NUREG/CR-4219
ORNL/TM-9593/V9&N1
Vol. 9, No. 1

Heavy-Section Steel Technology Program

Semiannual Progress Report for October 1991 – March 1992

Prepared by
W. E. Pennell

Oak Ridge National Laboratory

Prepared for
U.S. Nuclear Regulatory Commission

AVAILABILITY NOTICE

Availability of Reference Materials Cited in NRC Publications

Most documents cited in NRC publications will be available from one of the following sources:

1. The NRC Public Document Room, 2120 L Street, NW., Lower Level, Washington, DC 20555

2. The Superintendent of Documents, U.S. Government Printing Office, P.O. Box 37082, Washington, DC 20013-7082

3. The National Technical Information Service, Springfield, VA 22161

Although the listing that follows represents the majority of documents cited in NRC publications, it is not intended to be exhaustive.

Referenced documents available for inspection and copying for a fee from the NRC Public Document Room include NRC correspondence and internal NRC memoranda; NRC bulletins, circulars, information notices, inspection and investigation notices; licensee event reports; vendor reports and correspondence; Commission papers; and applicant and licensee documents and correspondence.

The following documents in the NUREG series are available for purchase from the GPO Sales Program: formal NRC staff and contractor reports, NRC-sponsored conference proceedings, international agreement reports, grant publications, and NRC booklets and brochures. Also available are regulatory guides, NRC regulations in the *Code of Federal Regulations*, and *Nuclear Regulatory Commission Issuances*.

Documents available from the National Technical Information Service include NUREG-series reports and technical reports prepared by other Federal agencies and reports prepared by the Atomic Energy Commission, forerunner agency to the Nuclear Regulatory Commission.

Documents available from public and special technical libraries include all open literature items, such as books, journal articles, and transactions. *Federal Register* notices, Federal and State legislation, and congressional reports can usually be obtained from these libraries.

Documents such as theses, dissertations, foreign reports and translations, and non-NRC conference proceedings are available for purchase from the organization sponsoring the publication cited.

Single copies of NRC draft reports are available free, to the extent of supply, upon written request to the Office of Administration, Distribution and Mail Services Section, U.S. Nuclear Regulatory Commission, Washington, DC 20555.

Copies of industry codes and standards used in a substantive manner in the NRC regulatory process are maintained at the NRC Library, 7920 Norfolk Avenue, Bethesda, Maryland, for use by the public. Codes and standards are usually copyrighted and may be purchased from the originating organization or, if they are American National Standards, from the American National Standards Institute, 1430 Broadway, New York, NY 10018.

NUREG/CR-4219
ORNL/TM-9593/V9&N1
Vol. 9, No. 1
RF

Heavy-Section Steel Technology Program

Semiannual Progress Report for October 1991 – March 1992

Manuscript Completed: October 1992
Date Published: November 1992

Prepared by
W. E. Pennell

Oak Ridge National Laboratory
Managed by Martin Marietta Energy Systems, Inc.

Oak Ridge National Laboratory
Oak Ridge, TN 37831-6285

Prepared for
Division of Engineering
Office of Nuclear Regulatory Research
U.S. Nuclear Regulatory Commission
Washington, DC 20555
NRC FIN B0119
Under Contract No. DE-AC05-84OR21400

Abstract

The Heavy-Section Steel Technology (HSST) Program is conducted for the Nuclear Regulatory Commission (NRC) by Oak Ridge National Laboratory (ORNL). The program focus is on the development and validation of technology for the assessment of fracture-prevention margins in commercial nuclear reactor pressure vessels. The HSST Program is organized in 11 tasks: (1) program management, (2) fracture methodology and analysis, (3) material characterization and properties, (4) special technical assistance, (5) fracture analysis computer programs, (6) cleavage-crack initiation, (7) cladding evaluations, (8) pressurized-thermal-shock technology, (9) analysis methods validation, (10) fracture evaluation tests, and (11) warm prestressing. The program tasks have been structured to place emphasis on the resolution fracture issues with near-term licensing significance. Resources to execute the research tasks are drawn from ORNL with subcontract support from universities and other research laboratories. Close contact is maintained with the sister Heavy-Section Steel Irradiation (HSSI) Program at ORNL and with related research programs both in the United States and abroad. This report provides an overview of principal developments in each of the 11 program tasks from October 1, 1991 to March 31, 1992.

Contents

List of Figures

List of Tables

Preface

The Heavy-Section Steel Technology (HSST) Program, which is sponsored by the Nuclear Regulatory Commission, is an engineering research activity devoted to extending and developing the technology for assessing the margin of safety against fracture of the thick-walled steel pressure vessels used in light-water-cooled nuclear power reactors. The program is being carried out in close cooperation with the nuclear power industry. This report covers HSST work performed in October 1991–March 1992. The work performed by the Oak Ridge National Laboratory (ORNL) and by subcontractors is managed by the Engineering Technology Division (ETD) of ORNL. Major tasks at ORNL are carried out by the ETD and the Metals and Ceramics Division. Prior progress reports on this program are listed below.

ORNL-4176
ORNL-4315
ORNL-4377
ORNL-4463
ORNL-4512
ORNL-4590
ORNL-4653
ORNL-4681
ORNL-4764
ORNL-4816
ORNL-4855
ORNL-4918
ORNL-4971
ORNL/TM-4655 (Vol. II)
ORNL/TM-4729 (Vol. II)
ORNL/TM-4805 (Vol. II)
ORNL/TM-4914 (Vol. II)
ORNL/TM-5021 (Vol. II)
ORNL/TM-5170 (Vol. II)
ORNL/NUREG/TM-3
ORNL/NUREG/TM-28
ORNL/NUREG/TM-49
ORNL/NUREG/TM-64
ORNL/NUREG/TM-94
ORNL/NUREG/TM-120
ORNL/NUREG/TM-147
ORNL/NUREG/TM-166
ORNL/NUREG/TM-194
ORNL/NUREG/TM-209
ORNL/NUREG/TM-239
NUREG/CR-0476 (ORNL/NUREG/TM-275)
NUREG/CR-0656 (ORNL/NUREG/TM-298)
NUREG/CR-0818 (ORNL/NUREG/TM-324)
NUREG/CR-0980 (ORNL/NUREG/TM-347)
NUREG/CR-1197 (ORNL/NUREG/TM-370)
NUREG/CR-1305 (ORNL/NUREG/TM-380)
NUREG/CR-1477 (ORNL/NUREG/TM-393)
NUREG/CR-1627 (ORNL/NUREG/TM-401)
NUREG/CR- 1806 (ORNL/NUREG/TM-419)
NUREG/CR-1941 (ORNL/NUREG/TM-437)
NUREG/CR- 2141, Vol. 1 (ORNL/TM-7822)
NUREG/CR-2141, Vol. 2 (ORNL/TM-7955)
NUREG/CR-2141, Vol. 3 (ORNL/TM-8145)
NUREG/CR-2141, Vol. 4 (ORNL/TM-8252)
NUREG/CR-2751, Vol. 1 (ORNL/TM-8369/V1)
NUREG/CR-2751, Vol. 2 (ORNL/TM-8369/V2)
NUREG/CR-2751, Vol. 3 (ORNL/TM-8369/V3)
NUREG/CR-2751, Vol. 4 (ORNL/TM-8369/V4)
NUREG/CR-3334, Vol. 1 (ORNL/TM-8787/V1)
NUREG/CR-3334, Vol. 2 (ORNL/TM-8787/V2)
NUREG/CR-3334, Vol. 3, (ORNL/TM-8787/V3)
NUREG/CR-3744, Vol. 1 (ORNL/TM-9154/V1)
NUREG/CR-3744, Vol. 2 (ORNL/TM-9154/V2)
NUREG/CR-4219, Vol. 1 (ORNL/TM-9593/V1)
NUREG/CR-4219, Vol. 2 (ORNL/TM-9593/V2)
NUREG/CR-4219, Vol. 3, No. 1 (ORNL/TM-9593/V3&N1)
NUREG/CR-4219, Vol. 3, No. 2 (ORNL/TM-9593/V3&N2)
NUREG/CR-4219, Vol. 4, No. 1 (ORNL/TM-9593/V4&N1)
NUREG/CR-4219, Vol. 4, No. 2 (ORNL/TM-9593/V4&N2)
NUREG/CR-4219, Vol. 5, No. 1 (ORNL/TM-9593/V5&N1)
NUREG/CR-4219, Vol. 5, No. 2 (ORNL/TM-9593/V5&N2)
NUREG/CR-4219, Vol. 6, No. 1 (ORNL/TM-9593/V6&N1)
NUREG/CR-4219, Vol. 6, No. 2 (ORNL/TM-9593/V6&N2)
NUREG/CR-4219, Vol. 7, No. 1 (ORNL/TM-9593/V7&N1)
NUREG/CR-4219, Vol. 7, No. 2 (ORNL/TM-9593/V7&N2)
NUREG/CR-4219, Vol. 8, No. 1 (ORNL/TM-9593/V8&N1)
NUREG/CR-4219, Vol. 8, No. 2 (ORNL/TM-9593/V8&N2)

Executive Summary

W. E. Pennell

The Heavy-Section Steel Technology (HSST) Program is conducted for the Nuclear Regulatory Commission (NRC) by Oak Ridge National Laboratory (ORNL). The program focus is on the development and validation of a fracture-mechanics-based technology for the evaluation of fracture-prevention margins in nuclear reactor pressure vessels (RPVs). Prior phases of a program generated the required technology, which was then transferred to national consensus codes and standards. Subsequent large-scale fracture tests have revealed the need for further development and refinement of the technology. Irradiation effects research programs and reactor vessel surveillance programs have identified further areas where extension of the fracture technology is required. Recent experience with licensing application of the technology has also identified areas in which additional development is required. Current HSST Program activities are structured to provide the necessary fracture technology developments and to support NRC in the licensing application of that technology.

1 Program Management

At the close of the current reporting period, the program cost and schedule variances were –25% and 4.4%, respectively. A principal cause of the schedule variance was a delay in preparation for the biaxial test caused by implementation of unscheduled cost control measures.

Subcontracts were placed with all of the HSST Program major subcontractors and consultants. Discussions were held with potential subcontractors for the large-scale biaxial tension fracture toughness test. In the case of AEA Technology, it was determined that there could be cost advantages to the program if the testing were performed as a part of the existing U.S.-U.K. collaborative program on pressure vessel integrity, because this would permit cost sharing. Responsibility for the interface with AEA Technology was therefore transferred to the NRC. A decision on the large-scale testing program will be made after exploratory tests have been completed on smaller scale test specimens.

Arrangements were completed for sessions on Pressure Vessel Fracture, Fatigue, and Life Management to be presented at the 1992 ASME Pressure Vessel and Piping Division Conference in New Orleans in June. The sessions were organized by an international team comprised of S. Bhandari, Framatome, France; P. P. Milella, ENEA/DISP, Italy; and W. E. Pennell, ORNL.

Papers by the HSST Program Manager were presented at the 19th NRC Water Reactor Safety Meeting on October 28, 1991, and at the NRC Aging Research Information Conference in the period March 24–27, 1992. The papers included scoping analyses and test data evaluations indicating that out-of-plane stresses, such as those generated during a pressurized thermal-shock (PTS) event, may act to increase crack-tip constraint and thereby reduce the material fracture toughness.

HSST Program personnel published one semiannual progress report, five NUREG/CR reports, one presentation, (as a NUREG/CP document), and two letter reports. Thirteen presentations were given at NRC-sponsored conferences and international fracture technology exchange meetings.

2 Fracture Methods and Analysis

Investigation of the effect of out-of-plane stresses on fracture toughness continued. This investigation is motivated by the fact that the loading conditions of primary concern in a nuclear RPV all produce biaxial stress fields with one of the principal stresses aligned parallel to the crack front for both longitudinal and circumferential flaws. There is no counterpart of these far-field stresses in the fracture toughness test specimens used to generate the fracture toughness data currently used to assess pressure vessel fracture-prevention margins. There is a concern that out-of-plane stresses may act to increase crack-tip constraint and thereby decrease fracture toughness.

During the current reporting period, results from the previously reported shallow-flaw and thermal-shock tests were evaluated as a set. This was possible because both sets of test data were produced using similar shallow-flaw depths. The results show a substantial elevation in toughness for shallow flaws loaded by uniaxial tensile stress. When similar flaws are loaded by a biaxial stress field however, the toughness elevation is much reduced. This result tends to support the postulate that out-of-plane stresses can influence crack-tip constraint and thereby influence fracture toughness.

Development of analytical models for the prediction of crack-tip constraint effects on fracture toughness continued. Crack-tip micromechanical models using both stress-based [Ritchie-Knott-Rice (RKR)] and ductility-based [McClintock-Hancock-MacKenzie (MKM)] fracture

criteria have been developed together with a correlation parameter based on the area of material at the crack-tip in which the stress exceeds a critical value. Emphasis in the current reporting period has been on validating these models using available fracture toughness data obtained in the plane stress-to-plane strain domain. To date none of the models has been able to match results from tests involving a range of crack-tip constraint conditions.

Near-term fracture model development and validation efforts will now focus on a detailed analysis of the thermal-shock test crack-tip stress and strain fields with the objective of identifying parameters that responded strongly to the biaxial loading condition present in those tests. The thermal-shock tests represent the only currently identified source of test data in which the effects of a 1:1 stress ratio on fracture toughness are present and potentially capable of isolation. It has become evident, however, that existing test data on biaxial loading effects cannot provide all of the information required for development of the constraint effects fracture toughness models.

The program has initiated development of a biaxial fracture toughness test specimen specifically designed to generate the data required to determine the effects of biaxial loading on fracture toughness in a manner that will facilitate identification of the underlying causes. In the current reporting period, 2-D and 3-D finite-element analyses have been performed to define the geometry of a cost-effective test specimen and confirm that the test specification requirements are met. One of these requirements is that stresses in the remaining ligament remain elastic at the fracture load. This requirement has dictated the use of a large (5-in.-thick) specimen that, in turn, dictates the use of a large high load-capacity test machine. Test machines with a currently existing capability to test the large biaxial specimens are all located overseas.

Analyses were performed to evaluate the performance of a RKR fracture model in predicting existing fracture toughness results in the plane stress-to-plane strain domain. Test results were drawn from the HSST Program wide-plate and shallow-flaw test series. Detailed plane strain finite-element models were constructed for both types of test specimen, and the J-Q loci were defined up to the test fracture load. Results showed a significant difference in the Q-stress dependence of fracture toughness for the two test specimens. In each case the fracture toughness predicted using the RKR model was significantly less than the measured value.

Analysis of the effect of out-of-plane stress on the constraint at the tip of a circumferential crack in a pressure vessel was continued at the University of Maryland (UM). In the current reporting period, the amplified pressure loading used in the previously reported analysis was replaced with a more prototypical combination of thermal and mechanical loading. The results obtained were similar to those previously reported. The presence of an out-of-plane stress had no significant influence on the crack-tip constraint as expressed in terms of the Q-stress. The conclusion from this study is that out-of-plane stresses do not influence the constraint element of the crack-driving force expressed in terms of the Q-stress. The previously discussed biaxial tests will be required to address the separate issue of the potential effect of out-of-plane stress effects on the material fracture toughness.

Studies of the effect of reactor vessel inertia on crack arrest behavior during a PTS event continued. During the current reporting period, dynamic fracture toughness estimates derived from data obtained from the HSST Program wide-plate tests were used in the analysis. Results again indicated that the final arrest depth is critically dependent on the dynamic crack reinitiation toughness relationship used in the analysis. A dynamic fracture toughness data base will be required if the dynamic crack arrest concept is to be developed to the point where it can be included as a verified element of a PTS analysis.

A report was issued summarizing results from a study at the UM on crack reinitiation from an arrested cleavage crack. The study showed no significant difference between the fracture toughness measured using fatigue presharpened and arrested cleavage cracks. The study also identified potential improvements to the American Society for Testing and Materials (ASTM) E1221 crack-arrest specimen design.

Support for the Japanese EPI Program was continued during the current reporting period. This research activity aims to develop and validate methods for the prediction of elastic-plastic crack growth in inhomogeneous materials (EPI). This work has application to the analysis of crack growth at the weld-base material interface in an RPV. Testing and analysis elements of this program are proceeding on schedule. The final report from this 4-year project is scheduled to be issued in the next reporting period.

3 Material Characterization and Properties

Testing to characterize the tensile and crack initiation toughness properties of the plate material used in the shallow-flaw fracture toughness program was completed

during the current reporting period. The tensile tests showed a significant difference in yield stress between material from the midsection of the plate and that taken from the plate surface. This trend is similar to that previously reported for the Charpy V-notch (CVN) energy for this material.

Thermal aging of stainless steel cladding specimens continued with the objective of completing the 20,000-h aging cycle by November 1992. This work supplements the previously reported study of irradiation aging effects on the ductile tearing toughness of stainless steel cladding.

HSST Program personnel involvement in the development of ASTM fracture toughness testing standards continued. Significant progress was made in the development of a combined J_{Ic}/J-R standard. Progress was also made in testing procedures incorporated in a proposed standard for "Test Practice for Fracture Toughness in the Transition Region."

The initial phase of the investigation of the pop-in behavior associated with local brittle zones has been completed, and a report is in preparation. A significant conclusion from the investigation is that pop-ins must be given serious consideration as potential initiators of fast-running cracks.

4 Special Technical Assistance

A study was completed of the effect on calculated stress-intensity factors for semielliptical surface cracks of recently proposed methods for representing the stress distribution over the depth of the crack. The recent proposal by J. M. Lawrence and J. L. Hechmer of the Babcock and Wilcox Company involves replacing the actual nonlinear stress distribution with an equivalent linear distribution over the depth of the crack producing an equivalent end load and moment. This linear stress distribution differs from that defined in Sect. XI of the *American Society of Mechanical Engineers Boiler and Pressure Vessel Code* and is claimed to improve the accuracy of the K_I calculation. The study showed that results obtained using the equilibrium-based linear fit were identical with those obtained using a least-squares fit to the actual nonlinear stress distribution.

Analyses were performed to evaluate the influence of flaw shape and material modeling assumptions on longitudinal propagation of finite-length surface flaws in a clad reactor vessel under PTS loading. This work has application to the future treatment of finite-length flaws in a PTS analysis. Analysis results showed the computed K_I values at the ends of the flaw (near the surface of the vessel) to be very sensitive to the flaw shape assumptions. The near-surface K_{Ic} was higher for a canoe-shaped flaw than for a semielliptical flaw. The difference increased as the flaws became long and the surface-length to radial-depth ratio increased.

5 Fracture Analysis Computer Programs

This task is concerned with development of an advanced computer program to perform the probabilistic fracture mechanics analysis of RPVs. This analysis is required by Title 10, Part 50, Sect. 61-4 of the *Code of Federal Regulations* to support any proposal for operation of a nuclear RPV once the PTS screening limits have been exceeded. The advanced code has been named FAVOR. It will incorporate the best features of the current generation of PTS analysis programs (e.g. OCA-P and VISA-II) together with fracture technology and programming developments to make it more accurate, versatile, and user friendly than its predecessors.

In the current reporting period, the overall structure of the FAVOR code was defined and development progressed on individual modules of the code. Specific developments involve consolidating of certain analysis procedures, improving the user interface, and introducing features that permit the analysis of a vessel divided into regions and subregions, each with its own set of characteristics. The latter feature makes possible an improved representation of the spatial variability of fracture-related parameters throughout an RPV. Participation in the ongoing NRC/Electric Power Research Institute sponsored PTS code benchmarking exercise is contributing to the validation of the FAVOR code.

A paper entitled "The Application of Probabilistic Fracture Analysis to the Residual Life Assessment of Embrittled Reactor Vessels" was prepared and presented at the NRC Aging Conference in Rockville, Maryland, in March.

6 Cleavage Crack Initiation

Analysis of data from the portion of the shallow flaw fracture toughness testing program assigned to ORNL was completed during the current reporting period. K_{Ic} values calculated from measured J_{Ic} and crack-tip opening displacement (CTOD) data were found to agree. Fracture toughness for the shallow flaws was found to be substantially greater (60% at T = –60°C) than that for deep flaws in the lower transition region of the K_{Ic} vs T-RT_{NDT} curve. The measured toughness appeared to be insensitive

to beam thickness for thicknesses in the range of 2 in. < B < 6 in.

Testing of shallow flaws in prototypical clad reactor vessel material is planned in order to evaluate the effect of metallurgical gradients in the near-surface material on shallow-flaw fracture toughness. Full-thickness material for these tests has been obtained from a reactor vessel for a cancelled nuclear plant. The test specification for these tests was completed and issued during the current reporting period. In a parallel activity, metallurgical gradients in a structural weld cut from the cancelled Midland reactor vessel were investigated at the UM. A significant finding from that investigation was that the material hardness peaked markedly in the region where heat-affected zones from the structural welds and the cladding weld overlapped.

Planning was initiated for a series of tests to determine the effect of out-of-plane stresses on fracture toughness. An understanding of the effects of out-of-plane stresses is necessary for advances to be made in the treatment of shallow-flaw fracture toughness in PTS analysis. Tests previously reported have demonstrated an increase in fracture toughness for shallow flaws under uniaxial loading. Analysis indicates this to be due to a relaxation of in-plane crack-tip constraint due to the proximity of the free surface of the test specimen. Prior HSST Program thermal-shock tests with similar shallow flaws showed very little fracture toughness enhancement however. It is possible that the addition of the out-of-plane stress acts to increase the crack-tip constraint and thereby counteract some of the relief of in-plane constraint associated with shallow flaws. The planned tests will provide the data required for a quantitative evaluation of out-of-plane constraint effects. During the current reporting period, a test specification was produced and preliminary design and analysis initiated on a large-scale biaxial-tension test specimen.

Studies were completed at the UM on the use of crack-tip precompression to permit generation of lower-bound dynamic fracture toughness data using small-scale test specimens. This work has potential significance for the long-range development of reactor vessel surveillance specimens. Results from the test phase of this work have shown that precompression can be used to generate lower-bound fracture toughness properties using small specimens. The actual toughness obtained however can be dependent on the amount of precompression applied. The technique is therefore not yet at a stage of development where it is ready for surveillance program use. In the current reporting period UM has completed a draft report on this work. The report will be published in NUREG format in the next reporting period.

7 Cladding

Analytical studies in progress are aimed at refining the treatment of cladding effects in PTS analyses. Cladding has the potential to have both positive and negative effects on fracture margins. The negative potential derives from the reported low tearing toughness of irradiated cladding material. This leads to a concern that tearing initiated in the cladding could convert to cleavage fracture in the base material.

The positive potential derives from the high cleavage fracture toughness of stainless steel cladding. This can reduce the combinations of certain categories of finite-length surface flaws to convert to infinite-length flaws under thermal shock loading. Finite-length flaws produce lower peak stress-intensity factors than do infinite-length flaws with an equivalent depth. The potential exists, therefore, for a reduction in the predicted rate of initial crack initiations during a PTS event with the inclusion of this aspect of cladding behavior into the analysis model.

An evaluation of the potential for tearing initiation in low toughness cladding was completed in the current reporting period. The evaluation utilized an idealization of the Rancho-Seco PTS transient together with 25.4-mm (1-in.) and 38.1-mm-(1.5-in.) deep surface flaws with surface length/depth ratios of 2:1, 3:1, and 6:1. Results showed that cleavage crack initiation would not be predicted at the deepest point of the 25.4-mm-deep finite-length flaws, but would be predicted for a infinite-length flaw of equivalent depth. These results confirm the benefit to be derived from demonstrating that certain finite-length cracks will not propagate to become infinitely long. The estimated cladding -3σ J_{cr} curve falls below the applied J curve, whereas the -2σ curve is always well above the applied J curve. Therefore, a relatively low probability exists for tearing to initiate in the cladding.

8 Pressurized-Thermal-Shock Technology

No activity in the current reporting period.

9 Analysis Methods Validation

The objective for this task is to verify analysis methods for nuclear pressure vessel fracture margin assessment. Principal verification techniques used are (1) application of the analysis methods to predict results from large-scale fracture tests and (2) interaction with domestic and foreign

research organizations and regulatory agencies active in the fracture margin assessment field.

In the current reporting period, the HSST Program, acting jointly with GRS of Cologne, Germany, completed the draft of the report on the CSNI/FAG project FALSIRE. In this project several international large-scale fracture experiments were analyzed by fracture analysis organizations in Europe, Japan, and the United States. Results from these analyses focused attention on deficiencies in existing technology for the analysis of crack propagation by ductile tearing. Arrangements have been made for the next Specialists Meeting on Fracture Mechanics Verification by Large-Scale Testing to be held on Oak Ridge, Tennessee, on October 26–29, 1992.

10 Fracture Evaluation Tests

Shallow-flaw fracture toughness testing has been transferred from ORNL to the David Taylor Research Center. Material for use in that program has been identified and reserved at ORNL.

Shallow-flaw fracture toughness tests are scheduled to be performed on full-thickness beam specimens cut from a cancelled PWR reactor vessel. During the current reporting period, the test material was flame cut from the vessel shell segment and forwarded to the test specimen fabrication subcontractor. The tests will be performed for the HSST Program at the National Institute of Standards and Technology under an interagency agreement.

Preliminary design studies were completed for a large-scale membrane-tension biaxial test specimen tailored to fit the AEA Technology (U.K.) large biaxial test machine. Membrane loading was selected for the test specimen to minimize data interpretation problems. Estimated costs for the initial test specimen design were prohibitive however, due in large measure to the extensive precision machining required for the specimen to mate with the U.K. machine interface. Subsequent design studies produced a specimen with single-pin loading on each of the four arms. The estimated cost for this specimen was close to one order of magnitude less than the estimated cost for the original test specimen design. Specification, design, and analysis activities in preparation for the large-scale biaxial test are proceeding based upon the reduced cost test specimen configuration.

11 Warm Prestressing

An investigation into warm prestressing (WPS) effects was initiated during the current reporting period with the long-term objective of (1) defining the conditions under which WPS effects could have a significant influence on a reactor vessel fracture margin assessment and (2) developing an understanding of the WPS phenomenon sufficient to permit its inclusion in the RPV fracture margin assessment process. In the current reporting period, a survey of potential applications for WPS technology was completed, and a letter report was produced.

HEAVY-SECTION STEEL TECHNOLOGY PROGRAM SEMIANNUAL PROGRESS REPORT FOR OCTOBER 1991—MARCH 1992*

1 Program Management

W. E. Pennell

The Heavy-Section Steel Technology (HSST) Program is conducted for the Nuclear Regulatory Commission (NRC) by Oak Ridge National Laboratory (ORNL). The program focuses on the development and validation of technology for the assessment of fracture-prevention margins in commercial nuclear reactor pressure vessels (RPVs).

RPV licensing issues of current concern can be grouped into three primary categories: (1) low-temperature overpressure protection (LTOP) set-point criteria, (2) structural integrity of the pressure vessel when subjected to pressurized-thermal-shock (PTS) loading, and (3) criteria for the evaluation of fracture margins for reactor vessels containing low-upper-shelf (LUS) Charpy energy material. The current HSST Program is structured to provide the research results required for resolution of these issues. A summary of the program's principal research tasks is given in Fig. 1.1.

Management direction and control of the program are implemented using an 11-element Level 1 work breakdown structure (WBS) and a linked cost-schedule performance monitoring system. The current HSST Program Level 1 WBS is illustrated in Fig. 1.2. Each element of the Level 1 WBS represents a separate research or management task with a designated task leader.

At the close of the current reporting period, the program cost and schedule variances were –25% and –4.4%, respectively. A principal cause of the schedule variance was a delay in preparation for the biaxial test due to (1) the need to perform additional design and analysis work to reduce the test specimen cost and (2) the decision to implement any contractual arrangement with AEA Technology by means of an NRC – AEA Technology international agreement rather than an HSST Program subcontract. In addition the schedule was impacted by the addition of an analysis and test evaluation task to be completed before work was initiated on the design of a clad-cylinder crack propagation test. The analysis and test activities were integrated into the program plan, but the associated rescheduling of the clad-cylinder test design activities was not. The cost variance results from greater than anticipated analysis costs for (1) dual-parameter fracture correlation validation, (2) biaxial test specimen design support, and (3) dynamic crack arrest studies.

Staffing for the research tasks is drawn from the Engineering Technology, Metals and Ceramics, and Computing and Telecommunications Divisions at ORNL. Subcontracts with consultants, universities, and other research laboratories are used to gain access to special expertise and capabilities required for certain research tasks. A summary of resources applied to the HSST research tasks during this report period is given in Fig. 1.3.

Subcontracts were placed with all of the HSST Program major subcontractors and consultants. A new consulting subcontract with Professor F. Shih of Brown University provides the program with the expertise required to guide the development of dual-parameter fracture toughness correlations. The subcontract with Battelle Columbus provides the program with access to a technology with a potential for producing fracture toughness data for out-of-plane biaxial tensile loading using relatively small test specimens.

Discussions were held with potential subcontractors for the large-scale biaxial tension fracture toughness test. In the case of AEA Technology it was determined that there could be cost advantages to the program if the testing were performed as a part of the existing U.S.–U.K. collaborative program on pressure vessel integrity, because this would permit cost sharing. Responsibility for the interface with AEA Technology was therefore transferred to the NRC. Discussions were also held with personnel from the National Institute of Standards and Technology (NIST). Apparently the NIST 27-MN test machine could be fitted with an auxiliary loading frame that will make it capable of the required biaxial loading. A decision on the large-scale testing program will be made after exploratory tests have been completed on smaller scale test specimens.

Arrangements were completed for sessions on Pressure Vessel Fracture, Fatigue, and Life Management to be presented at the 1992 American Society of Mechanical

*This report is written in metric units. Conversion from SI to English units for all SI quantities are listed on a foldout page at the end of this report.

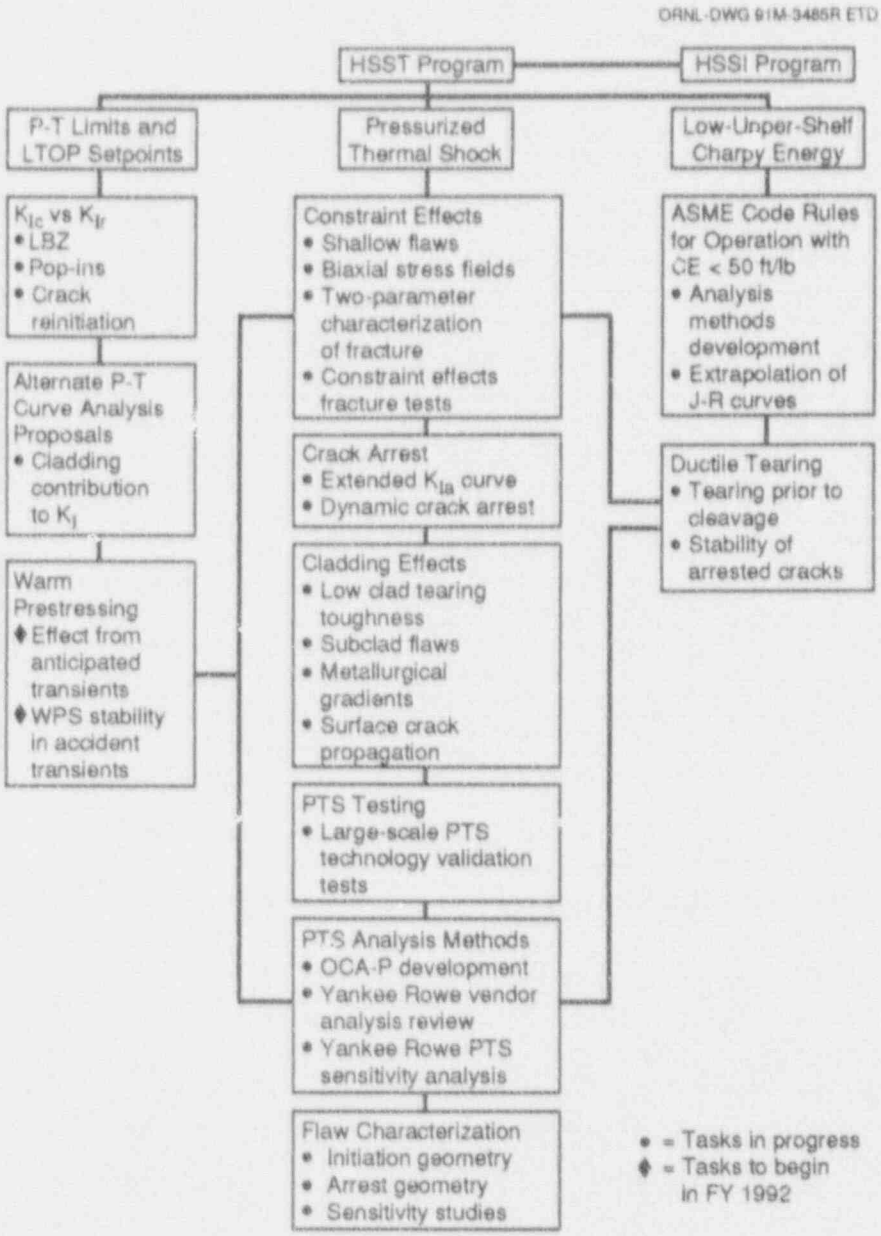

Figure 1.1 Summary of principal HSST Program research tasks

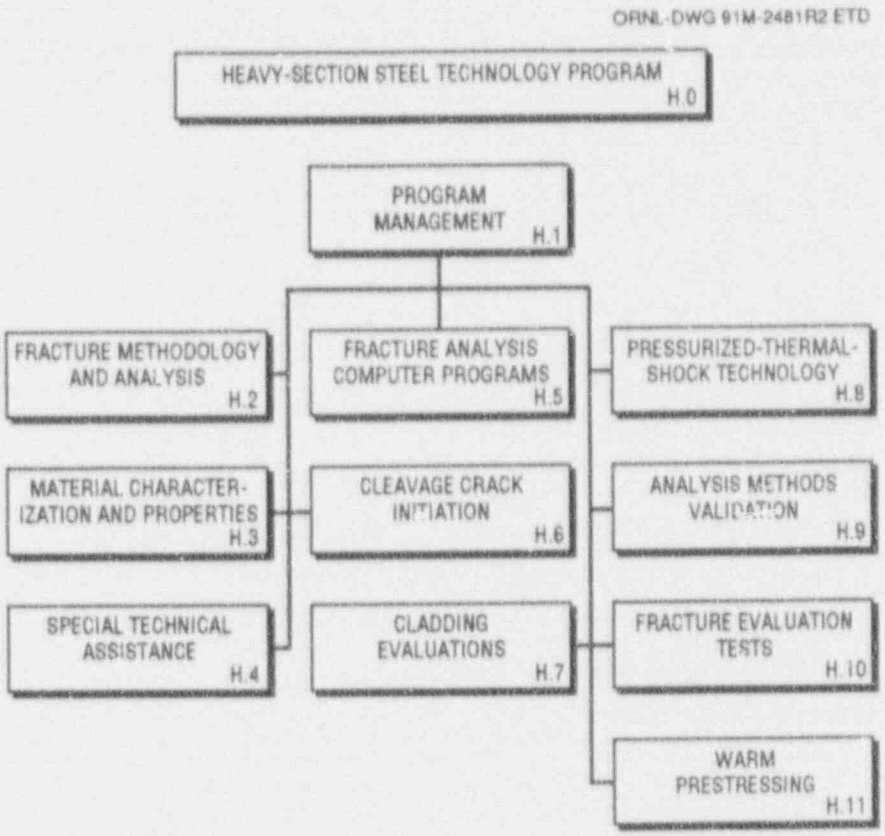

Figure 1.2 Level 1 breakdown structure for HSST Program

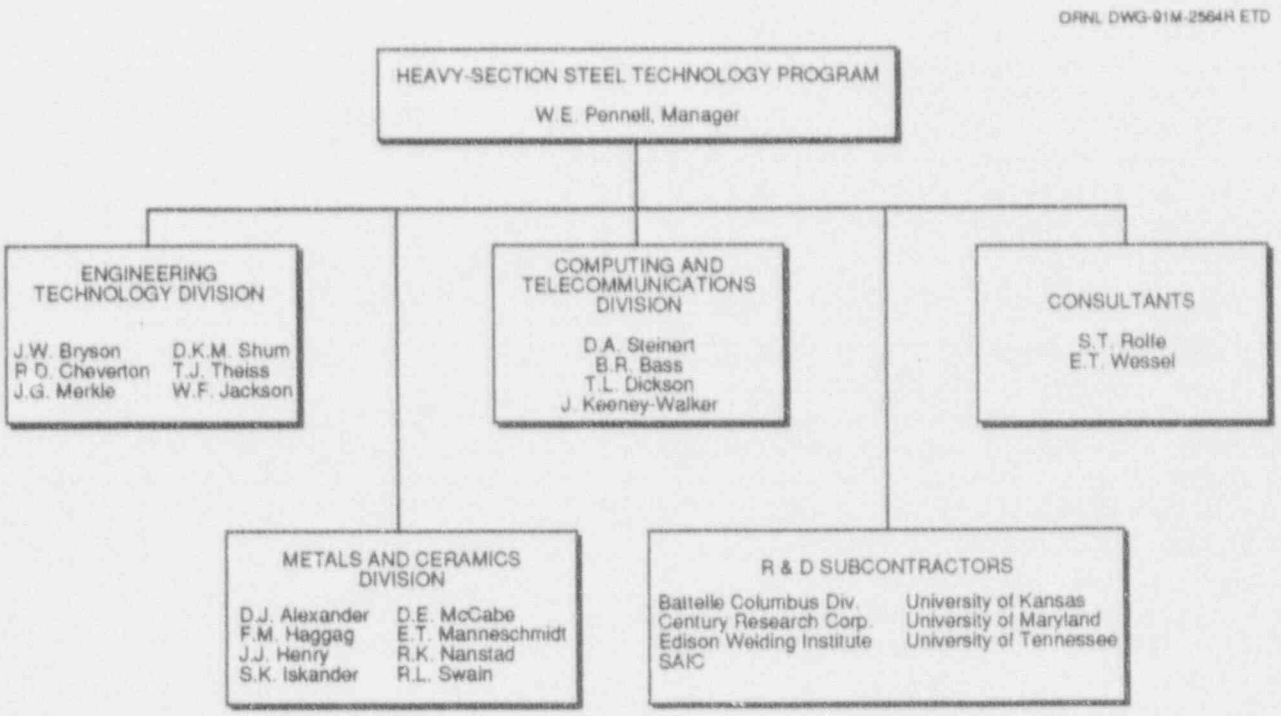

Figure 1.3 Resources applied to HSST Program R&D tasks

Engineers (ASME) Pressure Vessel and Piping Division Conference in New Orleans in June. A total of 37 papers will be presented in 9 sessions. The sessions were organized by an international team comprised of S. Bhandari, Framatome, France; P. P. Milella, ENEA/DISP, Italy; and W. E. Pennell, ORNL–USA. The volume of papers was assembled at ORNL and will be published by the ASME in June 1992 as PVP Vol. 223.

Two papers by W. E. Pennell were prepared and presented during this reporting period. The first, entitled "HSST Program: Recent Developments in Crack Initiation and Arrest Research" was presented at the 19th NRC Water Reactor Safety Meeting on October 28, 1991. This paper contained results from a scoping analysis which suggested that out-of-plane stresses could increase crack-tip constraint and thereby reduce fracture toughness. The second paper, entitled "Aging Impact on the Safety and Operability of Nuclear Reactor Pressure Vessels" was presented at the NRC Aging Research Information Conference in the period March 24–27, 1992. This latter paper included a review of results from the ORNL shallow-flaw and thermal-shock test programs. Both programs used test specimens with similar constant-depth shallow flaws. The shallow-flaw specimens were subjected to uniaxial loading, whereas the thermal-shock specimens were subjected to out-of-plane biaxial loading. Fracture toughness results for the uniaxial loading tests were significantly higher than those for the thermal-shock tests. These results lend support to the postulate that out-of-plane stresses can increase crack-tip constraint and thereby decrease fracture toughness. Research into out-of-plane and in-plane constraint effects continues with the aim of developing an improved definition of the fracture toughness for shallow flaws under out-of-plane biaxial loading. Results from this research are intended for application to the PTS analysis of pressure vessels where fracture initiation from shallow flaws is particularly important.

Other meetings with significant HSST Program management input during the current reporting period include the U.S.— U.S.S.R. Joint Coordinating Committee on Nuclear Reactor Safety Working Group Meeting (October 28–30, 1991), the HSST Program Review Meeting with NRC on February 25, 1992, and the NRC Constraint Effects on Fracture Meeting on March 3, 1992.

During the current reporting period HSST Program personnel published one semiannual progress report,[1] five NUREG/CR reports,[2–6] one presentation,[7] (as a NUREG/CP document) and two letter reports.[8,9] Three presentations were given at NRC-sponsored conferences,[7,10,11] three at NRC-sponsored international fracture technology exchange meetings,[12–14] two at technical society meetings,[15,16] and five at USNRC/Electric Power Research Institute fracture technology development meetings.[17–20]

References

1. W. E. Pennell, Martin Marietta Energy Systems, Inc., Oak Ridge Natl. Lab., *Heavy-Section Steel Technology Program Semiannual Progress Report for October 1990 — March 1991*, USNRC Report NUREG/CR-4219, Vol. 8, No. 1 (ORNL/TM-9593/V8 & N1), February 1992.*

2. J. W. Dalley et al., University of Maryland, *Lower-Bound Initiation Toughness with a Modified-Charpy Specimen*, USNRC Report NUREG/CR-5703 (ORNL/Sub/79-7778/7), November 1991.*

3. G. R. Irwin, University of Maryland, *Use of Thickness Reduction to Estimate Values of K*, USNRC Report NUREG/CR-5697 (ORNL/SUB/79-7778/5), November 1991.*

4. S. T. Rolfe, University of Kansas, *The Behavior of Shallow Flaws in Reactor Pressure Vessels*, USNRC Report NUREG/CR-5767 (ORNL/SUB/90-SH640/1), November 1991.*

5. D. E. McCabe, A Comparison of Weibull and β_{1c} Analysis of Transition Range Fracture Toughness Data, USNRC Report NUREG/CR-5788 (ORNL/TM-11959), January 1992.*

6. J. D. Landes, *Extrapolation of the J-R Curve for Predicting Reactor Vessel Integrity*, USNRC Report NUREG/CR-5650 (ORNL/SUB/89-99732/1), January 1992.*

7. W. E. Pennell, "Heavy-Section Steel Technology Program: Recent Developments in Crack Initiation and Arrest Research," in *Proceedings of U.S. Nuclear Regulatory Commission Nineteenth Water Reactor Safety Information Meeting, October 28-30, 1992, Rockville, Maryland*, USNRC Proceeding NUREG/CP-0119, Vol. 1, April 1992.*

8. D. K. M. Shum et al., "Potential Change in Flaw Geometry of an Initially Shallow, Axially Oriented, Inner-Surface Finite-Length Flaw During a PTS Transient," ORNL/NRC/LTR-92/1, January 31, 1992.

9. D. K. M. Shum, "Implications of Warm Prestress on Safety-Margin Assessment of Reactor Pressure Vessels," ORNL/NRC/LTR-92/9, March 31, 1992.

10. T. L. Dickson, The Application of Probabilistic Fracture Analysis to Residual Life Evaluation of Embrittled Reactor Vessels presented at the 1992 NRC Aging Research Conference, Bethesda, Maryland, March 25, 1992.

11. W. E. Pennell, "Aging Impact on the Safety and Operability of Nuclear Reactor Pressure Vessels" presented at the 1992 NRC Aging Research Conference, Bethesda, Maryland, March 25, 1992.

12. R. D. Cheverton, "Sensitivity of Calculated Conditional Probability of Vessel Failure to Variations in Methodology and Input for PTS Loading," presented at the U.S. — U.S.S.R. Joint Coordinating Committee on Civilian Nuclear Reactor Safety Working Group 3, Radiation Embrittlement of the Housing and Support Structures and Annealing of the Housing, Meeting, The Pavilion Hotel, Rockville, Maryland, October 24, 1991.

13. W. E. Pennell, "PTS — Current Issues and Research," presented at the U.S. — U.S.S.R. Joint Coordinating Committee on Civilian Nuclear Reactor Safety Working Group 3, Radiation Embrittlement of the Housing and Support Structures and Annealing of the Housing, Meeting, The Pavilion Hotel, Rockville, Maryland, on October 23, 1991.

14. W. E. Pennell, "Heavy-Section Steel Technology Program: Recent Developments in Crack Initiation and Arrest Research,"presented at Second USNRC/JAPEIC Specialized Topic Workshop, Marriott Hotel, LaJolla, California, November 11, 1991.

15. D. E. McCabe, "Unique Features of a Transition Range Standard," presented at ASME Committee E-24, San Diego, California, October 16, 1991.

16. D. K. M. Shum, "Application of Two-Parameter Fracture Methodologies to Large-Scale Fracture Experiments," presented at Society of Engineering Science 28th Annual Technical Meeting, Prager Medalist Session, University of Florida, Gainesville, Florida, November 11–15, 1991.

17. B. R. Bass, "Dynamic Crack Reinitiation Toughness," presented at Joint USNRC/EPRI Meeting, Anaheim, California, November 22, 1991.

18. T. L. Dickson, "OCA-P Structure and Modeling Assumptions," presented at Joint USNRC/EPRI Meeting, Anaheim, California, November 22, 1991.

19. J. Keeney-Walker, "Evaluation of Dynamic Effects and Fracture Toughness Relations on Crack Arrest/Reinitiation in RPVs," presented at the Joint USNRC/EPRI Meeting, Anaheim, California, November 22, 1991.

20. C. W. Schwartz and B. R. Bass, "Dynamic Fracture Toughness Relations Inferred from SEN Specimens of A 533 B Steel," USNRC/EPRI Meeting, Anaheim, California, November 22, 1991.

*Available for purchase from the National Technical Information Service, Springfield, VA 22161.

2 Fracture Methodology and Analysis

B. R. Bass*

2.1 Introduction

The following sections describe recent advances made in the coordinated effort being conducted under the Heavy-Section Steel Technology (HSST) Program by Oak Ridge National Laboratory (ORNL) and several subcontracting groups to develop the experimental data base and the analytical tools required to construct improved fracture models for reactor pressure vessel (RPV) steels.

During this report period, work continued on an investigation of the relationship between out-of-plane biaxial stress fields and crack-initiation toughness, an analysis of a proposed large-scale biaxial test specimen, an analysis of the near-crack-tip region using modified-boundary-layer models, analytical studies of dynamic crack arrest in RPVs subjected to pressurized-thermal-shock (PTS) loading, and the Joint Japanese/United States Elastic-Plastic Inhomogeneous (U.S. EPI) Program for the development of an engineering estimation scheme applicable to inhomogeneous materials and structures.

2.2 Constraint Effects on Fracture Toughness for Circumferentially Oriented Cracks in RPVs

(D. K. M. Shum, J. W. Bryson, T. J. Theiss, J. Keeney-Walker,* B. R. Bass*)

The objectives of this subtask are to develop and validate analytical methods for estimating the potential impact of out-of-plane biaxial far-field stresses on crack initiation toughness of inner surface cracks in nuclear RPVs.

PTS loading produces biaxial stress fields in an RPV wall with one of the principal stresses aligned parallel to postulated surface cracks in either longitudinal or circumferential welds. The limited quantity of existing biaxial test data all suggest a significant decrease in fracture toughness under out-of-plane biaxial stresses that would act in opposition to the in-plane constraint relaxation, which has been previously demonstrated for shallow cracks. Consequently, understanding of both in-plane and out-of-plane crack-tip constraint effects is necessary to a refined analysis of fracture initiation from shallow cracks under PTS transient loading.

*Computing and Telecommunications Division, Martin Marietta Energy Systems, Inc., Oak Ridge, Tenn.

A summary of existing biaxial test data indicating a significant decrease in fracture toughness under out-of-plane biaxial loading conditions is given in Table 2.1 and in Fig. 2.1. Comparisons of measured data from thermal-shock experiments[1] and shallow crack beam tests[2] conducted in the HSST Program at ORNL provide insight into the impact of biaxial far-field stress distributions on fracture toughness. The thermal-shock experiments employed shallow cracks having depths comparable to those in the shallow-crack beam tests, but with a very long crack front. Results in Fig. 2.2, from these thermal-shock tests show an increase in toughness relative to plane strain values, but not of a magnitude that would have been inferred from the shallow-crack data. It has been suggested[3] that the biaxial stress field produced by the thermal-shock loading had the effect of reducing fracture toughness well below (~40%) those values associated with uniaxial loading of the shallow-crack beams.

Table 2.1. Summary of experimental data exhibiting a decrease in toughness for out-of-plane biaxial stresses

Experiments(s)	Crack geometry	Biaxiality ratio	Reduction in K_c(%)
Shallow-crack and wide-plate data (HSST/ ORNL)	Through-crack	1:1 (equibiaxial)	40
Biaxial/tensile specimen data (BAM, Germany)	Through-crack	1:03	25
Spinning disk data (CNITMASH, Russia)	Finite-length surface crack	1:1 (equibiaxial)	37

Experimental and analytical studies[4–9] at Bundesanstalt für Materialprüfung (BAM), Germany, examined the influence of biaxial stress states on fracture toughness of pressure vessel steels. A nominal biaxial stress state was generated in small tensile specimens via a transverse bending stress that develops in conjunction with tensile loading. The ratio of tensile to transverse components of stress had maximum and mean values of 1:0.3 and 1:0.15, respectively. BAM reported that fracture toughness K values of the biaxially

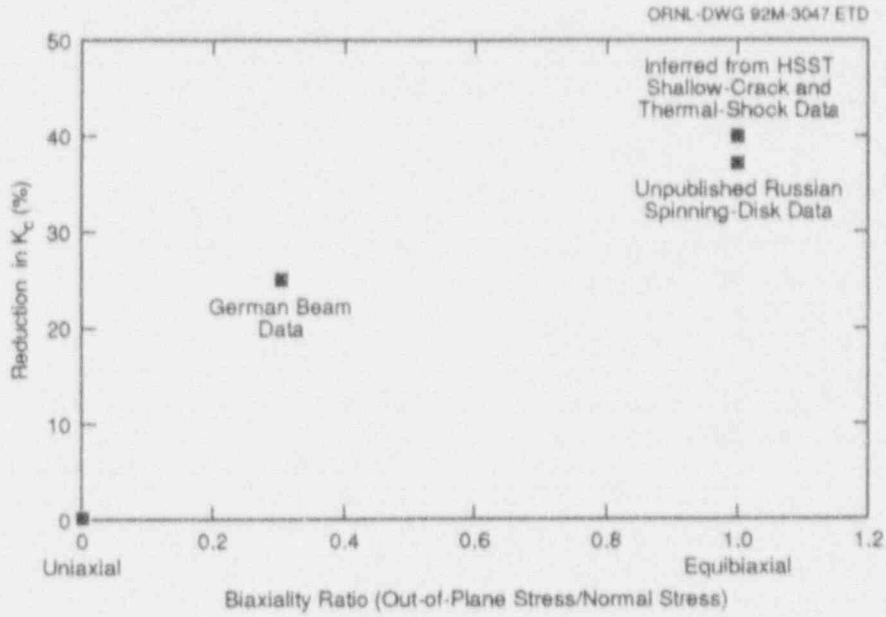

Figure 2.1 Experimental data indicating decrease in fracture toughness due to effects of out-of-plane biaxial stresses

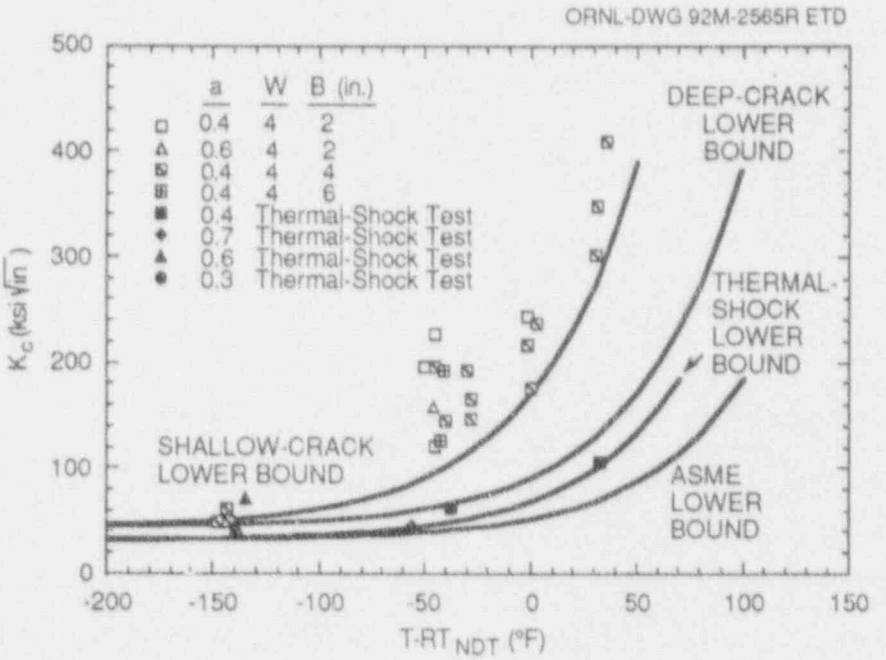

Figure 2.2 Comparison of cleavage initiation toughness data from shallow-crack beam test and from thermal-shock experiments

loaded specimens were ~25% lower than those of single-edge notched (SEN) specimens.

Unpublished data were reported from CNITMASH, Russia, concerning fracture toughness measurements under biaxial loading conditions produced in a spinning-disk facility.† These tests utilized circular disks having a diameter 450 to 600 mm, thickness of 150 mm, and surface cracks of maximum depth 40 mm and length 200 mm. In

†M. Brumovsky, personal communication to W. E. Pennell, Oak Ridge National Laboratory, May 11, 1992.

these experiments, an estimated 37% reduction in toughness K_c was reported for the biaxially loaded spinning disks, as compared with data from uniaxially loaded specimens.

The scarcity of experimental data addressing the effects of biaxial far-field stress distribution on fracture toughness provides the motivation for addressing the issue from an analytical perspective. Two different analytical approaches to the problem have been adopted.[10] The first approach addresses crack initiation by focusing on the near-crack-tip fields within a region extending a few crack-tip opening displacements (CTODs) directly ahead of the crack tip. Two-parameter fracture characterization methods, which incorporate the higher-order T-stress[11] and Q-stress[12] terms, are employed to provide the technical basis for addressing the shortcomings of conventional one-parameter methods based on the K and J parameters. The near-crack-tip results are then interpreted within the context of a selected number of micro-mechanical fracture models for the prediction of crack initiation. The Ritchie-Knott-Rice (RKR)[13] model is adopted for the prediction of cleavage fracture, and the McClintock-Hancock-MacKenzie (MHM) model[14–15] is adopted for the prediction of ductile fracture. These two models are chosen because they have been applied to A 533 B material, in the lower-transition and upper-shelf regions respectively, with some success under nonirradiated and irradiated conditions.[16–18]

The second approach focuses on the development of correlation parameters that relate fracture toughness with a volume of material loaded above nominal stress threshold states. Candidate correlation parameters include, but are not limited to, those based on a critical maximum principal stress contour methodology.[19–20] This methodology relates cleavage crack initiation with the attainment of a critical area enclosed within a selected maximum principal stress contour surrounding the crack tip. A correlation between fracture toughness and this numerically determined area parameter is provided through applications to measured data. This approach was applied to the analysis of existing fracture toughness data obtained from wide-plate specimens[20–21] and from compact tension (CT) specimens[22] having a common planform, but with varying thickness.

The fracture prediction models described above were applied to available measured data with the objective of validating the models in the plane stress-to-plane strain domain before applying them to positive out-of-plane strain conditions. Results from these applications are summarized in Table 2.2. The RKR model was applied to fracture initiation toughness data generated in the HSST Program from large-scale wide-plate experiments[21,23–24] and shallow-crack beam tests.[2] Finite-element analyses of these experiments were performed using loading conditions measured in the test. Full-field finite-strain solutions based on the plane strain assumption were generated from

Table 2.2. Summary of applications of fracture prediction models to measured data in plane stress-to-plane strain domain

Fracture prediction model	Test specimen configuration	Analysis objective	Analysis assessment
RKR cleavage initiation model	Wide plate	Comparison of model toughness predictions with measured values	No agreement (model substantially underpredicts measured values)
	Shallow-crack beam	Comparison of model toughness predictions with measured values	Marginal agreement (model underpredicts measured values)
	Thermally shocked cylinder	Comparison of model toughness predictions with measured values	(Analyses in progress)
Critical area/maximum principal stress contour model	CT specimens with 4T planform (thickness 1-, 2-, and 4 in.)	Determination of unique critical maximum principal stress at initiation	No calibration of model (no unique critical stress for three specimens)
MHM ductile initiation model	(No applications to existing measured data were performed in this study.)		

models having a highly refined crack-tip region. Correlations of measured and predicted toughness for the WP-1 and -2 series of wide-plate experiments based on the Q-stress parameter indicate that the RKR-model predictions fall substantially below the toughness values determined from analysis of the measured data. Fracture toughness predictions from the RKR model for the shallow-crack beam specimens were compared with measured toughness values for four values of critical stress. Again, the RKR model predictions were below measured values, but not to the extent observed in the wide-plate specimens. Additional details of these analyses are given in Sect. 2.3.

Inconsistencies between measured and predicted toughness for the wide-plate and shallow-crack beam experiments could be due to one or more factors. One possible difficulty may be the presence of three-dimensional (3-D) effects in the cheveroned wide-plate specimens that cannot be represented in the two-dimensional (2-D) plane strain models employed in the present analyses. It is unclear what modifications may be required to the J-Q methodology to represent these 3-D effects should they be present. Also, previous applications of the RKR prediction model to measure data have been confined to small-scale laboratory specimens. There may be difficulties with applications of this model to large-scale structures that have not yet been identified.

The correlations based on the stress contour method indicate that development of the methodology depends on establishing the existence of critical σ_{p1} stress values that correlate fracture toughness behavior over a range of transverse strain values. In analyses designed to validate and calibrate the model in the plane stress-to-plane strain domain, the stress contour method was applied to fracture toughness data for A 533 B steel previously generated by McCabe and Landes[22] for a study of thickness effects in the transition region. Analyses of 3-D finite-element models of compact specimens having a common planform of a 4T specimen and thickness ranging from 10.16 to 101.5 mm were performed in an attempt to estimate the critical σ_{p1} stress values in the negative transverse strain domain. The results were inconclusive because a critical σ_{p1} value common to three different thickness (of 1, 2, and 4 in.) of the specimens could not be established. However, note that the data set utilized in these analyses included only one cleavage initiation toughness value for each specimen thickness. Also, data for the specimen crack depth, material properties, and load vs load-line displacement were not sufficient to permit adequate modeling of the structural response of the test specimens.

The fracture models employed herein must be considered invalidated for predicting the effects of biaxial out-of-plane stress on fracture toughness, because applications to small- and large-specimen fracture data did not produce consistent results in predicting fracture behavior. Notwithstanding these general findings, toughness predictions implied by these models for out-of-plane strain effects were provided herein for reference purposes. Within the assumptions of the various models and analyses presented here, tensile transverse strains are predicted to produce a relatively small decrease in effective cleavage fracture toughness when compared to that of identical specimens loaded uniaxially. Applications of the RKR model (described in Sect. 2.3) and the stress contour methodology (described in a forthcoming report*) support a reduction of ~ 9% to 20% due to positive strains. The MKM model (described in a forthcoming report) predicted a minimal ductile toughness deviation. Analysis of circumferential cracks under PTS loading (described in Sect. 2.4) predicted a significant loss of constraint relative to corresponding plane strain configurations at higher J values. However, because the fracture methodologies considered in this study produced results that conflict with existing data considered relevant to this problem, these estimates cannot be applied with confidence in addressing questions that affect licensing and regulatory issues for RPVs.

Studies currently under way in the HSST Program are using methodologies described in this report to better understand the substantial differences in measured fracture toughness from the thermal-shock experiments and the shallow-crack beam tests. Although the outcome of this analysis is not yet known, it is clear that several different competing mechanisms affecting fracture toughness are present in these experiments. In addition to the biaxial stress field, other factors include shallow-crack effects, methods of structural loading, structural and crack geometries, and material properties. It is anticipated that the analytical studies of these data will provide significant information concerning relationships of some of these factors to fracture toughness. However, a *definitive* conclusion regarding biaxial effects still would require an understanding of the factor affecting toughness that is sufficient to permit an unambiguous separation of the individual contributions.

From these studies, it is apparent that testing under prototypical conditions is required (1) to determine the

*B. R. Bass et al., Martin Marietta Energy Systems, Inc., Oak Ridge Natl. Lab., "Constraint Effects on Fracture Toughness for Circumferentially Oriented Cracks in Reactor Pressure Vessels," NRC Report NUREG/CR-6008 (ORNL/TM-12131) in press.

magnitude of out-of-plane biaxial loading effects on fracture toughness and (2) to provide a basis for development of predictive models. The most desirable program would involve suitable test specimens and loading conditions for which the only variables are imposed biaxial loading components. This course of action is necessary to support a refined treatment of in-plane and out-of-plane constraint effects on crack initiation from shallow cracks under PTS loading conditions. As a consequence, criteria for a biaxial specimen are proposed in the next section that would form the basis of a testing program designed to close this gap between theoretical predictions and measured material behavior. Design studies are currently under way in the HSST Program to develop a set of geometric parameters, material and fracture properties, and loading conditions for the specimen satisfying these design criteria. Additional results of the design studies on the biaxial specimen will be presented in a future report from the HSST Program.

2.2.1 Design Criteria for Biaxial Specimen

The objective of the proposed biaxial fracture testing program is to obtain fracture toughness data under conditions of uniform far-field biaxial stresses that are selected (1) to produce prototypic crack-driving forces and out-of-plane stress and (2) to provide the simplest loading conditions for analysis. In addition, the experimental data from the proposed testing program will provide much needed data for the purpose of verifying and refining the fracture prediction methodologies that form the basis of the analytical predictions described in previous chapters. Tests would be conducted on uniaxially and biaxially loading specimens for comparative purposes.

Design of the biaxial test specimen is based on the following criteria:

1. Test specimen must remain elastic in the throat [i.e., linear-elastic fracture-mechanics (LEFM) conditions must apply].
2. Tests must only be influenced by out-of-plane biaxial loading (i.e., shallow-flaw effects, metallurgical gradients, etc., must not be prevalent).
3. Yield strength of material should be prototypic of irradiated conditions and achievable through heat treatment.
4. Test reference temperature T-RT_{NDT} must be prototypic of PTS temperatures (i.e., in lower transition region).
5. Flaw must be long to enhance crack initiation.
6. Biaxial loading ratio should be prototypic of that experienced by circumferential flaw under PTS loading (i.e., equibiaxial or 1:1 ratio).
7. Stress at failure should be prototypic of that in the vessel wall during PTS event.
8. Sufficient driving force should be present at the crack tip to reasonably ensure crack initiation at 27 MN load.

A preliminary set of parameters was selected to initiate the design process and to meet the above criteria. Criterion 2 may be satisfied by requiring a normalized crack depth a/W varying between 0.3 and 0.6 to eliminate any shallow-crack effects. Additionally, to eliminate influence of metallurgical gradients, test specimens should be cut such that the majority of the crack-tip region is located in the center region of the source plate. To satisfy criterion 3, all analyses presented here are based on a yield strength level of 620 MPa. This strength level is both prototypic of irradiated A 533 B grade B class 1 steel and is attainable in unirradiated A 533 B through heat treatment.

The material characterization of HSST Plate 13A (Ref. 21) was assumed for these studies. Examinations of integrated pressurized-thermal-shock (IPTS) studies[25] reveal that many crack initiations occur within a temperature range of $T - RT_{NDT}$ from –45 to 0°F. Testing at a temperature above RT_{NDT} would likely violate criterion 1. To ensure crack initiation and to satisfy criteria 4 and 8, the test temperature has been tentatively set at $T - RT_{NDT}$ = –45°C. The initiation fracture toughness at this temperature is taken to be 66 ksi$\sqrt{in}$. Further evidence that $T - RT_{NDT}$ = –45°C is a suitable temperature is provided by data from shallow-crack toughness tests.[2]

An essential test requirement is that the crack-driving force be sufficient to initiate the crack. However, scatter in the toughness data in the transition region often exceeds a factor of 2. In addition, some increase in toughness may be present in the biaxial specimens, because tension specimens generally are less constrained than bending specimens (CT or SENB specimens). The loss of constraint for tension loading should be minor if linear-elastic conditions are met. Also, the long flaw length dictated in criterion 5 provides more opportunities for crack initiation and should tend to bring about a lower initiation value. Therefore, a load ratio, K_J/K_{Ic} = 2.5 is assumed to be a requirement for these tests, satisfying part of criterion 8. This ratio implies that, at $T - RT_{NDT}$ from –45°F, K_I must exceed 165 ksi$\sqrt{in}$.

2.2.2 Far-Field Analyses of Biaxial Specimen

Design studies are currently under way to develop a set of geometric parameters, material and fracture properties, and loading conditions for the specimen satisfying the above design criteria. A candidate geometry for a biaxial specimen being analyzed in these studies is depicted in Fig. 2.3.

ORNL-DWG 92M-3408 ETD

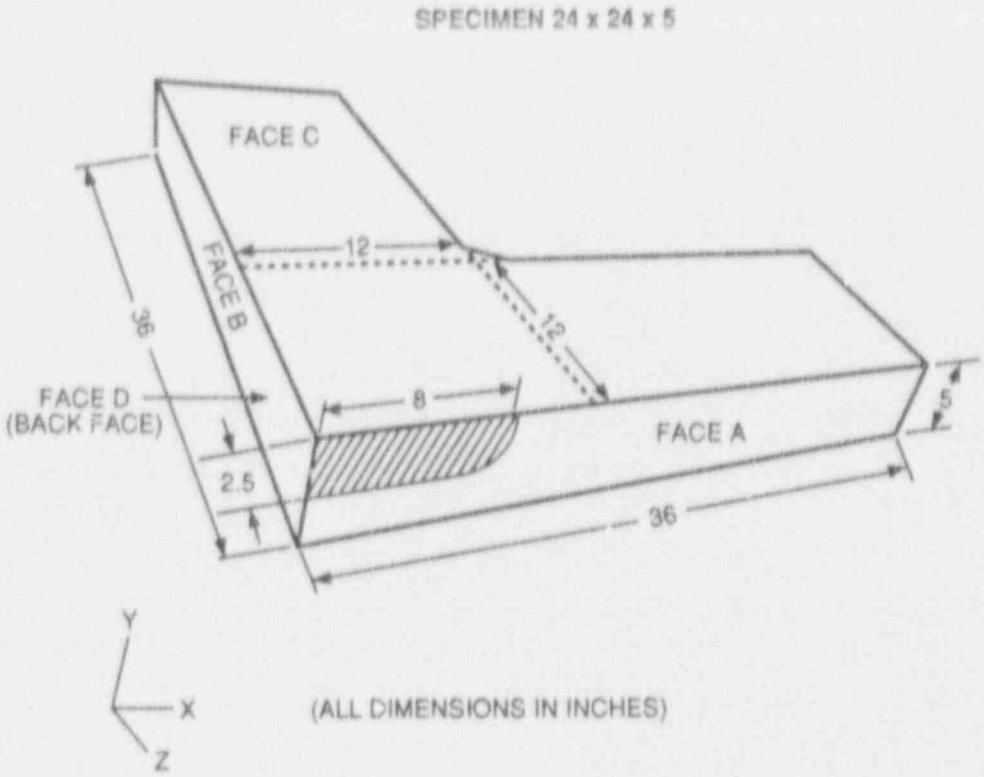

Figure 2.3 Schematic of candidate biaxial specimen for evaluating effects of out-of-plane stress on fracture toughness

2.2.2.1 Three-Dimensional Analyses

Figure 2.3 shows the dimensions of one-quarter of a test plate to which idealized tabs are attached for applying the biaxial loading component. A finite-element model employed in these analyses is shown in Fig. 2.4, which consists of 4194 nodes and 824 twenty-noded isoparametric brick element. Elastic and incremental elastic-plastic constitutive model representations of A 533 grade B class steel were taken from Ref. 8 material; properties were Young's Modulus E = 30,000 ksi, Poisson's ratio $\nu = 0.3$, yield stress $\sigma = 90$ ksi (additional explanation of the yield stress is necessary) and tangent modulus $E_T = 200$ ksi. Uniaxial and biaxial loads were applied to end surfaces of the pull-tabs. In the results presented here, these end surfaces were constrained in the normal direction using a generalized-plane strain (GPS) boundary conditions.

Depending upon the type of fixture used to apply the loads, other boundary conditions may be more appropriate for modeling the loading of the specimen. The loading was applied monotonically and incrementally to produce maximum resultant loads of 20 MN. At each load step iterations were performed to establish global equilibrium of the structure.

Shaded contours of the von Mises effective stress for the canoe-shaped crack geometry subjected to an applied load of 20 MN are shown in Figs. 2.5 and 2.6, respectively, for the B plane of Fig. 2.3. The small plastic zone contours around the crack tip corresponding to the initial yield stress of 90 ksi in shown for each loading condition. As expected, plastic zone development for the biaxial loading case is less than the uniaxial case; also, conditions of contained yielding exist at this load level.

2.2.2.2 Investigation of Clevis/Pin Far-Field Stress Distribution in Uncracked Biaxial Test Specimen

Two-dimensional plane stress analyses were performed to investigate the effects of a clevis/pin loading fixture on the far-field stress distribution in the biaxial specimen test plate. Figure 2.7 shows the preliminary design configuration of the biaxial test specimen. The test coupon itself is 24 × 24 × 5 in., and the total height and width of the

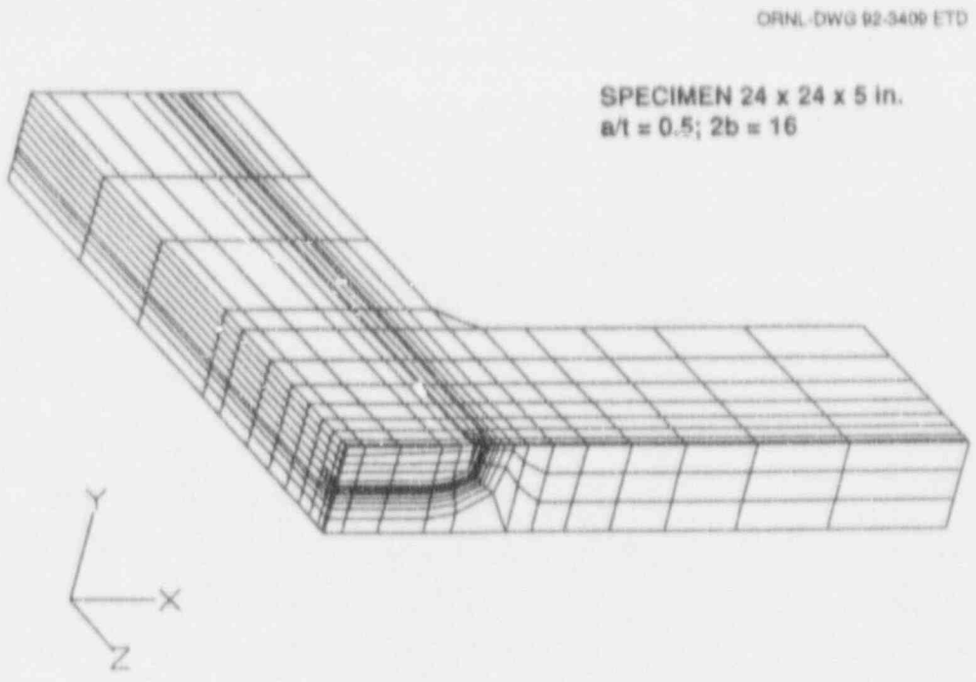

Figure 2.4 Finite-element model of biaxial specimen

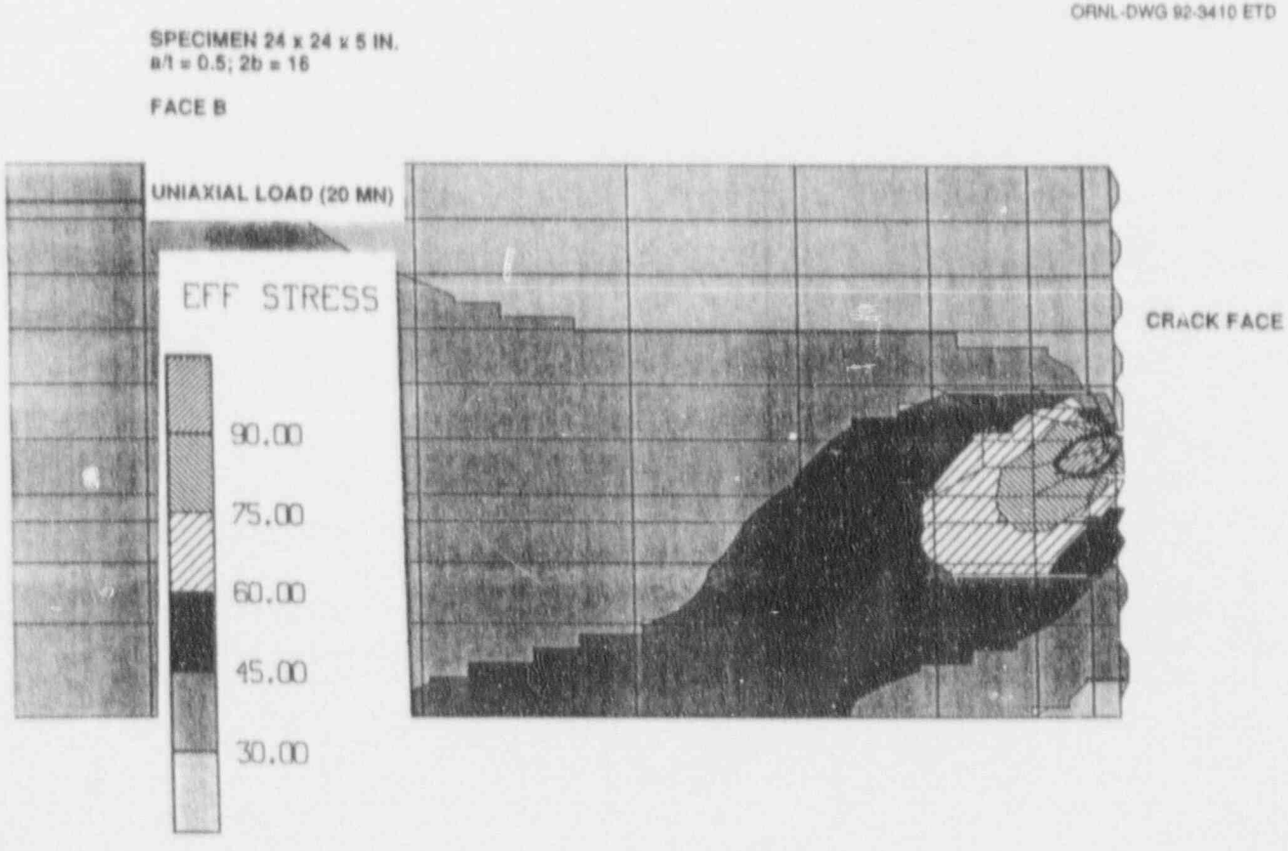

Figure 2.5 Contours of effective stress showing plastic zone size in Face B of specimen depicted in Fig. 2.3 for uniaxial loading of 20 MN

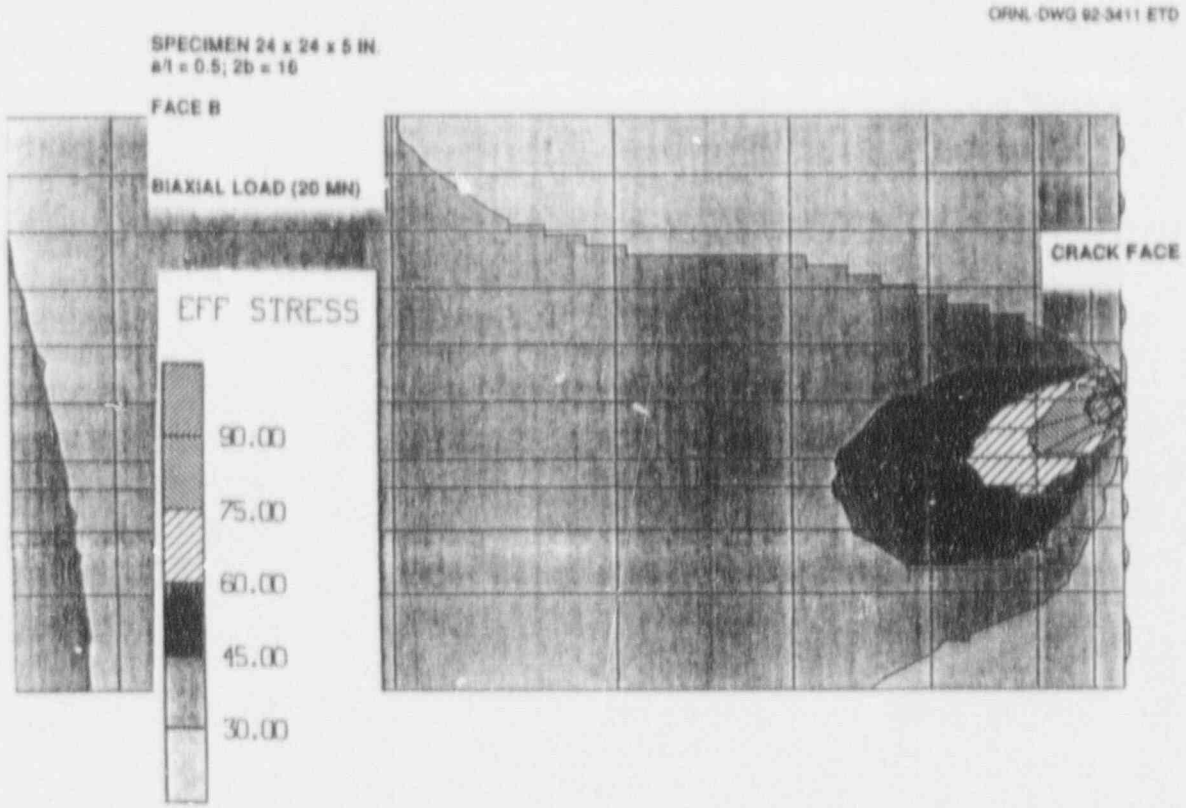

Figure 2.6 Contours of effective stress showing plastic zone size in Face B of specimen depicted in Fig. 2.3 for biaxial loading of 20 MN

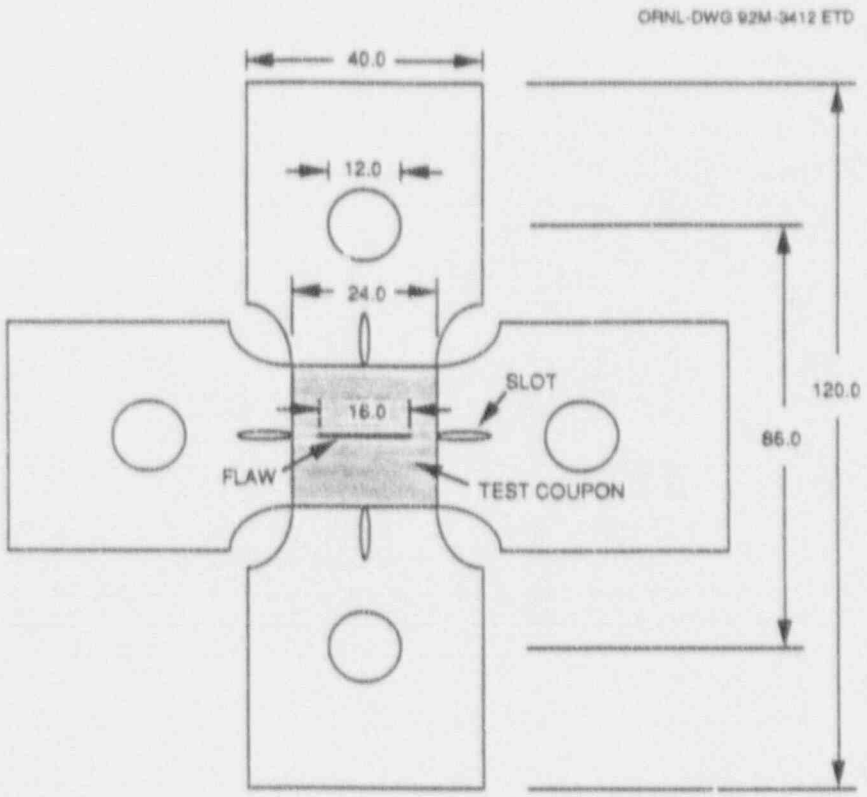

Figure 2.7 Preliminary design of biaxial test assembly showing plate specimen containing a surface crack, with attached pull tabs containing antiload diffusion slots

specimen including load arms is 120 in. Twelve-inch-diameter pins that are 86 in. apart are included in the present design. The loading arms are 40 in. wide. Slots adjacent to the test coupon (7 in., 20 in.) were simulated by releasing appropriate boundary conditions in the finite-element models. The slots help prevent stress redistribution into the arms and direct the load into the test coupon.

Elastic-plastic analyses were performed using a biaxial stress-strain representation (E = 300,000 ksi; v = 0.3; σ_o = 90 ksi; E_T = 200 ksi). Uniaxial loads to 20 MN were applied to each of two finite-element models; one having the load applied via a rigid pin or bolt (Fig. 2.8) while the other model represents a straight extension of the load arms with a uniform stress loading applied at the end (Fig 2.9). Eight-noded isoparametric quadrilateral elements were employed throughout the modeling. A crack-tip region was also modelled; however, the present studies assume that no crack exists (i.e., all nodes on the Z = 0 plane that are not in the slot have a Z-direction fixity).

Figures 2.10–2.11 show contour plots of the σ_{zz}-stress (ksi) for 7.0- and 20.0-in. slots, respectively, in the model loaded via rigid pin, Figs. 2.12–2.13 show the same plots for the model having straight arm extensions loaded with uniform stress (37.5 ksi) on the end. Additional plots of the σ_{zz}-stress in the test coupon at locations Z = 0.0 (crack plane), Z = 4.0, and Z = 8.0 are presented in Figs. 2.14–2.16.

The purpose of the present study was to determine whether the clevis/pin loading fixture would provide a stress field in an uncracked test coupon that was as uniform as that obtained if the loading were applied uniformly to the end of a test configuration having straight arm extensions. Figures 2.14–2.16 indicate that, for 7.0-in. slots, the clevis/pin arrangement does provide a stress field that is essentially identical to that given by a uniformly applied load. For 20.0-in. slots, the clevis/pin fixture gives a somewhat less uniform σ_{zz}-stress variation across the test coupon relative to a uniformly applied end load.

2.3 Application of RKR Fracture Model to Fracture Toughness Data
(D. K. M. Shum)

The RKR model was applied to fracture initiation toughness data generated in the HSST Program from large-scale wide-plate experiments[26–29] and shallow-crack beam tests.[4] The dual-parameter J-Q fracture characterization methodology described in Ref. 12 was employed in this analysis. The RKR model hypothesizes that cleavage fracture under Mode I conditions is governed by the attainment of a temperature-independent critical level of "opening-mode" stress over a minimum dimensional distance ahead of the crack front. The minimum dimensional distance necessary for cleavage fracture is often identified with the distance from the original crack front to cleavage initiation sites. Available data suggest that both the nature and location of the cleavage initiation sites vary considerably for nominal identical RPV-grade materials.[39,31] Consequently, a proper consideration of the micromechanics of fracture is an integral element in the application of this fracture model.

The HSST wide-plate experiments[21,23,24] utilized large plates with planar dimensions of 1 m × 1 m and thickness of 0.1 m or 0.15 m, to which long pull plates were welded to produce an assembly ~10 m in length. The plate assembly was tested as a SEN tension specimen containing a sharp crack having a normalized depth of a/W ≈ 0.2. The WP-1 series[21,23] of experiments utilized plate specimens fabricated from A 533 grade B class 1 steel (HSST Plate 13 A), while the WP-2 series[24,32] was based on a 2 1/4 Cr 1-Mo steel that had been specially heat treated to produce a low Charpy upper-shelf energy. Each side of the specimens was side-grooved to a depth equal to 12.5% of the specimen's thickness, and in most cases the crack front was further cut into a truncated chevron configuration. The beam specimens[2] were fabricated from the same source plate (HSST 13 A) as the WP-1 series of wide plates, with dimensions that varied from 500- to 610-mm length, 100-mm depth, and thickness of 50, 100, and 150 mm. Sharp cracks of depths 10 and 50 mm (a/W ≈ 0.1 and 0.5) were placed in the beams, which were then tested in three-point bend (TPB) loading at temperatures corresponding to the lower-shelf and the lower-transition region of the plate material.

Finite-element analyses of the wide-plate and shallow-crack beam experiments were performed using loading conditions measured in the test. Full-field finite-strain solutions based on plane strain assumptions were generated from models having a highly refined crack-tip region and a crack-tip profile with an initial root radius.

Specifically, detailed finite-strain, finite-element analyses were performed for

(1) seven specimens from the series-1 HSST wide-plate experiments; and
(2) six specimens from the production phase of the HSST shallow-flaw fracture toughness testing program: three of the specimens are deep-flaw specimens with nominal crack-depth to specimen-width ratio a/W = 0.5, while the remaining three are shallow-flaw specimens with nominal a/W = 0.1.

ORNL-DWG 92-3413 ETD

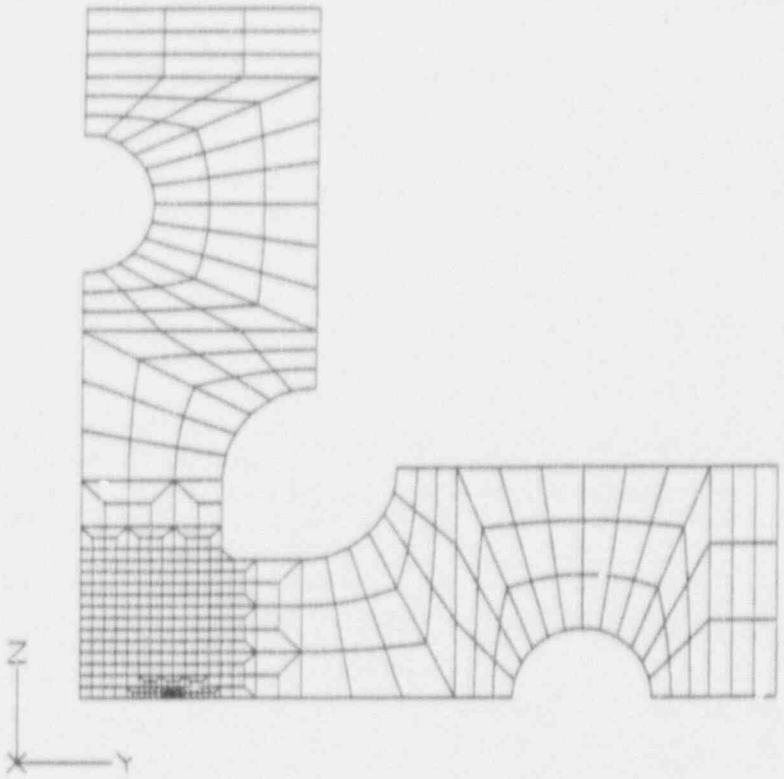

Figure 2.8 Finite-element model of biaxial test assembly depicted in Fig. 2.7

ORNL-DWG 92-3414 ETD

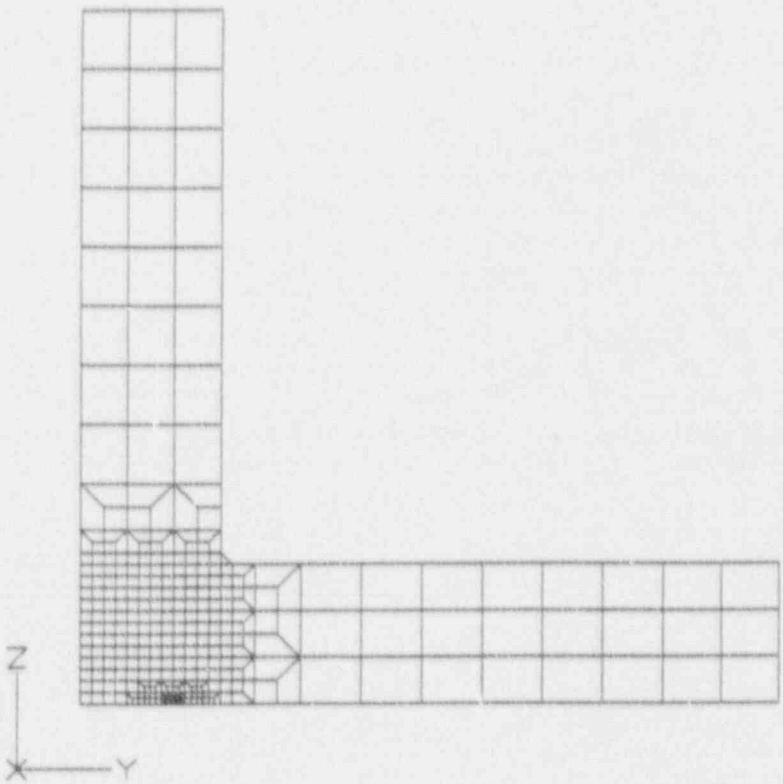

Figure 2.9 Finite-element model of biaxial test assembly for uniform end loading

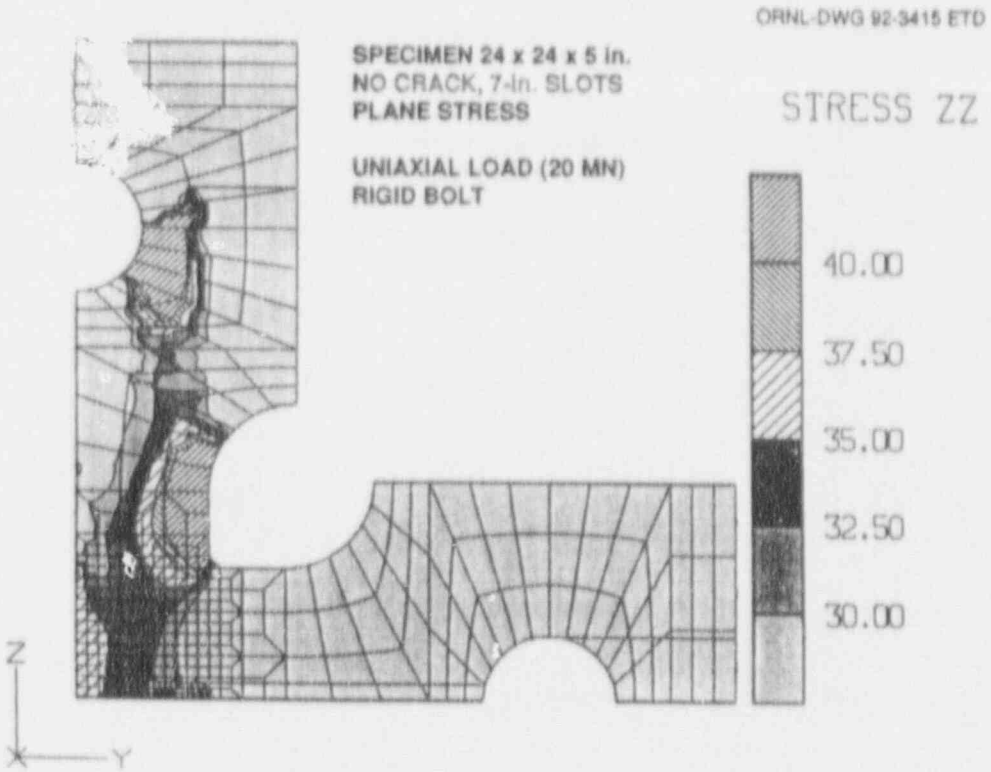

Figure 2.10 Opening-mode σ_{zz} stress contours for biaxial assembly model with 7-in. slots (see Fig. 2.3), subjected to uniaxial load of 20 MN

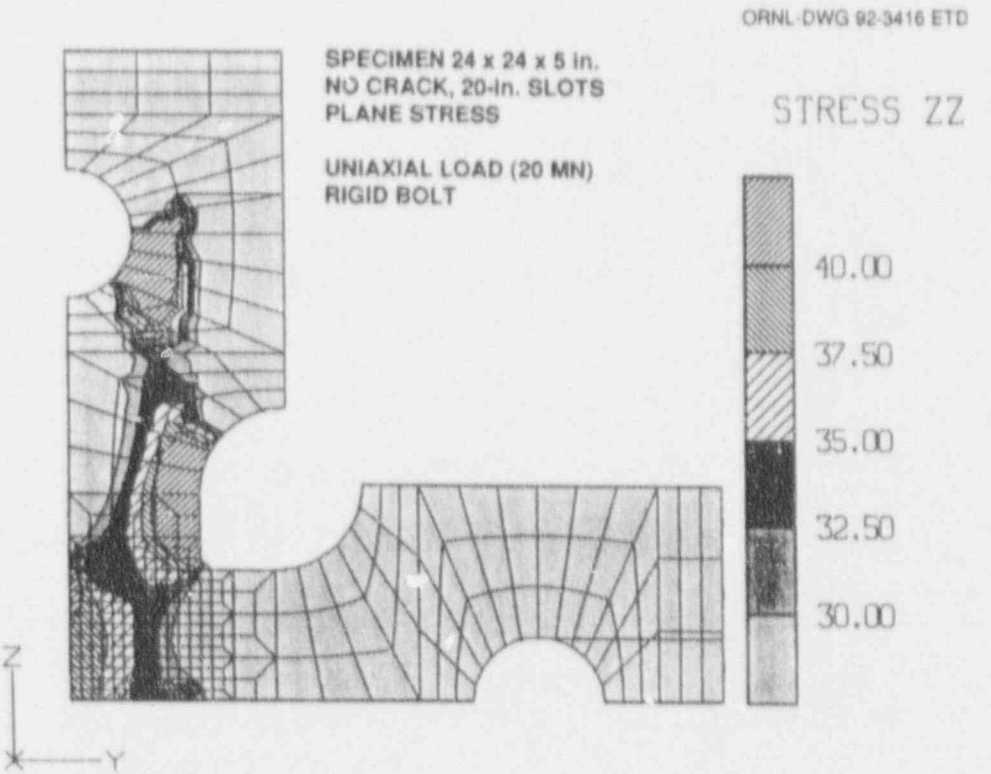

Figure 2.11 Opening-mode σ_{zz} stress contours for biaxial assembly model with 20-in. slots (see Fig. 2.3), subjected to uniaxial load of 20 MN

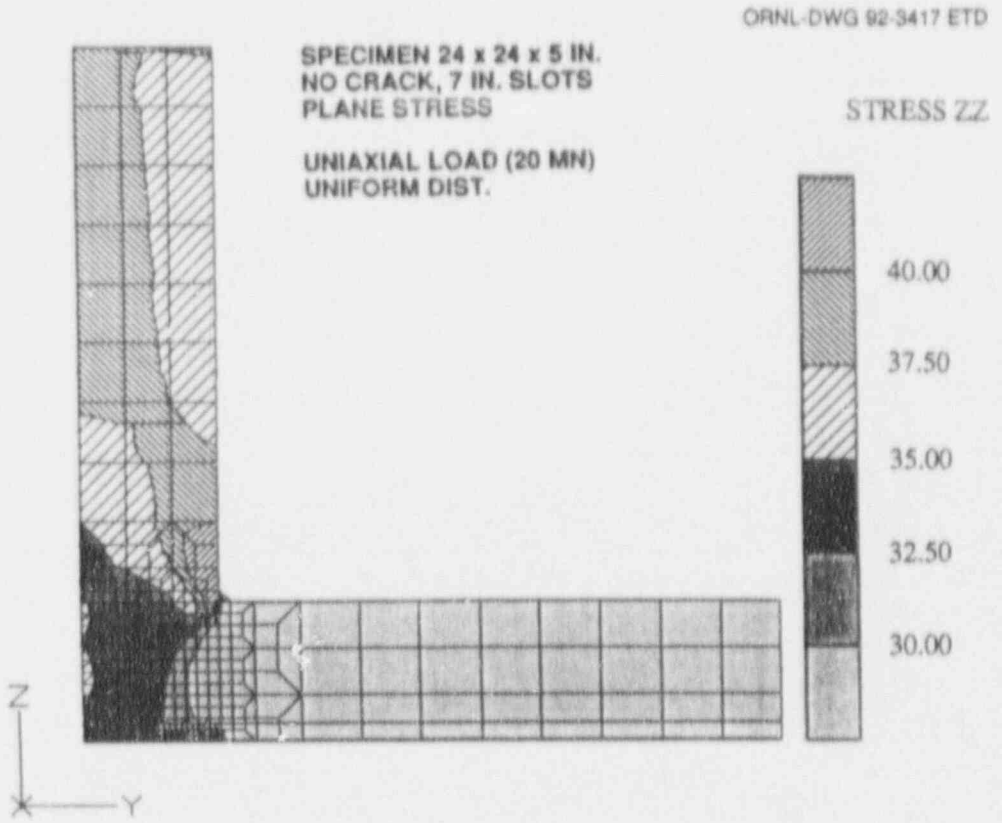

Figure 2.12 Opening-mode σ_{zz} stress contours for biaxial model with uniform loading (Fig. 2.9) and 7-in. slots, subjected to uniaxial load of 20 MN

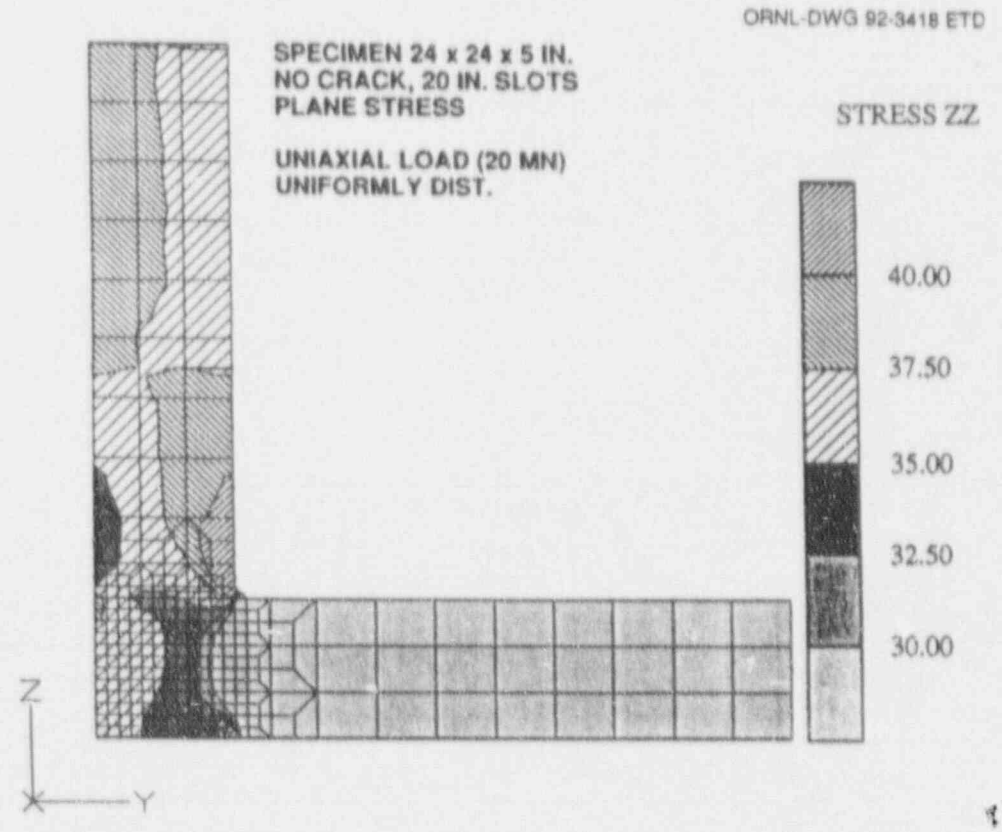

Figure 2.13 Opening-mode σ_{zz} stress contours for biaxial model with uniform loading (Fig. 2.9) and 20-in. slots, subjected to uniaxial load of 20 MN

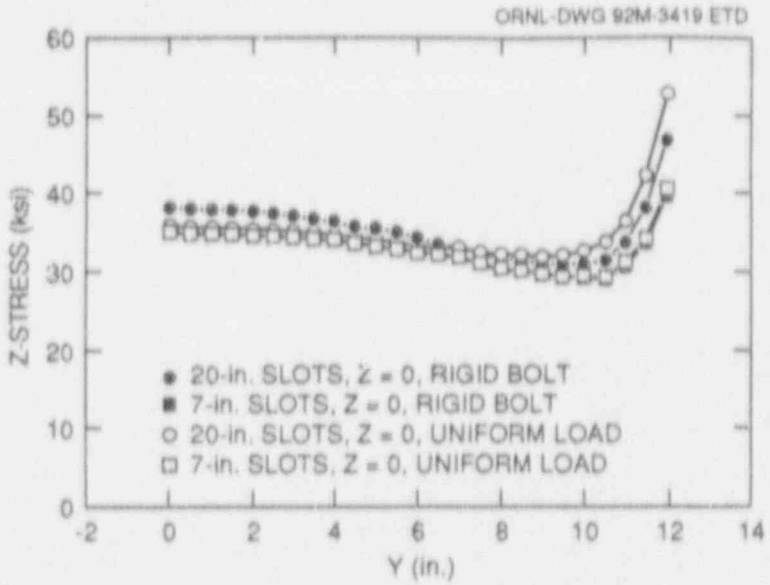

Figure 2.14 Variation of opening-mode σ_{zz} stress in crack plane defined by Z = 0.0 in.

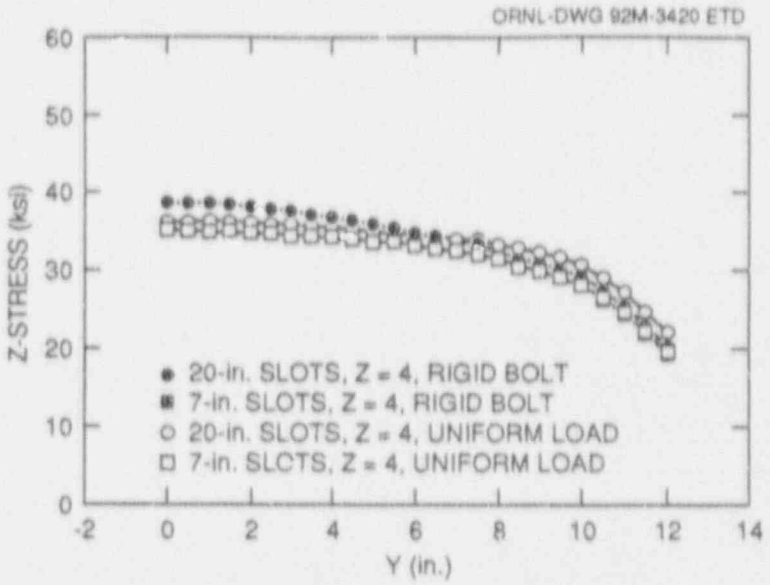

Figure 2.15 Variation of opening-mode σ_{zz} stress in plane defined by Z = 4.0 in.

2.3.1 J-Q Loci

Results from these analyses provide critical values of the J-Q parameters at cleavage initiation. Crack initiation for the WP-1 specimens occurred over a narrow temperature range that envelops the test temperature of the deep- and shallow-flaw beam specimens. Current understanding of the J-Q approach would suggest that the $J_c(Q)$ toughness loci from the WP-1 plates and the deep- and shallow-flaw specimens should be very similar. Instead, analysis results indicate a very different $J_c(Q)$ toughness locus for the WP-1 tests as compared to the deep- and shallow-flaw $J_c(Q)$ toughness loci presented in Fig. 2.17. Toughness values are expressed in terms of K, and they are further normalized by the plate 13-A small-specimen characterization toughness associated with the large-specimen crack-tip temperatures. In Fig. 2.17, the WP-1 results based on two sets of analysis assumptions are presented. The open-square symbols correspond to analysis results obtained from 2-D plane strain assumptions. The filled-square symbols correspond to

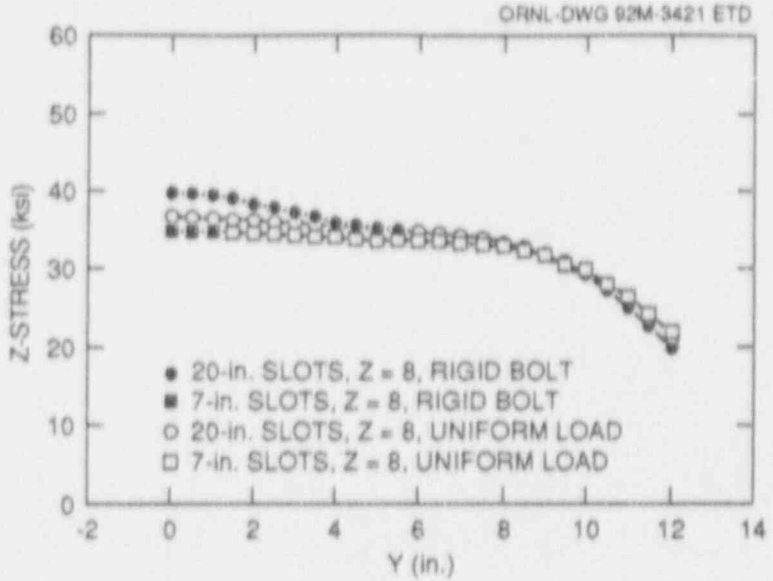

Figure 2.16 Variation of opening-mode σ_{zz} stress in plane defined by Z = 8.0 in.

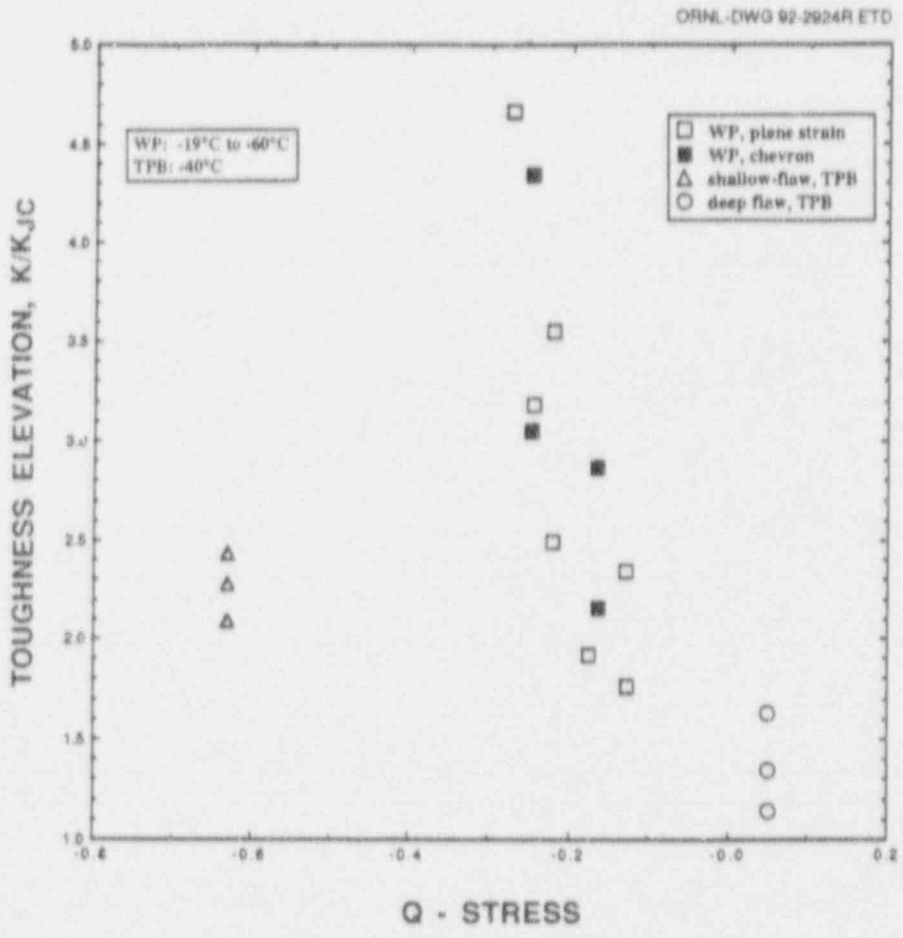

Figure 2.17 Comparison of shallow-crack and wide-plate crack-initiation toughness data showing different Q-stress dependence

analysis results based on an appropriate correction of the 2-D plane strain results to account for the inherently 3-D nature of the WP-1 crack fronts.

When the wide-plate and shallow-crack beam results are evaluated separately, each set of crack-initiation data appears to support a J-Q interpretation. That is, higher toughness values correspond to more negative Q-stresses, which imply a decrease in triaxiality and crack-tip constraint. Collectively, however, results in Fig. 2.17 indicate that the $J_c(Q)$ toughness locus for WP-1 is much steeper than that for the deep- and shallow-flaw specimens. The presence of 3-D effects in the WP-1 specimens is hypothesized to provide at least a partial explanation for the observed differences between the two $J_c(Q)$ toughness loci. (Tests were performed on three different thicknesses of the shallow-crack beams, and no 3-D effects were detected in the toughness data.)[2] Work is in progress to perform detailed 3-D analysis of the WP-1 and the shallow- and deep-flaw specimens to resolve this issue.

2.3.2 Possible 3-D Effects

The J-Q concept was originally formulated for the idealized conditions of plane strain constraint. Within the context of the (2-D) J-Q approach, departure of experimentally determined toughness values from the reference plane strain toughness is examined under the premise that the toughness deviation is due to "in-plane" effects on the crack-tip fields at the onset of crack initiation. The analysis results presented in this section are both consistent and accurate with respect to the (2-D) J-Q analysis assumption. The shallow-flaw and WP-1 specimens are, of course, 3-D in nature. In the case of the shallow-flaw specimens, for example, use of 2-D analysis conditions is thus premised upon the assumption that the thickness of the specimens (216 mm or 4 in.) is sufficient to maintain nearly plane strain constraint up to crack initiation.

The motivation for adopting a 3-D effects hypothesis to explain the observed differences between the deep- and shallow-flaw $J_c(Q)$ toughness locus and the WP-1 locus is newly obtained 2-D and 3-D finite-element analysis results for 2-in.- and 4-in.-thick 4T planform CT specimens. These specimens were examined as part of an investigation into the effects of specimen planform and thickness on fracture toughness.[33] These specimens were fabricated from unirradiated A 533 B material. These 4T-CT specimens are considered "high constraint" specimens because the crack-depth to specimen-width ratio a/W = 0.5, and the specimen thicknesses are substantial by conventional standards of small-specimen testing. When these 4T-CT specimens are examined in a 2-D plane strain context, the crack-tip fields up to crack initiation are essentially identical to the associated small-scale yielding (SSY) fields. In Fig. 2.18, the opening-mode stress component for the SSY and full-field solutions for the 4T-CT planform geometry up to crack initiation are indicated. The magnitude of K at the onset of crack initiation is reported to be 193 MPa•$\sqrt{m}$ for the 2-in.-thick specimen and 152 MPa•$\sqrt{m}$ for the 4-in.-thick specimen.

However, when these specimens are examined using 3-D finite-element models, the crack-tip fields for the 2-in.-thick 4T-CT specimen at normalized distances $r/(J/\sigma_o) > 5$ show progressive deviation from the SSY distributions up to the onset of crack initiation as indicated in Fig. 2.19. (The 3-D finite-element models for the 4T-CT specimens are not sufficiently refined to permit meaningful interpretation of the crack-tip fields and, hence, the Q-stress parameter, over normalized distances of $r/(J/\sigma_o) \leq 5$.) In Fig. 2.19, the midplane of the specimen corresponds to $\eta = 0$, while the free-surface of the specimen corresponds to $\eta = 1$. Results in Fig. 2.19 indicate that the deviation from SSY conditions occurred even at the midplane of the specimen. Corresponding results for the 4-in.-thick 4T-CT specimen are indicated in Fig. 2.20. The deviation from SSY conditions was less pronounced for the 4-in. than the 2-in. specimen.

The possibility of substantial 3-D effects on the crack-tip fields in the "high constraint" 2-in.- and 4-in.-thick 4T-CT specimen geometry is of concern here for the following reasons. The WP-1, deep- and shallow-flaw specimens are of nominally the same material as the 4T-CT specimen. These specimens either share or exceed the specimen thickness of the 4-in.-thick 4T-CT specimen. It is unclear whether the WP-1 and/or the deep- and shallow-flaw specimens might similarly experience 3-D effects on the crack-tip fields at the onset of crack initiation. Based on the 4T-CT results, the presence of substantial 3-D effects are expected to lower the magnitude of the Q-stress parameter as determined from a 2-D plane strain analysis. Furthermore, these 3-D effects are not expected to manifest themselves as an "effective" Q-stress contribution when the specimens are examined using a 2-D plane strain model.

2.3.3 RKR Model Prediction

Results from application of the RKR prediction model to the WP-1 series of experiments are given in Fig. 2.21. Correlations of measured and predicted toughness for the experiments based on the Q-stress parameter are expressed in terms of K-factors normalized by SSY values corresponding to initial conditions. For the WP-1 series

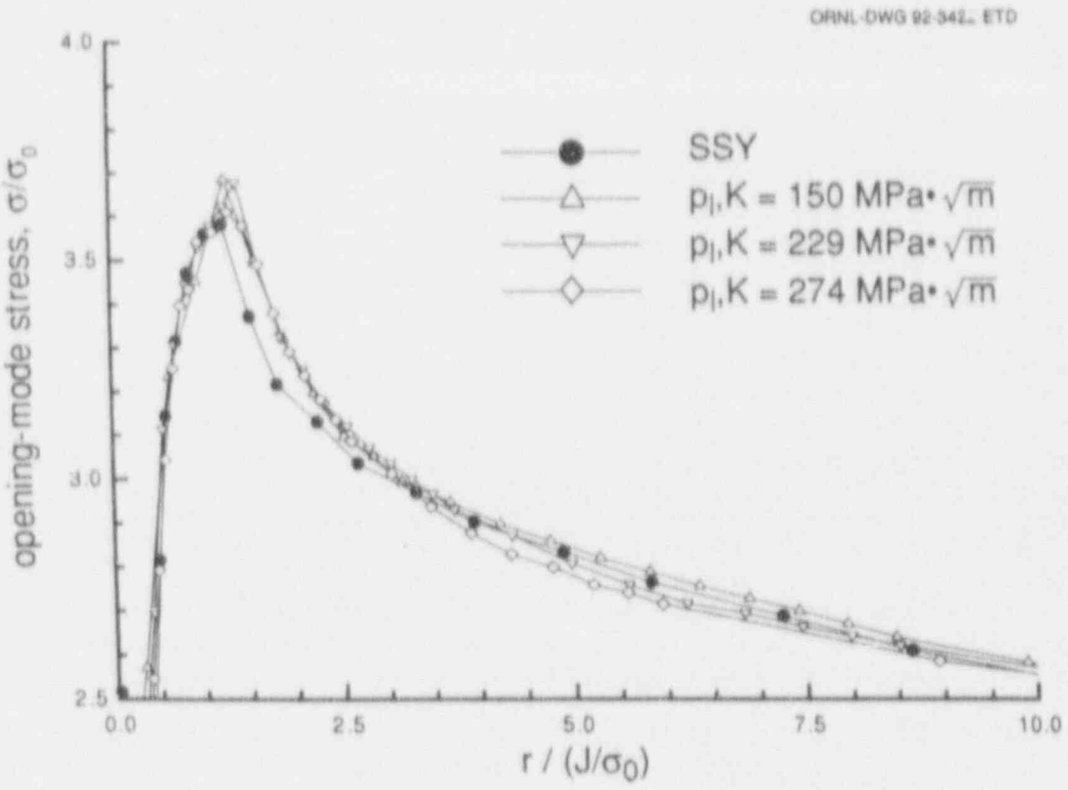

Figure 2.18 Opening-mode stress directly ahead of crack tip from 2-D plane strain solutions from a 4T-CT specimen at three load levels

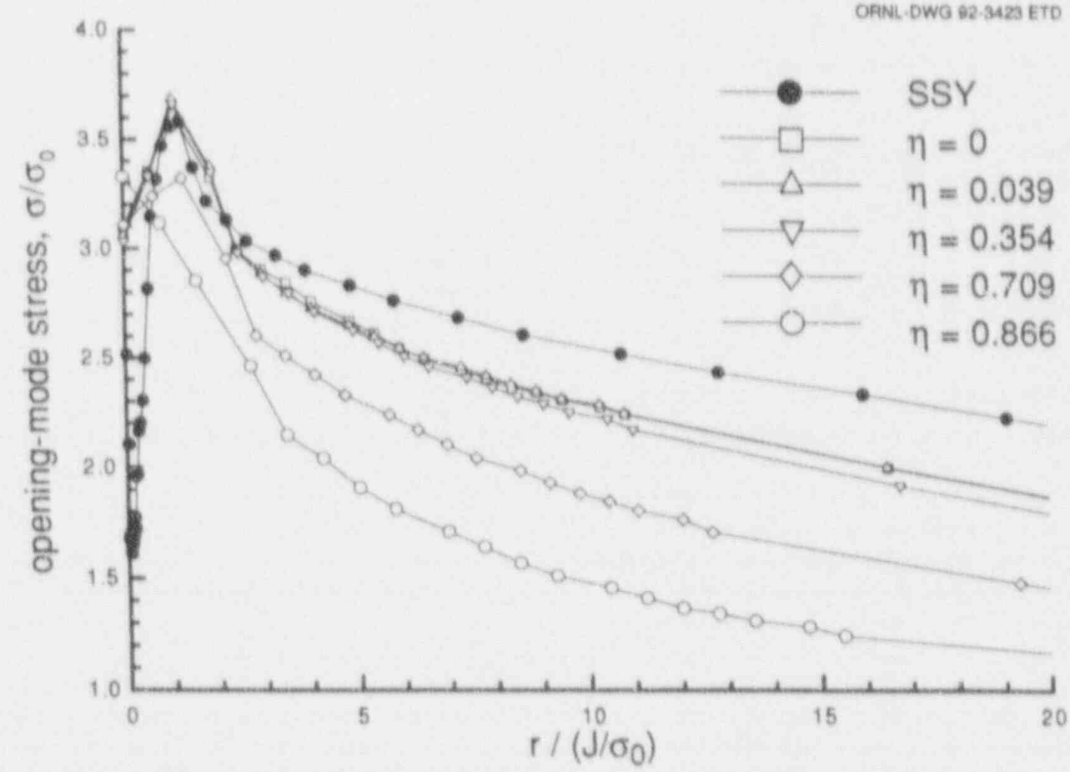

Figure 2.19 Opening-mode stress directly ahead of the crack tip obtained from 3-D finite-element model of 2-in.-thick 4T-CT specimen. The small-scale yielding solution is included for comparison

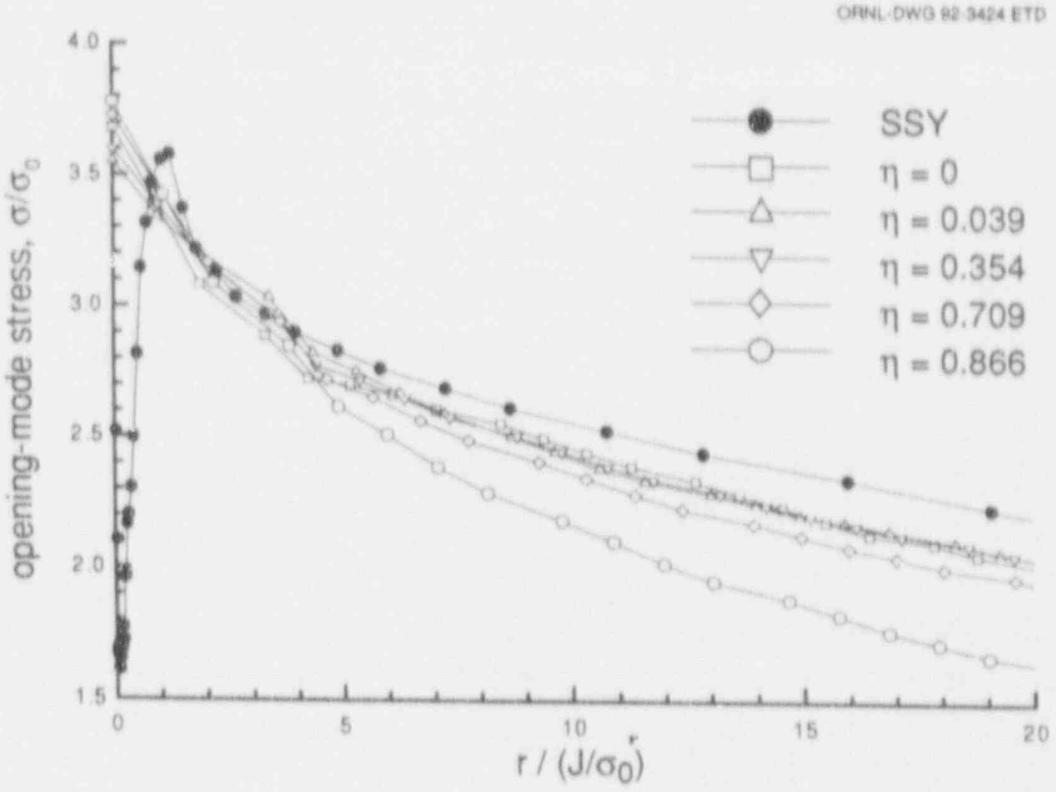

Figure 2.20 Opening-mode stresses directly ahead of crack tip at onset of crack initiation obtained from 3-D finite-element model of 4-in.-thick 4T-CT specimen. The small-scale yielding solution is included for comparison

(Fig. 2.21), toughness predictions are given for three values of the critical stress ratio, σ_c/σ_o = 2.2, 2.6, and 3.4, where σ_o = 465 MPa. Results for the WP-2 series of experiments will be given in a future report. For both series of experiments, the RKR model predictions fall substantially below the toughness values determined from the measured data. Fracture toughness predictions from the RKR model for the shallow-crack beam specimens are compared with measured toughness values in Fig. 2.22. Predictions are given for four values of the critical stress ratio, σ_c/σ_o = 2.7, 3.0, 3.4, and 4.0. Again, the RKR model predictions fall below measured values, but not to the extent indicated for the wide-plate specimens. Note that these results were obtained from a 2-D plane strain assumption, which was the basis for development of the J-Q methodology. It has not been established to what extent these differences are due to problems associated with representing 3-D stress states in the wide plates by a 2-D model or to problems with the RKR prediction model. Previous applications of the RKR prediction model to measure data have been confined to small-scale laboratory specimens. There may be difficulties with applications of the model to large-scale structures subjected to nominal 3-D stress states that have not yet been identified.

2.4 Crack-Tip Constraint For Circumferential Flaws

(C. W. Schwartz, University of Maryland)

Previous studies[12] have investigated the crack-tip constraint conditions for cleavage-dominated initiation of a circumferential flaw under pure mechanical loading conditions (i.e., where the axial and tangential loadings are induced solely by the vessel internal pressure). The results from this previous work suggested that crack-tip constraint is lower–and thus the "apparent" fracture toughness in the lower transition region is higher–for the circumferential flaw configuration under a combined internal pressure and axial loading than for the corresponding plane strain condition under axial loading only. This effect appears to be due more to in-plane than out-of-plane effects. Specifically, it is largely a consequence of the more negative in-plane stress biaxiality resulting from the radial loading applied to the inner surface of the vessel.

The comparatively simple pure mechanical loading condition considered in this earlier work represents an upper bound for the apparent toughness elevation caused by the

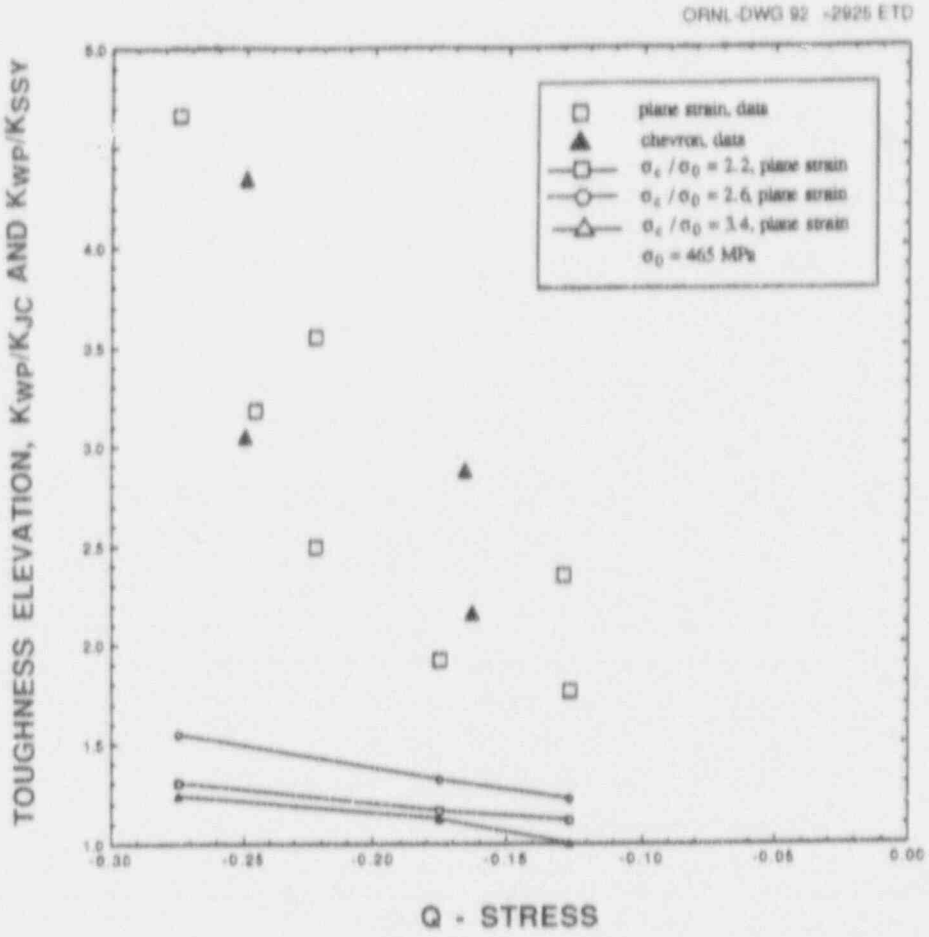

Figure 2.21 Correlation of measured and predicted toughness for WP-1 wide-plate series based on Q-stress parameter

radial compressive stresses. In a PTS transient during a loss-of-coolant accident, the radial compressive stress will likely become less important in comparison with the thermally induced crack-driving loads. Consequently, a second series of analyses has been performed to investigate crack-tip constraint for circumferential flaws under loading conditions that better represent actual reactor vessel conditions.

2.4.1 Analysis Model

The prototype reactor vessel considered in these analyses is a cylinder having an internal radius r_i of 2171.7 mm (85.5 in.) and a wall thickness W of 215.9 mm (8.5 in.). A continuous circumferential flaw with a crack length, a, equal to 53.98 mm in the radial direction (a/W = 0.25) was postulated around the inner beltline of the vessel. Because crack initiation is the focus of this study, crack extension was not considered in any of the analyses.

The finite-element model of the assumed cross-sectional geometry as generated using the PATRAN[34] pre-/post-processing system is illustrated in Fig. 2.23. Only the upper symmetric half of the vessel was considered. The mesh consists of 1727 nodes and 536 8-node reduced integration (2 × 2) isoparametric elements. The finite-element model is truncated above the crack plane at a height equal to three times the wall thickness (Fig. 2.23), and the axial loads were applied as uniform normal tractions along this boundary. No rotational restraint was imposed along the upper boundary of the model. Eight fans of elements converge on the crack tip (Fig. 2.24); the 17 initially coincident crack-tip nodes are free to deform independently during the analysis. The discretization is sufficiently fine to permit adequate resolution of the stress and strains within distances on the order of five CTODs from the crack tip; the radial dimension of the elements at the crack tip is ~ 0.02 mm (r/W = 0.000124). All finite-element calculations were performed using the ABAQUS analysis code.[35]

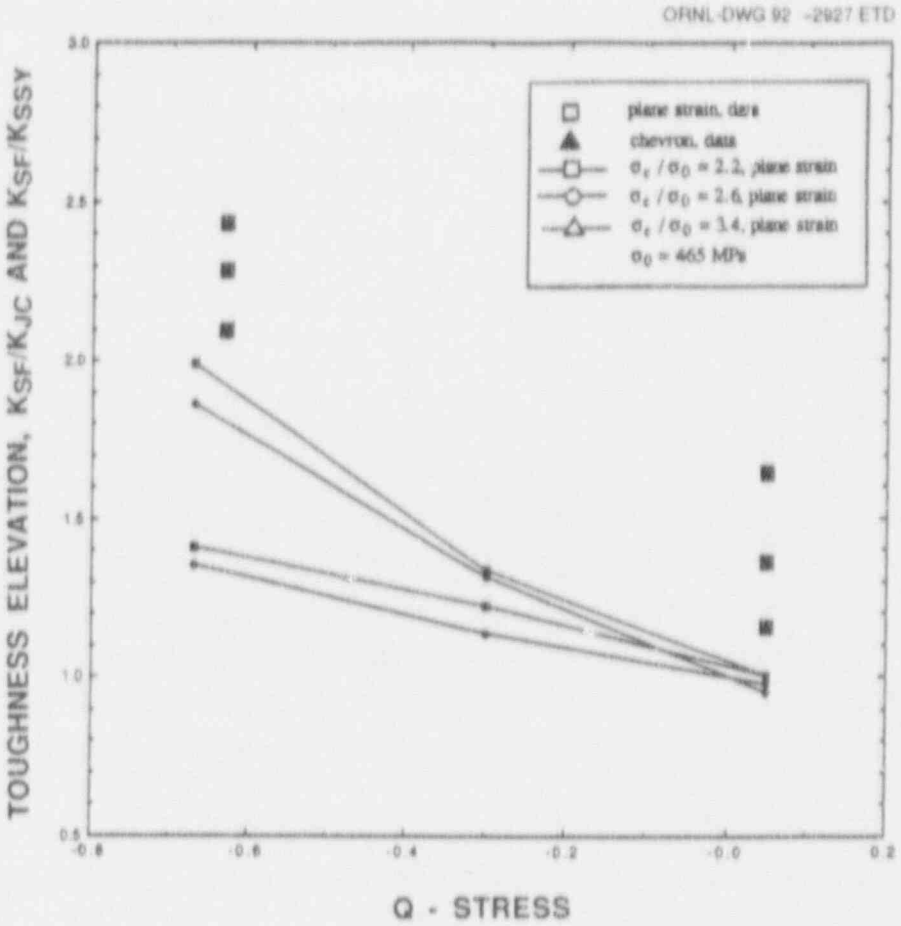

Figure 2.22 Correlation of measured and predicted toughness for shallow-crack beam specimens based on Q-stress parameter

The material stress-strain behavior was modeled using a normalized Ramberg-Osgood deformation plasticity constitutive model:

$$\varepsilon/\varepsilon_0 = \sigma/\sigma_0 + \alpha\,(\sigma/\sigma_0)^n \quad . \qquad (2.1)$$

The following values of the material constants were used in all analyses: initial tangent elastic modulus $E = \sigma_0/\sigma_0 = 300$; Poisson's ratio $\nu = 0.3$; $\sigma_0 = 1$; $\alpha = 1$; and $n = 10$. As shown in Fig. 2.25 the agreement between the normalized Ramberg-Osgood uniaxial stress-strain curve and the corresponding stress-strain curve for A 533 B steel at room temperature[71] is reasonably good. The largest discrepancies in the curves occur before and near the yield point, where the Ramberg-Osgood model cannot capture the relatively abrupt yield of A 533 B.

The Rancho Seco PTS transient[15] was used to determine the maximum loading conditions appropriate to an actual reactor vessel under a loss-of-coolant condition. The peak pressure during this transient approached 15 MPa, and the peak temperature differential across the vessel wall approached 180°C. Both peaks occurred roughly simultaneously at ~50 to 60 min into the transient.

The analysis of a typical reactor vessel under a particular PTS transient was not the objective of this study. Rather, the Rancho Seco transient was employed as an "envelope" defining the outer limits of the radial and out-of-plane loading for an actual pressure vessel. To analyze the crack-tip conditions at various loading combinations within this envelope, the axisymmetric reactor vessel geometry was modeled as a 2-D GPS problem. This permits independent control of the axial loading, the in-plane radial compressive stresses induced by the vessel internal pressure, and the out-of-plane tangential strains induced by the thermal shock loading. This, in turn, permits independent evaluation of the influence of each loading component on the crack-tip constraint.

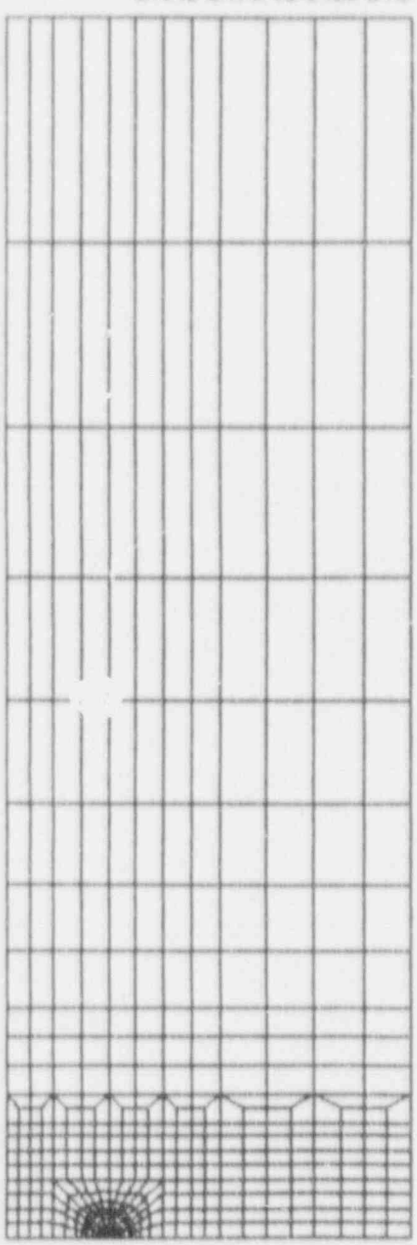

Figure 2.23 Finite-element mesh for analyses of circumferential crack subjected to PTS loading

Combinations of three internal pressure levels and three out-of-plane strain conditions were analyzed in this study. Table 2.3 summarizes the out-of-plane strain ratios $\varepsilon_z/\varepsilon_o$ corresponding to each combination. The internal pressure ratio p_i/σ_o ranged from 0, which represents a pure axial loading condition, to 0.035, which is approximately the peak internal pressure in the Rancho Seco PTS transient. An intermediate value of $p_i/\sigma_o = 0.020$ was also analyzed. The three out-of-plane strain conditions correspond to pure plane strain ($\varepsilon_z/\varepsilon_o = 0$, row 1 in Table 2.3), GPS with the prescribed $\varepsilon_z/\varepsilon_o$ dictated by the mechanical loads only (i.e., $\Delta T = 0$, row 2 in Table 2.3), and GPS with the prescribed $\varepsilon_z/\varepsilon_o$ dictated by the combined mechanical and thermal shock loads ($\Delta T = 180°C$, row 3 in Table 2.3). For the mechanical loads, the out-of-plane strain was approximated assuming an out-of-plane stress σ_z equal to ten times the internal pressure (based on the ratio of the vessel radius to the wall thickness) and $\sigma_z = \sigma_z/E$; this slightly overestimates the out-of-plane strain because it neglects the circumferential contraction induced by the tensile axial loads. For the thermal-shock loads, the out-of-plane strain was approximated assuming that the full ΔT occurs at the crack tip and that the rest of the vessel remains at its initial elevated temperature. The out-of-plane strain is then given as $\varepsilon_z = \alpha_T \Delta T$, in which α_T, the coefficient of thermal expansion, is equal to 11×10^{-6}/°C (typical for A 533 B steel) and $\Delta T = 180°C$. This approximation overestimates the thermally induced out-of-plane strain because it neglects the cooling and consequent contraction of the vessel at locations remote from the crack tip.

In the GPS idealization employed for these analyses, it is impossible to simulate the variation of the pressure-induced radial compressive stress across the vessel wall. Instead, a uniform radial compressive stress with a magnitude equal to the vessel internal pressure is applied. This pressure is also applied to the crack faces in the mode.

In all the analyses of this study, the full radial pressure and out-of-plane strain loading components were applied during the initial load step and then held constant throughout the analysis. The remote axial tractions p_a were applied incrementally to a maximum value $p_a/\sigma_o = 0.6$. This maximum loading was well short of full plasticity of the vessel wall.

The analysis loading conditions produced maximum $J/(a\sigma_o)$ values on the order of 0.015. The lower- and upper-shelf toughnesses of A 533 B steel are on the order of $J/(a\sigma_o) = 0.0005$ and 0.01 ($K_J \cong 50$ and 220 MPa$\cdot\sqrt{m}$), respectively. The actual loading conditions given by the Rancho Seco PTS transient correspond to $J/(a\sigma_o) \cong 0.003$, based on the approximate solution by Chen, Paris, and Tada;[36] this, in turn, corresponds to $p_a/\sigma_o \cong 0.4$ in the finite-element analyses.

A small strain formulation was employed in all of the finite-element calculations for several reasons. First, it is an adequate formulation for many of the phenomena being studied in this analysis series. Although it is true that the small strain formulation cannot correctly model the stress

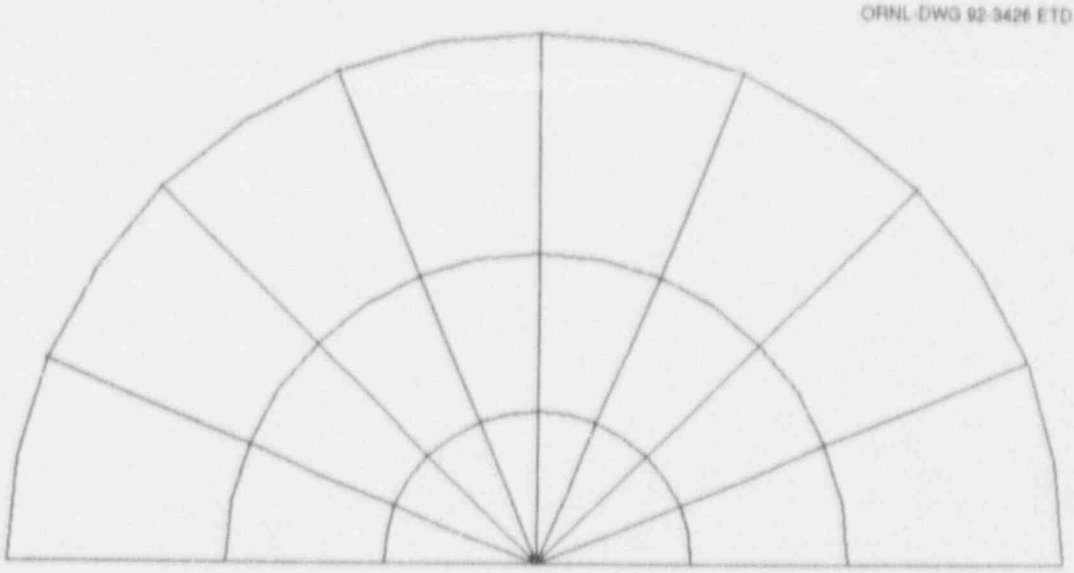

Figure 2.24 Detail of crack-tip region for finite-element model depicted in Fig. 2.23

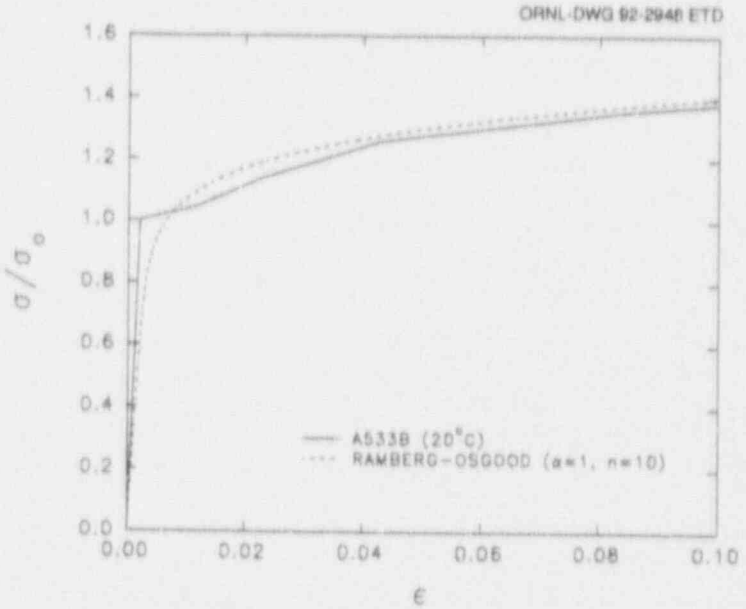

Figure 2.25 Stress-strain relations for Ramberg-Osgood material ($\alpha = 1$, $n = 10$, $E = \sigma_0/\varepsilon_0 = 300$) and for A 533 B steel at room temperature ($E = 207$ GPa, $\nu = 0.3$, $\sigma_y = 425$ MPa)

and strain fields and crack-tip blunting in the very high strain region immediately surrounding the crack tip, the stress and strain fields predicted by small strain and large strain formulations are similar at distances greater than approximately three CTODs from the crack tip under plane strain conditions.[37,38] This is sufficient for the purposes of the present study. Second, the small strain formulation is consistent with the asymptotic plasticity solutions for the crack-tip stress fields.[39,40] As will be shown later, these asymptotic plasticity solutions provide a reference condition for evaluation of crack-tip constraint effects. Finally, the small strain formulation eliminates the convergence problems associated with large strain analyses of highly refined meshes loaded over large ranges.

J-integral values were computed using the virtual crack extension algorithm as implemented in ABAQUS.[35,41]

Table 2.3. Out-of-plane tensile strain levels $\varepsilon_z/\varepsilon_o$ for loading combinations analyzed

ΔT (°C)	p_i/σ_o		
	0.0	0.020	0.035
0	0.00	0.00	0.00
0		0.20	0.35
180		0.79	0.94

Ten contours were evaluated at each load step to establish path independence for the J-integral value.

2.4.2 Results

The variation of $J/(a\sigma_o)$ with axial load level p_a/σ_o computed in all of the analyses are summarized in Fig. 2.26. The J vs load relations are roughly similar for all loading configurations.

This section will focus on the analysis results as interpreted in terms of the Q-stress approach of O'Dowd and Shih:[12]

$$\sigma_{ij}/\sigma_o \equiv [J/(\alpha\varepsilon_o\sigma_o I_n r)]^{1/(n+1)}\tilde{\sigma}_{ij}(\theta) + Q[r/(J/\sigma_o)]^q \tilde{\sigma}_{ij}(\theta) \qquad (2.2)$$

Equation (2.2) represents a two parameter expansion of the near-tip elastic-plastic stress fields in a power law hardening material. The first term represents the usual HRR singularity[38,39] with amplitude equal to J. The second order term has the dimensionless parameter Q as its amplitude; Q captures all constraint influences on the in-plane near-tip stress fields, regardless of whether these influences are the results of in-plane or out-of-plane factors. The functions $\tilde{\sigma}_{ij}(\theta)$ and $\tilde{\sigma}_{ij}(\theta)$ represent the angular variation of the stress fields and are expected to depend also upon the material hardening; the $\tilde{\sigma}_{ij}(\theta)$ functions are normalized such that $\tilde{\sigma}_\theta$ equals 1 at $\theta = 0$. Note that the second order expansion in Eq. (2.2) assumes a small strain formulation, as it is based upon the HRR solution. The material parameters α, n, ε_o, and σ_o have been defined previously Eq. (2.1), and values for I_n and $\tilde{\sigma}_{ij}(\theta)$ are tabulated graphically in Hutchinson[39] and Kanninen and Popelar.[26] For the material parameters used in this study, $I_n = 4.58$, $\tilde{\sigma}_{xx}(\theta) = 2.52$, and $\tilde{\sigma}_{yy}(\theta) = 3.53$.

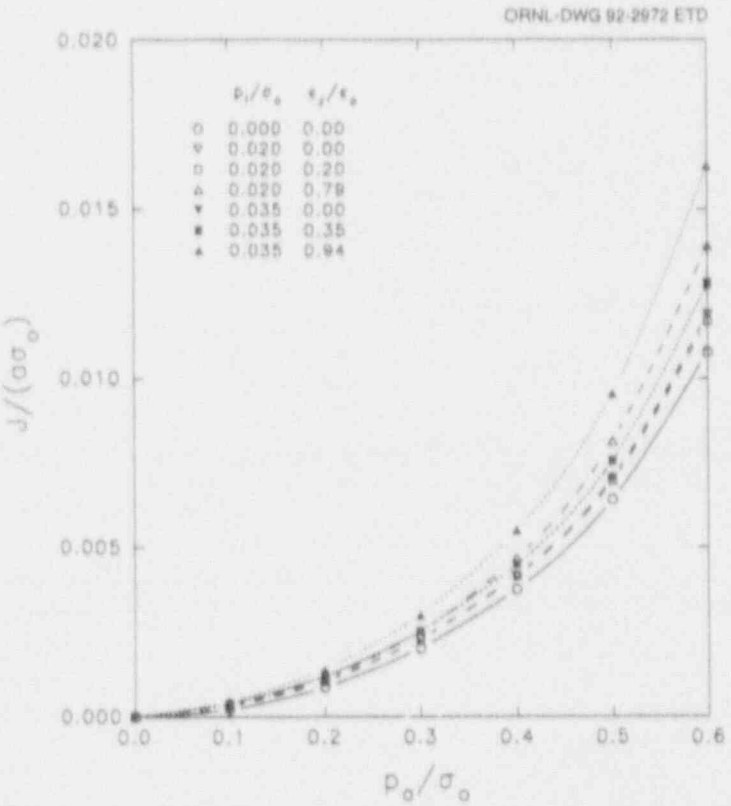

Figure 2.26 $J/(a\sigma_o)$ vs normalized axial load level p_i/σ_o for all analyses

The second-order fields are extracted by subtracting the HRR solution from numerical solution for the crack-tip stresses in the finite geometry configuration. The parameters Q and q in Eq. (2.3) can then be obtained from a nonlinear regression analysis of the second-order crack opening stresses $(\sigma_{yy}/\sigma_o)_2$ along the crack plane ahead of the crack tip:

$$\ln(\sigma_{yy}/\sigma_o)_2 = \ln(Q) + q \ln [r/(J/\sigma_o)] \qquad (2.3)$$

O'Dowd and Shih[12] concluded that the annulus in which the two-term expansion in Eq. (2.2) provides a reasonable estimate of the crack-tip stress is limited to ~20% of the plastic zone size. Using the standard Irwin estimate for the plastic zone radius for plane strain conditions:

$$r_p = (K_I/\sigma_o)^2/(3\pi\sigma_o^2) \ , \qquad (2.4)$$

the range of validity of Eqs. (2.2) and (2.3) is thus estimated as $r/(J/\sigma_o) \leq 5$ ($r \leq 4.4$ mm, $r/a \leq 0.082$). The regressions of Eq. (2.3) therefore included only those computed stress points at distances along the crack plane within this limit. The first four nodal points ahead of the crack tip ($r \leq 0.04$ mm, $r/a \leq 0.082$) were also excluded from the regressions because of lack of fidelity of the numerical solution in this region. The fit of the computed regressions was very good in all cases, with R^2 values approaching 0.99 at low J values and decreasing slightly to a minimum $R^2 \cong 0.80$ at the highest J values.

The variation of Q with load level $J/(a\sigma_o)$ is shown in Fig. 2.27. For both p_i/σ_o values analyzed, Q starts at a value of about –0.2 at low load levels and decreases with increasing load, as expected. A value of Q = 0 corresponds to complete agreement with the HRR solution (i.e., ideal plane strain constraint). The negative Q values computed from the present analyses are caused by the moderate depth of the flaw (e.g., see Al-Ani and Hancock[27]) the radial compressive loading (Leevers and Radon,[28])the out-of-plane tensile strains, and the increasing plasticity at higher load levels.

The variation of q with load level is shown in Fig. 2.28. For both internal pressure values analyzed, q starts at a moderate to a value of ~0.6 at low load levels and decreases asymptotically to a value of ~0.1 at higher load values. This contradicts the findings of O'Dowd and Shih, who concluded that the variation of the second-order stress fields with radial distance ahead of the crack tip was very weak (i.e., $|q| << 1$). However, O'Dowd and Shih extracted their second-order stress fields from large strain finite-element calculations; it is possible that the slight differences in the computed stress distributions from the small vs large strain formulations over the range $1.5 \leq r/(J/\sigma_o) \leq 5$ may be concentrated in slight changes in the radial variation of the stresses. Whatever the cause, the influence of constraint on both Q and q, if generally true, reduces the effectiveness of the J-Q approach as a two-parameter fracture toughness criterion.

The dependence of Q and q on the internal radial pressure load p_i/σ_o under pure plane strain conditions is shown in Figs. 2.29 and 2.30, respectively. In these figures, the curves for the axial load level $p_a/\sigma_o = 0.4$ best represent the vessel loading at the peak of the Rancho Seco PTS transient; the curves for $p_a/\sigma_o = 0.2$ and 0.6 are provided for comparison purposes at lower and higher J values, respectively. Both Q and q decrease slightly with increasing radial compressive load, as expected, but the dependence is very slight. The reduction in Q caused by the radial compressive stresses in the present analyses is much less than that observed in our earlier study.[42] One reason for this is that the ratio of p_i/p_a in the earlier analysis series was up to 6 times larger than in the present computations.

The dependence of Q and q on the out-of-plane tensile strain $\varepsilon_z/\varepsilon_o$ is shown in Figs. 2.31 and 2.32, respectively. The curve for $p_i/\sigma_o = 0.035$ and $p_i/\sigma_o = 0.4$ best represents the vessel loading at the peak of the Rancho Seco PTS transient. The decreases in Q and q with increasing out-of-plane strain is negligibly small. This observed lack of influence of out-of-plane strain on constraint is consistent with the results from our earlier study and with the results from other researchers (Parks,[29] Hancock,* Wang,[43] and Shum et al.[10]).

2.4.3 Conclusions

The analyses in this study have quantified the crack-tip constraint for a continuous inner circumferential flaw in a pressure vessel under loadings consistent with actual PTS transients. The primary focus of this study is cleavage initiation in the lower transition region of the fracture toughness vs temperature curve.

In all cases, the crack-tip constraint as quantified by the Q-stress approach is less than that under ideal plane strain conditions. For the given crack length a/W = 0.25 considered in this study, load level $J/(a\sigma_o)$ had the largest effect on constraint, with increasing load levels producing lower constraint (i.e., more negative Q values). The internal

*J. W. Hancock, personal communication, 1991.

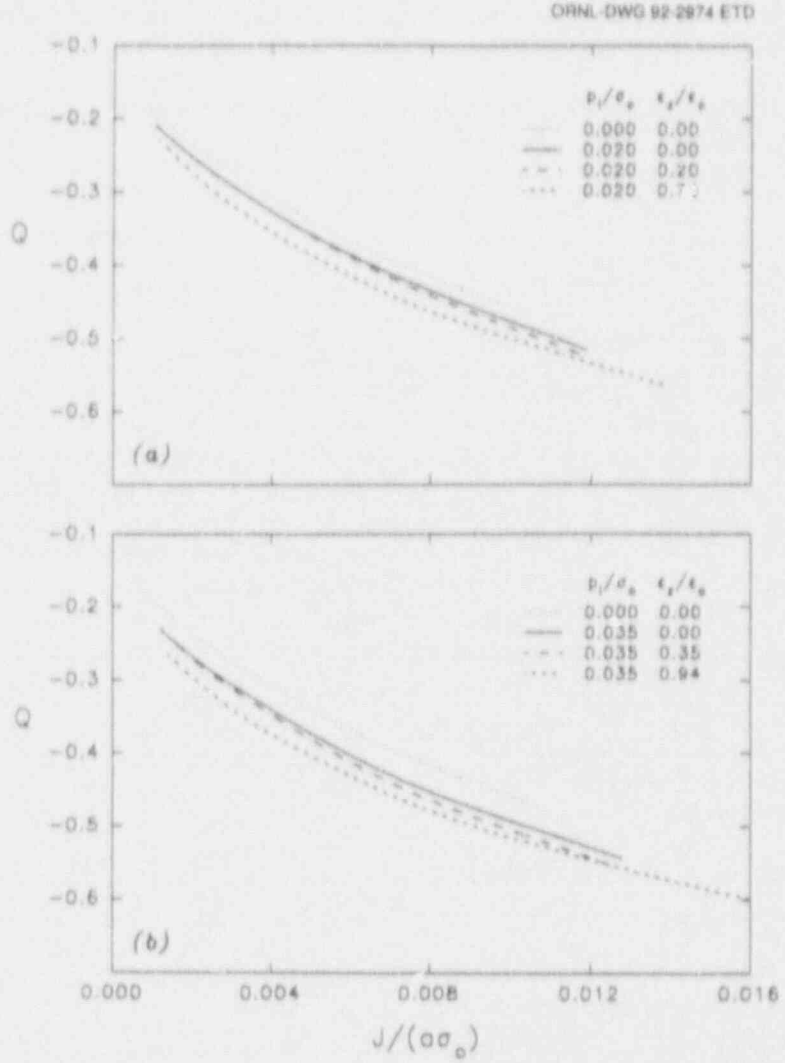

Figure 2.27 Variation of Q with load level $J/(a\sigma_0)$ as computed from finite-element analyses and the reference plane strain HRR solution: (*a*) $p_i/\sigma_0 = 0.020$; (*b*) $p_i/\epsilon_0 = 0.035$

pressure loading and the out-of-plane tensile strain exhibited slight to negligible influence on the crack-tip constraint. Although not explicitly investigated in this study, crack length is also expected to have a significant effect on constraint (e.g., Al-Ani and Hancock,[27] Thiess[2]).

The analyses in this study demonstrated that the constraint variables may influence both the Q and q parameters in the two-term expansion for the near-tip stress fields [Eq. (2.2)]. This observation contradicts the findings of O'Dowd and Shih,[12] and, if generally true, it reduces the effectiveness of the J-Q approach as a two-parameter fracture toughness criterion.

Although cleavage-dominated fracture initiation was the primary focus of this study, questions remain regarding the influence of out-of-plane tensile ductile strain upon crack extension. The out-of-plane strains elevate the magnitude and volumetric extent of the high-stress triaxiality region ahead of the crack tip, suggesting that cavity growth may be significantly accelerated. A full understanding of the influence of constraint on the competition between cleavage and ductile fracture mechanisms in the transition region may not be possible through analytical studies alone. Specialized constraint-controlled biaxial loading tests will also be required.

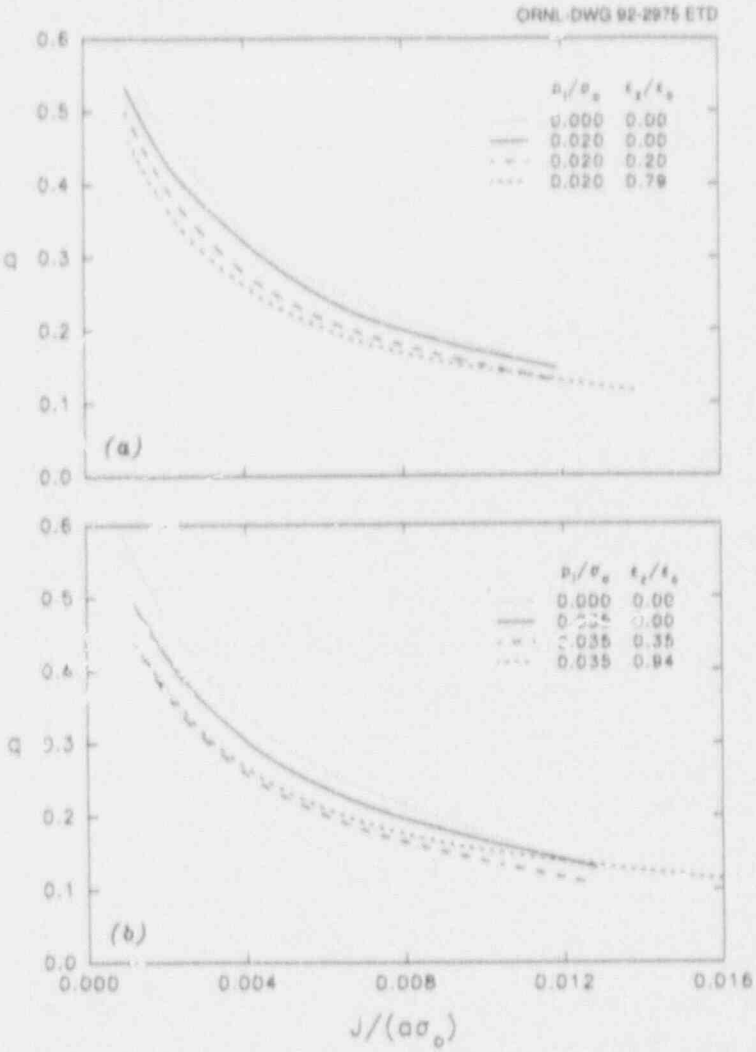

Figure 2.28 Variation of q with load level $J/(a\sigma_0)$ as computed from finite-element analyses and reference plane strain HRR solution: (*a*) $p_l/\sigma_0 = 0.020$; (*b*) $p_l/\sigma_0 = 0.035$

2.5 Dynamic Fracture Analysis of Pressure Vessels

(J. Keeney-Walker, B. R. Bass)

2.5.1 Introduction

In a previous study,[33] several issues related to the modeling and analysis of dynamic fracture events in an RPV were examined quantitatively through static and dynamic analyses of a hypothetical RPV subjected to a PTS transient. Analyses were performed with the OCA-P code[44] to identify shallow cracks that initiate in cleavage and arrest deep in the wall of the RPV as a result of PTS transient loading. The OCA-P predictions were compared with both application- and generation-mode dynamic analysis results based on postulated dynamic fracture toughness models. The potential for cleavage reinitiation of the arrested cracks was investigated using both static and dynamic initiation toughness relations. A radially constrained static model,[45] to approximate certain dynamic conditions at the time of crack arrest, was applied to the same PTS transient, and the results were comparable with those from the dynamic analyses.

The static and dynamic models of the previous study are extended herein to incorporate additional capabilities for the analysis of a PTS event in RPVs. The application-mode dynamic model was modified to include a second dynamic fracture toughness relation developed by Schwartz* from

*C. W. Schwartz, Martin Marietta Energy Systems, Inc., Oak Ridge Natl. Lab., "Crack Speed Relations Inferred from Large SEN Specimens of A 533 B Steel," USNRC Report NUREG/CR-5861 (ORNL/Sub/79/7778/9), to be published.

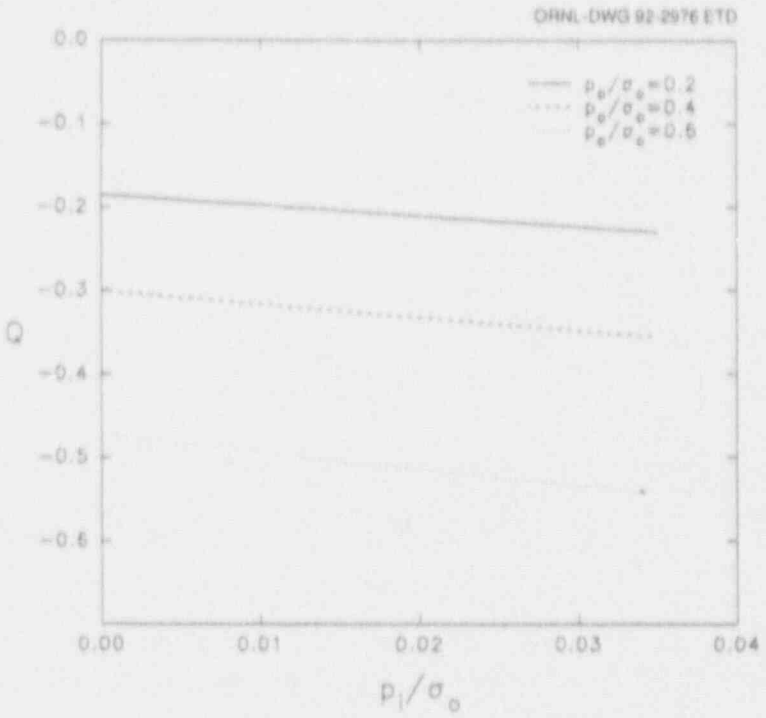

Figure 2.29 Variation of Q with radial compressive load level p_i/σ_o under pure plane strain conditions. Axial load level p_i/σ_o = 0.4 best represents peak PTS conditions for actual vessel

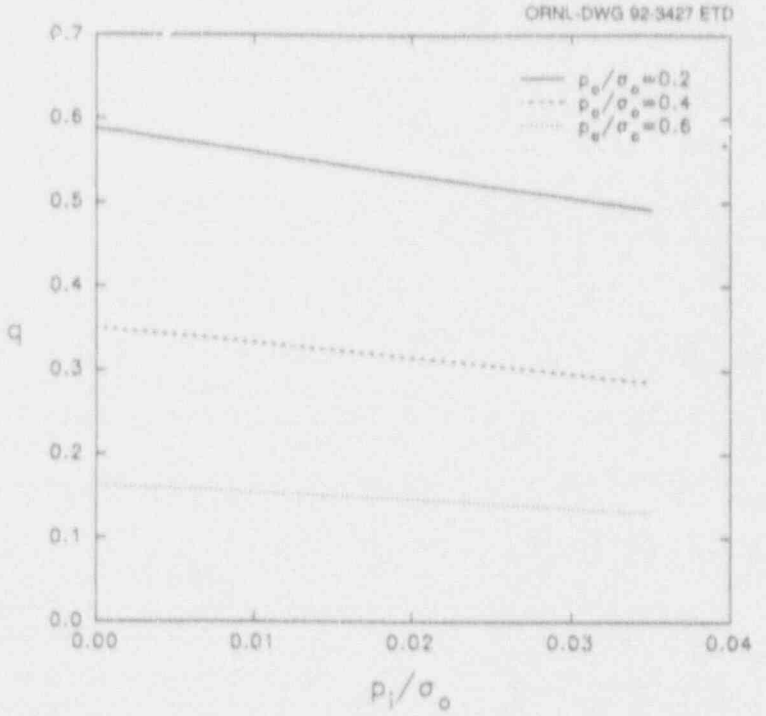

Figure 2.30 Variation of q with radial compressive load level p_i/σ_o under pure plane strain conditions. Axial load level p_i/σ_o = 0.4 best represents peak PTS conditions for actual vessel

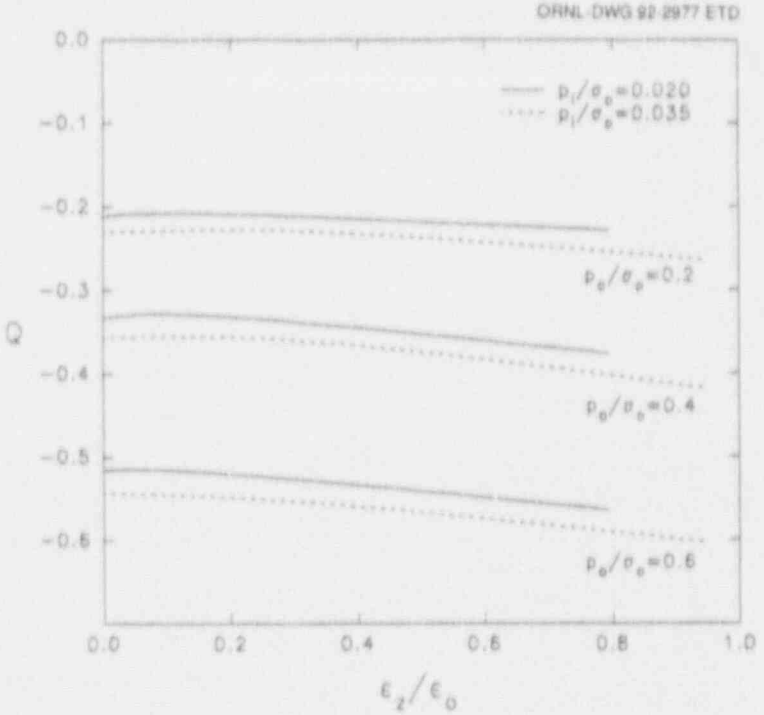

Figure 2.31 Variation of Q with out-of-plane tensile strain level ϵ_z/ϵ_0. Radial compressive load level $p_i/\sigma_0 = 0.035$ and axial load level $p_a/\sigma_0 = 0.4$ best represent peak PTS conditions for actual vessel

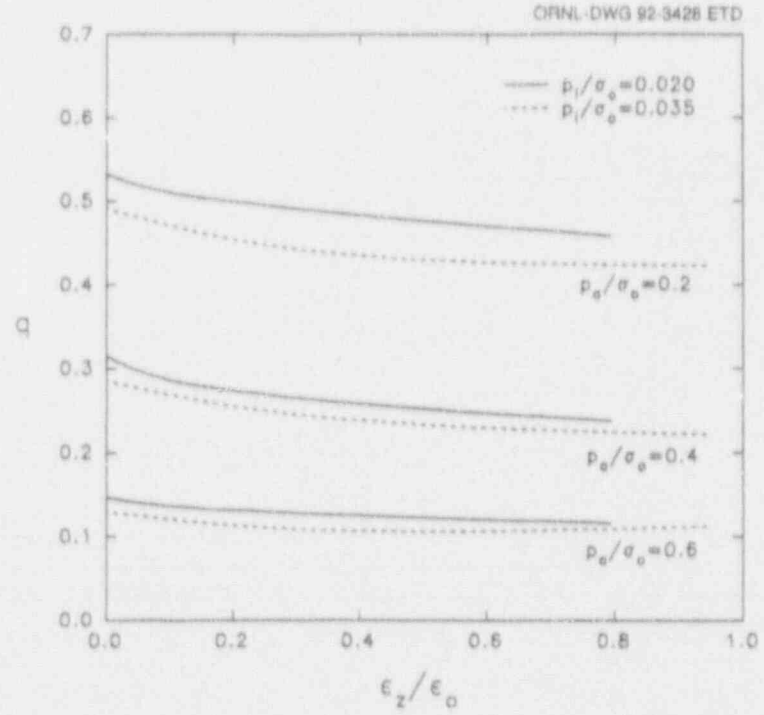

Figure 2.32 Variation of q with out-of-plane tensile strain level ϵ_z/ϵ_0. Radial compressive load level $p_i/\sigma_0 = 0.035$ and axial load level $p_i/\sigma_0 = 0.4$ best represent peak PTS conditions for actual vessel

dynamic data generated in the WP-1 series of HSST wide-plate tests. This relation provides a model that is more relevant to RPV steels than the previously applied fracture toughness model[46] developed from Japanese wide-plate data.[47] Also, the radially constrained static model[45] was evaluated in applications to dynamic crack-reinitation event in RPVs. Results from these applications are compared with previous studies in the following sections.

2.5.2 Fracture Analyses

The PTS event selected for analysis from the Nuclear Regulatory Commission (NRC)/IPTS studies was the H. B. Robinson transient 9.22B (Ref. 48) (modified for a constant value of the heat-transfer coefficient). The vessel has an inner radius of 1981.2 mm, a wall thickness of 236.5 mm, and a cladding thickness of 5.6 mm. Based on an OCA-P analysis, a flaw having a depth of a_0 = 0.0239 m (a/W = 0.101) is predicted to initiate in cleavage at time t = 36 min and to arrest at a depth of a_f = 0.1189 m (a/W = 503).

2.5.2.1 Finite-Element Model

In the static and dynamic thermoelastic analyses, a 2-D plane-strain, finite-element formulation was used to model the test vessel. The finite-element model employed in these analyses, depicted in Fig. 2.33, consists of 1994 nodes and 613 eight-noded isoparametric elements. An MNLO formulation and a 2 × 2 numerical integration order was used in all the analyses. The values of the radial temperature distribution and internal pressure at the time of cleavage-crack propagation for this transient were used as the boundary conditions and assumed to be constant during the run-arrest event. The pressure at crack initiation was applied to the inner surface of the model using 2-D pressure surfaces; crack-face pressure was not included. To provide the proper constraint for the thermal stresses, the material stress-free temperature was lowered, so the average out-of-plane stress through the vessel wall approximated the average axial stress given by the relation (Pr/2t).

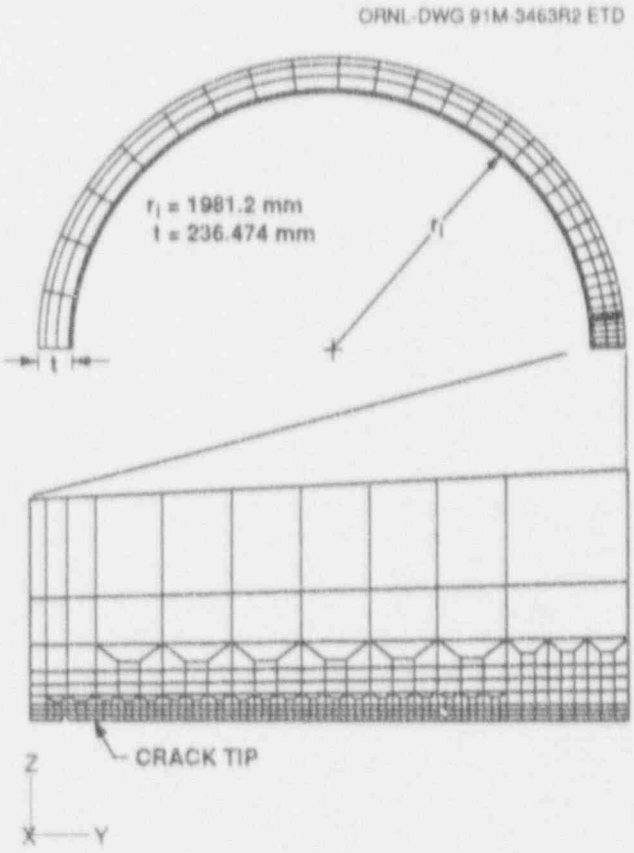

Figure 2.33 Finite-element model used in dynamic fracture analyses of a reactor pressure vessel

2.5.2.2 Finite-Element Analyses

Initially, quasi-static analyses were performed with ORNL-modified ADINA[49,50] at the initial crack depth (a/W = 0.101) and at two other crack depths (a/W = 0.494 and a/W = 0.507) that were close to the arrest location determined by OCA-P. The computed K_I values compare well with the OCA-P calculations (2% difference).

The application-mode analyses of the present study employed two empirical dynamic fracture toughness relations, which were developed in support of the HSST wide-plate testing program.[21] The first of these relations (pretest model) was developed by Kanninen et al.[46] from Japanese wide-plate data[47] primarily for use in pretest planning analysis of the wide-plate experiment. The second relation (posttest model) was developed by Schwartz* from dynamic data generated in the WP-1 series of HSST wide-plate tests, which employed specimens fabricated from A 533 grade B class 1 steel. According to Schwartz, a linear form was assumed for the K_{Id} (ȧ, T) relation, the coefficients of which were estimated from test data using generation-mode computational methodology. The first application-mode dynamic analysis was performed using the ASME Sect. XI lower-bound toughness curves.[51] In this case, the crack was assumed to arrest if K_I fell below K_{Ia} or if the crack velocity dropped below a threshold velocity of 2% of the shear wave velocity (~60 m/s).

Analysis results predicted crack arrest at a/W = 0.358 for the pretest fracture toughness model (path A to B in Fig. 2.34) and at a/W = 0.31 for the posttest model (path A to D in Fig. 2.34). After the initial arrest, K_I oscillates due to vessel bending and reaches peak values of 262 MPa•$\sqrt{m}$ at 19.5 ms (point C in Fig. 2.34) and 209 MPa•$\sqrt{m}$ at 2.9 ms (point E in Fig. 2.34) for the pretest and posttest models, respectively. If crack reinitiation is assumed to occur when the applied K_I increases above the static K_{Ic} value, then the results depicted in Fig. 2.34 do not predict reinitiation for either of the fracture toughness models.

*C. W. Schwartz, Martin Marietta Energy Systems, Inc., Oak Ridge Natl. Lab., "Crack Speed Relations Inferred from Large SEN Specimens of A 533 B Steel," USNRC Report NUREG/CR-5861 (ORNL/Sub/79/7778/9), to be published.

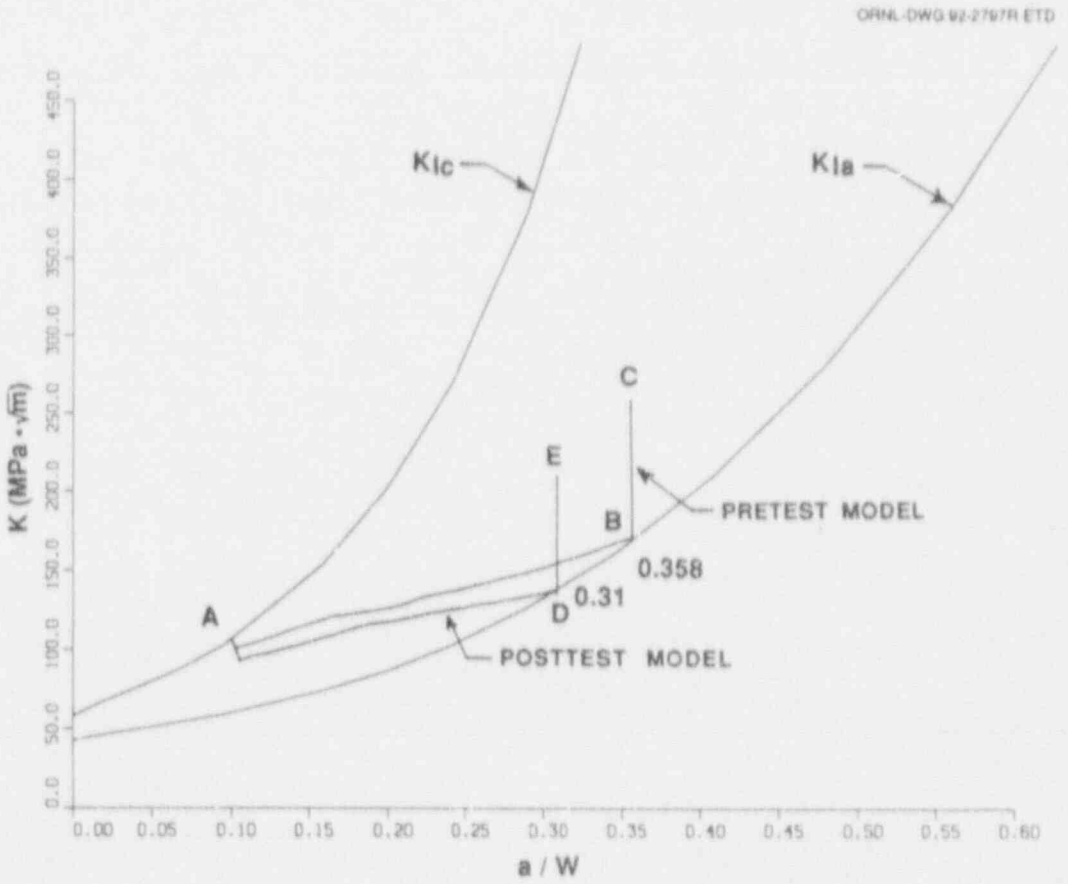

Figure 2.34 Results from application-mode analyses at a/W = 0.358 for pretest fracture toughness model (path A-B) and at a/W = 0.31 for the posttest model (path A-D). Reinitiation is based on the ASME lower-bound K_{Ic} curve

In general, the lower-shelf and transition fracture toughness of structural steels decreases with increasing loading rate. So for any given temperature, the fracture toughness measured in a high rate loading test (K_{Id}) is generally lower than the fracture toughness measured in a static test (K_{Ic}).

A procedure was developed for this study to estimate the dynamic initiation toughness from measured data.[52] The application-mode dynamic analyses were repeated using the generated K_{Id} curve in place of the ASME lower-bound K_{Ic} curve to determine the propensity for crack reinitiation. As shown in Fig. 2.35, the crack reinitiated for the pretest model at a K_I value for 262 MPa•$\sqrt{m}$, and then arrested at a K_I of 261 MPa•$\sqrt{m}$ and a/W of 0.46 (path A-B-C-F). After arrest K_I again oscillates with a peak value of 335 MPa•$\sqrt{m}$ and a/W of 24.5 ms (point G), which is below the K_{Id} curve. For the posttest model, the crack reinitiated and arrested because of low velocity at an a/W of 0.36 (path A-D-E-H). K_I reached a peak value of 263 MPa•$\sqrt{m}$ at 19.3 ms (point I) and missed the reinitiation value by 1 MPa•$\sqrt{m}$. If reinitiation had occurred, the crack would have arrested at an a/W of ~0.46, which is consistent with the OCA-P prediction. This is shown as a dashed line in Fig. 2.35.

It has been proposed[45] that the stress-intensity factor during crack extension can be approximated by a static analysis that assumes that the vessel is essentially stationary. The technique proposed in Ref. 45 was investigated in the present study through an application to the same RPV model and PTS loading transient defined earlier. A series of static thermoelastic analyses were performed at various crack lengths with the vessel fixed radially on the outer surface at the radial displacement calculated for the initial crack depth. The results of these analyses are depicted in Fig. 2.36. In Fig. 2.36, calculated K_I values from OCA-P, application-mode dynamic analysis (post-test model and K_{Id} curve), and static (radially constrained outer-surface) are plotted as functions of a/W. Note that the K_I computed from the static radially constrained model intersects the K_{Ia} curve at about the same point as the first arrest of the application-mode dynamic analysis using the posttest model (3% difference). The unconstrained value of K_I at an a/W of 0.30 is 193 MPa•$\sqrt{m}$, and when this value is amplified by 1.07 the K_I value is 207 MPa•$\sqrt{m}$,which would predict reinitiation because K_{Id} is 205 MPa•$\sqrt{m}$. The amplification factor of 1.07 was calculated from the posttest model application-mode dynamic analysis and the OCA-P analysis at an a/W of 0.31. To propagate the crack after reinitiation, a series of analyses was performed with

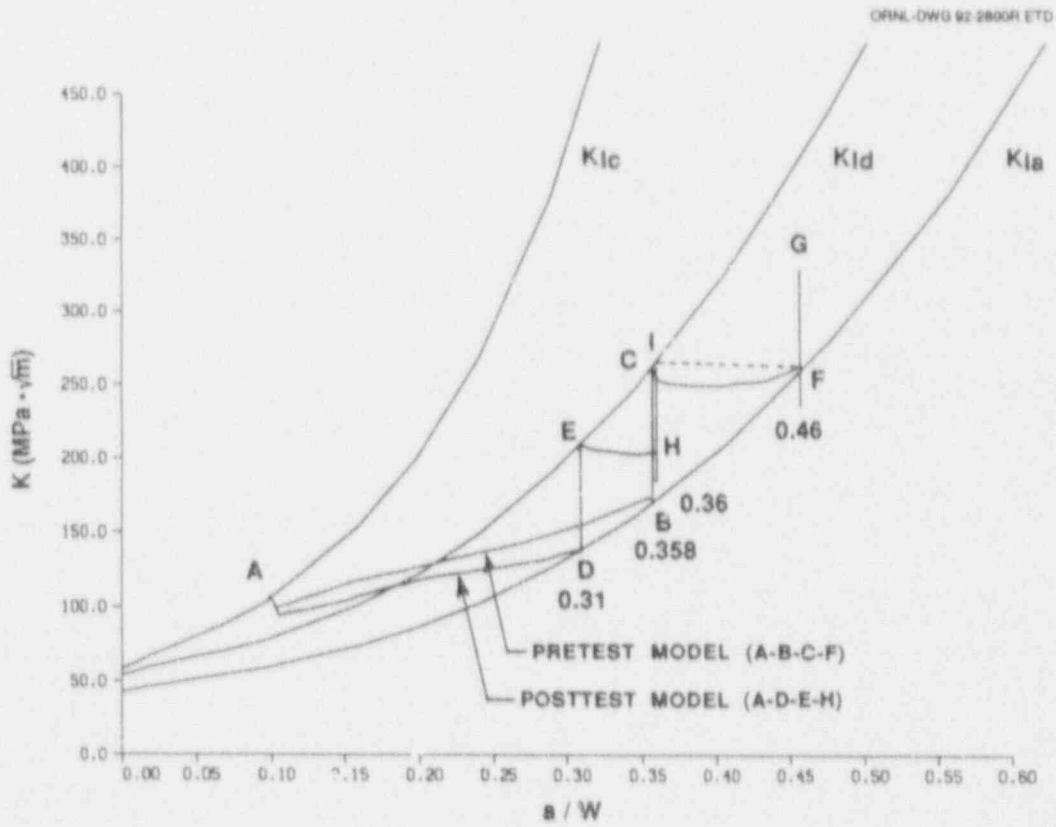

Figure 2.35 Results from application-mode analysis with reinitiation based on dynamic initiation toughness estimated from measured data given in Ref. 52

the vessel fixed radially on the outer surface at the radial displacement calculated for the unconstrained model with a crack at an a/W of 0.30. The computed K_I values at each crack depth were amplified by 1.07. The crack arrested at an a/W of 0.39 when K_I intersected the K_{Ia} curve. This is between the two application-mode analyses. The amplification factor was determined to be 1.2 at this crack depth. The unconstrained value of K_I at the arrest location is 240 MPa•$\sqrt{m}$, which gives an amplified value of 288 MPa•$\sqrt{m}$. Reinitiation at this location is not predicted. A comparison of predicted crack-arrest values for some of the previously described analyses is also depicted in Fig. 2.36. The differences in these results are clearly dependent upon whether the crack reinitiates.

2.5.3 Summary and Conclusions

Comparisons of crack-arrest predictions from the static and dynamic analyses indicate that the radially constrained static model shows good agreement with the posttest dynamic model for both crack-arrest depths, while the full-bending static model (OCA-P) leads to an overprediction of the first and second arrest depth. The magnitude of these differences is dependent upon whether cleavage reinitiation is predicted by the dynamic models.

Five factors that influence postcleavage arrest predictions in dynamic models of the type employed in this study include (but are not limited to) the following:

1. dynamic initiation toughness of the vessel material,
2. dynamic fracture toughness of the vessel material,
3. precleavage and postcleavage ductile tearing (such as that observed in the HSST/PTSE-2 experiment),
4. constitutive modeling and fracture parameters of the material (e.g., plasticity, strain-rate effects,etc),
5. geometric model of the crack (e.g., 2-D vs 3-D representation of the propagating crack).

The differences in predictions of reinitiation of the arrested crack are predominantly controlled by the assumed toughness. The issue condenses to the relevance of the rate dependency described in Ref. 52 to the realistic situations of interest.

Clarification of any one of the five issues represents a formidable research challenge, but the development of an effective model of the complete fracture event is dependent upon substantial progress being made in several of these areas.

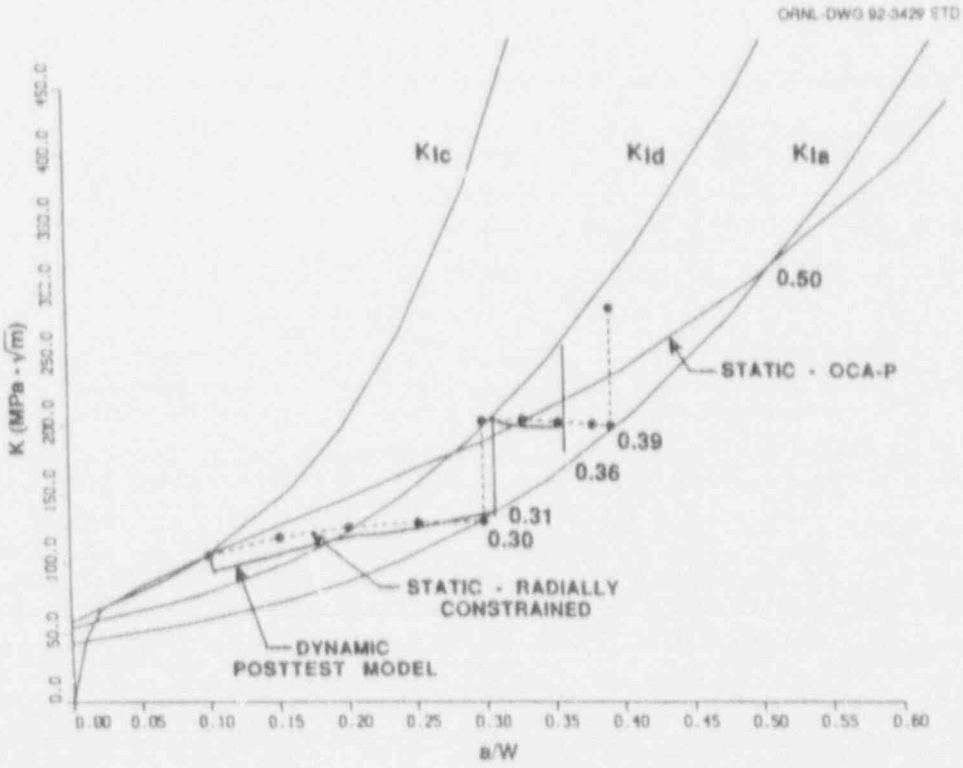

Figure 2.36 Comparison of analysis results from a static method implemented in OCA-P code, radially constrained static method from Ref. 45, and application-mode dynamic model utilizing the dynamic fracture toughness model from Schwartz.

2.6 Cleavage Initiation Studies

(W. L. Fourney, G. R. Irwin, University of Maryland)

A report was completed giving the final results of cleavage initiation toughness comparisons between specimens precracked with fatigue and similar specimens precracked with cleavage arrest. Tables 2.4 and 2.5, from that report, summarize the test results. Crack front irregularities, natural for crack arrest, tended to lower the K values for cleavage initiation and caused more numerous pop-in (short run-arrest) events. The K value estimates for crack arrest furnished lower bounds for the scatter of K values for cleavage initiation at each of the three test temperatures, regardless of whether the cleavage initiation resulted in complete specimen fracture or merely a short run-arrest event.

Introduction of a cleavage-arrest precrack into a TPB specimen caused initial problems. However, a method for doing this was developed, using a combination of chevron-style side grooving and wedge loading, which consistently produced useful arrest positions for the cleavage precracks. It is now apparent that a modification of ASTM E1221 (for K_{Ia} measurements) to permit use of chevron style grooving deserves attention. A modification of that kind has good

Table 2.4 Test results of SENB specimens of A 508 steel with cleavage precracks. σ_{YS} = 90 ksi, RT_{NDT} = 60°C

Specimen	Temperature (°C)	a_i/W	$(B_n/B)_i$	P_p (klp)	Kp (MPa•√m)	$K_p(r_y)$ (MPa•√m)	a_a/W	$(B_n/B)_a$	K_a (klp)	K_a (MPa•√m)	p_c (klp)	K_c (MPa•√m)	$K_c(r_y)$ (MPa•√m)
T5	23	0.52	0.68	14.2	73	73	0.54	0.71	13.0	70	13.5	73	73
T7	23	0.51	0.65	15.5					15.3		17.3	93	95
T6	65	0.54	0.70	20.7					20.5		23.5	132	143
T8	65	0.54	0.63	22.5	132	144	0.60	0.76	17.0	115	20.0	135	147
T4	85	0.51	0.56	20.7	117	124	0.54	0.63	19.0	112	27.6	163	179
T9	85	0.56	0.69	18.5	114	119	0.59	0.75	17.1	112	19.6	129	138

Note:
a_i/W and $(B_n/B)_i$ pertain to the initial precrack.
P_p and K_p are load and K at start of pop-in.
a_a/W and $(B_n/B)_a$ are based upon estimates of crack size after pop-in.
P_p minus P_a is the pop-in load drop.
P_c and K_c are load and K at start of final fracture.
K values with r_y adjustment are shown as K (r_y).
W = 89 mm, B = 38 mm.

Table 2.5 Test results of SENB specimens of A 508 steel with fatigue precracks

Specimen	Temperature (°C)	a_i/W	$(B_n/B)_i$	P_p (klp)	Kp (MPa•√m)	$K_p(r_y)$ (MPa•√m)	a_a/W	$(B_n/B)_a$	K_a (klp)	K_a (MPa•√m)	p_c (klp)	K_c (MPa•√m)	$K_c(r_y)$ (MPa•√m)
T11	23	0.52	0.79								16.0	81	81
T13	23	0.51	0.77	14.7	73	73	0.53	0.77	13.8	71	15.7	81	84
T14	62	0.49	0.75								25.1	119	123
T15	62	0.51	0.76								25.5	127	135
T16	80	0.45	0.61								34.2	152	168
T17	85	0.42	0.55								35.8	159	169
T18	85	0.43	0.57								37.8	173	189

Note:
a_i/W and $(B_n/B)_i$ pertain to the initial precrack.
P_p and K_p are load and K at start of pop-in.
a_a/W and $(B_n/B)_a$ are based upon estimates of crack size after pop-in.
P_p minus P_a is the pop-in load drop.
P_c and K_c are load and K at start of final fracture.
K values with r_y adjustment are shown as K (r_y).
W = 89 mm, B = 38 mm.

prospects toward improved efficiency of small-specimen K_{Ia} measurements.

2.7 Elastic-Plastic Fracture Mechanics in Inhomogeneous Materials and Structures [B. R. Bass, G. Yagawa (University of Tokyo)]

The principal purpose of the EPI Program is to investigate the elastic-plastic crack growth phenomena in inhomogeneous materials and structures, aiming at the development of estimation schemes of fracture resistance through the cooperative work between U.S. and Japanese research consortia. The HSST Program, on behalf of the NRC, is the sole U.S. participant in the EPI Program.

The Japanese consortium in charge of the EPI Program was organized in July 1988 as one of the subcommittees of the Nuclear Engineering Research Committee of The Japan Welding Engineering Society (JWES). The EPI subcommittee consists of 9 universities, 3 research institutes, and 21 companies. Three working groups (WGs) have been set up under the subcommittee: Theoretical WG, Experimental WG and Estimation Scheme WG.

The experimental WG conducts tests and generates experimental data of crack growth behavior in planned inhomogeneous specimens, which are used for numerical analyses to examine the applicability of various elastic-plastic fracture mechanics parameters to the inhomogeneous material regime. This WG also examines the effects of various factors on fracture behavior, including crack-tip location and crack orientation with respect to fusion line (FL), specimen thickness, and residual stress.

The theoretical WG analyzes the experimental results using various numerical as well as analytical methods not only to understand the crack growth phenomena in inhomogeneous materials but also to provide the fundamental data for the development of the estimation schemes of crack growth resistance.

The estimation scheme WG, which was established in the fall of 1989, analyzes the experimental results using conventional estimation schemes to examine the applicability of these to the inhomogeneous material regime and also works on the investigation and the development of new estimation schemes based on those experimental as well as numerical results. Results from studies of the three WGs are reported in detail in interim reports.[53-55]

The fourth EPI report, the English version of which is to be published at the end of May 1992, describes the results of the subtasks performed during April 1991 through March 1992. The principal results of the subtasks are summarized in the next section.

2.7.1 Literature Survey

Crack growth phenomena in inhomogeneous materials and structures can be roughly divided into the following two categories: (1) crack growth parallel to the phase boundary of different materials and (2) crack growth across the phase boundary. A circumferential crack that occurs in the weldment of a welded pipe is an example of the former phenomena. The latter phenomena are found in irradiated RPVs, cladded RPVs, and welded joints. The latter phenomena, which involve theoretical difficulties such as the J-integal not possessing path-independence even in stationary crack problems, seem more critical to the integrity assessment of RPVs. Thus, we have decided to mainly study cracks growing perpendicular to the phase boundary of different materials.

To study these phenomena, we consider the following two kinds of estimation schemes of elastic-plastic fracture resistance: (1) J-integral formula utilized in 2-D fracture toughness and resistance tests, and (2) J-integral formula for the integrity assessment of 3-D structures with through-wall and surface cracks. The former category involves the Merkle-Corten's formula J_{M-C} for CT specimens in stationary crack problems and the J-deformation J_D and the J-modified J_M in growing crack problems. Incremental fracture mechanics parameters such as the J and T^* integrals are also selected as references in the present study.

Among several conventional estimation schemes for integrity studies of structures, we have selected the General Electric (GE)/Electric Power Research Institute (EPRI) approach, the R6 approach, and the references stress approach. The applicability of these fracture mechanics parameters and the simplified assessment approaches to the evaluation of crack growth resistance in the inhomogeneous material regime are examined in detail.

2.7.2 Material and Welding Procedure

In the previous fiscal years, we performed fracture tests using specimens taken from welded plates of A 533 grade B class 1 steel. The material and the welding procedure were commercial quality and the differences between

material properties of the base metal and the weld metal was not very significant (i.e., only ~15% difference in yield stress for the two metals.) In this fiscal year, we have performed fracture tests using bimaterial specimens consisting of A 533 B class 1 steel and a high strength HT80 steel. The yield stress of HT80 steel is about twice as much as that of A 533 B class 1 steel. The welding procedure employed here was the electron beam welding method. The A 533 grade B class 1 steel was produced by the same procedure as in the previous study. The weldment was ~3 mm wide and the size of the heat-affected zone (HAZ) was negligible.

To maintain the original difference of material properties for the two materials, all specimens were machined from the as-weld plates and used for several tests.

2.7.3 Fundamental Material Properties

Unaxial tensile tests of A 533 grade B class 1 steel and HT80 steel were performed. A hardness test of the welded plates was also performed. The principal results are summarized as follows:

- The stress-strain curve of A 533 grade B class 1 steel was found to be almost the same as that of A 533 grade B class 1 steel tested in the previous years. Thus, the stress-strain relation of A 533 B class 1 steel formulated in the previous years is again utilized to analyze experimental results for the bimaterial specimens.
- The yield stress of HT80 steel is about twice as much as that of A 533 B class 1 steel.
- The order of hardness is weldment > HT80 steel > A 533 grade B class 1 steel.

2.7.4 Residual Stress Measurement

Nondestructive measurements of residual stress that occurred in the welded plates of A 533 grade B class 1 steel and HT80 steel were performed using an acoustoelastic technique. A compressive residual stress on the order of 100 MPa occurred in the vicinity of the weldment region. The distribution of the residual stress is to be used for fracture analyses to evaluate its effects precisely.

2.7.5 Fracture Experiments on 2-D Specimens

(1) Specimens

Homogeneous and bimaterial CT specimens were machined from the welded plate of A 533 grade B class 1 steel and HT80 steel. The plane dimensions of all the specimens are the same as those of the standard 1T-CT specimen, whereas the thickness is chosen to be 10, 15, or 19 mm. As for the bimaterial specimens, initial cracks were prepared normal to the phase boundary, and locations of initial crack tips were varied with respect to the phase boundary. The bimaterial CT specimens tested are as follows:

- AH-(A 533 B) specimen, in which holes for loading and an initial crack are machined in the A 533 grade B class 1 portion, and an initial crack-tip is placed about 3 mm in front of the centerline of the weldment. As a result, a crack grows across the phase boundary from the A 533 grade B class 1 portion to the HT80 portion.
- AH-(HT80) specimen, in which an initial crack tip is placed about 3 mm ahead of the phase boundary. Then, a crack grows only in the HT80 portion.
- HA-(PB) specimen, in which holes for loading and an initial crack are machined in the HT80 portion, and an initial crack-tip is placed on the phase boundary of HT80 and the weldment. Then a crack grows from weldment to the A 533 grade B class 1 portion.
- HA-(A 533 B), in which an initial crack-tip is placed ~3 mm ahead of the phase boundary. Then a crack grows only in the A 533 B class 1 portion.

To avoid any confusion due to different testing procedures, these experiments were performed in only two research groups. A multiple-specimen method and an unloading compliance method were utilized to precisely measure crack growth amount.

(2) Effects of specimen thickness on initiation toughness

The experimental results showed that initiation toughness was independent of specimen thickness for the welded specimens whose thickness ranges from 10 mm to 19 mm.

(3) Effects of crack-tip locations on crack growth resistance

The J-integrals evaluated here are the J-deformation J_D and the J-modified J_M. The principal results are summarized as follows:

- The comparison between homogeneous HT80 specimens and inhomogeneous AH-(HT80) specimens and the comparison between homogeneous A 533 B specimens and inhomogeneous HA-(A 533 B) specimens clearly showed that, even if a crack grows in the same material, global inhomogeneity of specimen significantly influences crack growth behavior. Qualitative discussions of these results will be presented in Sect. 2.7.8 together with numerical results.
- As for AH-(A 533 B) specimens and HA-(PB) specimens, a crack grows across the phase boundary of different materials. In these cases, crack growth behavior become more complicated than the above locally homogeneous specimens.

The above results are mainly attributed to local yielding that occurred in portions other than the crack tip (i.e., holes for loading and the phase boundary). These phenomena are influenced by material combinations and crack-tip locations.

(4) Direct measurement of crack-tip behavior

The Moire interferometry method, which is assisted by a computer image processing technique, was applied to measure crack-tip fields of the welded specimens of A 533 B class 1 steel and HT80 steel. The principal results are summarized as follows:

— In AH-(A 533 B) specimens, the yielding region is restricted to the field between the crack tip and the phase boundary.
— In HA-(HT80) specimens, yielding occurs in the vicinity of the crack tip as well as the phase boundary.

2.7.6 Fracture Experiments on Surface-Cracked Specimens

In this fiscal year, TPB type specimens were tested at the center of which a semi-elliptical surface crack was prepared. The surface crack was machined to cross the weldment perpendicularly. Half of the crack was placed in the A 533 B class 1 steel portion and the other half was in the HT80 steel portion, and then the weldment was located at the center of the crack. The crack-mouth-opening displacement (CMOD) was measured with an optical method. After loading experiments, the CTOD was measured with the silicon rubber casing method, while crack growth amount (Δa) was measured directly using scanning electron microscopy (SEM). The crack-tip opening angle (CTOA) was evaluated using both CTOD and Δa values.

The homogeneous and welded specimens were tested to examine the effects of inhomogeneity on crack growth behavior. The results obtained are summarized as follows:

— CTOD is slightly larger in the HT80 portion than in the A 533 B class 1 portion.
— Crack growth amount is much larger in the HT80 portion than in the A 533 B class 1 portion.
— CTOA is smaller in the HT80 portion than in the A 533 B class 1 portion.

In the welded specimens of A 533 B class 1 steel tested in previous years, such significant inhomogeneity effects were not observed. These experimental results are to be analyzed by the 3-D finite element method to calculate the distribution of the J-integral along a crack front.

2.7.7 Fracture Experiment Under Anisothermal Condition

As one of the fundamental problems related to the EPI Program, fracture experiments under an anisothermal condition were performed using the SEN specimens taken from the heat-treated base plate of A 533 grade B class 1 steel. The purpose of the present experiments is to examine the effects of gradual changes of material toughness on fracture behavior.

Last year, crack-tip temperature and temperature gradient were set to be 0°C, and 0.250°C/mm respectively. We could not observe any significant effects of anisothermal conditions on fracture behavior. This year, the crack-tip temperature was set to –50°C, and the temperature gradient was increased to 0.5°C/mm to increase the gradient in material properties, including fracture toughness. The results showed that the fracture toughness of A 533 B class 1 steel in the current anisothermal condition was by ~15% smaller than that of a uniform temperature condition.

2.7.8 Elastic-Plastic Finite Element Analyses of 2-D Crack

Fracture phenomena of inhomogeneous materials and structures are influenced by several factors such as the inhomogeneity of material properties, residual stresses and the location of crack tip. Fracture experiments are not sufficient to quantify the effect of each factor on fracture behaviors. Thus, numerical analyses were performed based on experimental results. The elastic-plastic finite element analyses of crack growth performed in this year are summarized below:

(1) Crack analyses of the welded specimens of A 533 grade B class 1 and HT80 steels

To confirm the effects of the difference of material properties on crack behavior, elastic-plastic finite element analyses were performed of the welded specimens of A 533 B class 1 and HT80 steels. The specimen types analyzed are AH-(A 533 B), AH-(HT80), HA-(A 533 B) and HA-(HT80) defined previously. Crack length a/W varied from 0.1 to 0.6. The results are summarized as follows:

— Load vs load-line displacement curves of HA specimens are greater than AH specimens.
— Plastic yielding regions are observed either in the vicinity of the crack-tip, the phase boundary, or the loading point. Sizes of the yielding regions depend on specimen type and crack length.

- At a smaller loading level J_{path}, T^*, and $\hat{J}$ integrals are path-independent, irrespective of specimen types and crack length. These parameters coincide with J_{M-C}. With increasing load, J_{path} becomes path-dependent, and later T^* and $\hat{J}$ integrals also become path-dependent. Modification of the integration paths for calculating these integrals can make them path-independent.
- At a higher loading level, the J_{M-C} value becomes larger than the J_{path} value calculated along a small integration path set in the vicinity of a crack-tip. This tendency is more significant in AH specimens possibly because of plastic yielding at the loading point affecting the evaluation of J_{M-C}. On the other hand, the difference between J_{M-C} and J_{path} values is small for HA specimens with deeper cracks. J_{M-C} values may be reliable in HA specimens with deeper cracks.
- As for AH specimens and specimens with shorter cracks, it is necessary to take into account some modification of plastic yielding at the loading point to evaluate J_{M-C}.

(2) Crack growth analysis of welded specimens of A 533 B class 1 steel with consideration given to residual stresses.

Residual stresses measured by an acoustoelastic method were taken into account to perform the generation-phase crack growth analysis of the H5G specimen. In the H5G specimen, the crack-tip was placed in front of the phase boundary of the base metal and the weld metal (i.e., HAZ portion). The results showed that residual stresses did not affect crack growth behavior.

2.7.9 Elastic-Plastic Finite Element Analyses of 3-D Cracks

(1) Crack growth simulation of CT specimens

Based on the measured distribution of crack growth along the crack front, the generation-phase crack growth simulation of a CT specimen was performed. The J-integral was evaluated using a line integration technique. The results are summarized as follows:

- The calculated load vs load-line displacement agreed well with the measured one.
- During stable crack growth, the J_{path} distribution along the crack front remained uniform.
- The HRR field formed before a crack starts to grow did not move during crack growth. As a result, the HRR field gradually shrank as an elastic unloading region expanded.

(2) Analyses of cracks on the interface

A 3-D finite element analysis of a crack on the interface was performed. The results clarified yielding behavior of a crack-tip field at the intersection of interface and the free surface.

2.7.10 Estimation Scheme Development for 2-D Cracks

The GE/EPRI approach, the R6 approach, and the reference stress approach were applied to analyze crack growth behavior in welded CT specimens made of A 533 B class 1 steel, and those for welded CT specimens consisting of A 533 B class 1 steel and HT80 steel. The specimens analyzed are as follows:

- M5G specimen that is a homogeneous CT specimen made of A 533 B class 1 steel
- H5G specimen in which a crack tip is placed in front of the phase boundary, (i.e., HAZ part)
- F5G specimen in which a crack tip is placed on the phase boundary
- D5G specimen in which a crack is placed across the phase boundary

The yield stress of the base metal is ~15% larger than that of the weld metal.

- AH-(A 533 B) specimen, in which holes for loading and an initial crack are machined in the A 533 B class 1 portion and an initial crack tip is placed ~3 mm in front of the centerline of the weldment. The crack grows across the phase boundary from A 533 B class 1 portion to the HT80 portion.
- AH-(HT80) specimen, in which an initial crack tip is placed ~3 mm ahead of the phase boundary. Thus, a crack grows only in the HT80 portion.
- HA-(PB) specimen, in which holes for loading and an initial crack are machined in the HT80 portion and an initial crack tip is placed on the phase boundary of HT80 and the weldment. Then a crack grows from weldment to A 533 B class.
- HA-(A 533 B), in which an initial crack tip is placed ~3 mm ahead of the phase boundary. Then, a crack grows only in the A 533 B class 1 portion.

The yield stress of HT80 steel is about double that of the A 533 B class 1 steel. The principle results are summarized as follows for the GE/EPRI method

- The crack growth phenomenon in the M5G specimen can be assessed accurately.
- In the H5G, F5G, and D5G specimens, the measured load vs load-line displacement curves are well simulated by using the material properties of the base metal

in the beginning stage and by using the material properties of the weld metal in the later stage. As a result, the magnitude of the measured maximum load is well estimated by using the averaged values of the material properties of the base metal and the weld metal.

— In H5G, F5G, and D5G specimens, the measured J-R curves are well simulated by using the averaged values of the material properties of both metals.

The GE/EPRI method was also applied to analyze crack growth phenomena in the HA and AH specimens. Because the HT80 steel has a high hardening number n, a fully plastic solution corresponding to this material has to be extrapolated. This extrapolation resulted in some errors in evaluating fully plastic solutions. The present analyses of the HA and AH specimens are not considered reliable. Further examination is still necessary.

The R6 approach was applied to crack growth analyses of both kinds of specimens. The results showed that the assessment using the material properties and the J-R curves of the material in the uncracked ligament portion gives a good estimation of a load vs load-line displacement curve.

The reference stress approach gave results similar to the GE/EPRI approach.

2.7.11 Estimation Scheme Development for 3-D Cracks

The GE/EPRI approach was established for semi-elliptical surface cracks. Fully plastic solutions of a semi-elliptical surface crack in a plate subjected to tensile and bending stress were obtained by using the nonlinear finite-element analysis, which takes into account incompressibility by the penalty function method. The results were formulated with polynomials in terms of crack aspect ratio a/c and crack depth a/t of a semi-elliptical surface crack and a hardening exponent of material n.

References

1. R. D. Cheverton et al., Martin Marietta Energy Systems, Inc., Oak Ridge Natl. Lab., "Review of Pressurized-Water-Reactor-Related Thermal-Shock Studies," ASTM Special Technical Publication 969, 752–766 (1988).*

2. T. J. Theiss, Martin Marietta Energy Systems, Inc. Oak Ridge Natl. Lab., pp. 43–50 in "Heavy-Section Steel Technology Program Semiannual Progress Report for April-September 1991," USNRC Report NUREG/CR-4219 (ORNL/TM-9693/V8&N2), 1992.†

3. W. E. Pennell, "Aging Impact on the Safety and Operability of Nuclear Reactor Pressure Vessels," presented at the NRC Aging Research Information Conference, Rockville, MD, March 24–27, 1992.

4. D. Aurich, "The Influence of the Stress State on the Plastic Zone Size," *Eng. Fract. Mech.* 7, 761–765 (1975).

5. D. Aurich et al., "The Influence on the Stress State of K_{Ic}," Paper G 5/2 in *Proceedings of the 4th International Conference on Structural Mechanics in Reactor Technology, San Francisco, California, August 15–19, 1977.*

6. D. Aurich et al., "The Influence of Stress State on Fracture Toughness – Further Results," Paper G 2/3 in *Transactions of the 5th International Conference on Structural Mechanics in Reactor Technology, Berlin, Germany, August 13–17, 1979.*

7. J. Olschewski et al., "The Influence of Biaxial Loading on Fracture Toughness – Further Results," Paper G/F 3/3 in *Transactions of 7th International Conference on Structural Mechanics in Reactor Technology, Chicago, IL, August 1983.*

8. D. Aurich, "Übertragbarkeit von Bruchkennwerten von Proben auf Bauteile im Hinblick auf die Sicherheitsanalyse von Kernkraftwerks-komponenten," Report RS 275, BAM, Berlin, Germany, September 14, 1984 (text in German).

9. D. Aurich et al., "The Influence of Multiaxial Stress States on Characteristic Parameters for Cleavage Fracture in the Elastic-Plastic Range," pp. 345–356 in *Proc. Intl. Conf. Appl. Fracture Mechanics to Materials and Structures, 1984.*

10. D. K. M. Shum, Martin Marietta Energy Systems, Inc., Oak Ridge Natl. Lab., "Analytical Studies of Transverse Strain Effects on Fracture Toughness for Circumferentially Oriented Cracks," USNRC Report NUREG/CR-5592 (ORNL/TM-11581), April 1991.†

11. S. G. Larsson and A. J. Carlsson, "Influence of Non-Singular Stress Terms and Specimen Geometry on Small-Scale Yielding at Crack Tips in Elastic-Plastic Materials," *J. Mech. Phys. Solids* 21, 263-277 (1973).*

12. N. P. O'Dowd and C. F. Shih, "Family of Crack-Tip Fields Characterized by a Triaxiality Parameter: Part I – Structure of Fields," *J. Mech. Phys. Solids* (1991).*

13. R. O. Ritchie, J. F. Knott, and J. R. Rice, "On the Relationship Between Critical Tensile Stress and Fracture Toughness in Mild Steel," *J. Mech. Phys. Solids* 21, 395-41 (1973).*

14. A. McClintock, "A Criterion for Ductile Fracture by the Growth of Holes," *J. Appl. Mech.* 35, 363-371 (1968).*

15. J. W. Hancock and A. C. MacKenzie, "On the Mechanisms of Ductile Fracture in High-Strength Steels Subjected to Multi-Axial Stress-States," *J. Mech. Phys. Solids* 24 147-169 (1976).*

16. D. M. Parks, "Interpretation of Irradiation Effects on the Fracture Toughness of a Pressure Vessel Steel in Terms of Crack Tip Stress Analysis," *Journal of Engineering Materials and Technology*, 98, 30–36 (1976).*

17. R. O. Ritchie, W. L. Server, and R. A. Wullaert, "Critical Fracture Stress and Fracture Strain Models for the Prediction of Lower and Upper Shelf Toughness in Nuclear Pressure Vessel Steels," *Met. Trans. A*, Vol. 10A, 1557-1570 (1979).*

18. R. A. Wullaert and W. L. Server, "Small Specimen Predictions of Fracture Toughness for Nuclear Pressure Vessel Steels," *Nucl. Eng. Des.* 57, 153–173 (1980).*

19. T. L. Anderson and R. H. Dodds, Jr., "Specimen Size Requirements for Fracture Toughness Testing in the Transition Region," Report MM-6585-90-5, Mechanics and Materials Center, Texas A&M University, College Station, Texas, May 1990.

20. J. Keeney-Walker, B. R. Bass, and J. D. Landes, Martin Marietta Energy Systems, Inc., Oak Ridge Natl. Lab., "An Investigation of Crack-Tip Stress-Field Criteria for Predicting Cleavage-Crack Initiation," USNRC Report NUREG/CR-5651 (ORNL/TM-11692), September 1991.†

21. D. J. Naus et al., Martin Marietta Energy Systems, Inc., Oak Ridge Natl. Lab., "Crack-Arrest Behavior in SEN Wide Plates of Quenched and Tempered A 533 Grade B Steel Tested Under Nonisothermal Conditions," USNRC Report NUREG/CR-4930 (ORNL-6388), August 1987.†

22. D. E. McCabe and J. D. Landes, "The Effect of Specimen Plan View Size and Material Thickness on the Transition Temperature Behavior of A 533 B Steel," Research Report 80-1D3-REVEM-R2, Westinghouse R&D Center, November 1980.

23. D. J. Naus et al., Martin Marietta Energy Systems, Inc., Oak Ridge Natl. Lab., "High-Temperature Crack-Arrest Behavior in 152-mm Thick SEN Wide Plates of Quenched and Tempered A 533 Grade B Class 1 Steel," USNRC Report NUREG/CR-5330 (ORNL/TM-11083), April 1989.†

24. D. J. Naus et al., Martin Marietta Energy Systems, Inc., Oak Ridge Natl. Lab., "High-Temperature Crack-Arrest Tests Using 152-mm-Thick SEN Wide Plates of Low-Upper-Shelf Base Material: Tests WP-2.2 and WP-2.6," USNRC Report NUREG/CR-5450 (ORNL/TM-11352), February 1990.†

25. D. L. Shelby et al., Martin Marietta Energy Systems, Inc. Oak Ridge Natl. Lab., "Pressurized Thermal Shock Evaluation of the H. B. Robinson Unit 2 Nuclear Power Plant," USNRC Report NUREG/CR-4183 (ORNL/TM-9567/V1 and V2), September 1985.†

26. M. F. Kanninen and C. H. Popelar, *Advanced Fracture Mechanics*, Oxford University Press, New York, 1985.

27. A. M. Al-Ani and J. W. Hancock, "J-Dominance of Short Cracks in Tension and Bending," *J. Mech. Phys. Solids*, 39 (1), 23-43 (1991).†

28. P. S. Leevers and J. C. Radon, "Inherent Stress Biaxiality in Various Fracture Specimen Geometries," *Int. J. Fract.*, 19, 311–325 (1982).

29. D. M. Parks, "Three-Dimensional Aspects of HRR-dominance," *Symposium on Elastic-Plastic Fracture*, European Group on Freiburg, West Germany, October 1989.

30. J. Heerens and D. T. Read, "Fracture Behavior of a Pressure Steel in the Ductile to Brittle Transition Region," National Institute of Standards and Technology Report NISTIR 88/3099 (PB89-189195/AS), December 1988.

31. S. G. Druse, G. P. Gibson, and M. Capel, "Microstructural Control of Cleavage Fracture in an A508 Class 3 Pressure Vessel Steel," presented at the 22nd National Symposium on Fracture Mechanics, Atlanta, Georgia, June 26-28, 1990.

32. D. J. Naus et al., Martin Marietta Energy Systems, Inc., Oak Ridge Natl. Lab., "Crack-Arrest Behavior in SEN Wide Plates of Low-Upper-Shelf Base Metal Tested Under Nonisothermal Conditions: WP-2 Series," USNRC Report NUREG/CR-5451, (ORNL/TM-6584), August 1990.†

33. J. D. Landes and D. E. McCabe, "Effect of Section Size on Transition Temperature Behavior of Stuctural Steels," pp. 378–392, *Fracture Mechanics: Fifteenth Symposium, ASTM STP 833*, R. J. Sanford, Ed., American Society for Testing and Materials, Philadelphia, 1984.

34. *Patran Plus User Manual–Release 2.4*, PDA Engineering, Inc., Costa Mesa, California (1989).

35. *ABAQUS User Manual–Version 4.8.5*, Hibbit, Karlsson, and Sorenson, Inc., Providence, R.I., 1989.

36. L. Chen, P. C. Paris, and H. Tada, "A Deep Part-Through All Around Circumferential Crack in a Cylindrical Vessel Subject to Combined Thermal and Pressure Loads," *23rd National Symposium on Fracture Mechanics*, College Station, Tex., June 1991.

37. J. R. Rice and M. A. Johnson, "The Role of Large Crack Tip Geometry Changes in Plane Strain Fracture," in *Inelastic Behavior of Solids*, Kanninen et al., Eds., (McGraw-Hill, New York 1970) 641–670.

38. R. M. McMeeking, "Finite Deformation Analysis of Crack Tip Opening in Elastic-Plastic Materials and Implications for Fracture," *J. Mech. Phys. Solids*, 25, 357–381 (1982).*

39. J. W. Hutchinson, "Singular Behavior at the End of a Tensile Crack in a Hardening Material," *J. Mech. Phys. Solids*, 16, 13-31 (1968).*

40. J. R. Rice and G. F. Rosengren, "Plane Strain Deformation Near a Crack Tip in a Power-Law Hardening Material," *J. Mech. Phys. Solids*, 16, 1–12 (1968).

41. D. M. Parks, "The Virtual Crack Extension Method for Nonlinear Material Behavior," *Computer Methods in Applied Mechanics and Engineering*, 12, 353–364 1977.†

42. C. W. Schwartz, "Influence of Out-of Plane Loading on Crack Tip Constraint," *ASTM Symposium on Constraint Effects in Fracture*, Indianapolis, Ind., May 1991.

43. Y. Y. Wang "On the Tow-Parameter Characterization of Elastic-Plastic Crack-Front Fields in Surface Cracked Plates," *ASTM Symposium on Constraint Effects in Fracture*, Indianapolis, IN, May 1991.

44. R. D. Cheverton and D. G. Bell, Martin Marietta Energy Systems, Inc., Oak Ridge Natl. Lab., "OCA-P, A Deterministic and Probabilistic Fracture-Mechanics Code for Application to Pressure Vessels," USNRC Report NUREG-3618 (ORNL-5991), May 1984.†

45. R. J. Fabi and D. J. Ayers, "Combustion Engineering Inc., "Calculating Dynamic Crack Arrest by Static Analogy," Electric Power Research Institute, Report NP-6223, March 1989.

46. M. F. Kanninen et al., "Preliminary Analysis of Japanese Wide-Plate Dynamic Crack Propagation-Arrest Experiments," p. 89 in Heavy-Section Steel Technology Program Semiannual Progress Report for April-September 1984, USNRC Report NUREG/CR-3744, Vol. 2 (ORNL/TM-9154/V2) December 1984.

47. T. Kanazana, S. Machida, T. Teramoto, and H. Yoshimura, "Study on Fast Fracture and Crack Arrest," *Experimental Mechanics* 21(2), 78–88, (February 1981).*

48. R. D. Cheverton and D. G. Ball, Martin Marietta Energy Systems, Inc., Oak Ridge Natl. Lab., "Pressurized-Thermal-Shock Evaluation of the H. B. Robinson Nuclear Power Plant," pp. 263-306, USNRC Report NUREG/CR-4183, Vol. 1 (ORNL/TM-9567/V1), September 1985.

49. K. J. Bathe, Massachusetts Institute of Technology, "ADINA — A Finite Element Program for Automatic Dynamic Incremental Nonlinear Analysis," Report 82448-1, 1975 (revised 1978).

50. B. R. Bass et al., "Applications of ADINA to Viscoplastic-Dynamic Fracture Mechanics Analysis," *Computers and Structures* 23(3/4), 815–824, 1989.

51. *The American Society of Mechanical Engineers Boiler and Pressure Vessel Code*, Section XI, Rules for Inservice Inspection of Nuclear Power Plant Components, 1986.‡

52. W. O. Shabbits, "Dynamic Fracture Toughness Properties of Heavy Section A 533 Grade B Class 1 Steel Plate," Westinghouse R&D Center, WCAP-7623, HSST Technical Report No. 13, December 1970.

53. G. Yagawa, Century Research Corporation, Tokyo, Japan, "Study on Elastic-Plastic Fracture Mechanics in Inhomogeneous Materials and Structures I," CRC-EPI-1, March 1989.

54. G. Yagawa, Century Research Corporation, Tokyo, Japan, "Study on Elastic-Plastic Fracture Mechanics in Inhomogeneous Materials and Structures II," CRC-EPI-2, March 1990.

55. G. Yagawa, Century Research Corporation, Tokyo, Japan, "Study on Elastic-Plastic Fracture Mechanics in Inhomogeneous Materials and Structures III" CRC-EPI-3, March 1991.

---

*Available in public technical libraries.
†Available for purchase from the National Technical Information Service, Springfield, VA 22161.
‡Available from American National Standards Institute, 1430 Broadway, New York, NY 10018, Copyrighted.

3 Material Characterization and Properties

R. K. Nanstad

Primarily for internal management and budgetary control, the Heavy-Section Steel Technology (HSST) Program created a separate task (Task H.3) for the work on material characterization and properties determinations. However, for the reader's convenience, some contributions to this report are placed within other chapters according to the larger tasks that correspond to the particular material studied.

3.1 Characterization of HSST Plate 013B in the L-S Orientation

(S. K. Iskander, R. L. Swain, J. J. Henry)

The purpose of the Shallow Flaws Task is to investigate the toughness of materials in the presence of shallow flaws (ones with a depth to thickness a/W ≈ 0.05 to 0.10) as compared to toughness measured by the standard American Society for Testing and Materials (ASTM) tests with a/W = 0.5.

The testing phase for characterizing HSST Plate 013B for the Shallow Flaws Task is almost complete. Tests to determine the Charpy V-notch (CVN) curves in the L-S and T-L orientations, the drop-weight nil-ductility transition (NDT) temperature, and the reference temperature, RT_{NDT}, for both surface and midthickness material have been completed and reported in the previous semiannual progress report. Tests to determine tensile properties in the L orientation as a function of temperature for both surface and midthickness material have now been completed. Crack initiation toughness tests (K_{Ic}, K_{Jc}, or J-R) have also been performed over the temperature range of interest using 25-mm 1T C(T) compact specimens in the L-S orientation from the midthickness positions. Preliminary results from both tensile and crack initiation toughness testing will be reported here. The approximate 10 remaining 1T C(T) specimens will be tested at temperatures that will improve the statistics of the 18 specimens already tested. The experimental load extension curves from the X-Y plotter obtained during tensile testing of material from the surface and midthickness have been digitized for use in the analysis of the shallow-flaw bending tests. The load extension data will be recalculated to give stresses and strains, and the initial slope modified to reflect a more accurate Young's modulus. The analysis of all data and the preparation of a report are in progress. A small number of 25-mm-thick, 50-mm-deep single-edge three-point bend (TPB) SE(B) specimens will be tested at a single temperature and their results compared to those from the C(T) specimens to determine the effect of specimen geometry on the initiation toughness.

Results of the tests performed to date have shown that a significant difference exists in the CVN impact energy test results between specimens from the midthickness and those from the surface of the characterization block. The results of drop-weight and tensile testing have confirmed the difference in properties between the surface and midthickness of the plate.

HSST Plate 013 was manufactured by Lukens Steel, melt C4453, in accordance with ASTM Specification for Pressure Vessel Plates, Alloy Steels, Quenched and Tempered, Manganese-Molybdenum and Manganese-Molybdenum-Nickel Grade B, Class 1 (A 533 grade B class 1). A characterization block, designated 13 BA/5, was flame-cut from the 187-mm-thick (7 3/8-in.) HSST Plate 013B. The characterization block, together with other flame-cut material destined to be machined into the shallow-flaw beam specimens, was given a postweld heat treatment (PWHT) in May 1991 of 621 ± 14°C (1150 ± 25°F) for 40 h to simulate the PWHT given to reactor pressure vessels. The characterization has been performed in the same L-S orientation as that in which the Shallow Flaws Task TPB beam tests are performed. HSST Plate 013A (the other half of HSST Plate 013) has been previously quite extensively characterized, but not in the L-S orientation, and may not have had a PWHT.

The results of tensile testing at five temperatures for two specimens from each of the surface and midthickness material are shown in Fig. 3.1. The experimental data have been regression fitted with a second-order polynomial. The results obtained to date from crack initiation toughness testing are shown in Fig. 3.2. Note that only material from the midthickness has been tested because it is not practicable to sample the surface layer in the L-S orientation using 1T C(T) specimens. Note also that the results from side-grooved specimens are similar to those from those with no side grooves.

3.2 Thermal Aging of Stainless Steel Cladding (F. M. Haggag, R. K. Nanstad)

Thermal aging at relatively low temperatures (343°C) has been shown to significantly degrade the Charpy impact toughness of type 308 stainless steel welds. The stainless

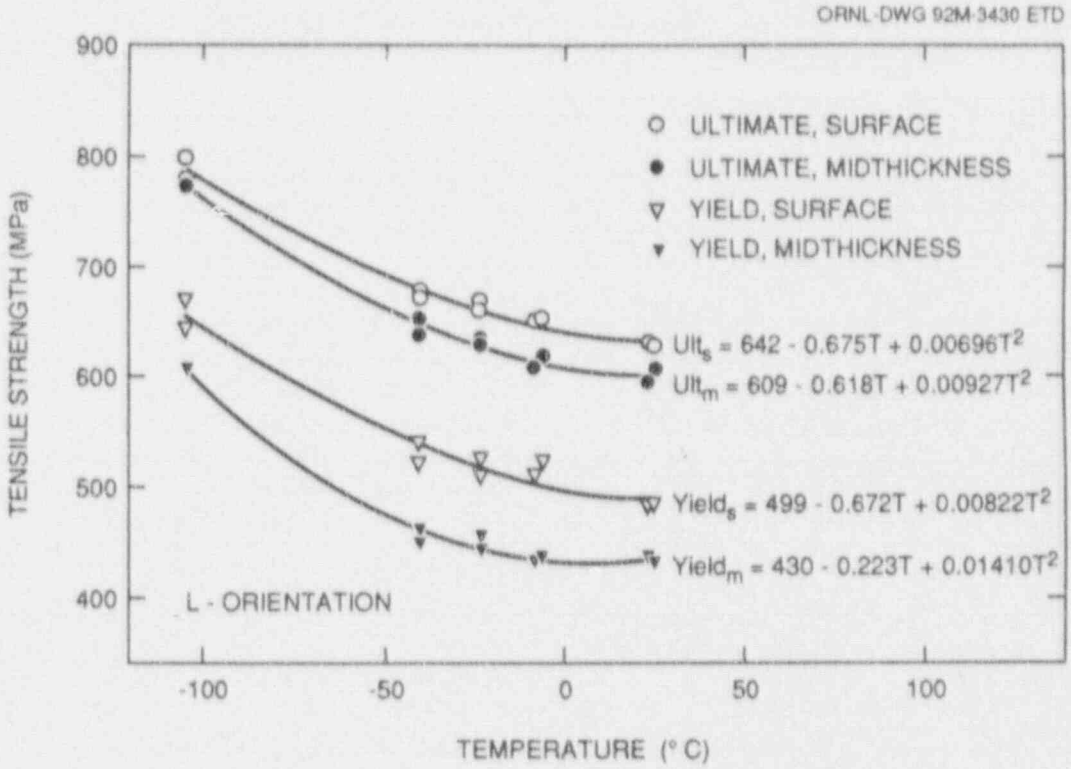

Figure 3.1 Yield and ultimate tensile strengths of surface and midthickness material in L orientation of characterization block 13BA/5 from HSST Plate 013B, postweld-heat-treated in May 1991 at 621°C (1150°F) for 40 h. The test results were regression fit with a second-order polynomial shown

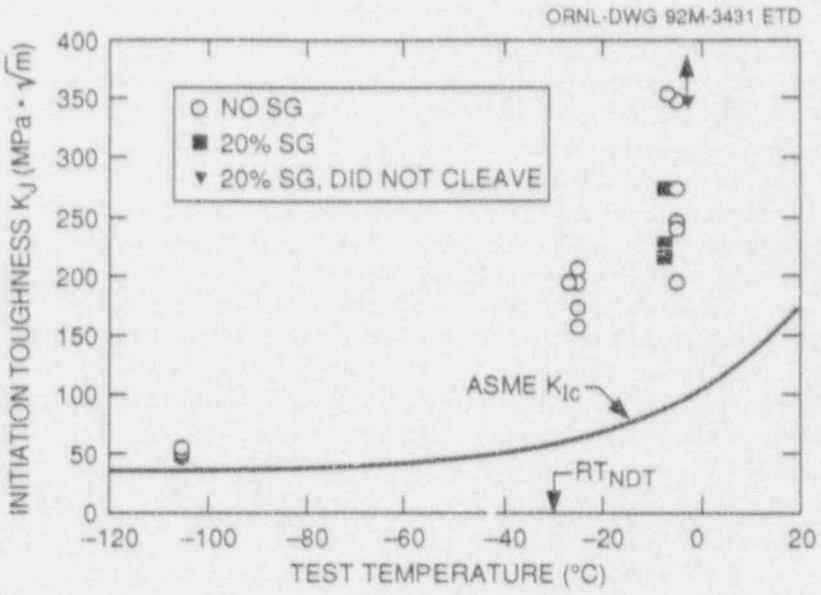

Figure 3.2 Crack initiation toughness test results

steel cladding applied to the inner surface of RPVs is very similar to that material. Hence, an experimental program was initiated to evaluate the effects of thermal aging on stainless steel cladding relative to its contribution to toughness degradation during irradiation experiments as well as long-term effects.

Results from testing of unaged material and material aged for 1600 h were presented in the last progress report. Thermal aging at 288°C of stainless steel cladding and the ferritic steel on which it is overlaid to accumulated times of 20,000 h (expected to be completed by November 1992) and 50,000 h is in progress. Other cladding specimens are being aged at 343°C together with a type 308 stainless steel weld from another NRC program.

3.3 ASTM Fracture Toughness Testing Standards Development

(D. E. McCabe, D. J. Alexander, R. K. Nanstad)

HSST Program personnel participated in another group meeting of the combined J_{Ic}/J-R curve standard committee. This group has now adopted a simple scheme to adjust compliance-generated Δa (crack growth) values for initial offset: a problem that has escaped a mutually agreeable solution for ~2 years. The combined standard will also contain fracture toughness determinations on test specimens that fracture in a brittle manner (by cleavage). The practice was modified according to our recommendations to enable appropriate specimen preparation for such data.

Standard practice E 561 on K_R curves has been updated with three proposed changes, and these were submitted to E-24 for balloting. All negative votes were resolved, and the revised practice has been forwarded to the ASTM staff representative.

Work is continuing on the "Test Practice for Fracture Toughness in the Transition Range." An extensive amount of supporting data has been collected, and the recommendations of the practice are being tested with these data. In the last reporting period it was realized that there is potential to use established statistical practices to define lower-bound fracture toughness with associated probability limits. Involvement of Dr. K. Wallen of VTT (Finland) in this element of the research program has accelerated progress considerably.

3.4 Study of Low Toughness Zones

(D. E. McCabe)

The evaluation of pop-ins and their significance to safety issues is currently being documented in a draft NRC report. Evidence in pop-in behavior was gathered from several sources. The bottom line is that pop-ins must be given serious consideration as potential initiators of fast-running cracks. A single test record of a pop-in event does not provide all the evidence needed to judge the relevance of the event. The report will show that pop-in discontinuities on test records are a function of specimen size. Some pop-ins can be ignored, but this requires extensive data generation to prove that the pop-in was an outliner toughness index, apart from the main body of cleavage fracture behavior for that material. The issue of reliability of toughness development after pop-in crack arrest will be discussed.

4 Special Technical Assistance

J. G. Merkle

4.1 Examination of Equilibrium-Based Linearly Varying Stress Distribution for Estimating K_I for Surface Cracks

4.1.1 Introduction

At the American Society of Mechanical Engineers (ASME) Pressure Vessel and Piping Conference in 1991, Lawrence and Hechmer[1] compared four different approximations for fitting stress distributions and calculating K_I values for surface cracks in plates. One of these involved fitting the stress distribution over the depth of the crack with a straight line such that the force and moment of the actual stress distribution are preserved. This procedure was shown to produce K_I values generally differing by <10% from those calculated on the basis of a cubic polynomial fit to the actual stress distribution. For this and other practical reasons, the equilibrium-based straight-line fit to the actual stress distribution, over the depth of the crack, was proposed* as an improvement to the K_I calculation procedure for surface cracks in *ASME Code*, Sect. XI, Appendix A. Because least-squares fits are commonly considered rational means for approximating curves, the question naturally arose concerning the relation between a least-squares linear fit and an equilibrium-based linear fit to the same curve. As will be shown below, the two fits are identical. In addition, if a least-squares linear fit to the stress distribution produces good K_I approximations, then it should be possible to estimate the higher order polynomial K_I coefficients from the constant and linear K_I coefficients. This will also be discussed below. The subject of K_I estimates based on least-squares linear fits to nonlinear stress distributions has been discussed in a previous progress report.[2]

4.1.2 Relation Between Statically Equivalent and Least-Squares Linear Fits

Let $\hat{\sigma}$ represent a linear approximation to an arbitrary stress distribution, over the depth a of a surface crack. Then at a depth x from the surface,

$$\hat{\sigma} = \sigma_m + \sigma_b \frac{\left(\frac{a}{2} - x\right)}{\frac{a}{2}} \qquad (4.1)$$

describes the linear approximation in terms of the stress at midcrack-tip depth σ_m and the bending stress at the surface and the crack-tip depth σ_b. Equation (4.1) can be rearranged to read

$$\hat{\sigma} = (\sigma_m + \sigma_b) - 2\sigma_b \left(\frac{x}{a}\right) . \qquad (4.2)$$

The sum of the squares of the deviations between $\hat{\sigma}$ and the actual stress σ over the crack depth, denoted by S, is given by

$$S = \int_o^a (\hat{\sigma} - \sigma)^2 \, dx . \qquad (4.3)$$

The least-squares fit of $\hat{\sigma}$ to σ is based on minimizing S with respect to both $(\sigma_m + \sigma_b)$ and σ_b. Thus

$$\frac{\partial S}{\partial(\sigma_m + \sigma_b)} = \frac{\partial S}{\partial \hat{\sigma}} \cdot \frac{\partial \hat{\sigma}}{\partial(\sigma_m + \sigma_b)} = 0 , \qquad (4.4)$$

and

$$\frac{\partial S}{\partial \sigma_b} = \frac{\partial S}{\partial \hat{\sigma}} \cdot \frac{\partial \hat{\sigma}}{\partial \sigma_b} = 0 . \qquad (4.5)$$

From Eqs. (4.2), (4.4), and (4.5)

$$\int_o^a \hat{\sigma} dx = \int_o^a \sigma dx , \qquad (4.6)$$

and

$$\int_o^a \hat{\sigma} x dx = \int_o^a \sigma x dx . \qquad (4.7)$$

Then, using Eq. (4.2) again,

$$\int_o^a \hat{\sigma} dx = \sigma_m a , \qquad (4.8)$$

and

$$\int_o^a \hat{\sigma}\, x dx = \frac{1}{2}\sigma_m a^2 - \frac{1}{6}\sigma_b a^2 . \qquad (4.9)$$

Combining Eqs. (4.6) through (4.9) gives

$$\sigma_m = \frac{1}{a}\int_o^a \sigma dx \qquad (4.10)$$

*J. M. Bloom, Babcock & Wilcox Co., "Proposed Revision to Stress Intensity Factor Correction Factors in Appendix A (ISI-81-29)," letter to R. C. Cipolla, ASME Code Section XI WG on Flaw Evaluation, November 7, 1991.

and

$$\sigma_b = \frac{6}{a^2}\int_0^a \sigma\left(\frac{a}{2} - x\right) dx \quad , \qquad (4.11)$$

which are the average stress and extreme fiber bending stress, respectively, for a rectangular beam of depth, a, subject to the force and moment calculated from the nominal stress acting over the depth of the crack. Thus the statically equivalent linear fit is also a least-squares linear fit. Note that the term static equivalence is only a description of the uncracked stress distribution and has nothing to do with a finite-length surface crack because it takes no account of crack shape.

4.1.3 Estimation of Higher Order Polynomial K_I Coefficient from the Constant and Linear Coefficients

Numerical finite-element solutions exist[1] for estimating stress-intensity factors for finite-length surface cracks in plates by means of fitting the actual stress distribution over the depth of the crack with a polynomial series of the form

$$\sigma = A_o + A_1 x + A_2 x^2 + A_3 x^3 \quad , \qquad (4.12)$$

which can be rewritten in the form

$$\sigma = A'_o + A'_1\left(\frac{x}{a}\right) + A'_2\left(\frac{x}{a}\right)^2 + A'_3\left(\frac{x}{a}\right)^3 \quad . \qquad (4.13)$$

The numerical results for K_I are expressed in the form

$$K_I = \left(A'_o G_o + A'_1 G_1 + A'_2 G_2 + A'_3 G_3\right)\sqrt{\frac{\pi a}{Q}} \quad , \qquad (4.14)$$

where the quantity in parentheses is the nominal stress at the crack-tip depth. The terms G_i are calculated, one at a time, from separate cases in which the stress distribution is assumed to be represented by a single polynomial term. If the linear approximation is accurate, then it should be possible to fit each of the individual higher order polynomial stress distributions with a straight line and then estimate the higher order G_i from G_o and G_1 by equating the resulting K_I values to the polynomial based values.

For a single-term polynomial stress distribution,

$$\sigma = \sigma_a\left(\frac{x}{a}\right)^n \quad . \qquad (4.15)$$

Substituting Eq. (4.15) into Eqs. (4.10) and (4.11) gives

$$\sigma_m = \frac{\sigma_a}{n+1} \qquad (4.16)$$

and

$$\sigma_b = 6\sigma_a\left[\frac{1}{2(n+1)} - \frac{1}{(n+2)}\right] \quad . \qquad (4.17)$$

For n = 2

$$\sigma_m = \frac{\sigma_a}{3} \qquad (4.18)$$

and

$$\sigma_b = \frac{\sigma_a}{2} \quad . \qquad (4.19)$$

For n = 3

$$\sigma_m = \frac{\sigma_a}{4} \qquad (4.20)$$

and

$$\sigma_b = -\frac{9}{20}\sigma_a \quad . \qquad (4.21)$$

For a linear representation of the stress, referring to Eq. (4.13),

$$A'_o = \sigma_m + \sigma_b \qquad (4.22)$$

and

$$A'_o = -2\sigma_b \quad . \qquad (4.23)$$

Substituting Eqs. (4.22) and (4.23) into Eq. (4.14) gives

$$K_I = \left[(\sigma_m + \sigma_b)G_o - 2\sigma_b G_1\right]\sqrt{\frac{\pi a}{Q}} \quad . \qquad (4.24)$$

From Eq. (4.13)

$$K_I = A'_j G_j \sqrt{\frac{\pi a}{Q}} \quad . \qquad (4.25)$$

For a single-term polynomial,

$$A'_j = \sigma_a \quad , \qquad (4.26)$$

so that substituting Eq. (4.26) into Eq. (4.25) and equating the right sides of Eqs. (4.24) and (4.25) gives

$$G_j = \left(\frac{\sigma_m + \sigma_b}{\sigma_a}\right) G_o - 2\left(\frac{\sigma_b}{\sigma_a}\right) G_1 \quad . \qquad (4.27)$$

For n = 2, substituting Eqs. (4.18) and (4.19) into Eq. (4.27) gives

$$G_2 = -\frac{1}{6} G_o + G_1 \quad , \qquad (4.28)$$

and for n = 3, substituting Eqs. (4.20) and (4.21) into (4.27) gives

$$G_3 = -\frac{1}{5} G_o + \frac{9}{10} G_1 \quad . \qquad (4.29)$$

Bounds on the accuracy of the linear approximation method can be obtained with Eqs. (4.28) and (4.29). Preliminary calculations using the tables in Ref. 1 indicate that at the deepest point of the crack the estimates are 10 to 15% low for G_3 and 5 to 10% low for G_2. Crack shape does not seem to have much effect. At the surface of a finite-length crack, errors are greater, but the coefficients are smaller and thus the nonlinear terms contribute less to K_I.

Additional calculations are needed to firmly establish the accuracy of the G_3 and G_2 estimates, especially for points away from the deepest point of the crack. The accuracy of the least-squares linear approximation, for a range of load cases including thermal shock, was investigated in Ref. 1. Those studies may need to be extended to cases of greater stress nonlinearity, especially those involving thermal and residual stresses in stainless steel cladding.

4.2 Effect of Crack Shape Near the Ends of a Finite-Length Surface Crack on Computed K_I Values at the Surface

At the request of the Nuclear Regulatory Commission (NRC), work was performed to provide estimates on the potential change in flaw geometry of an initially shallow, axially oriented, inner-surface, finite-length flaw in a reactor pressure vessel (RPV) during the course of a postulated pressurized-thermal-shock (PTS) transient. Specifically, the question being addressed was whether a shallow finite-length surface [three-dimensional (3-D)] flaw would tend to elongate along the axial direction to become an essentially two-dimensional (2-D) flaw during the transient. The analyses were performed within the context of linear-elastic fracture mechanics. Results from this study are expected to contribute toward an assessment of the degree of conservatism associated with the use of 2-D axial flaws in a probabilistic fracture mechanics assessment of an RPV. A letter report[3] that discusses the analysis method and some preliminary findings from this work has been forwarded to NRC.

Following the analyses of semicircular and long surface flaws subjected to PTS loadings reported in Ref. 3, additional closed-form approximate calculations were done to estimate the stress-intensity factor at the surface for long surface flaws. The values obtained by the Raju-Newman[4] and Merkle[5] equations were almost equal and considerably less than the values reported in Ref. 3. Issues that may influence the computed K_I values along the crack front include (1) crack-front geometry within the cladding and (2) the role of cladding plasticity. Additional 3-D finite-element calculations were performed to resolve the apparent discrepancies.

Three crack-front geometries have been considered: (1) modified-ellipse—the crack-front is elliptical in the base material and is perpendicular to the vessel's inner surface in the cladding region; (2) canoe—the crack front in the base material is essentially a straight line parallel to the vessel's longitudinal axis with two semicircular regions that intersect the clad/base interface at 90°, and the crack front in the cladding is perpendicular to the vessel's inner surface; and (3) ellipse—the crack front is elliptical in shape throughout the base and cladding material [see Fig. 4.1(*a*) and (*b*)]. In Fig. 4.1(*a*) the vertical and horizontal axes are drawn to vastly different scales to emphasize the differences in crack-front geometries. In Fig. 4.1(*b*), crack-front geometries are redrawn with similar vertical and horizontal axes to emphasize the observation that the differences in flaw geometries in Fig. 4.1(*a*) are minor in comparison with the overall geometry of the nominal flaw shape. Material models considered are (1) elastic base and cladding material (bimaterial elastic); (2) elastic base with cladding material assigned base material properties (one-material elastic); and (3) elastic-plastic base and cladding material (bimaterial elastic-plastic). Maximum loading of the flawed cylinder, in terms of the magnitude of the applied stress-intensity factor K_I, occurs at ~20 min into the transient. In subsequent discussions, analysis results are presented for 25 min into the transient.

Analysis results suggest that the crack-front geometry within the cladding can significantly influence the computed K_I values along the crack front within the cladding region, especially for the case of elongated surface flaws with large aspect ratios. Specifically, for the one-material elastic case with a nominal flaw half-length to flaw depth ratio of 80 to 1, analysis results indicate that (1) computed K_I values at the deepest point of the crack front agree for all three flaw geometries; and (2) computed K_I values near

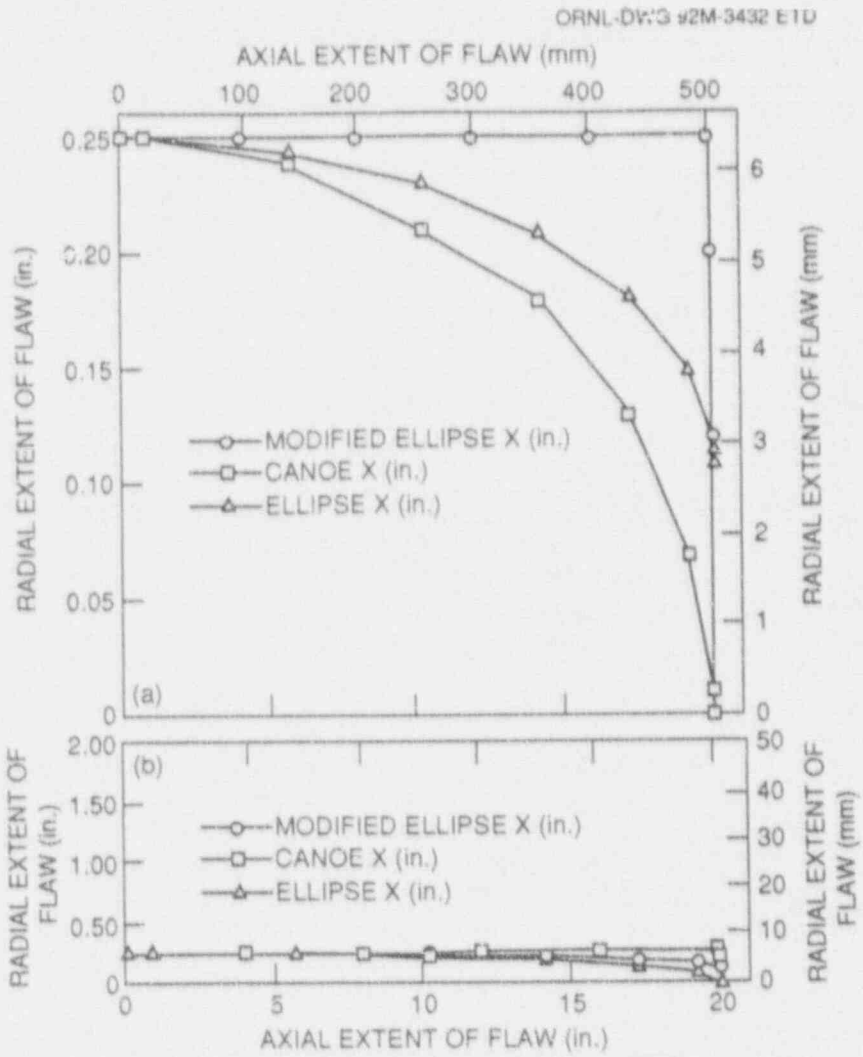

Figure 4.1 **(*a*) Overall crack-front geometries assumed in PTS analysis: (1) modified ellipse, (2) canoe, (3) ellipse. Vertical and horizontal axes are drawn to vastly different scales to emphasize differences in crack-front geometries. (*b*) Crack-front geometries redrawn with similar vertical and horizontal axes to emphasize observation that differences in flaw geometries in (*a*) are minor in comparison with overall geometry of nominal flaw shape**

the inner surface, along the cladding portion of the crack front, can differ by up to a factor of 5 among the flaw geometries considered, with the maximum value being for the canoe flaw geometry and the minimum value being for the ellipse flaw geometry (see Fig. 4.2). Evidently, conversion of an initially 3-D shallow surface flaw to an essentially 2-D axial flaw geometry due to PTS loading can be substantially enhanced or inhibited based on the actual flaw geometry. Note that while the computed K_I values are very sensitive to the flaw geometries investigated, the differences in flaw geometries are minor in comparison with the overall geometry of the nominal flaw shape. It thus appears that care must be taken to represent the crack-front shape realistically near its ends to avoid inaccuracies in the value of K_I there and thus the tendency for axial extension.

Analysis results also indicate that the computed K_I values are very sensitive to whether the cladding and base materials are modeled as elastic or elastic-plastic, with the latter analysis assumption being more realistic. Specifically, the computed K_I values near the inner surface along the cladding portion of the crack front and along a substantial portion of the crack front within the base material are lower for the case of elastic-plastic material response than the elastic analysis conditions (Fig. 4.3). While not evident in Fig. 4.3, analysis results indicate that as the nominal

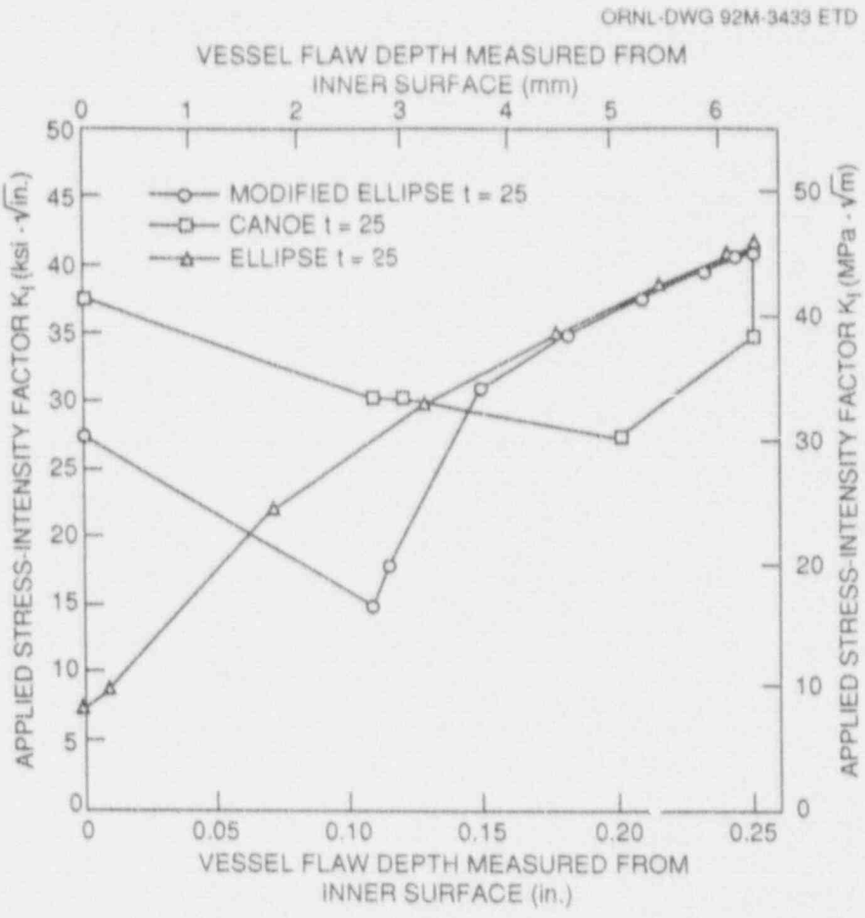

Figure 4.2 **Crack-front geometry within the cladding that can significantly influence computed K_I values along the crack front within the cladding region, especially for the case of elongated surface flaws with large aspect ratios. Results are for 25 min into the transient**

flaw shape in terms of the overall aspect ratio increases, the assumption of elastic-plastic material response leads to the maximum K_I value being located away from the inner surface of the vessel toward the deepest point of the crack front. Migration of the location of maximum K_I toward the deepest point of the crack front is suggestive of an enhanced tendency toward radial rather than axial crack propagation and, therefore, lessens the likelihood of the conversion of an initially 3-D shallow-surface flaw to an essentially 2-D axial flaw geometry. A NUREG report that details these findings is being prepared.

References

1. J. M. Lawrence and J. L. Hechmer, "Closed Form Stress Intensity Factors for a Semi-Elliptical Crack in a Flat Plate Under a Gradient Stress Field," PVP-Vol. 213/MPC-Vol. 32, Pressure Vessel Integrity, American Society of Mechanical Engineers, 1991.*

2. J. G. Merkle, Martin Marietta Energy Systems, Inc., Oak Ridge Natl. Lab., "Stress-Intensity Factor Estimates for Cracks Subject to Nonlinear Stress Distributions," pp. 11–19 in HSST Program Quarterly Progress Report for October–December 1974, ORNL-TM-4805, Vol. II, March 1975.†

3. D. K. M. Shum et al., Martin Marietta Energy Systems, Inc., Oak Ridge Natl. Lab., "Potential Changes in Flaw Geometry of an Initially Shallow, Axially Oriented, Inner-Surface Finite-Length Flaw During a Pressurized-Thermal-Shock Transient," USNRC Report ORNL/ NRC/LTR-92/11, January 31, 1992.‡

4. J. C. Newman and I. S. Raju, "Stress-Intensity Factor Equations for Cracks in Three-Dimensional Finite Bodies Subjected to Tension and Bending Loads," Chap. 9 in *Computational Methods in the Mechanics of Fracture*, S. N. Atluri (ed.), Elsevier Science Publishers B.V., 1986.

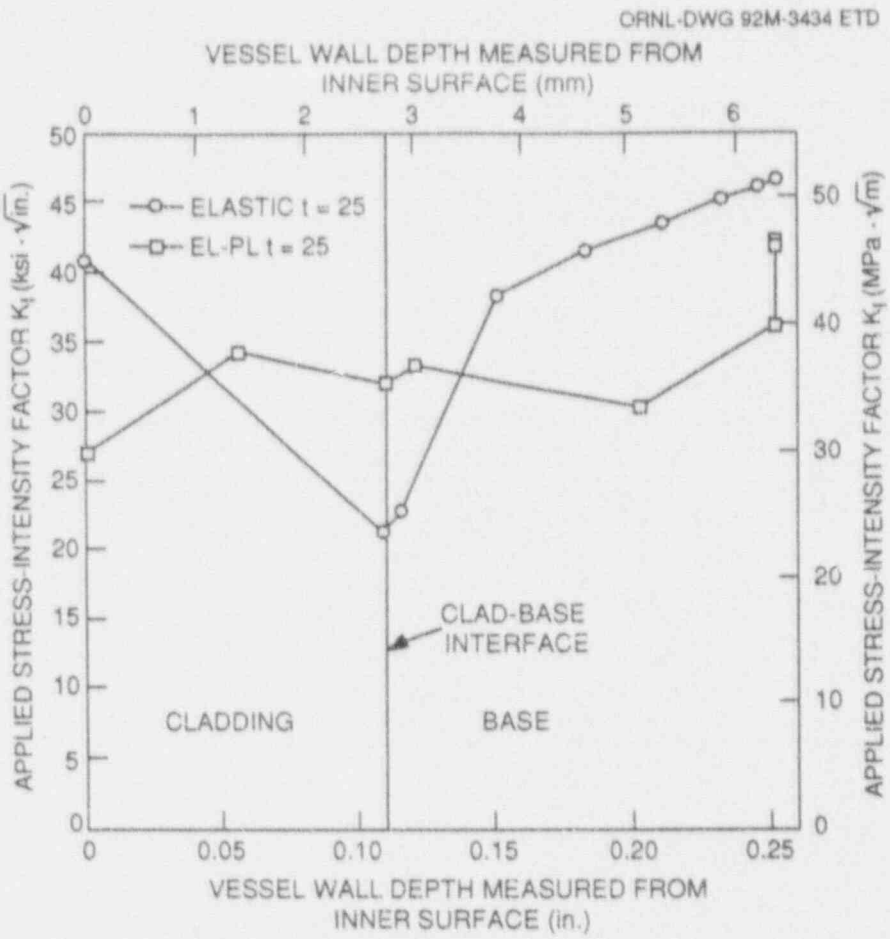

Figure 4.3 **Computed K_I values are sensitive to whether cladding that is modeled as elastic or elastic-plastic, with latter analysis assumption being more realistic. Results are for 25 min into the transient**

5. J. G. Merkle, Union Carbide Corp. Nuclear Div., Oak Ridge Natl. Lab., "Heavy-Section Steel Technology Program Quar. Prog. Rep. July–September 1974," ORNL-TM-4729, Vol. II, pp. 3–22 and 31–32, November 1974.†

---

*Available in public technical libraries.
†Available for purchase from National Technical Information Services, Springfield, VA 22161.
‡Available in NRC Public Document Room.

5 Fracture Analysis Computer Programs

T. L. Dickson*

5.1 Development of New Pressurized-Thermal-Shock (PTS) Vessel Fracture Simulation Code

The current objective of this task is to develop a new, rigorous, validated, quality assured, "user-friendly," modularly designed, self-contained, and well documented computer code for performing reactor vessel probabilistic PTS analysis. The new code will incorporate the best features of existing codes, such as OCA-P[1] and VISA-II,[2] as well as some new features. The new code, named Fracture Analysis of Vessels: Oak Ridge (FAVOR), will provide a fully validated tool for performing the plant-specific vessel fracture analysis for the PTS required by U.S. Nuclear Regulatory Commission, *Regulatory Guide 1.154*.[3]

Work accomplished during this period included the following:

1. Planned the overall structure of the code.
2. Consolidated calculation of the total vessel load response to a specific PTS event (through-wall temperature time histories, stress time histories, and K_I time histories) into one analysis (computer execution).
3. Developed a "user-friendly" input data format for the load analysis.
4. Incorporated the ability to perform a single probabilistic fracture analysis for the entire vessel beltline region, containing any number of flaws, distributed over the beltline region in any user-specified manner. This methodology eliminates any potential for unplanned conservatisms due to "double-counting."
5. Initiated work on a methodology to make the program totally "self contained," that is, to eliminate the need for having to use external files that contain stress-intensity factor influence coefficients.

Each of these five items will be discussed below.

*Computing and Telecommunication Division, Martin Marietta Energy Systems, Inc., Oak Ridge, Tenn.

5.1.1 FAVOR Code Structure

The FAVOR code structure is divided into three main modules: load analysis, deterministic fracture analysis, and probabilistic fracture mechanics (PFM) analysis, as shown in Fig. 5.1. This code structure lends itself to a modular programming approach that will facilitate code maintenance and future code enhancements to incorporate future enhancements and/or fracture technology developments. Also, the output reports from any single fracture analysis

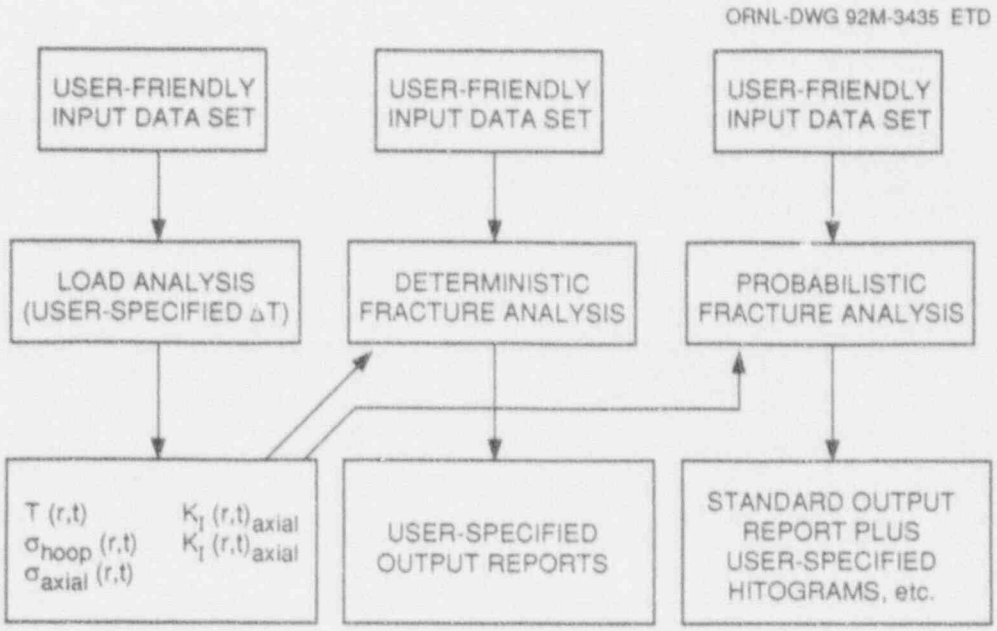

Figure 5.1 FAVOR code structure

can be user-tailored to contain only the desired information.

5.1.2 Consolidation of Vessel Load Response into a Single File

The load analysis consists of accurate validated one-dimensional (1-D) finite-element analyses/solutions for the vessel thermal and stress response and a determination of stress-intensity factors (K_I) using influence coefficients and superposition techniques. All load parameters required to perform a fracture analysis of a reactor vessel subjected to a specific PTS event (thermal analysis, stress analysis, and K_I analysis for both surface axial flaws and surface circumferential flaws) are created in one analysis (computer execution) and are consolidated into a single output file. This user-named load result file will be used as input into any vessel fracture analysis.

The load file can be easily interrogated to give temperature, stress, or K_I time-histories for user-specified location(s) in the vessel wall or through-wall variations at user-specified time(s) in the transient. This type of load data can be retrieved quickly and output in an array format that lends itself to external data packages (LOTUS, CricketGraph, etc.) for further postprocessing and/or graphics. This will be an option in the deterministic fracture module, which has not yet been developed.

The time increment to be used for saving the vessel response parameters is also a user-specified parameter. The results of PFM analyses have shown some sensitivities to the size of the time increment used, particularly for those transients that exhibit sudden load spikes, such as those caused by sudden repressurizations. In any case, this generality allows the user to generate the vessel response at "any time" in the transient.

This structure is more computationally efficient than VISA-II and OCA-P because the load analysis for any PTS scenario has to be executed only one time and the user-named load file repeatedly used as input into any deterministic or probabilistic fracture analysis. This methodology accommodates the usual situation of performing PTS sensitivity analyses for various fracture-related parameters such as chemistries, fluence distributions, flaw densities, etc., for a specified PTS transient definition (vessel load response).

5.1.3 "User-Friendliness" of Load Analysis Input Data

One of the problems with both VISA-II and OCA-P is the lack of user-friendliness regarding input data. The user must spend a considerable amount of time referring to the user manual to determine the record, field location, and format required for input data. Figure 5.2 is an example of input data required to perform a load analysis with the FAVOR code. The input format is key-word, free-format driven, that is, the correct location for input parameters is easily found by using key words (or abbreviations), and the data do not have to be located in specific fields. The dataset may be internally documented because all records that have an asterisk in column 1 are comment cards. The user should almost never have to refer to a user manual to create an input file because the example dataset contains all of the instructions required to create an input dataset. It is a simple matter to modify an existing file to accommodate a new vessel and/or transient scenario using the instructions included in the dataset.

5.1.4 Global PFM Modeling Methodology

Global PFM modeling methodology is the term used to describe the FAVOR ability to perform a PFM analysis for an entire vessel beltline region (or any portion of it) containing any number of flaws in a single probabilistic analysis. This methodology provides the user with a lot of generality for creating a PFM model and also eliminates the potential for double-counting, which is inherent in OCA-P and VISA-II due to adjustments for the correct number of flaws and/or combining results of PFM analyses that were performed for individual beltline regions.

The entire vessel beltline region is modeled by dividing the vessel into major regions such as plates, axial welds, and circumferential welds. Each region can be further divided into subregions. Figure 5.3 shows an example of a vessel beltline layout that is modeled by dividing it into five major regions and subregions as follows:

Major regions	Number of subregions
Upper axial weld	4
Lower axial weld	2
Circumferential weld	10
Upper plate	40
Lower plate	20

Each subregion can be modeled with its own distinguishing fracture-related parameters such as best-estimate "mean"

ORNL-DWG 92-3436 ETD

```
*****************************************************************
*      INPUT DATASET TO DETERMINE THE LOADING ON VESSEL
*      DUE TO PRESSURIZED THERMAL SHOCK (PTS) LOADING
*
*      ALL RECORDS WITH AN ASTERICK(*) IN COLUMN 1 ARE COMMENT CARDS
*      THERE IS NO LIMIT TO THE NUMBER OF COMMENT CARDS ALLOWED IN
*      INPUT DATASET
*
*      IRAD:   INTERNAL RADIUS OF PRESSURE VESSEL (INCHES)
*      W:      THICKNESS OF PRESSURE VESSEL WALL,INCLUDING CLADDING (INCHES)
*      CLTH:   CLADDING THICKNESS (INCHES)
*****************************************************************
GEOM  IRAD=78.0 W=9.31  CLTH=0.156
*****************************************************************
*  THERMAL-ELASTIC MATERIAL PROPERTIES OF CLAD AND BASE
*
*  K:      THERMAL CONDUCTIVITY (BTU/HR-FT-F)
*  C:      SPECIFIC HEAT (BTU/LB F)
*  RHO:    DENSITY (LB/FT**3)
*  E:      MODULUS OF ELASTICITY (KSI)
*  ALPHA:  THERMAL EXPANSION COEFFICIENT ( /F)
*  V:      POISSON'S RATIO
*
*****************************************************************
BASE  K=24  C=0.12  RHO=489  E=28000  ALPHA=.00000800   V=0.3
CLAD  K=10  C=0.12  RHO=489  E=27000  ALPHA=.00000990   V=0.3
*****************************************************************
*           INITIAL TEMPERATURE OF PRESSURE VESSEL AT t=0
*        (WILL BE USED AS STRESS-FREE REFERENCE TEMPERATURE)
*****************************************************************
VITP  TO=550
*****************************************************************
*      TIME PERIOD FOR WHICH ANALYSIS IS TO BE PERFORMED (TOTIME)
*      INCREMENT AT WHICH RESULTS ARE TO BE STORED AND REPORTED (DT)
*            DT SHOULD BE AN INTEGER FACTOR OF TOTIME
*               (ALL TIME ARE IN MINUTES)
*****************************************************************
TIME  TOTIME=120  DT=5
*****************************************************************
*           CONVECTIVE HEAT TRANSFER COEFFICIENTS
*           TIME: MINUTES   h(t): BTU/HR-FT**2-F
*
*        NC=2 PAIRS OF TIME - h(t) P DATA INPUT BELOW
*           (CAN INPUT UP TO 100 PAIRS OF t, H(t) )
*****************************************************************
NHTC  NC=2
      0.00      400.
    120.0       400.
*****************************************************************
*                  PLANT XYZ THERMAL TRANSIENT 123
*                    TIME: MINUTES   T(t): F
*
*        NT=12 PAIRS OF TIME-FLUID TEMPERATURE DATA INPUT BELOW
*                 (CAN INPUT UP TO 100 PAIRS OF t, T(t) )
*****************************************************************
NTTH  NT=12
      0.          550.
      2.          429.
      5.          372.
      7.          311.
     11.          291.
     16.          260.
     29           230.
     45.          195.
     63.          178.
     87.          165.
    109.          159.
    120.          150.
*****************************************************************
*                  PLANT XYZ PRESSURE TRANSIENT 123
*                  TIME:  MINUTES     PRESSURE:  KSI
*
*           NPR=2 PAIRS OF TIME-PRESSURE DATA INPUT BELOW
*              (CAN INPUT UP TO 100 PAIRS OF t, P(t) )
*****************************************************************
NTRP  NPR=2
      0.000     1.0
      120.0     1.0
```

Figure 5.2 Example "user-friendly" input data to FAVOR load analysis module

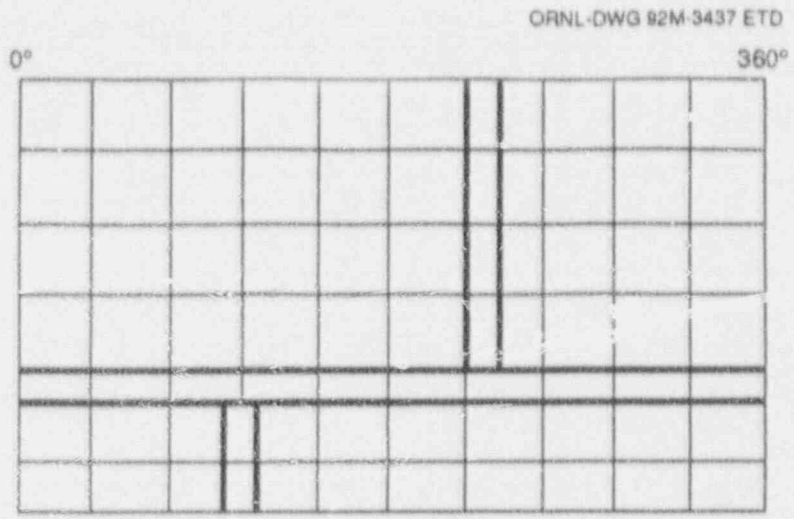

Figure 5.3 Example of PFM global modeling: dividing beltline region into major regions and subregions

chemistry, initial RT_{NDT}, RT_{NDT} shift correlation, flaw orientation, and fluence. This allows the inclusion of very detailed beltline fluence maps and also allows inclusion of axial and circumferential flaws in the same PFM analysis. The total number of flaws in the vessel are proportionally distributed over the vessel beltline by assigning each subregion its own volume and flaw density.

For each vessel analyzed in a Monte Carlo PFM analysis, a flaw is located in a specific beltline subregion, and a value for each critical parameter is sampled from its distribution. The code then steps through the transient time history, and at each time step, the applied K_I at the crack tip is compared with the sampled K_{Ic} at the crack tip. If initiation does not occur, the simulation advances to the next time step. If initiation does occur, the crack tip is extended by a small increment, and the new K_I value is compared to K_{Ia}. If crack arrest does not occur, the crack tip advances another small increment, and again a check is made for arrest. If the crack does arrest, the code continues stepping through time checking for reinitiation. The simulation advances until either the vessel fails or the transient is over. If the vessel does not fail, the code proceeds to locate another flaw in a subregion of the same vessel and repeats the process until one of the flaws either causes vessel failure or none of the flaws result in failure. A simplified logic diagram of this process is shown in Fig. 5.4.

A tentative example output generated by a FAVOR PFM analysis for a beltline region divided into eight major regions is shown in Fig. 5.5. The report is broken into four main parts: global summary, major region summary, average value of key parameters, and flaw size summary. The conditional probability of failure for the entire vessel (reported in the global summary) is the sum of the probability of failure reported for each of the major regions (reported in the major region summary). The major region summary also includes detailed information regarding the flaw distribution, number of initiations, and arrests (total and stable). Additional histogram data will be available upon request.

The global methodology of analyzing the entire vessel for a large number of flaws necessarily involves the simulation of possibly a very large number of flaws in order to converge to solution with an acceptably small error, particularly for those cases having a relatively low probability of failure. An algorithm was developed and incorporated into FAVOR that significantly enhances the computational efficiency. This algorithm identifies those combinations of flaw sizes, beltline subregions, and transient times for which cleavage initiation could not possibly occur, even for the "minimum worst case" prediction of fracture toughness. This eliminates actually analyzing those combinations that could never possibly cause cleavage fracture. The effectiveness of this enhancement increases when evaluating those cases having relatively low probabilities of failure. As can be seen from the example global summary, the number of flaws actually analyzed is considerably less than the number of simulated flaws.

5.1.5 Program Self Containment

A plane was developed to eliminate the need for having to use external files that contain stress-intensity factor influence coefficients, which were generated outside of

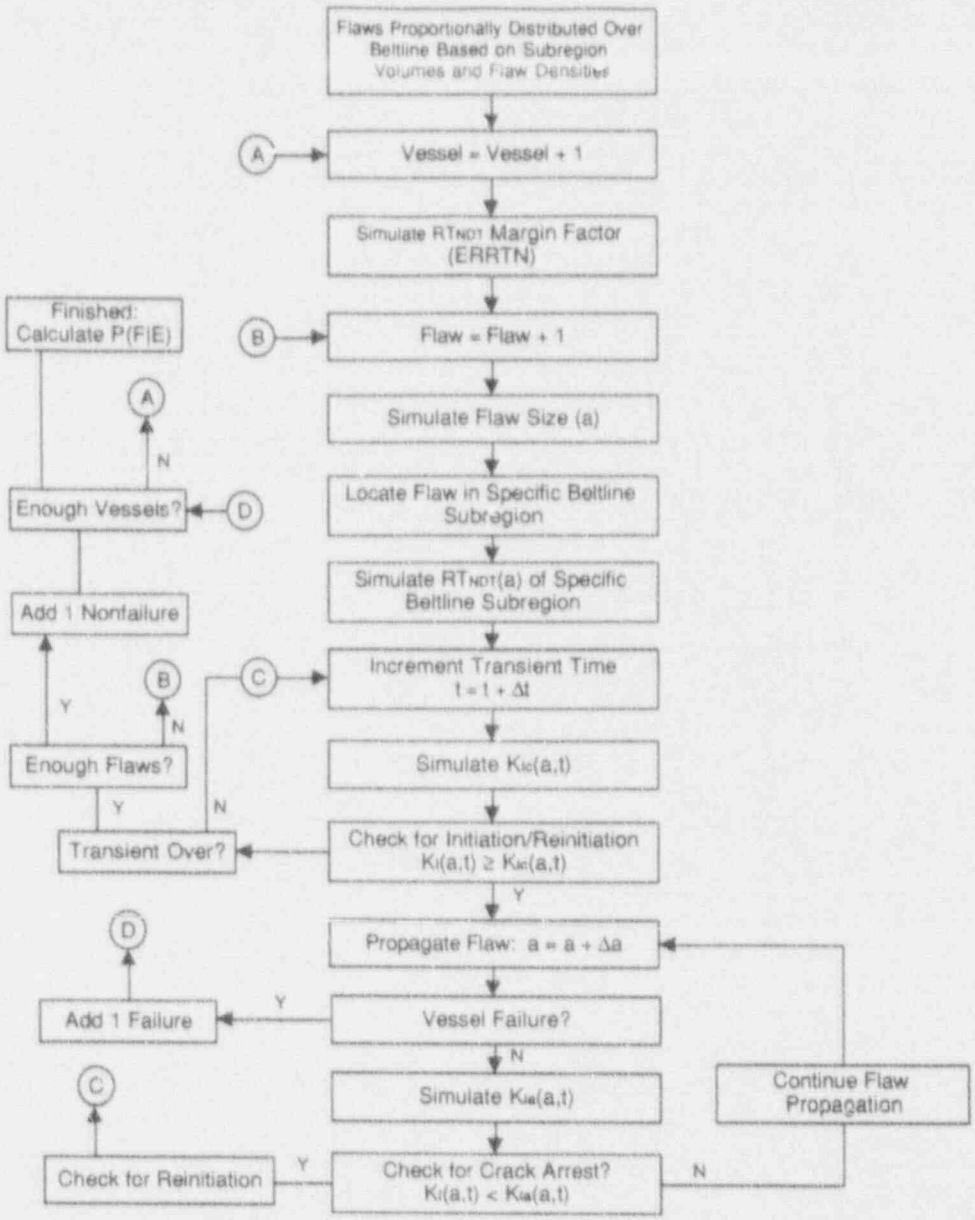

Figure 5.4 Simplified logic diagram of FAVOR global PFM methodology

FAVOR. The plan is to generate a data base of stress-intensity influence coefficients for a range of vessel geometries ($7 < R/t < 12$), which will be contained in FAVOR. The coefficients will be generated using the NQA-1 ABAQUS code.[4] An interpolative routine will be developed so that FAVOR can internally generate the appropriate coefficients for the user-specified vessel geometry. To date, these coefficients have been generated for infinite-length, axial surface flaws for a vessel geometry of $R/t = 10$. Future work will generate the remaining data base for both axial and circumferential infinite-length flaws as well as generate coefficients for three-dimensional (3-D) (finite-length flaws) for a range of vessel geometries and flaw lengths.

5.2 PTS Computer Code Benchmarking Exercise

An Electric Power Research Institute/Nuclear Regulatory Commission (EPRI/NRC)-sponsored exercise of benchmarking different PTS fracture mechanics computer programs was initiated. The Heavy-Section Steel Technology

ORNL-DWG 92-3439 ETD

EIGHT MAJOR VESSEL REGIONS AS FOLLOWS:

1.) UPPER SHELL AXIAL WELDS (3)
2.) NOZZLE SHELL PLATE
3.) UPPER CIRCUMFERENTIAL WELD
4.) INTERMEDIATE SHELL AXIAL WELDS (3)
5.) INTERMEDIATE SHELL PLATE
6.) LOWER CIRCUMFERENTIAL WELD
7.) LOWER SHELL AXIAL WELDS (3)
8.) LOWER SHELL PLATE

FLUENCE DISTRIBUTION FOR 40 EFPY
4.5 FLAWS/CUBIC METER FOR PLATE REGIONS
45. FLAWS/CUBIC METER FOR WELD REGIONS

TOTAL NUMBER OF FLAWS IN VESSEL= 39.969

TYPE I MARK-PRESTRESS NOT CONSIDERED IN ANALYSIS

PFM TIME STEPPING INCREMENT = 5 MINUTES

MONTE CARLO CONVERGENCE: PER CENT ERROR = 4.704330

PFM GLOBAL SUMMARY

NUMBER OF SIMULATED VESSELS	=	80000
NUMBER OF VESSEL WHICH INITIATE	=	1757
NUMBER OF VESSEL FAILURES	=	1699
NUMBER OF VESSEL NONFAILURES	=	78300
PROBABILITY OF INITIATION	=	0.021962
PROBABILITY OF FAILURE	=	0.021238
NUMBER OF SIMULATED FLAWS	=	3086510
ACTUAL SIMULATED FLAWS	=	952453
NUMBER OF INITIAL INITIATIONS	=	1760
TOTAL NUMBER OF ARRESTS	=	134
TOTAL NUMBER OF STABLE ARRESTS	=	61

MAJOR REGION SUMMARY

MAJ REG	REGION FLAWS	SIMULATED FLAWS	INITIAL INITIATIONS	ARRESTS TOTAL	ARRESTS STABLE	FAILED VESSELS	FLAWS PER FAILURE	P(F|E)
1	0.311	23928	25	0	0	25	16.20	0.000312
2	5.251	404944	14	0	0	14	13.86	0.000175
3	2.589	200407	38	35	22	16	17.88	0.000200
4	2.352	181264	1305	35	9	1296	19.39	0.016200
5	23.668	1827692	151	7	6	145	19.21	0.001812
6	2.589	200063	65	55	23	42	17.45	0.000525
7	0.621	47950	160	2	1	159	20.45	0.001988
8	2.589	200262	2	0	0	2	16.50	0.000025

AVERAGE VALUE OF KEY PARAMETERS

	ALL	INITIAL INITIATION	FAILURE
ERRTN:	-0.001	1.292	1.292
SCU :	0.122	0.154	0.154
SFID :	4.010	3.745	3.775
SIZE :	+0.163	0.496	7.062
ERKIC:	1.000	0.782	0.801
KI	:	59.551	496.223
TIME	:	73.688	75.533
TEMP	:	244.208	327.038

FLAW SIZE SUMMARY

INITIAL LAW SIZE	NUMBER SIMULATED	% OF TOTAL	NUMBER INITIATED	% OF INITIAL INITIATIONS	NUMBER FAILED	% OF FAILURES
0.085	2134057	69.1	0	0.0	0	0.0
0.263	687937	22.3	566	32.2	547	32.2
0.458	198820	6.4	655	37.2	633	37.3
0.671	51161	1.7	342	19.4	329	19.4
0.904	11639	0.4	148	8.4	141	8.3
1.159	2349	0.1	34	1.9	34	2.0
1.437	446	0.0	13	0.7	13	0.8
1.742	88	0.0	2	0.1	2	0.1
2.076	13	0.0	0	0.0	0	0.0

Figure 5.5 Example output generated by FAVOR PFM analysis

(HSST) Program is an active participant in this exercise, the objective of which is to identify and resolve differences in results and methodologies between the various PTS fracture computer codes presently in use. Westinghouse, Combustion Engineering, Babcock and Wilcox, Pacific Northwest Laboratories, and private consultants are also participants in this on-going exercise. The HSST Program is using the FAVOR code to solve all benchmark problems.

During this report period, two meetings were held. In the first meeting, a sample prototypical PTS baseline problem was chosen and Phase I of the benchmarking exercise defined. The objective of Phase I is mutual validation of the deterministic and probabilistic solutions to the baseline problem. After mutual validation is achieved for Phase I, the benchmarking exercise will include identifying and resolving differences in methods used to model the effect of additional PTS sensitivity considerations, such as the inclusion of the mechanical effects of cladding, flaw shape, flaw distribution, etc.

In the second meeting, several exercise participants presented their results to the Phase I baseline problem. The tentative conclusion is that most, but not all, of the participants appeared to agree reasonably well regarding the deterministic solutions; however, there appeared to be more divergences in the probabilistic solutions.

More precise comparisons and discussions of the Phase I solutions and a definition of Phase II benchmark problems are to be presented at the next PTS benchmarking meeting to be held in San Antonio on May 6, 1992.

5.3 Paper Presented at 1992 NRC Aging Conference

T. L. Dickson was the senior author of a paper entitled "The Application of Probabilistic Fracture Analysis to Residual Life Evaluation of Embrittled Reactor Pressure Vessels" that was presented on March 25 at the NRC Aging Conference.

References

1. R. D. Cheverton and D. G. Ball, Union Carbide Corp. Nuclear Division, Oak Ridge Natl. Lab., "OCA-P, A Deterministic and Probabilistic Fracture Mechanics Code of Application to Pressure Vessels," USNRC Report NUREG/CR-3618 (ORNL-5991), May 1984.*

2. F. A. Simonen et al., Pacific Northwest Lab., Richland, Wash., "VISA II—A Computer Code for Predicting the Probability of Reactor Pressure Vessel Failure," USNRC Report NUREG/CR-4486 (PNL-5775), March 1986.*

3. U.S. Nuclear Regulatory Commission, Regulatory Guide 1.154, "Format and Content of Plant-Specific Pressurized Thermal Shock Safety Analysis Reports for Pressurized Water Reactors."†

4. *ABAQUS User Manual*, Version 4-9-1, Hibbit, Karlsson & Sorenson, Inc., Providence, Rhode Island, 1991.

*Available for purchase from National Technical Information Services, Springfield, VA 22161.

†Available in NRC Public Document Room for inspection and copying for a fee.

6 Cleavage Crack Initiation

T. J. Theiss

This task emphasizes cleavage initiation toughness and the specimens that are used to evaluate cleavage fracture toughness. The task was begun in FY 1990 and is currently divided into five subtasks: (6.1) Shallow-Crack Fracture Toughness Testing, (6.2) Gradient Effects on Fracture Toughness, (6.3) Thickness Effects on Fracture, (6.4) Biaxial Specimen Testing, and (6.5) Lower-Bound Initiation Toughness.

6.1 Shallow-Crack Fracture-Toughness Program

Currently, the Shallow-Crack Fracture-Toughness Program is divided into two areas. (1) the HSST Shallow-Crack Fracture-Toughness Testing Program, and (2) the full-thickness shallow-crack clad beam tests. The HSST Shallow-Crack Fracture-Toughness Testing Program has been ongoing since FY 1990, producing data by testing 100-mm-deep (4-in.) single-edge notch bend specimens.[1–4] The shallow-crack full-thickness clad beam tests were initiated during this report period and will test 230-mm-thick (9-in.) clad beams taken from a cancelled nuclear plant.

6.1.1 Heavy-Section Steel Technology (HSST) Shallow-Crack Fracture-Toughness Testing Program [T. J. Theiss, T. S. Rolfe (University of Kansas)]

The HSST Shallow-Flaw Program is a joint experimental/analytical program that has produced a limited data base of shallow-flaw fracture-toughness values and analyses to aid in the transferability of the specimen data to an RPV. The experimental portion of the program was divided into two phases: a development phase and a production phase. All testing was conducted on three-point-bend specimens with a beam depth of ~100 mm (4 in.) The beams were taken from the homogeneous center of the source plate with the crack oriented in the thickness (S) direction. The development phase established the techniques appropriate for shallow-crack testing, verified the existence of a shallow-flaw effect in A 533 B steel, and compared beams of three thickness from which to choose the most appropriate thickness for the production phase of the program. The production phase developed a limited data base of shallow-crack toughness values as prototypic as possible of reactor pressure vessel (RPV) pressurized-thermal-shock (PTS) conditions. All HSST shallow-crack fracture toughness testing at Oak Ridge National Laboratory (ORNL) has been completed. During this report period, the production data were reanalyzed based on the final measured crack depths and the techniques established during the development phase of the program.

A summary of the experimental results of the program is reported later in this section. Analytical results are included in the report on Task 2.

Critical crack-tip-opening displacement (CTOD) (δ_c) and J-integral (J_c) toughness expressions were determined for each test from available crack-mouth-opening displacement (CMOD) and load-line-displacement (LLD) data, respectively. Because J_c and δ_c, are related according to $J_c = m\,\sigma_f\,\delta_c$, where m is the constraint parameter and σ_f is the flow stress (average of yield and tensile strength),[5] additional checks on the test data were made. The constraint parameter m was determined for each test and found to average 1.5 for deep-crack tests and 1.1 for shallow-crack tests. The δ_c data were converted to K_c according to $K_c = \sqrt{(m \cdot \sigma_f \cdot \delta_c \cdot E')}$, where m = 1.5 and m = 1.1 and $E' = E/(1 - \nu^2)$. Comparison of K_c from the J-integral and δ_c calculations reveals very consistent results (see Table 6.1).

The toughness data expressed in terms of critical stress-intensity factor (K_c) vs temperature are presented in Table 6.1 and Fig. 6.1 along with the material characterization curve. These data show a significant increase in the fracture toughness for shallow-crack specimens in the transition region of the A 533 B toughness curve. All of the specimens failed in cleavage except the data point indicated in Fig. 6.1 with the arrow. As expected, the shallow-crack specimens on the lower shelf where plane-strain behavior occurs showed little to no toughness increase. All of the specimens had crack depths that were deep (~50 mm) or shallow (~10 mm) except for one beam with a crack depth of 14 mm. This intermediate crack-depth specimen also appears to show a shallow-crack toughness elevation.

Toughness data are plotted as a function of beam thickness for all of the tests conducted at $T - RT_{NDT} = -25°C$ (–45°F) and –11°C (–20°F) in Fig. 6.2. As indicated in Figs. 6.1 and 6.2, the toughness values for the shallow- and

Table 6.1 HSST shallow-crack test data

HSST beam No.	S (mm)	B (mm)	W (mm)	a (mm)	a/W	Failure load (kN)	CTOD total (mm)	J integral (MPa-mm)	K_c from CTOD (MPa·$\sqrt{m}$)	K_c from J (MPa·$\sqrt{m}$)
Development phase										
3	406	51	100	10.0	0.10	600.0	0.586	261	282	243
4	406	51	100	51.8	0.52	128.1	0.048	42	97	97
5	406	51	99	51.2	0.52	139.7	0.049	48	97	105
6	406	51	100	51.9	0.52	184.6	0.117	102	151	152
7	406	51	94	10.2	0.11	483.5	0.137	92	140	145
8	406	51	94	9.6	0.10	657.4	0.476	284	262	215
9	406	51	94	9.5	0.10	552.4	0.352	173	225	198
10	406	51	94	14.0	0.15	489.3	0.235	143	184	180
11	406	102	94	8.4	0.09	472.4	0.196	101	168	152
12	864	102	95	49.8	0.53	116.5	0.061	50	109	106
13	864	102	94	8.8	0.09	501.7	0.657	208	226	218
14	864	152	93	8.7	0.09	723.2	0.346	225	222	139
15	864	153	94	8.7	0.09	684.1	0.146	85	145	
16	864	153	94	50.0	0.53	170.4	0.060	46	108	102
Six deep-crack beams phase										
12A	406	102	94	51.0	0.54	251.8	0.077	60	120	117
13A	406	102	94	50.8	0.54	293.1	0.111	86	144	140
14A1	406	51	93	50.2	0.54	135.2	0.121	93	150	145
14A2	406	51	93	50.8	0.55	102.7	00.43	39	90	94
15A	406	153	94	50.7	0.54	435.0	00.84	79	133	134
16A	406	153	94	51.9	0.55	348.3	00.62	51	107	108
Production phase										
17	610	102	102	52.6	0.52	245.1	0.116	96	142	148
18	610	101	102	10.6	0.10	777.1	0.466	238	251	233
20	610	101	101	10.8	0.11	823.3	1.733	985	473	472
21	610	101	102	10.7	0.11	724.1	0.306	152	202	186
22	610	101	102	10.9	0.11	793.5	0.942	564	349	358
24	610	102	102	52.0	0.51	269.1	0.367	268	253	247
25	610	102	102	52.0	0.51	238.4	0.110	85	144	139
26	610	102	102	11.0	0.11	740.1	0.355	175	222	200
27	610	101	102	10.7	0.11	787.3	0.559	242	274	235
28	610	101	102	10.3	0.10	832.7	1.242	786	400	422
31	610	102	102	51.5	0.51	205.5	0.063	51	109	108
32	610	102	102	11.1	0.11	417.7	0.018	20	55	68
33	610	102	102	10.7	0.11	339.8	0.010	13	42	53
34	610	101	102	10.4	0.10	431.0	0.019	21	57	70
35	610	102	102	51.7	0.51	244.2	0.121	95	146	147
36	610	102	102	51.6	0.51	176.1	0.042	35	89	89
37	610	102	102	10.8	0.11	745.9	0.263	135	191	175
38	610	102	102	10.8	0.11	755.3	0.206	106	170	155

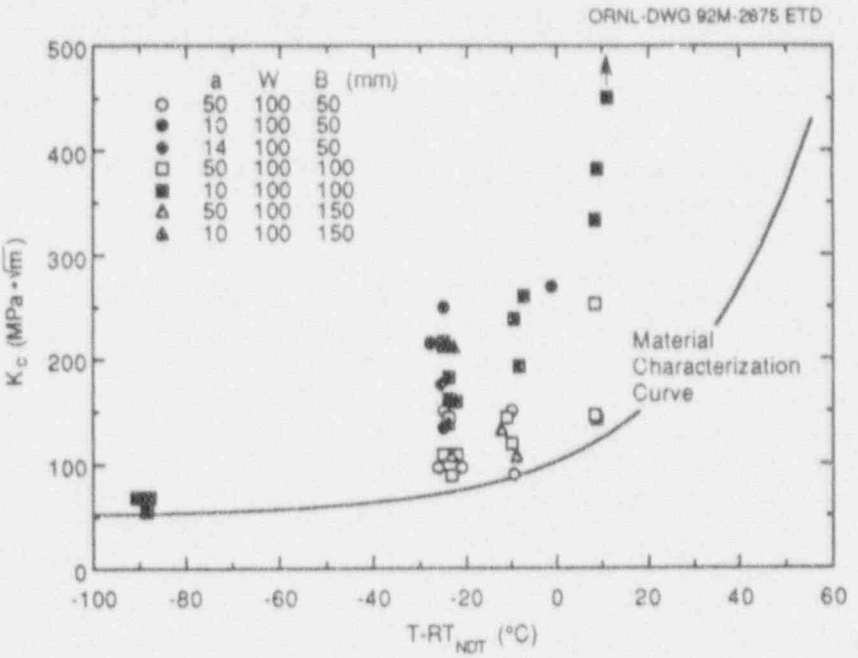

Figure 6.1 All toughness (K_c) data vs normalized temperature for the shallow- and deep-crack specimens

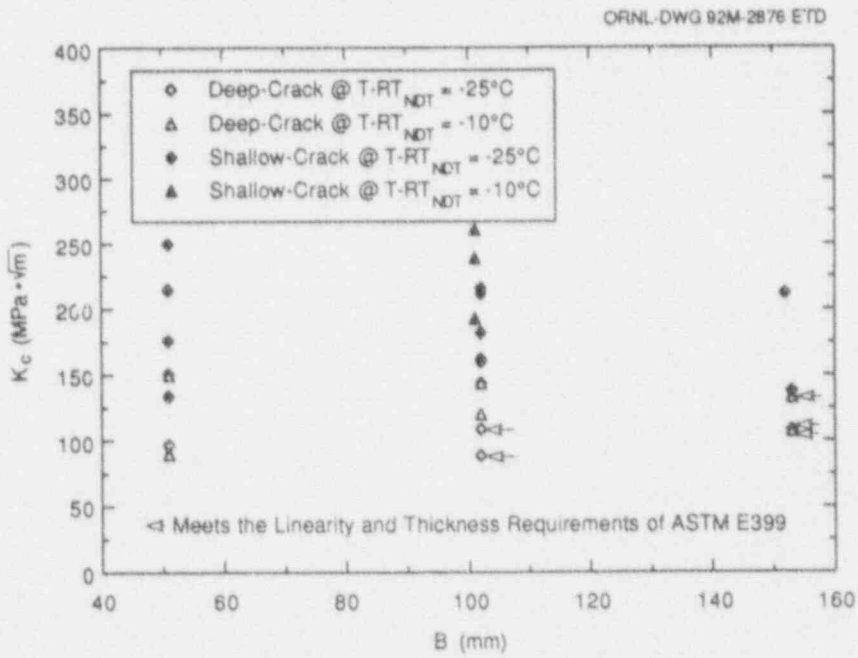

Figure 6.2 Toughness (K_c) data vs beam thickness for shallow- and deep-crack specimens at T = 60°C, –45°C, and –40°C

deep-crack specimens from the 100- and 150-mm-thick (4- and 6-in.) beams generally are consistent with the 50-mm-thick (2-in.) data. However, there appears to be slightly more data scatter associated with the 50-mm-thick (2-in.) beams than with the 100- and 150-mm-thick (4- and 6-in.) beams. It is interesting to note that the lowest shallow- and deep-crack toughness values were both from beams with the least thickness (B = 50 mm). None of these deep-crack tests strictly meet the requirements of American Society of Mechanical Engineers ASTM E399 for a valid K_{Ic} result

due to insufficient crack depth (a = 50 mm). The beams that had linear-elastic test records and are sufficiently thick for valid results per ASTM E399 are marked in Fig. 6.2.

The shallow-crack toughness increase can be quantified in terms of a ratio of toughness values at one temperature or a temperature shift. The ratios of the shallow-to-deep lower-bound δ_c at T = –60°C (–75°F) and –40°C (–40°F) are 2.4 and 4.9, respectively, which are consistent with the A36 and A517 results from the University of Kansas.[6,7] In terms of K_c, the shallow-crack toughness increase is ~60% at T = –60°C (–75°F). Figure 6.3 shows the shallow- and deep-crack test data with approximate lower-bound curves. The shallow-crack lower-bound curve was formed using the deep-crack curve and a temperature shift of 35°C (63°F). The shifted deep-crack lower-bound curve fits the shallow-crack data well at all test temperatures.

6.1.2 Shallow-Crack Full-Thickness Clad Beam Tests (T. J. Theiss)

Current RPV life assessments are based on data from deep-flaw fracture-toughness specimens. These specimens are tested in the L-T orientation and taken from the center homogeneous region of the source plate, which yields a toughness significantly different from the actual material toughness in an RPV. The limiting condition of the RPV is most often governed by PTS accident conditions. Reactor vessel analyses are based on the Marshall flaw[8] distribution and the U.S. Nuclear Regulatory Commission, *Regulatory Guide 1.154*.[9] The Marshall flaw distribution predicts more small than large flaws, while *Regulatory Guide 1.154* requires that all flaws be considered as surface flaws. The shallow-surface flaw is therefore of major importance in RPV life assessments.

As discussed in Sect. 6.11, shallow-flaw specimens cut from homogeneous plate material have been shown to exhibit an effective toughness greater than that shown in deep-crack specimens. Shallow flaws in an RPV, however, are located near the plate surface where large metallurgical gradients exist. Axial flaws in an RPV are oriented in the L-S material direction rather than the L-T orientation. These metallurgical differences may have a significant impact on the resulting fracture toughness.

To quantify the fracture toughness of shallow flaws in reactor vessels, several full-thickness, clad beams will be tested under prototypic PTS conditions. The flaws in these beams will be located in material in which metallurgical conditions are prototypic of those found in RPVs. Comparison of results from these tests with those from homogeneous shallow-flaw test specimens will provide a quantitative definition of the effect of near-surface conditions on fracture toughness. The effective fracture toughness from these large beams will also be compared with the

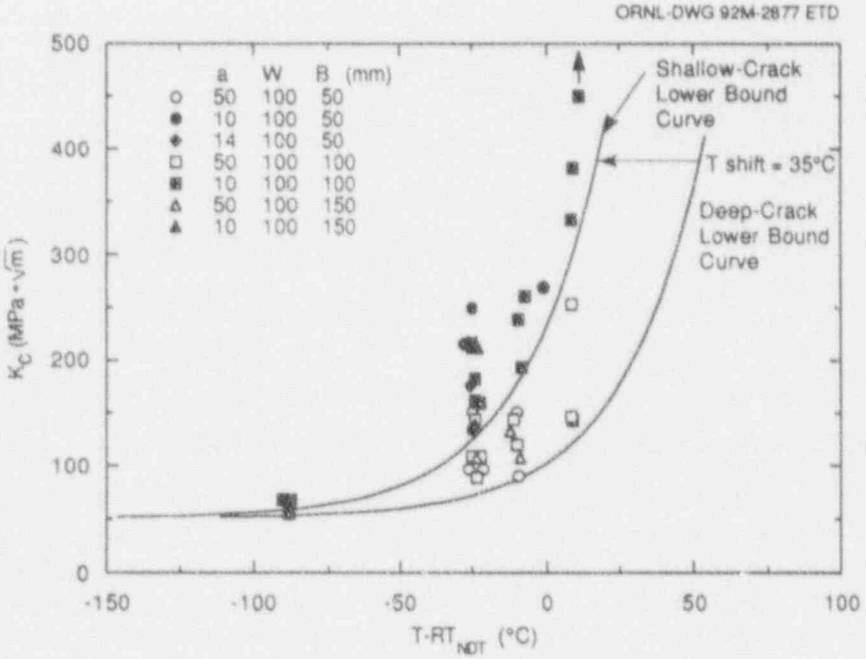

Figure 6.3 All toughness (K_c) data vs normalized temperature for shallow- and deep-crack specimens with shallow- and deep-crack lower bound curves

toughness as determined by current ASME Sect. XI rules. The objective of these tests, therefore, is to determine the fracture toughness of prototypic, clad, full-thickness RPV weld and plate material with shallow flaws. Three-point-bend specimens with a 230- by 230-mm (9- by 9-in.) cross section will be tested to simulate RPV loading conditions. Figure 6.4 shows the full-thickness clad beam with pertinent dimensions.

The source plate of the specimens is A 533 grade B class 1 steel with stainless steel cladding. This material was taken from a cancelled pressurized-water reactor (PWR) vessel. The plate material, cladding, and weldment are completely prototypic of a production quality RPV. ORNL plans to determine the transition region for the weld in the L-S orientation using Charpy specimens and generate stress-strains curves at the appropriate test temperature for the weldment.

One development beam and two test beams will be tested during FY 1992, each with the flaw located in axial weld material. The development beam shall be tested to verify and validate the testing procedures for the other tests. The first test beam (i.e., the development beam) will be deep-cracked (a/W = 0.5). If the development beam test produces usable test data, then that test will be considered test beam 1, and test beams 2 and 3 will be tested as shown in the first table below. If the development beam does not produce usable test data, then one deep- and one shallow-crack beam will be tested at the depths shown in the second table below. The crack depths, a, shown below for the beams, are after fatigue precracking. The shallow-flaw depths will simulate possible vessel conditions even though the notch tip will not be located in the cladding. However, the results should provide valuable information regarding the behavior of full-thickness prototypic vessels with cladding. The tentative test temperature for all three beams has been set at –46°C (–50°F), which is at or below the nil-ductility temperature (NDT) for this material. Final test temperature will be determined following material characterization.

These results assume that the development beam produces usable test data.

Test beam	Crack depth, a [mm (in.)]	a/W
1 (development)	114 (4.50)	0.50
2	23 (0.09)	0.10
3	10 (0.40)	0.04

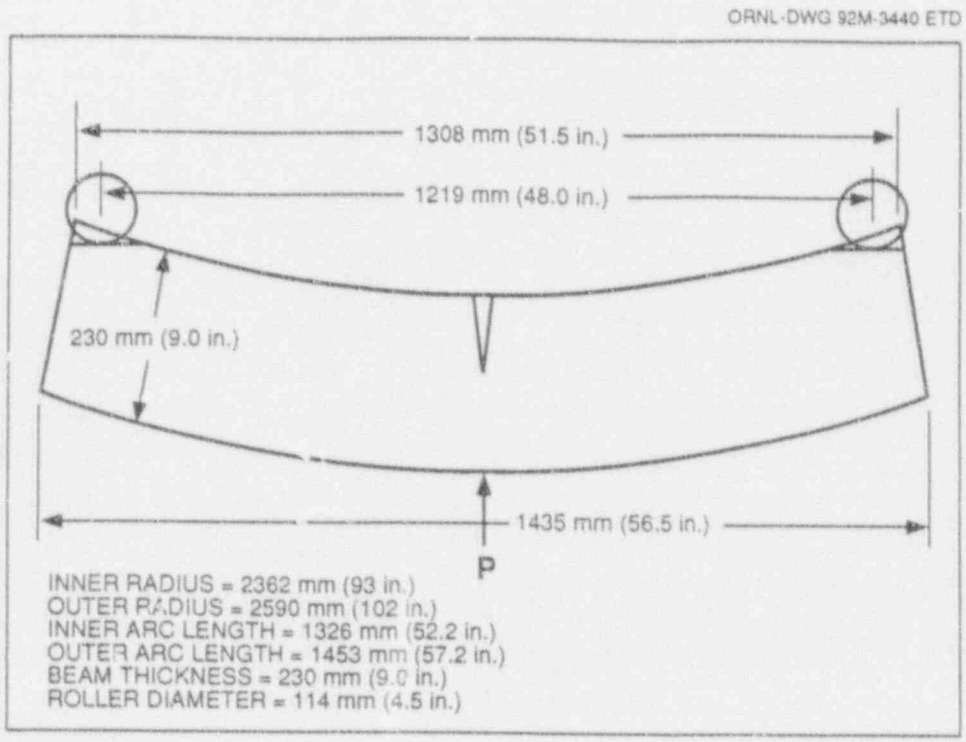

Figure 6.4 Full-thickness clad beam specimen

Cleavage

These results assume that the development beam does not produce useable test data.

Test beam	Crack depth, a [mm (in.)]	a/W
1 (development)	114 (4.50)	0.50
2	114 (4.50)	0.50
3	15 (0.60)	0.07

During the current reporting period, the test specification for the full-thickness, clad-beam tests was issued. The specification (Spec. No. HSST-H10-92-001, Rev. 1) will be subject to formal change control procedures and revised as needed so that the final test specification will reflect the conditions of the test. Details of the contract and testing aspects of the full-thickness, clad-beam tests are discussed in Chap. 10. Pretest analysis of the full-thickness clad beams and cladding evaluations will begin soon as a part of Task 7, Cladding.

6.2 Gradient Effects on Fracture Toughness (G. R. Irwin, X. J. Zhang—University of Maryland, College Park)

A report entitled "Gradient Study of a Large Weld Joining Two Forged A 508 Shells of the Midland Reactor Vessel" has been forwarded to ORNL by the University of Maryland to be issued as NUREG/CR-5867 (ORNL/Sub-79-7778/10). A summary of the findings is given here.

As a portion of the HSST study of the influence of metallurgical gradients on toughness, a slab containing a large weldment and the adjacent nuclear vessel steel was examined. The weldment joined two forged shells of A 508 steel through a wall thickness of 317 mm (12.5 in.). The specimen came from the Midland reactor. Attention was given to local regions where grain coarsening and hardness elevation indicated low toughness relative to initiation and spreading of cleavage (as shown in Fig. 6.5). As would be expected, regions of that type were observed in the A 508 heat-affected zone (HAZ) adjacent to each weld run layer.

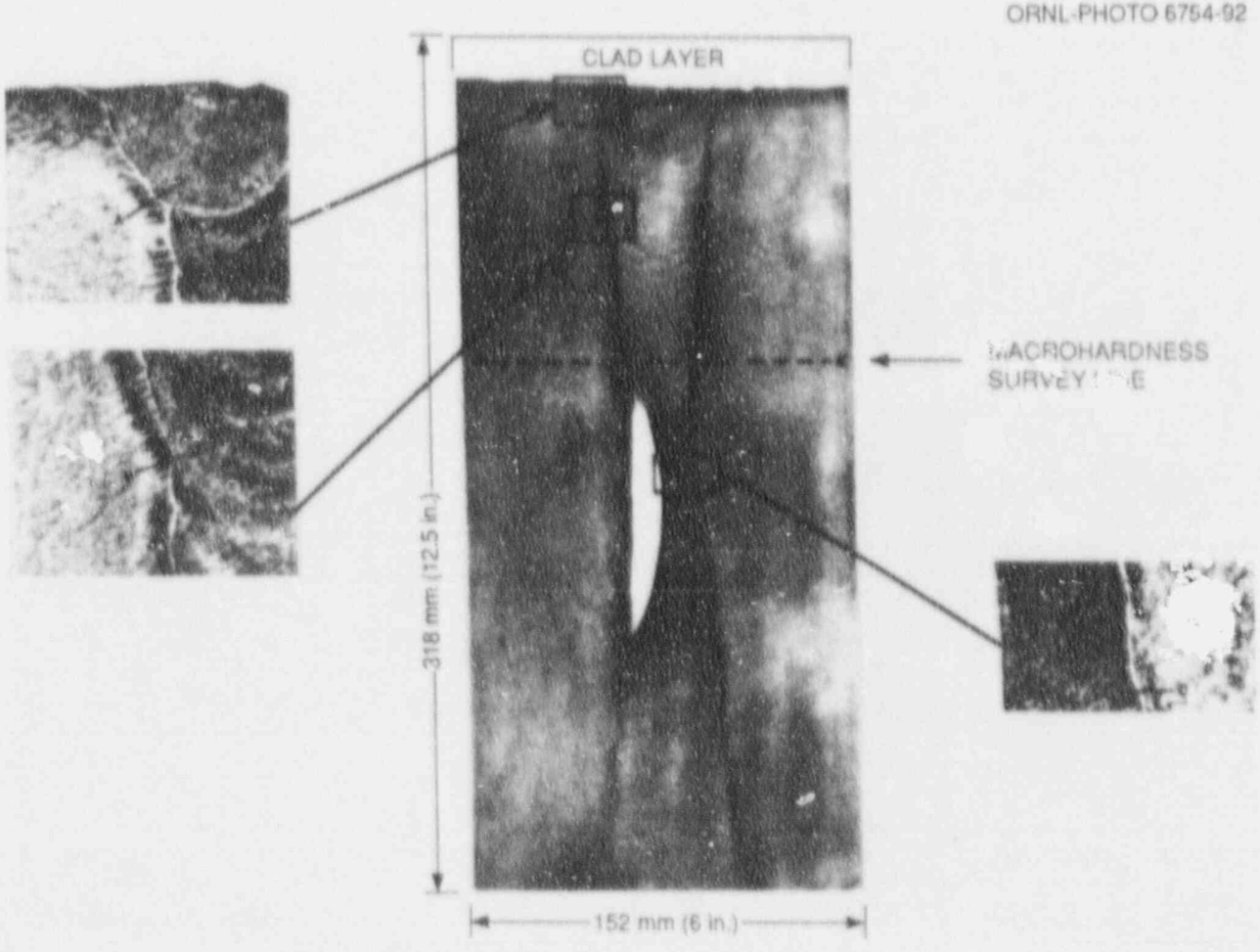

Figure 6.5 Macrostructure of midland weld section

The severity was largest where the carbide density in the A 508 was locally elevated by carbide banding. Figure 6.6 shows the results from microhardness indents across a region of that kind and roughly normal to the fusion boundary. The microhardness numbers within the weld (WF67) and the A 508 (beyond 3 mm from the fusion line) are typical for those materials remote from the HAZ. The tensile strength estimate for the 2.5-mm (0.1-in.) region with HV 300 hardness is nearly 965 MPa (140 ksi). The reported tensile strength for the A 508 shell was 676 MPa (98 ksi). Previous austenite grain sizes in the range 150 to 250 μm are frequent in these weld border HAZ regions.

One might consider the possibility for a complete fracture to form through a sequence of separations within the HAZ. However, experience with weld border fractures has rarely shown this to occur. The most dangerous local HAZ region is the one adjacent to the topmost layer of welding, close to a free surface, and, often, with a notch-type stress elevation due to crowning of the weldment. In the section examined, the weld surface had been smoothed even with the shell surface. However, application of cladding supplied a number of small undercladding cracks and a HAZ region at least as large and severe as that shown in Fig. 6.6.

Figure 6.7 shows microstructure and microhardness indents across the boundary between the cladding and A 508 steel. Figure 6.8 shows a portion of this boundary region after repolishing and etching to increase visibility of grain boundaries in the cladding. The small cracks in the A 508 appear to be separations on previous austenite grain boundaries and to connect with austenite grain boundaries in the cladding. Figure 6.9 provides the microhardness results in graphical form. A very narrow strip of cladding at the fusion boundary has a microhardness of HV 400. However, this region of penetration of the small cracks in the A 508 through that region were not visible. A narrow strip of the cladding covering the low carbon weld metal showed an equal degree of hardness elevation. Reheat of the weld metal by the cladding process did not produce a HAZ of significant severity, and no small cracks were observed in that region. Because of its location, close to a free surface, to small cracks, and to the HAZ region beneath the cladding, the A 508 HAZ region adjacent to the topmost weld run may be the region most likely to assist cleavage fracture initiation.

6.3 Biaxial Specimen Testing (T. J. Theiss)

Current RPV life assessments are most often limited by PTS accident conditions. The fracture resistance for an RPV is based on K_{Ic} and K_{Ia} fracture-toughness curves, which are developed using specimens with zero out-of-plane strain (i.e., plane-strain conditions). However, PTS loads produce both a significant positive stress perpendicular to the crack and a significant positive out-of-plane stress along the crack front for circumferential and axial flaws. Out-of-plane stresses cause an increase in the hydrostatic stress to deviatoric adjacent to the crack-tip plastic zone.[10] The increase in the hydrostatic to deviatoric stress ratio outside the plastic-zone infers (1) an increase in the

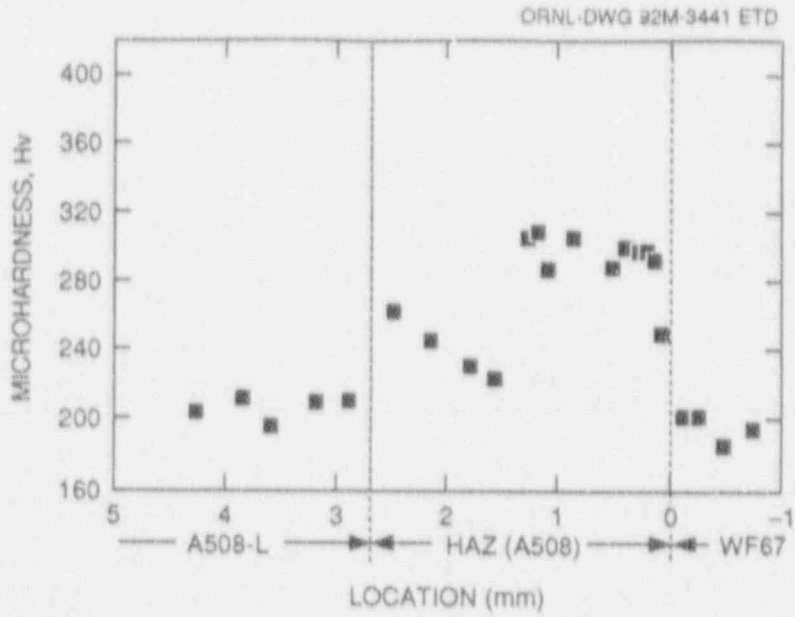

Figure 6.6 Microhardness results along line B in WF67 and the A 508-L HAZ

ORNL-PHOTO 6755-92

Figure 6.7 Microhardness indents in cladding and in A 508-L HAZ produced by cladding process

ORNL-PHOTO 6756-92

Figure 6.8 Enlargement of Fig. 6.6 after repolishing and etching to enhance grain boundaries in cladding

maximum principal stress within the crack-tip plastic zone and (2) a decrease in the ductility of the material. The stress-state at the crack-tip is influential on the resulting fracture toughness.[10]

Experimental evidence of the influence of out-of-plane stress on fracture toughness can be found by comparing HSST shallow-crack data (see Sect. 6.1.1) and previous HSST thermal-shock data.[11] Recent testing on 100-mm-deep (4-in.) single-edge-notch-bending (SENB) specimens has shown an increase in the toughness associated with shallow-flaw specimens in the transition region over conventional, deep-flaw specimens. These specimens were tested under uniaxial conditions. However, thermal-shock data also tested in the transition region and with shallow cracks showed little to no increase in toughness over those from deep-crack results. Thermal-shock tests (like PTS transients) create significant out-of-plane stresses along the crack-tip that are absent in fracture-toughness tests. The implication is that the thermal-shock test data include two offsetting effects: the shallow-crack effect, which elevates the fracture toughness; and an out-of-plane (biaxial) stress effect, which reduces the toughness.

Because two potential offsetting effects have been identified, the influence of positive out-of-plane stress on fracture toughness needs to be understood. To determine the influence of out-of-plane stresses prototypic of those in an RPV during a PTS event on toughness, the HSST Program is planning to conduct a series of out-of-plane biaxial loading fracture-toughness tests. The objective of these tests is to determine the influence of out-of-plane loading on the effective fracture toughness of RPV plate material. Large double-tension specimens with a test section measuring 610 × 610 × 127 mm (24 × 24 × 5 in.) thick and a 3-D surface flaw are being investigated for potential use in these tests.

To ensure that the biaxial test conditions are prototypic of those conditions in an RPV during a PTS transient, the following conditions must be met:

1. The throat of the test section must remain elastic at the point of failure (i.e., linear-elastic fracture-mechanics conditions must apply).
2. Yield strength and transition temperature (RT_{NDT}) of the test material (A 533 B) must simulate irradiated material properties. The minimum allowable yield is 621 MPa (90 ksi); the target RT_{NDT} is –7°C (20°F).

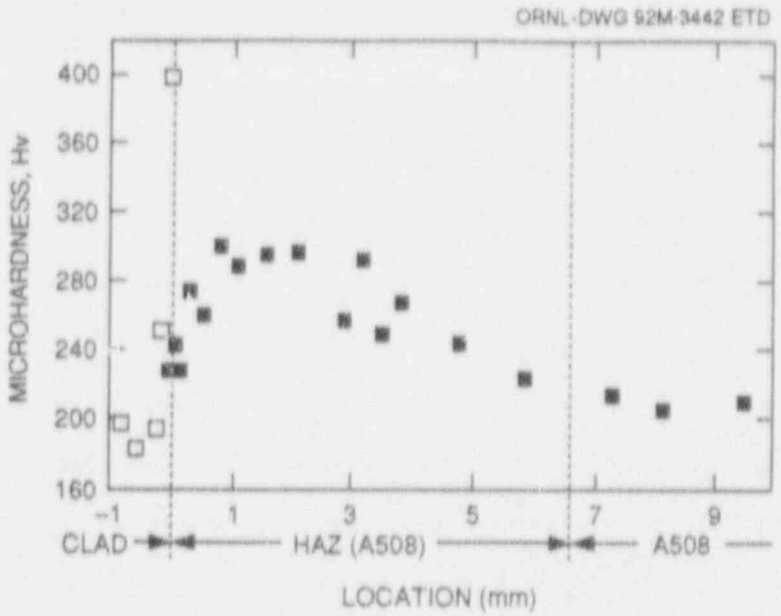

Figure 6.9 Microhardness results for Fig. 6.6 shown in graph form

3. The test temperature must be in the low transition region ($T - RT_{NDT} = -25°C$). Most PTS initiations take place in the low transition region. In addition, fracture phenomenon such as biaxial effects would not be expected on the lower shelf.
4. Biaxial loading ratio must be equibiaxial (1:1).

The far-field stress at the point of failure must be ~345 MPa (50 ksi). To be able to interpret the biaxial data, possible alternate influences (metallurgical gradients, shallow-crack effects, etc.) must be eliminated. For this reason, both the uniaxial and biaxial tests are planned to be performed with identical double-tension specimens. To enhance a lower-bound initiation result, the flaw must be as long as possible. Finally, to ensure that initiation can take place, sufficient crack driving force must be attained within load limits of the test machine. A K_I/K_{Ic} ratio of 2.5 is required based on small-specimen characterization data.

ORNL initially plans to test two specimens, with additional specimen testing at a later date. The first specimen is planned to be loaded in uniaxial tension, and the second specimen will be loaded in equibiaxial tension. Both specimens will be tested at the same temperature. Identical specimens will be used for both of these tests. The test temperature for these tests will be selected such that the K_{Ic} is ~71 MPa•$\sqrt{m}$ (65 ksi•$\sqrt{in.}$). Current characterized A 533 B material has a toughness of 71 MPa•$\sqrt{m}$ (65 ksi•$\sqrt{in.}$) at a temperature ≈25°C (45°F) below RT_{NDT}. It is anticipated that RT_{NDT} for the heat-treated material will be between 4 and –17°C (40 and 0°F), resulting in a test temperature above –40°C. The heat treatment development will determine whether the test temperature is above or below –40°C. The final test temperature will be determined following material characterization. The flaw configuration for both beams will be identical with the maximum notch depth, a = 61 mm (2.4 in.). Fatigue precracking should extend the flaw ~2.5 mm (0.1 in.) along the bottom.

During this reporting period a test specification for the out-of-plane biaxial loading tests was prepared. The specification (Spec. No HSST-H10-92-002) has not yet been issued but will be when questions concerning the final specimen and fixture design are completed. Additional information on the test specimen design and analysis is included in Chap. 2. Details of the fabrication of a specimen for the biaxial tests and interaction with a testing vendor are included in Chap. 10.

6.4 Lower-Bound Initiation Toughness (J. W. Dally, G. R. Irwin, X. J. Zhang, R. J. Bonenberger—University of Maryland)

A report entitled "The Influence of Precompression on the Lower-Bound Initiation Toughness of A 533 B Reactor-Grade Steel" has been forward to ORNL by the University of Maryland to be issued as NUREG/CR-5847 (ORNL/Sub-79-7778/8). A summary of the findings is given here.

Cleavage

The lower-bound initiation toughness (K_{Id}) of two different heats of A 533 B reactor-grade steel was determined over temperatures in the brittle-to-ductile transition region. The lower-bound toughness was measured by depressing the initiation toughness with dynamic loading, high constraint offered by notched round bars, and axial precompression of the material in the fracture process zone. The effect of the amount of precompression on cleavage initiation and K_{Id} was examined at two temperatures ($T^* = 43$ and 65°C) where $T^* = T - RT_{NDT}$.

Results for the cleavage initiation toughness for the two different heats of A 533 B reactor-grade steel are shown in Figs. 6.10 and 6.11. In both figures, the temperature T^* is relative to RT_{NDT}, which was –2 and –23°C (28 and –9°F) for heats 1 and 2, respectively. The results from the notched round-bar tests are compared with toughness determinations made by others using different specimens that were larger in size. These determinations include PTSE-1, ORNL TSE, COOP program, and the round-robin experiments.[12]

The data from the notched round bar compares favorably with the initiation toughness determined in the other test programs except for the ORNL TSE, which generally gave higher values. The scatter in the data from the notched round bar was somewhat smaller than the scatter observed in the round robin crack-arrest testing.

The amount of precompression required to minimize ductile tearing increases with the temperature T^*. For heat 1 of A 533 B steel with $RT_{NDT} = 2$°C (28°F), it was observed that the amount of precompression required ranged from 0.4 mm (0.016 in.) at $T^* = -5$°C (–9°F) to 1.2 mm (0.047 in.) as T^* increased to 52°C (94°F). However, it should be noted that the application of this amount of precompression did not ensure cleavage initiation in every test. Instead, the effect of the precompression was to increase to probability of cleavage initiating from several sites with a very small extension of the crack by ductile tearing.

The amount of precompression required for specimens fabricated from heat 2 of A 533 B steel, with $RT_{NDT} = -23$°C (–9°F) was examined in more detail. At $T^* = 43$°C (77°F), cleavage initiation occurred for precompressions ranging from 0.36 to 1.35 mm (0.014 to 0.053 in.), although the useful range of precompression is much smaller. The K_{Id} associated with cleavage initiation appeared to depend on the amount of precompression. Specimens with precompressions of 0.7 to 0.9 mm (0.028 to 0.035 in.) gave valid measures of K_{Id}. Specimens having precompressions <0.7 mm (0.028 to 0.035 in.) gave valid measures of K_{Id}. Specimens having precompressions <0.7 mm (0.028 in.)

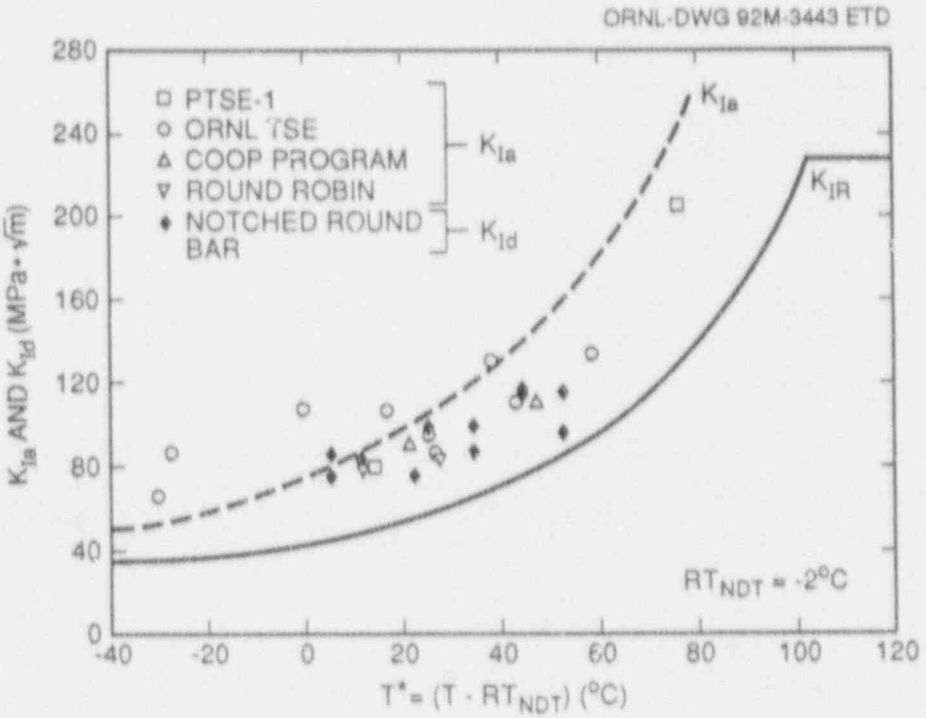

Figure 6.10 Lower-bound initiation toughness as a function of temperature T* for A 533 B reactor-grade steel, heat No. 1 with $RT_{NDT} = -2$°C

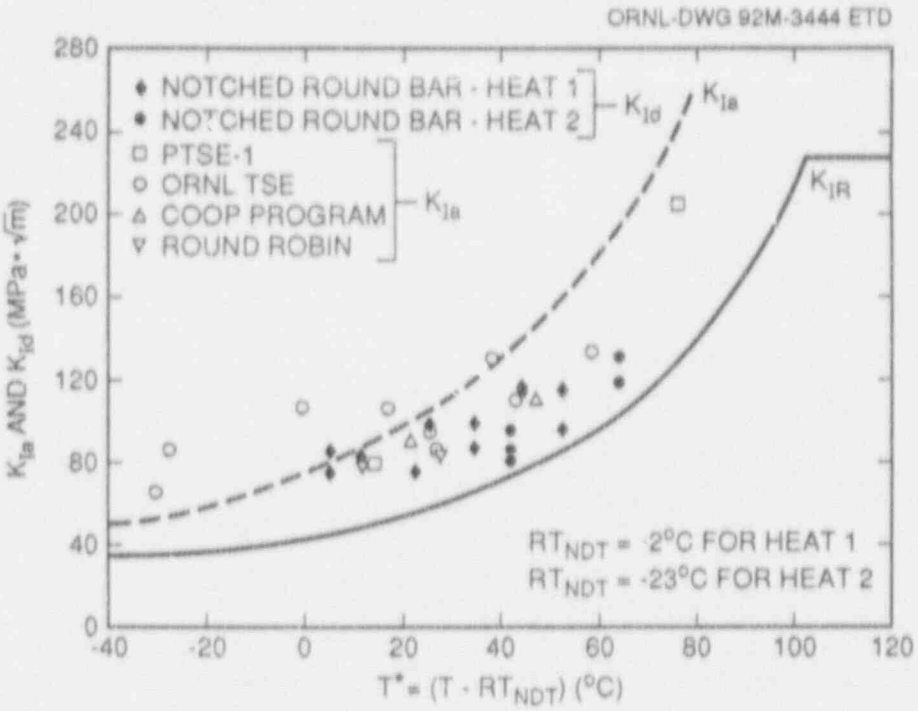

Figure 6.11 Lower-bound initiation toughness as a function of temperature T^* for A 533 B reactor-grade steel, heat Nos. 1 and 2

did not reliably initiate cleavage, and specimens with precompressions >0.9 mm (0.035 in.) initiated cleavage prematurely (i.e., at artificially low stress fields).

As the temperature increased to $T^* = 65°C$ (117°F), the initiation toughness increased, and the range of precompression required to determine a valid K_{Id} increased from 1.5 to 1.6 mm (0.059 to 0.063 in.). In this set of experiments, it was noted that the cleavage initiation toughness and the tearing initiation toughness were about the same.

The notched-round-bar test procedure provides an inexpensive method to determine lower-bound initiation toughness with relatively small scatter. Measurements of the lower-bound toughness were made with A 533 B reactor-grade steel, a relatively tough material, to a temperature $T^* = 65°C$ (117°F). The lower-bound toughness varied from 74 to 130 MPa•$\sqrt{m}$ (67 to 118 ksi•$\sqrt{in.}$) as the temperature T^* was increased from 5 to 65°C (9 to 117°F).

References

1. T. J. Theiss, Martin Marietta Energy Systems, Inc., Oak Ridge Natl. Lab., "Recommendations for the Shallow-Crack Fracture Toughness Testing Task Within the HSST Program," USNRC Report NUREG/CR-5554 (ORNL/TM-11509), August 1990.*

2. T. J. Theiss, G. C. Robinson and S. T. Rolfe, "Preliminary Test Results from the Heavy-Section Steel Technology Shallow-Crack Toughness Program," *Proceedings of the ASME Pressure Vessel & Piping Conference*, PVP Vol. 213/MPC-Vol. 32, pp. 125-129, Pressure Vessel Integrity, ASME, 1991.†

3. T. J. Theiss and J. W. Bryson, "Influence of Crack Depth on the Fracture Toughness of Reactor Pressure Vessel Steel," presented at the ASTM Symposium on Constraint Effects, May 18, 1991, Indianapolis, Ind.

4. S. T. Rolfe, University of Kansas for Martin Marietta Energy Systems, Inc., Oak Ridge Natl. Lab., "The Behavior of Shallow Flaws in Reactor Pressure Vessels: Status Report," USNRC Report NUREG/CR-5767 (ORNL/Sub/90-SH640/1), November 1991.*

5. J. M. Barsom and S. T. Rolfe, *Fracture and Fatigue Control in Structures*, Prentice-Hall, Englewood Cliffs, N.J., 1987.

6. W. A. Sorem, R. H. Dodds, Jr., and S. T. Rolfe, "An Analytical Comparison of Short Crack and Deep Crack CTOD Fracture Specimens of an A36 Steel," *WRC Bulletin 351*, Welding Research Council, New York, NY 10017, February 1990.†

7. J. A. Smith and S. T. Rolfe, "The Effect of Crack Depth to Width Ratio On the Elastic-Plastic Fracture Toughness of a High-Strength Low-Strain Hardening Steel," *WRC Bulletin 358*, Welding Research Council, New York, NY 10017, November 1990.†

8. W. Marshall, "An Assessment of the Integrity of PWR Pressure Vessels," October 1976.‡

9. U. S. Nuclear Regulatory Commission, *Regulatory Guide 1.154*, "Format and Content of Plant-Specific Pressurized Thermal Shock Safety Analysis Reports for Pressurized Water Reactors."§

10. W. E. Pennell, HSST Program: Recent Developments in Crack Initiation and Arrest Research," in *Proc. of the U.S. Nuclear Regulatory Commission Nineteenth Water Reactor Safety Meeting, Rockville, Md., October 28–30, 1991*, USNRC Report NUREG/CP-0119, Vol. 1, April 1992.

11. R. D. Cheverton, S. K. Iskander, and D. G. Ball, "Review of Pressurized-Water-Reactor-Related Thermal Shock Studies," *Fracture Mechanics: Nineteenth Symposium, ASTM STP 969*, T. A. Cruse, ed., American Society for Testing and Materials, Philadelphia, 1988, pp. 7520–766.†

12. D. B. Barker et al., University of Maryland for Martin Marietta Energy Systems, Inc., Oak Ridge Natl. Lab., "A Report on the Round Robin Program Conducted to Evaluate the Proposed ASTM Standard Test Method for Determining the Plane-Strain Crack-Arrest Toughness, K_{Ia}, of Ferritic Materials," USNRC Report NUREG/CR-4966 (ORNL/Sub/79-7778/4), 1988.*

---

*Available for purchase from National Technical Information Service, Springfield, VA 22161.

†Available in public technical libraries.

‡Available from U.S. Government Printing Office, Washington, D.C. 20402. ATTN: Regulatory Guide Account.

§Available in NRC Public Document Room for inspection and copying for a fee.

7 Cladding Evaluations

J. Keeney-Walker*

7.1 Objective

Cladding effects are regarded as one of the fracture technology issues with significance for reactor pressure vessel (RPV) fracture-margin-safety assessments under pressurized-thermal-shock (PTS) loading conditions. The objective of this task is to achieve a more comprehensive representation of the effects of cladding in the probabilistic analysis of vessel fracture. Specific parameters of interest are (1) the effects of irradiation on the toughness of cladding, (2) the possibility of fracture-mode conversion due to high strain rates associated with a propagating crack, (3) the propensity for ductile tearing of shallow through-clad surface cracks in low-toughness cladding, and (4) the potential role of cladding in inhibiting the initiation and longitudinal propagation of finite-length surface cracks.

During this report period, analytical studies have continued to assess the overall effects of cladding on the fracture behavior of small surface cracks in an RPV subjected to an overcooling accident. A methodology is being developed and validated to include these effects in the probabilistic fracture analysis computer codes. This study will later be used to assess the need for additional thermal-shock tests.

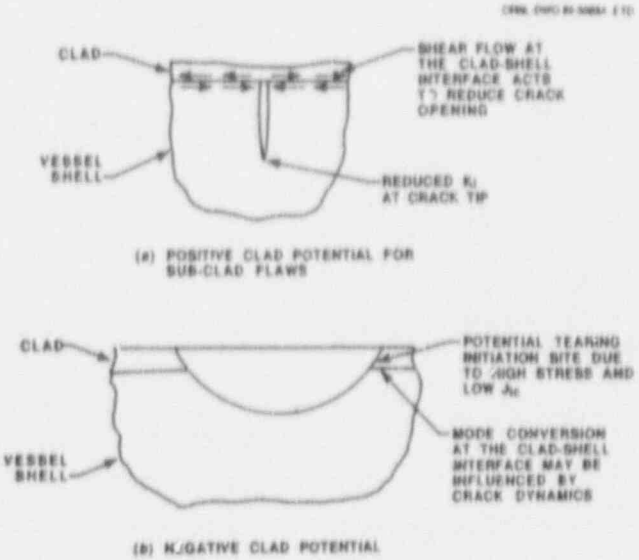

Figure 7.1 **Effect of vessel cladding not yet fully included in reactor vessel PTS analysis models (OCA-P). Additional research is required to determine if their introduction will have net positive or negative effect on calculated reactor vessel failure probability**

7.2 Introduction

Cladding has typically been regarded as a tough inner skin to the reactor vessel with a capability to impart an additional increment of fracture margin by acting to reduce the crack-tip opening of submerged cracks. This condition is illustrated in Fig. 7.1(*a*). While thermal expansion and heat transfer properties of the stainless steel cladding were included in the PTS analysis of Ref. 1, effects of the enhanced cleavage fracture toughness of cladding were conservatively neglected.

Data generated recently in the reactor materials irradiation program (detailed in Ref. 2) have raised a concern relative to a possible negative effect of cladding on pressure vessel fracture margins during a PTS event. The concern derives from the low ductile tearing toughness of irradiated cladding. Figure 7.2 shows the test results of concern. Tearing toughness of irradiated stainless steel cladding is similar to that of irradiated low-upper shelf (LUS) weld material and substantially less than that of irradiated A 533 grade B vessel shell material. A concern exists that tearing could initiate in the cladding and convert to cleavage fracture at the cladding-base material interface. Strain-rate effects induced by the initial tearing process may be greater than strain rates associated with steady-state tearing. These effects add to the cleavage fracture-initiation concern.

The objective for this phase of the study is to define combinations of conditions that will or will not result in crack initiation. The variables in this parameter study include PTS transient, flaw geometry, clad thickness, and RT_{NDT}.

7.3 Cladding Analysis

Semielliptical surface cracks having length-to-depth ratios of 6:1, 3:1, and 2:1 and depths of 25.4 to 38.1 mm (1.0 to 1.5 in.) were evaluated in this study. The three-dimensional (3-D) finite-element model of the cylinder is shown in Fig. 7.3. The RPV has an inner radius of 1979 mm

*Computing and Telecommunications Division, Martin Marietta Energy Systems, Inc., Oak Ridge, Tenn.

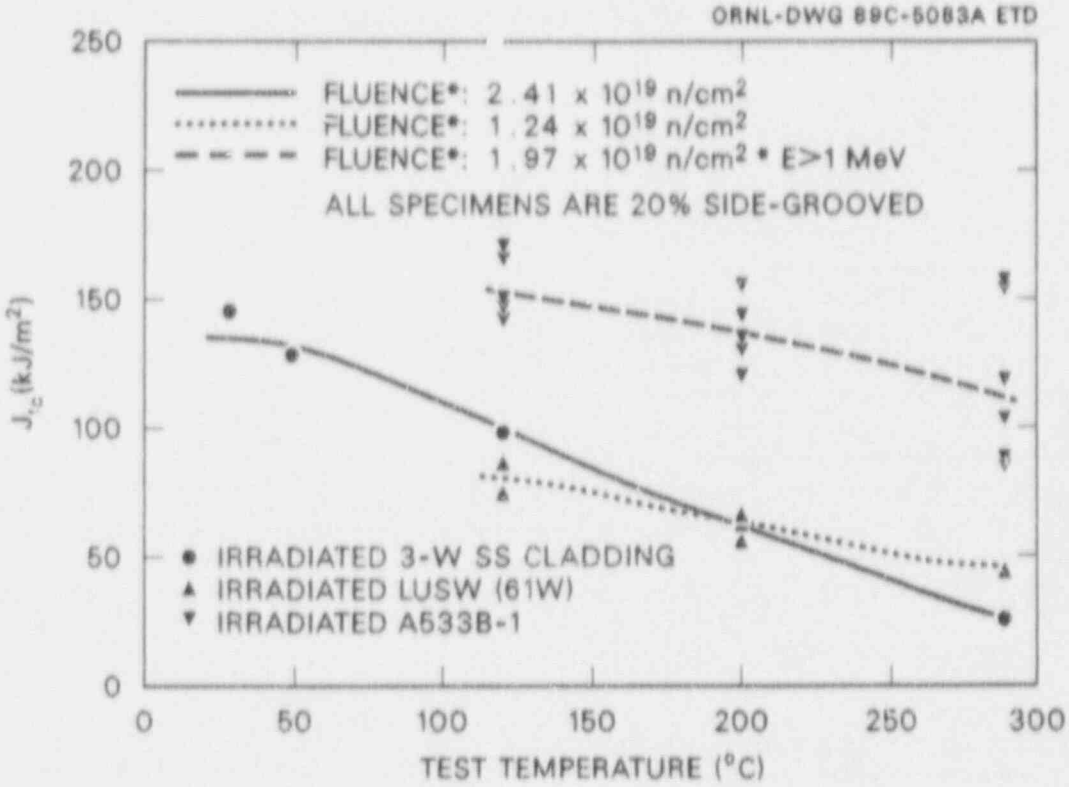

Figure 7.2 Recently completed tests to measure the ductile tearing toughness of reactor vessel materials showing ductile-tearing initiation toughness of both LUS weld materials and cladding in irradiated conditions to be approximately half that of irradiated A 533 B material

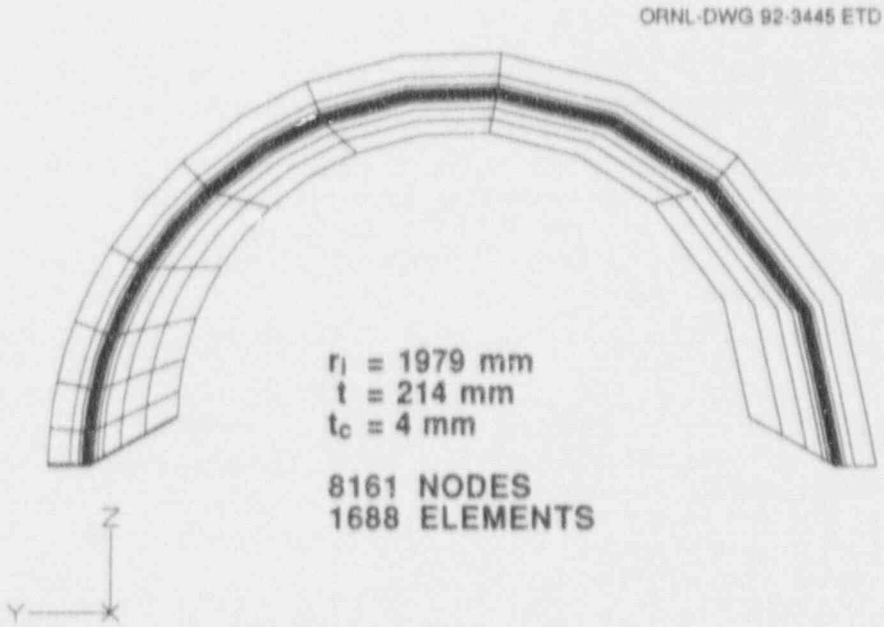

Figure 7.3 3-D finite-element model of cylinder used to evaluate the effects of cladding on crack initiation under PTS-transient loading

(77.91 in.), a wall thickness of 218 mm (8.58 in.), and a cladding thickness of 4.1 mm (0.16 in.). Generalized plane-strain boundary conditions were imposed on the surface of the model opposite to the symmetry plane to simulate the closed end of an RPV. Mechanical and physical properties for irradiated three-wire cladding and A 533 B steel were used for the cladding and base material, respectively.

Transient pressure and temperature loading used in the thermoelastic analyses are given in Fig. 7.4. The loading condition time histories shown in this figure were derived from an idealization of the Rancho Seco PTS transient. Therefore, they provide a realistic basis for assessing the potential for crack initiation under PTS loading conditions.

Values of applied J are plotted as a function of the angle around the crack (0°—surface and 90°—deepest point of the crack) in Figs. 7.5 and 7.6 for the 6:1 and 2:1 flaw, respectively. From these figures one can observe that the applied J values are larger at the deepest part of crack for the 6:1 flaw, whereas J is larger at the surface for the 2:1 flaw.

In Fig. 7.7, values of applied K at the deepest point in the 25.4-mm flaw are shown for three aspect ratios and an infinite-length flaw (generated by OCA-P). The *American Society of Mechanical Engineers Boiler and Pressure Vessel (ASME B&PV) Code*, Sect. XI, fracture-toughness curves (-2σ) for an RT_{NDT} of 132°C (270°F) and an estimated -3σ curve are shown superimposed on the applied K curves in Fig. 7.7. The K values do not intersect the fracture-toughness curves, so crack initiation would not be expected. An analysis was also performed with OCA-P with the results included in Fig. 7.7. Because OCA-P assumes an infinite flaw, the K values are much higher than the finite-length flaws and predict crack initiation.

The results for the three-flaw configurations are compared with the ASME fracture-toughness curves for an RT_{NDT} of 146°C (295°F) in Fig. 7.8. In this case, the 6:1 flaw K values intersect the -3σ fracture-toughness curve because the material toughness decreases with increasing RT_{NDT}. The choice of RT_{NDT} has an impact on crack initiation predictions.

In Figs. 7.9 and 7.10, the K values of the three flaws at the clad/base interface are plotted with the ASME fracture-toughness curves with an RT_{NDT} of 132 and 146°C, respectively. The K values of the 2:1 and 3:1 flaws are now higher than the 6:1 flaw because it is closer to the surface. Also the fracture-toughness curves are slightly lower because the temperatures are lower at the inner surface. The applied K curves for the 2:1 and 3:1 flaws intersect the -3σ curve in Fig. 7.9 and the -2σ curve in Fig. 7.10. The 6:1 flaw curve intersects the -3σ curve in Fig. 7.10.

Estimated lower-bound J_R toughness curves for cladding, LUS-weld metal, and A 533 B plate material are shown superimposed on the applied J curves in Figs. 7.11 and 7.12. These material toughness curves were derived from

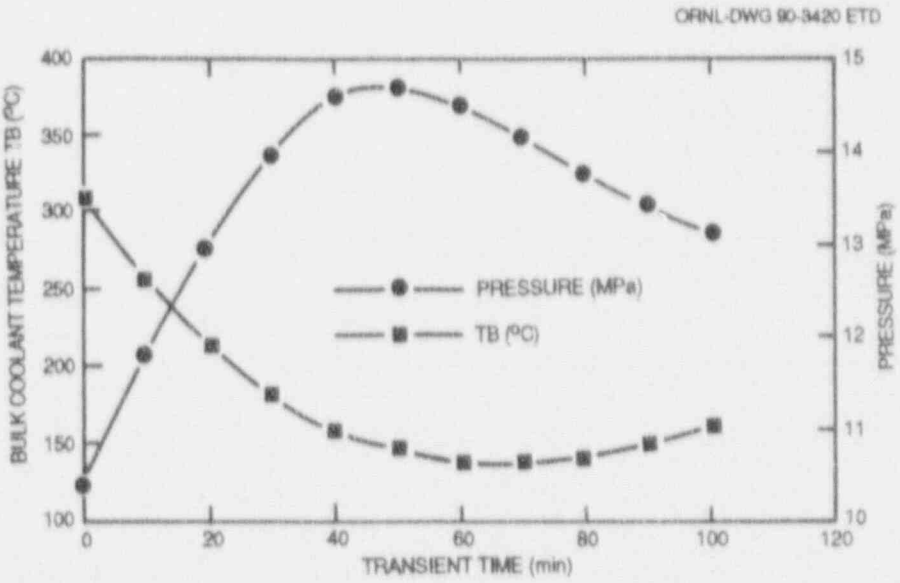

Figure 7.4 Rancho Seco PTS transient used in preliminary evaluation of effect of cladding on crack initiation in surface flaws

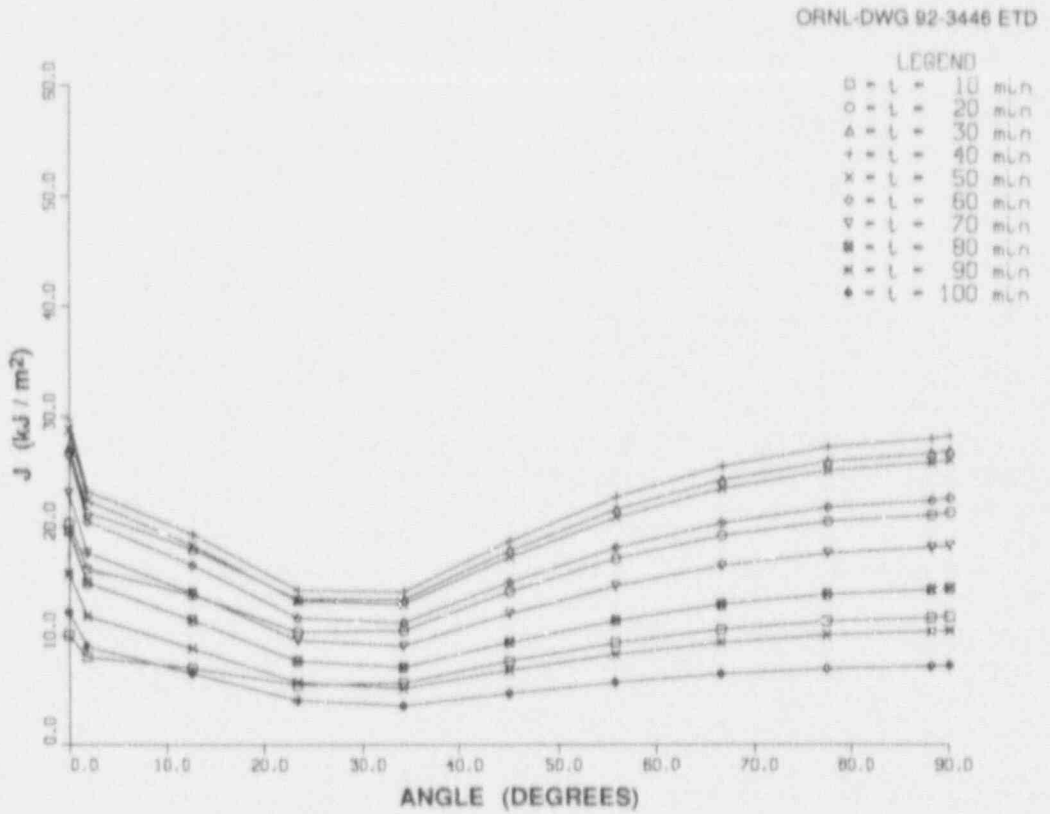

Figure 7.5 J vs angle for a 6:1 flaw and 25.4-mm depth for various times in transient

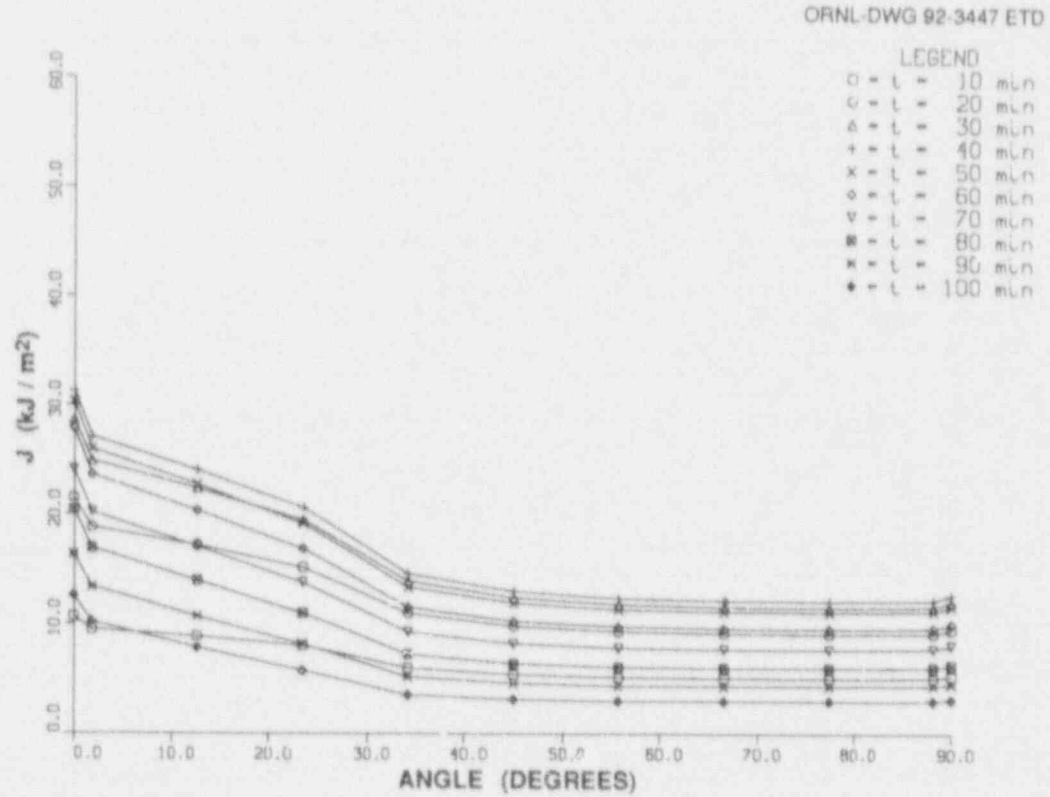

Figure 7.6 J vs angle for a 2:1 flaw and 25.4-mm depth for various times in transient

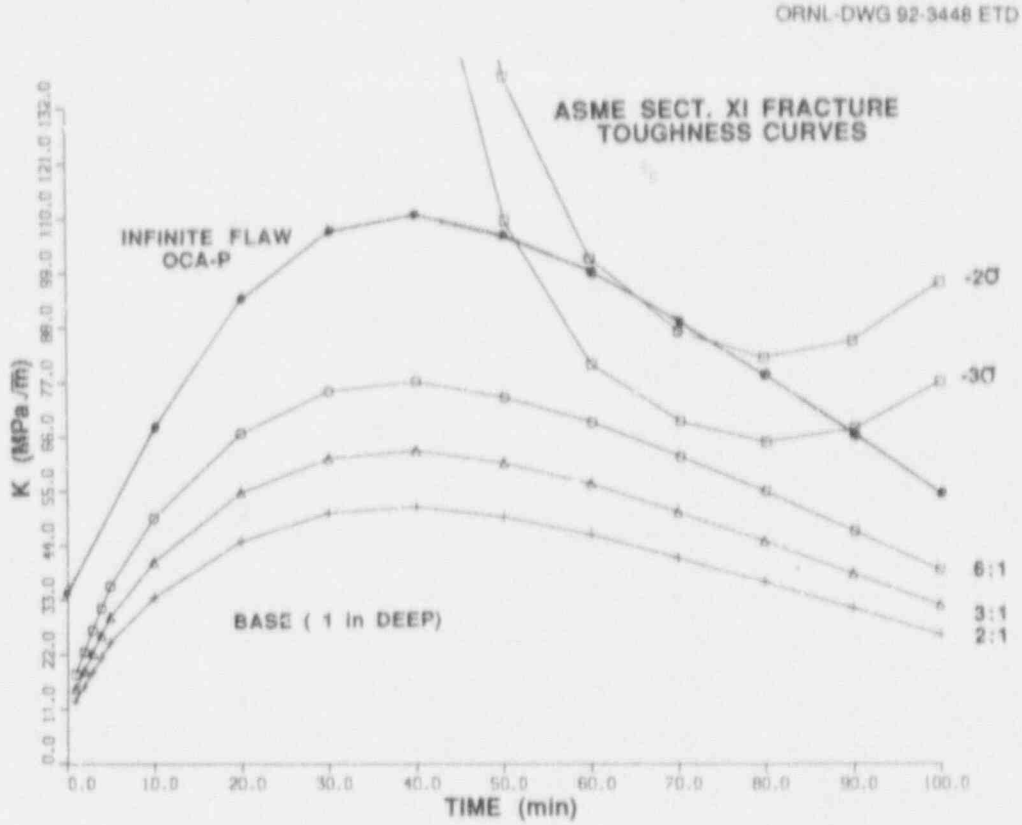

Figure 7.7 K vs time for 25.4-mm-deep flaws with various aspect ratios and RT_{NDT} of 132°C (270°F)

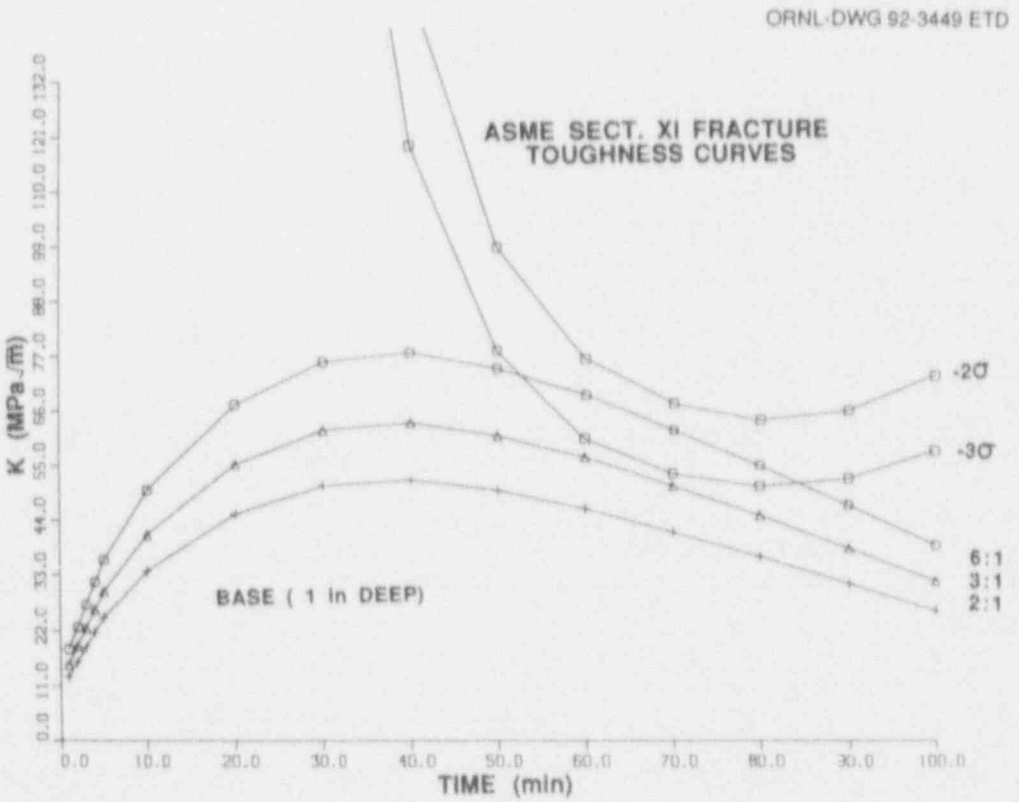

Figure 7.8 K vs time for 25.4-mm-deep flaws with various aspect ratios and RT_{NDT} of 146°C (295°F)

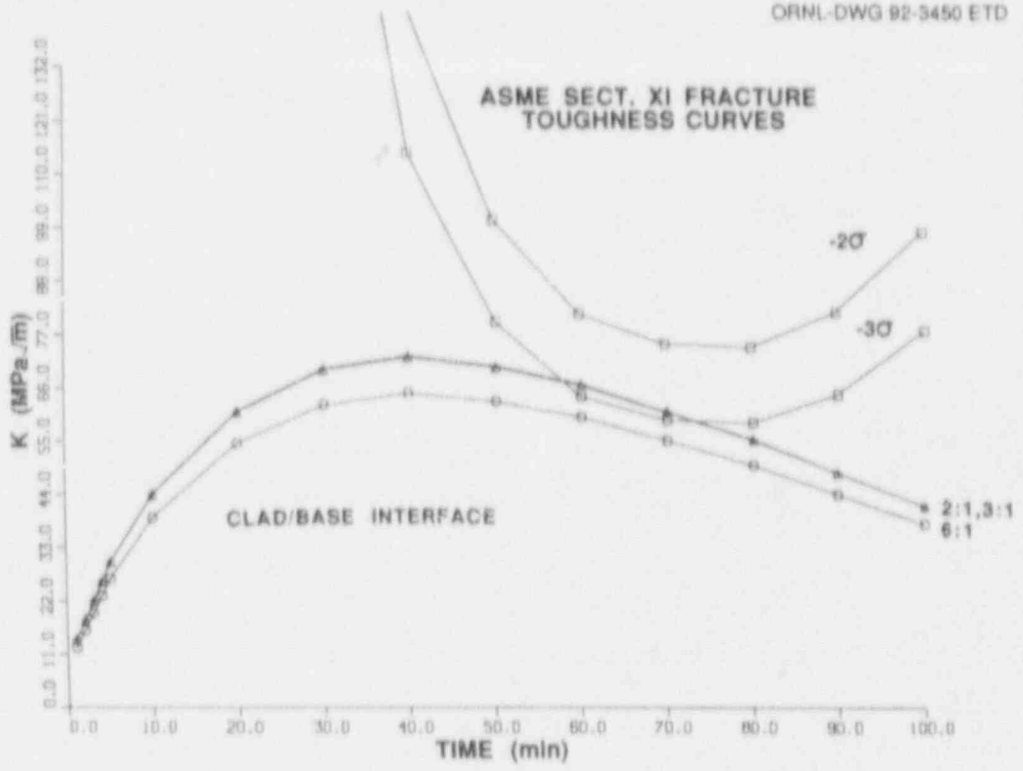

Figure 7.9 K vs time at clad/base interface for 25.4-mm-deep flaws with various aspect ratios and RT_{NDT} of 132°C (270°F)

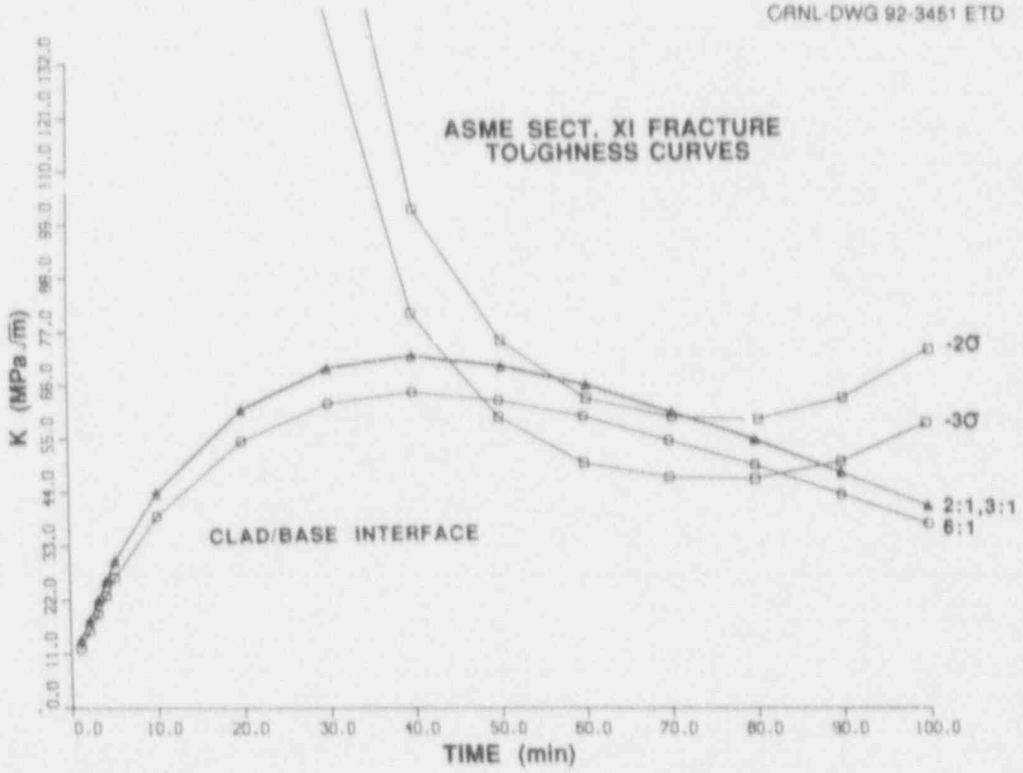

Figure 7.10 K vs time at clad/base interface for 25.4-mm-deep flaws with various aspect ratios and RT_{NDT} of 146°C (295°F)

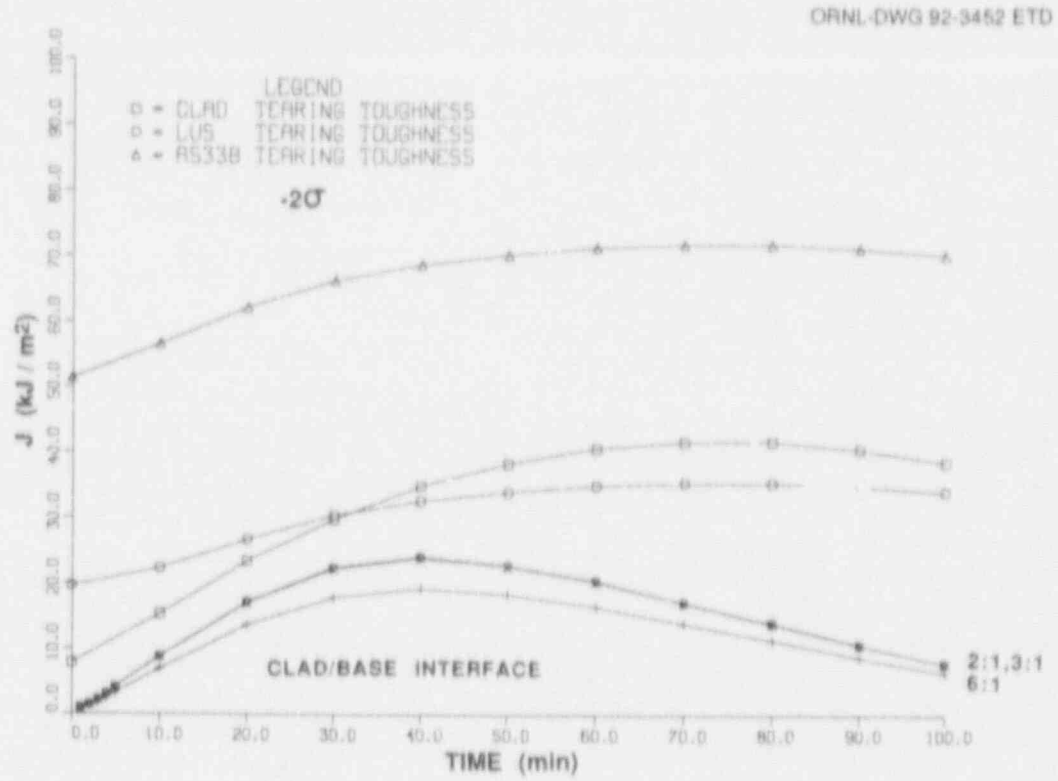

Figure 7.11 J vs time at clad/base interface for 25.4-mm-deep flaws with various aspect ratios and -2σ tearing toughness curves

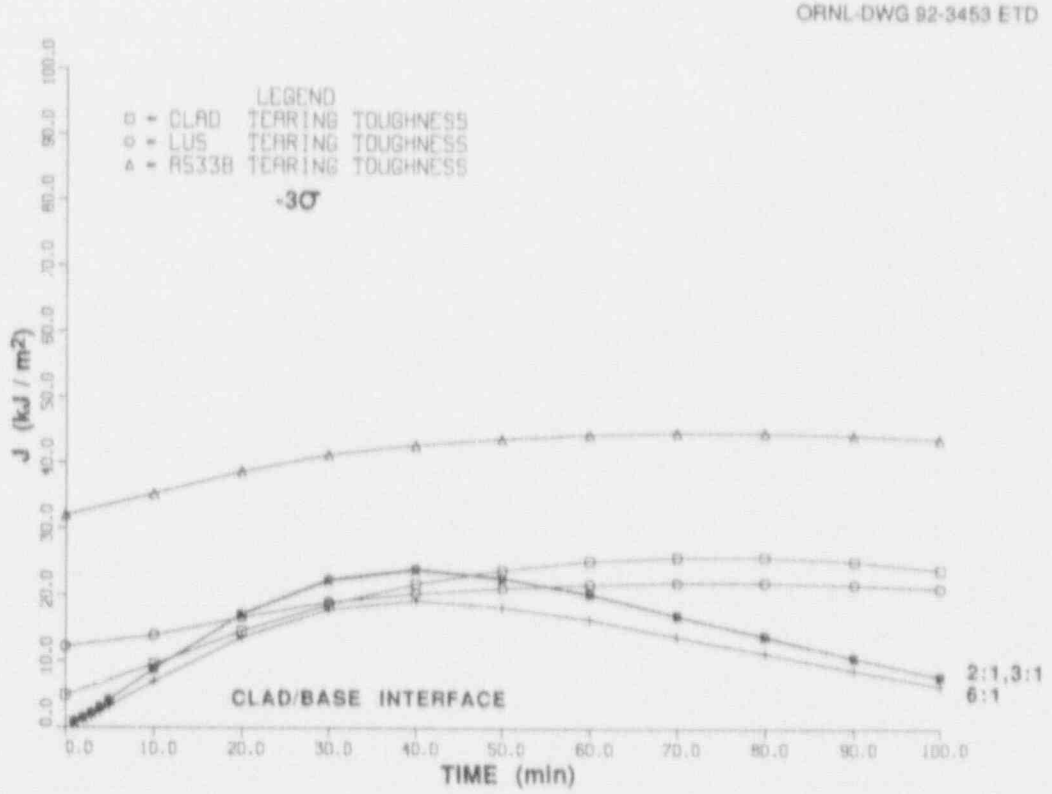

Figure 7.12 J vs time at clad/base interface for 25.4-mm-deep flaws with various aspect ratios and -3σ tearing toughness curves

the ductile-tearing toughness curves of Fig. 7.2 by means of reducing the mean curves by the factor 1/2.05 to obtain estimated -2σ curves and the factor 1/3.28 to obtain estimated -3σ curves. The factor 2.05 used to generate the J-resistance curves corresponds to the factor 1.43 employed by Cheverton et al.,[1] 1985 [Eq. (5.1)], to derive a mean cleavage-toughness curve from the *ASME Code* lower-bound curve. Implicit in the above procedure is the assumption that the ductile tearing-toughness curves of Fig. 7.2 represent the mean tearing toughness of the material.

It is evident from the curves of Fig. 7.11 that the applied J value at the clad-base material interface does not come close to the estimated -2σ-clad-tearing toughness curve at anytime during the transient, but the 2:1 and 3:1 flaw J values do intersect with the -3σ-clad- and LUS-tearing toughness curves (see Fig. 7.12). Based on the magnitude of the tearing margins derived from the curves of Figs. 7.11 and 7.12, the possibility of propagation of surface cracks into the base material could be induced by the low ductile tearing toughness of irradiated stainless steel cladding material for this flaw configuration and PTS transient.

7.4 Conclusion

The next phase of this study will examine the impact of plasticity effects, flaw geometry, and PTS transient. It is evident from the results of Figs. 7.7–7.10, that longitudinal crack propagation may not occur for a significant subset of the PTS transient: flaw geometry combinations considered in a PTS analysis. Results from the completed cladding study will provide a basis for introducing a refinement in PTS analysis procedures by considering surface-flaw initial geometry.

References

1. R. D. Cheverton and D. G. Ball, Martin Marietta Energy Systems, Inc., Oak Ridge Natl. Lab., Chap. 5 in "Pressurized-Thermal-Shock Evaluation of the H. B. Robinson Unit 2 Nuclear Power Plant," USNRC Report NUREG/CR-4183, Vol. 1 (ORNL/TM-9597/V1), September 1985.*

2. F. M. Haggag, W. R. Corwin, and R. K. Nanstad, Martin Marietta Energy Systems Inc., Oak Ridge Natl. Lab., "Irradiation Effects on Strength and Toughness of Three-Wire Series-Arc Stainless Steel Weld Overlay Cladding," USNRC Report NUREG/CR-5511 (ORNL/TM-11439), February 1990.*

*Available for purchase from National Technical Information Service, Springfield, VA 22161.

8 Pressurized-Thermal-Shock Technology

T. L. Dickson

No activity in the current reporting period.

9 Analysis Methods Validation

B. R. Bass,* J. Keeney-Walker,* C. W. Schwartz†

During this report period, work continued on several subtasks being performed in support of the Project for Fracture Analysis of Large-Scale International Reference Experiment (Project FALSIRE). A draft final report incorporating results, conclusions, and recommendations of the Project FALSIRE workshop was completed and distributed to participants for review comments.

Substantial progress was made in the development of plans for presenting Project FALSIRE results at an International Atomic Energy Agency (IAEA) Specialists meeting in 1992 at Oak Ridge, Tennessee.

9.1 CSNI/FAG Final Report on Project FALSIRE Workshop

Project FALSIRE was sponsored by the Fracture Assessment Group (FAG) of Principal Working Group No. 3 (PWG/3) of the Organization for Economic Cooperation and Development (OECD)/Nuclear Energy Agency's (NEA's) Committee on the Safety of Nuclear Installations (CSNI). On behalf of the CSNI/FAG, the Heavy-Section Steel Technology (HSST) Program at Oak Ridge National Laboratory (ORNL) and the GRS, Köln, Germany, were responsible for organization arrangements related to Project FALSIRE. The chairman of the CNSI/FAG is H. Schulz of GRS-Köln. Motivation for the project was derived from recognition by the CSNI/PWG-3 that inconsistencies were being revealed in predictive capabilities of a variety of fracture assessment methods, especially in ductile-fracture applications. As a consequence, the CSNI/FAG was formed to evaluate fracture prediction capabilities currently used in safety assessments of nuclear components. Members were from laboratories and research organizations in Western Europe, Japan, and the United States.

The CSNI/FAG planned Project FALSIRE to assess various fracture methodologies through interpretive analyses of selected large-scale fracture experiments. Six reference experiments given in Table 9.1 were eventually selected by CSNI/FAG for detailed analysis and interpretation. The CSNI/FAG established a common format for comprehensive statements of these experiments, including supporting information and available analysis results.[1]

These statements formed the basis for evaluations performed by an international group of analysts using a variety of techniques. At a 3-d workshop in Boston, in May 1990, all participating analysts examined these evaluations in detail.

Table 9.1. Large-scale fracture experiments analyzed in CSNI/FAG Project FALSIRE

Experiment	Testing organization	Country
NKS-3	Materialprüfungsanstalt (MPA) der Universität Stuttgart	FRG
NKS-4	Materialprüfungsanstalt (MPA) der Universität Stuttgart	FRG
PTSE-2	Oak Ridge National Laboratory	USA
Spinning Cylinder I	Atomic Energy Authority (AEA) Risley, United Kingdom	UK
Spinning Cylinder II	Atomic Energy Authority (AEA) Risley, United Kingdom	UK
Step-B PTS	Japan Power and Engineering Inspection Corporation (JAPEIC)	JAPAN

Comparative assessments of the solutions presented at the Project FALSIRE Workshop were performed by GRS, ORNL, and other participants in the workshop. A comprehensive report of the findings, conclusions, and recommendations was prepared based on these assessments as a cooperative effort between GRS, ORNL, and other member of the CSNI/FAG. An initial draft of the report was completed in January 1992 and submitted to the individual workshop participants for review and comments. GRS transmitted copies of the report to participants in western Europe, while ORNL was responsible for participants in Japan and the United States.

An updated draft incorporating recommendations from reviews is scheduled for completion jointly by GRS and ORNL in May 1992. Following completion, the draft will be submitted to members of the CSNI/ PWG-3 committee in June 1992. The report will be finalized in the summer of

*Computing and Telecommunications Division, Martin Marietta Energy Systems, Inc., Oak Ridge, Tenn.,
†University of Maryland, College Park, Maryland.

1992 after comments and approval have been obtained from the CSNI/PWG-3.

9.2 Joint IAEA and OECD/NEA Meeting on Fracture Mechanics Verification by Large-Scale Testing

The IAEA International Working Group on Life Management of Nuclear Power Plants and OECD/NEA-CSNI are organizing an International Specialists Meeting on Fracture Mechanics Verification by Large-Scale Testing. The meeting will be sponsored by the U. S. Nuclear Regulatory Commission (NRC) and will be hosted by ORNL. The meeting will be held October 26–29, 1992, in the Pollard Auditorium in Oak Ridge, Tennessee.

J. Stronsnider of the NEA Nuclear Safety Division and L. Ianko of the IAEA Division of Nuclear Power have been nominated as coscientific secretaries responsible for organizing the meeting. The U.S. member of the IAEA International Working Group for Life Management of Nuclear Power Plants is C. E. Pugh, who also chairs the technical program for the 1992 Specialists' Meeting.

This jointly sponsored meeting will provide researchers an opportunity to review recent large-scale fracture (brittle and/or ductile) experiments and to discuss them relative to verification of fracture-mechanics methods. The objective of the meeting is to assess the ability of analytic methods to model the fracture behavior of nuclear reactor components and structures. Specialists will be provided an opportunity to discuss the validity of fracture mechanics models under prototypic and laboratory conditions, and it is expected that, based on these discussions, they will reach conclusions regarding the capabilities and limitations of fracture-mechanics analysis methods.

The meeting will address the application of all forms of fracture-mechanics methodology and experimental verification, including correlations between small and large specimens and components. The emphasis will be on experimental results and the evaluation of fracture mechanics models and analysis methods through individual and comparative studies. The scope will include all pressure boundary components with special emphasis on vessels, piping, and closures under normal operating, upset, and accident conditions.

The CSNI/PWG-3 has agreed to support the Specialists' Meeting through the work of the Fracture Assessment Group (FAG) of the CSNI and the participants in Project FALSIRE. In particular, the first day of the meeting will be devoted completely to presentations on the six reference experiments of Project FALSIRE (see Table 9.1). Briefly, the 1-d agenda proposed jointly by the program chairman and by H. Shulz on behalf of CSNI/FAG calls for an overview talk on Project FALSIRE, followed by two presentations for each experiment used in Project FALSIRE, and, finally, a panel discussion. The first presentation for each experiment, to be given by a representative of the testing organization, will review the results of the experiment and provide an overview of the analysis results presented at the FALSIRE Workshop with respect to the Phase I FALSIRE-Report described in Sect. 9.1. A second presentation will focus on recent analysis results compiled since the workshop with emphasis on applications of more advanced fracture methodologies.

Staff members and subcontractors of the HSST Program are providing support to the program through organizational efforts concerning the technical program and through presentations of analysis results for the second HSST pressurized thermal-shock-experiment (PTSE-2) and for the Japanese Step-B PTS experiment (see Table 9.1). The analyzes of the Step-B experiment currently being performed by the University of Maryland for the HSST Program represents the first non-Japanese analysis of the experiment.

The agenda on the second and third days will cover other experimental and analytical work performed in IAEA and CSNI member countries.

Topics to be addressed during these sessions include:

- large-scale fracture experiments relating to pressure vessels and piping;
- analyses of available experiments to assess the applicability of fracture models to identify limitations and to relate to regulatory issues;
- assessments of experimental data and fracture models for studying constraint effects on fracture toughness;
- assessments of ductile fracture models including ranges of applicability, interactions with cleavage fracture, and comparative evaluations;
- advancements of experimental techniques for large-scale tests to characterize fracture and deformation behavior;
- fracture data bases that support understanding the applicability of laboratory data to prototypical situations, including size effects, rate effects, multiaxial conditions, and temperature dependence; and

- recommendations for experiments and analytical activities needed to advance the verification of fracture analysis methods for applications to nuclear reactor pressure vessels and components.

The morning of the third day will include either a tour of the ORNL experimental fracture facilities or a technical session, depending on the number of papers proposed and accepted. The final program for the meeting will be distributed in August 1992.

Reference

1. B. R. Bass et al., "Assessment of Ductile Fracture Methodology Based on Applications to Large-Scale Experiments," pp. 25–36 in *SMiRT II Transactions*, Vol. G, August 1991. *

*Available in public technical libraries.

10 Fracture Evaluation Tests

T. J. Theiss

10.1 Introduction

The purpose of this task is to provide experimental support for all remaining tasks within the HSST program. Currently, Task 10 is divided into five subtasks: (10.1) Shallow-Crack Fracture Toughness Testing (coordinated with Task 6, Cleavage Crack Initiation); (10.2) Full-Thickness Clad Beam Tests (coordinated with Task 6, Cleavage Crack Initiation, and Task 7, Cladding); (10.3) Large-Scale Biaxial Tests (coordinated with Task 2, Fracture Methodology and Analysis, and Task 6, Cleavage Crack Initiation); (10.4) Large-Scale Fracture Methodology Experiments (for future ORNL fracture testing); and (10.5) Material Requests (supply A 533 B material on an as-needed basis).

10.2 Shallow-Crack Fracture-Toughness Testing Program

Testing for the shallow-crack fracture-toughness program at Oak Ridge National Laboratory (ORNL) has ceased and was transferred to David Taylor Research Center (DTRC). Crack-depth measurements for previously tested production beams were completed this reporting period. Final crack-depth values are included in Table 6.1. DTRC requested through the Nuclear Regulatory Commission (NRC) a section of HSST Plate 11A measuring 3.175 m (125 in.) by full width (1.65 m) and thickness (184 mm) for their shallow-crack and constraint testing. HSST Plate 11A is the companion plate to HSST Plate 11B, which will be used for the large-scale biaxial tests.

10.3 Full-Thickness Clad Beam Tests

Design of the full-thickness, clad beam fracture-mechanics specimens; program objectives; test matrix; and issuance of the test specification (Spec. No. HSST—H10-92-001, Rev. 1) are detailed in Chap. 6.

The full-thickness, clad beam tests will be performed at the National Institute of Standards and Technology (NIST) using the 26.7-MN (6-million-lb) testing machine. An Interagency Agreement with NIST for the full-thickness clad beam, shallow-crack tests was placed this reporting period. The Interagency Agreement is based on the test specification that was the basis of the NIST research proposal.

A portion of an actual cancelled PWR reactor vessel will be used as a source material for the full-thickness, clad beam tests. The material is A 533 grade B steel with stainless steel cladding on the inner surface. The PWR shell contains an axial weld in the center of the shell and two circumferential welds. One circumferential weld connects the upper and lower and shell courses; the other circumferential weld connects the upper shell to the nozzle course. The nominal radius of curvature of the shell is 2.49 m (98 in.). The circumferential length is 1447 mm (57 in.). The section of material necessary for fabrication of the clad beams was flame cut from the reactor shell during the current reporting period. A suitable vendor(s) has been located to fabricate the specimens using a saw to cut the shell into specimens. Saw cutting is required to minimize the amount of wasted or degraded material.

10.4 Large-Scale Biaxial Tests

Objectives for the out-of-plane biaxial tests are defined in Chaps. 2 and 6 of this report. Design of the biaxial specimen is described in Chap. 2. Design criteria are specified in Chap. 6.

Initial plans were to test a biaxial specimen with a test section measuring 1524 × 1524 × 127 mm (60 × 60 × 5 in.) thick. A preliminary cost assessment of the 1524 × 1524 × 127 mm (60 × 60 × 5 in.) biaxial test specimen was developed by the Engineering Division of Martin Marietta Energy Systems, Inc. The specimens were designed to be tested in the 100-MN (22.5-million pound) machine located at the U.K. Atomic Energy Authority (AEA) Risley facility. This facility is capable of equibiaxial loading up to 50 MN. Each biaxial specimen, complete with necessary attachments for testing, would cost ~$250K. The primary cause of the high cost is the size of the specimen (18 ton each) and the large amount of precision drilling and tapping required to mount the specimen in the 100-MN machine. The end arms with the drilled and tapped holes cold not be reused. Due to the expense of the larger specimen, two alternate specimen designs were considered and cost estimates developed. Both additional specimen designs involve a 610 × 610 × 127 mm (24 × 24 × 5 in.) test section. One design mounts the specimen directly into the machine with expendable end arms. The other design uses a reusable clevis that loads the specimen through a pin. The U.K. AEA facility has five sets of actuators for biaxial loading, each with a 10-MN (2250-kip) capacity

spaced every 12 in. apart. Therefore, two sets of actuators can stress a 610 × 610 × 127 mm (24 × 24 × 5 in.) plate to the same level as five sets of actuators can stress a 1524 × 1524 × 127 mm (60 × 60 × 5 in.) plate. A planform dimension of 610 mm (24 in.) was chosen so that two specimens could be cut from the 1626-mm (64-in.) source plate (HSST Plate 11B). Based on an estimated cost of $4.50/lb of machined material, the 610 × 610 × 127 mm (24 × 24 × 5 in.) designs with expendable end arms and reusable clevises would cost $70K and $32K, respectively, for the test specimen only. Based on this information, the decision was made to proceed with the 610 × 610 × 127 mm (24 × 24 × 5 in.) design with reusable clevises. The biaxial test specification is written to reflect the new test 610 × 610 × 127 mm (24 × 24 × 5 in.) specimen with reusable clevises.

Potential vendors with large-scale testing capabilities in the U.S. were surveyed for performing the out-of-plane biaxial loading tests. Seven U.S. testing facilities were contacted and given the load requirements of 10 million pound in both the longitudinal and transverse directions. None of these seven firms had existing facilities capable of performing the biaxial tests. However, one firm (Wyle Labs) returned a preliminary budgetary quote based on modifying existing facilities to test the biaxial specimens.

HSST Plate 11B is the source material selected for the biaxial specimen tests. Because the biaxial test is a new program, with the potential for more testing in the future, a new plate was used as the source material. Plate 11B was chosen because it has a rather high yield strength for A 533 B according to the mill certification reports. The biaxial test material will be heat treated to increase the yield strength of the material to simulate irradiated conditions. A small piece of material (533 × 686 mm) was cut from the plate and sent to Task 3 for development of the heat treatment necessary to increase the yield strength to ~620 MPa (90 ksi).

10.5 Material Requests

Requests for material (A 533 B) have been received from numerous sources and are being handled on a case-by-case basis. Three requests were for remains from the HSST shallow-crack, fracture-toughness beams. The largest request has come from Southern University for their testing program. Sketches from Southern University were received this reporting period for 240 specimens from 3 different materials. ORNL has been directed by NRC to supply the steel specimens (80 total). ORNL is interacting with Southern University to determine their testing requirements. Based on preliminary cost estimates, only 40 specimens can be fabricated within existing budgetary constraints.

11 Warm Prestressing

D. K. M. Shum

11.1 Introduction

The overall objective of this task is to quantify the potential benefits from the inclusion of warm prestress (WPS) effects toward the safety-margin assessment of reactor pressure vessels (RPVs). The near-term objectives of the task are to

1. identify potential regulatory issues that would benefit from the inclusion of WPS effects,
2. establish a framework for interpreting available WPS data,
3. investigate the mechanics and mechanisms of WPS,
4. provide preliminary estimates on the potential benefits from the inclusion of type-I WPS effects toward RPV start-up and cool-down procedures, and
5. evaluate the stability of type-I WPS for RPV applications where monotonic unloading of the crack tip cannot be guaranteed.

Contingent upon favorable near-term outcomes, recommendations on analytical and experimental research efforts that are necessary to provide both a better understanding of WPS and a technical basis for its application to the safety-margin assessment of RPVs will be presented. These recommended research efforts will become integral elements in the long-term objectives of this task, including

1. developing criteria and methods for the inclusion of WPS effects in plant-specific safety-margin assessment of RPVs under normal operations and postulated accident conditions, and
2. developing a predictive WPS model.

This semiannual report summarizes the first-phase activities in this task, the focus of which is a comprehensive literature search on the phenomenon of WPS and its relation to RPV analysis and applications. A letter report entitled "Implications of Warm Prestress on Safety-Margin Assessment of Reactor Pressure Vessels" has been completed. The following discussion is extracted from this report.

11.2 Characteristics of WPS

The primary characteristic of WPS is the apparent increase in fracture toughness due to prior loading (above K_{Ic} for the test temperature) at a higher temperature. It is emphasized that available experimental results on apparent WPS-induced toughness enhancement are limited to mode I, quasi-static, plane strain, cleavage crack-initiation toughness values.[1–4] As shown in Fig. 11.1, three types of WPS benefits in relation to crack initiation are considered in this study.

- Type I: The mode I stress-intensity factor (K_I) does not increase with time ($K_I \leq 0$), and crack initiation is not anticipated.
- Type II: WPS loading histories that involve final reload to fracture from K values that are less than K_{Ic}. Magnitude of K at failure (K_f) after WPS is greater than or equal to K_{Ic} ($K_f/K_{Ic} \geq 1$).
- Type III: WPS loading histories that involve final reload to fracture from K values that are greater than K_{Ic}. Magnitude of K_f after WPS is greater than K_{Ic} ($K_f/K_{Ic} \geq 1$).*

11.3 WPS and RPV Regulatory Issues

Current RPV fracture-margin assessment methods are based on the *American Society of Mechanical Engineers (ASME) Boiler and Pressure Vessel (B&PV) Code* fracture-toughness curves indexed by RT_{NDT}.[5–7] Depending on the vessel application such as low-temperature overpressure (LTOP) set points, P-T limits, and pressurized-thermal-shock (PTS) transients (to be discussed shortly), the Code fracture-toughness K_{Ic} (lower-bound crack-initiation toughness) or K_{Ia} (lower-bound crack-arrest toughness) curve forms the basis of regulatory reference toughness K_{IRef}.[6,7,†] Consequently, both the magnitude and rate-of-change of K_{IRef} due to embrittlement depend on the choice of reference toughness.

Because the majority of available WPS data are only applicable to conditions of quasi-static crack initiation, inclusion of WPS effects would at present only beneficially impact regulatory issues that use K_{Ic} as the basis of regulatory reference toughness K_{IRef}. Nevertheless, potential regulatory issues that would benefit from the inclusion of WPS effects are as follows:

---

*The present definition of type-III WPS is motivated by, but different than, that proposed by G. R. Irwin in "Benefits of Warm Prestressing," presentation made at ASME Sect. XI Working Group on Flaw Evaluation, Sept. 2, 1982.

†The symbol K_{IRef} is used, in the present context, to denote the reference toughness value appropriate to the specific vessel application under discussion. The symbol K_{IRef} should not be confused with the symbol K_{IR}, which is often associated with the *ASME Code* lower-bound, dynamic-toughness curve, which in turn is identified with the lower-bound K_{Ia} curve.

Warm

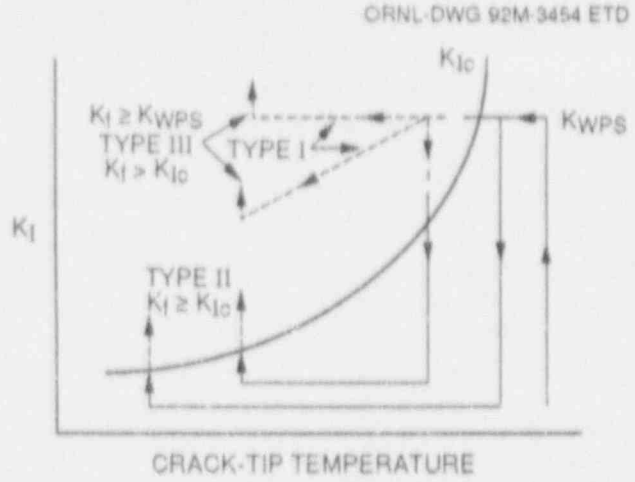

Figure 11.1 Schematic illustrating three types of warm prestress benefits in relation to crack initiation. Type I: $K_I \leq 0$, no fracture. Type II: $K_f/K_{Ic} \geq 1$. Type III: $K_f/K_{Ic} > 1$

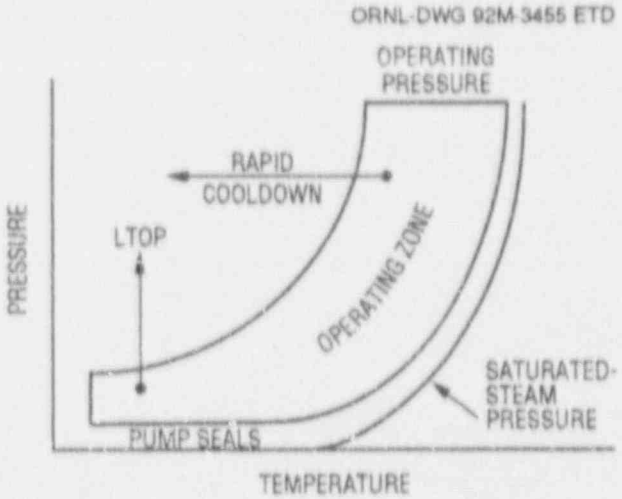

Figure 11.2 Schematic from Ref. 11 indicating operating P-T window, along with potential loading paths due to overcooling and LTOP conditions. Upper P-T limit is based on reference toughness $K_{IRef} = K_{Ia}$ up to the LTOP enabling temperature of (RT_{NDT} + 90°F). Beyond LTOP enabling temperature, RPV operating pressure determines the upper pressure limit. The lower P-T limit is based on the larger of either the minimum coolant-pump pressure with margin terms or the minimum coolant-pump pressure needed to prevent cavitation within the pump.

1. LTOP set points for adjustable and nonadjustable LTOP relief valves,
2. RPV operating pressure-temperature (P-T) limits, and
3. calculated probability of vessel failure under postulated PTS transient conditions.

In the following discussion on potential regulatory issues that would benefit from the inclusion of WPS effects, one source of WPS effects would be vessel operation before vessel start-up or cool-down. In this scenario, vessel operation constitutes prior loading at a higher temperature. The WPS benefits would apply over the entire range of operating temperatures from start-up to core operation. Another source of WPS effects would be the preservice and in-service hydrostatic tests. In this case, the WPS benefits would strictly apply over the range of temperatures from start-up to the hydrostatic test temperature. In the case of thermal shock (TS) and PTS loading conditions, yet another source of WPS effects would be the transient itself in a manner to be described in Sect. 11.3.2.

11.3.1 LTOP Set Points

Various P-T limits that govern reactor design and operations are set forth in Sect. III, Appendix G, and Sect. XI, Appendix G, of the *ASME B&PV Code*.[6,7] The P-T limits that are applicable to normal vessel start-up and cool-down and LTOP conditions separate the RPV operating zone from conditions hazardous to vessel integrity.[8–10] In Fig. 11.2, the operating P-T "window" is schematically indicated, along with the potential loading paths due to overcooling and LTOP conditions.[11] The upper P-T limit is based on reference toughness $K_{IRef} = K_{Ia} = K_{Id}$. The LTOP system is required to be operable during start-up and shut-down conditions below the LTOP enable temperature of (RT_{NDT} + 90°F).[8] Beyond the LTOP enable temperature, the RPV operating pressure determines the upper pressure limit. The effects of embrittlement of the RPV during plant operation result in a decrease in that portion of the upper P-T limit that is based on K_{Ia}, thereby decreasing the range of allowable operating pressure at a given temperature and resulting in a narrowed P-T window.

Current guidelines from the Standard Review Plan (SRP)[8,9] require the LTOP system to protect the upper P-T limit during normal start-up and cool-down and related transient conditions. Operational considerations such as pressure overshoot, margin to avoid inadvertent lifting of the LTOP relief valves, and instrument gage error result in LTOP set points that are below the allowable upper P-T

limit as indicated in Fig. 11.3.[10] If the LTOP set points are allowed to transgress the upper P-T limit, the LTOP set points would benefit from the inclusion of WPS effects in the following sense. Permissible transgression of the upper P-T limit by the LTOP set points implies a change in LTOP philosophy from ensuring crack arrest to prevention of crack initiation.* The immediate benefit thus comes from a "consistent" interpretation of this philosophy change, which would result in the use of K_{Ic} (as opposed to K_{Ia}) as the reference toughness K_{IRef} in determining the LTOP set points. In addition, use of K_{Ic} as the reference toughness K_{IRef} would make possible the inclusion of WPS effects in providing additional elevation of the

*Acceptance of this philosophy change will require a consensus on the issue of the existence of local brittle zones (LBZs) and the associated issue of dynamic crack pop-ins for RPV-grade materials under irradiated conditions.

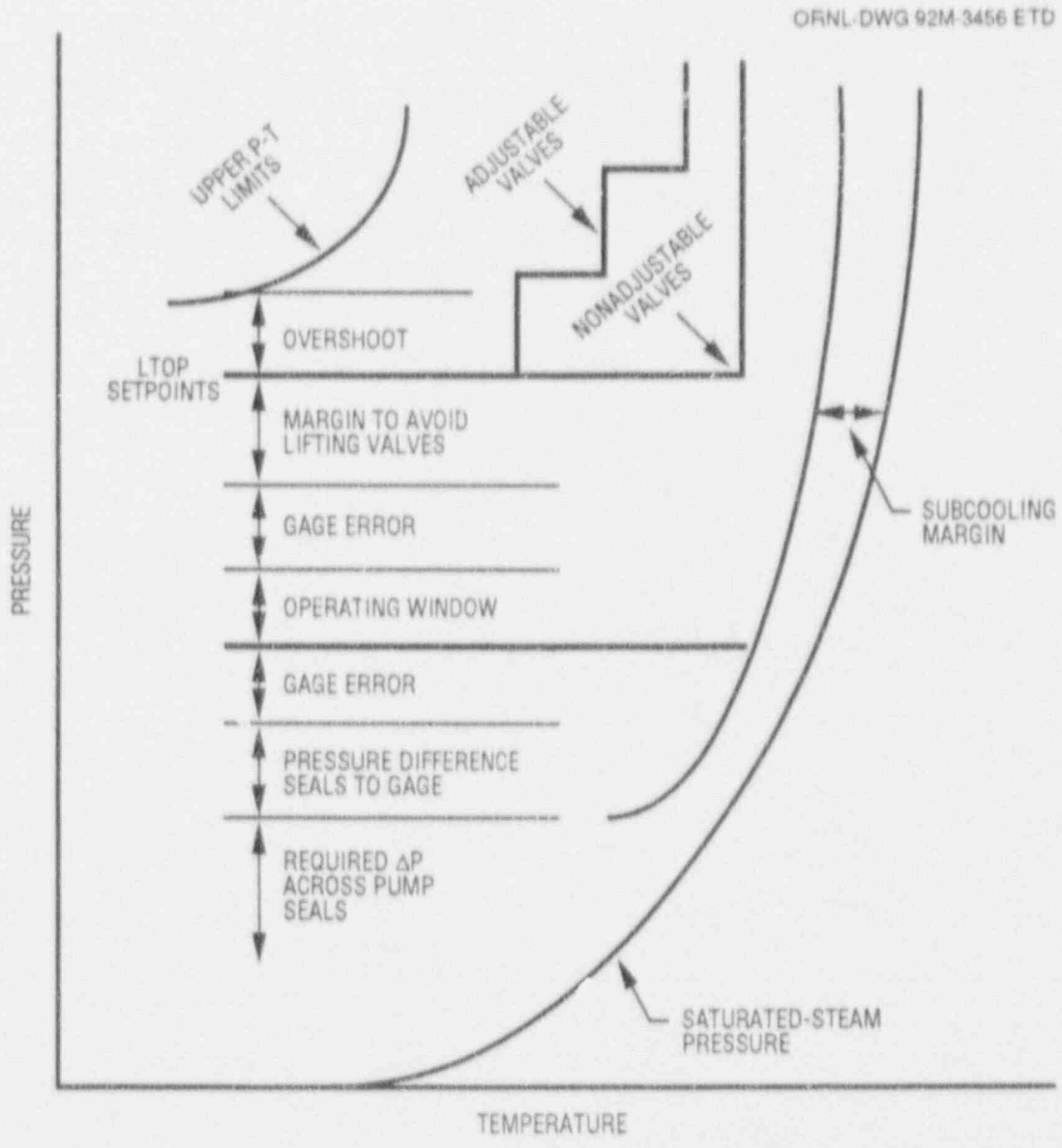

Figure 11.3 Schematic from Ref. 10 indicating LTOP set points for both nonadjustable and adjustable LTOP relief valves in relation to the P-T limits. Operational considerations such as pressure overshoot, margin to avoid inadvertent lifting of the LTOP relief valves, and instrument gage error result in LTOP set points that are below the allowable upper P-T limit. Potential benefits from inclusion of WPS effects are more significant for nonadjustable LTOP relief-valve systems as compared to adjustable systems

reference toughness. Obviously, potential benefits are more significant for nonadjustable LTOP relief-valve systems as compared to adjustable systems. As indicated in Fig. 11.3, the range of P-T conditions that permit continuous P-T operation from low temperature/pressure to operating temperature-pressure is much more restrictive for nonadjustable LTOP systems as compared with adjustable systems.

11.3.2 RPV Operating P-T Limits

If the basis for establishing the P-T limits is changed from ensuring crack arrest to prevention of crack initiation, reactor operating P-T limits would likewise benefit from the inclusion of WPS effects. In a manner analogous to the LTOP set points, the potential benefits come from an elevation of the reference toughness, with respect to K_{Ia}, based on K_{Ic} and the inclusion of WPS effects on K_{Ic}. As indicated in Fig. 11.4, the potential benefits are to

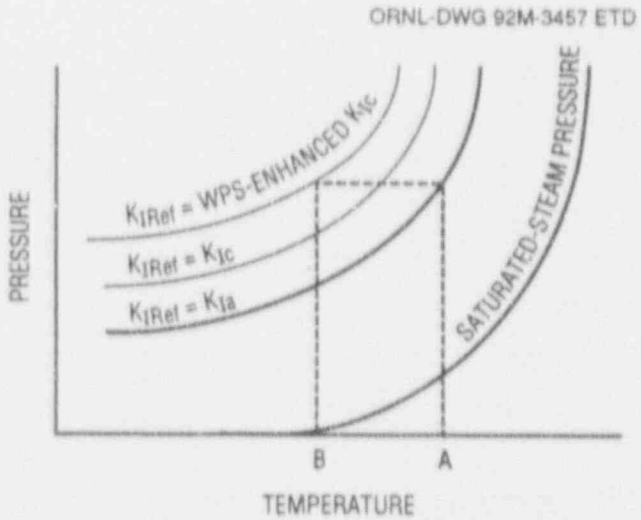

Figure 11.4 Schematic indicating potential benefits to operating P-T limits from inclusion of WPS effects. Inclusion of WPS effects would lower the required test temperature for in-service leak and hydrostatic tests from A (based on K_{Ia}) to B (based on WPS-enhanced K_{Ic}). Potential benefits with respect to higher start-up and cool-down rates, and an enlarged operating P-T window during core operation, also follow from replacing K_{Ia} with WPS-enhanced K_{Ic}

1. lower the required test temperature for in-service leak and hydrostatic tests,
2. permit higher vessel start-up and cool-down rates, and
3. enlarge the operating P-T window during core operation.

The benefits relating to preservice and in-service leak and hydrostatic tests are applicable to both pressurized-water reactors (PWRs) and boiling-water reactors (BWRs). In the absence of WPS benefits, the in-service leak and hydrostatic test temperatures might, through irradiation embrittlement, be sufficiently elevated to require an external heating source to provide the temperature elevation necessary to perform these tests.[10] Inclusion of WPS effects, based upon a "consistent" interpretation of P-T-limits philosophy based on $K_{IRef} = K_{Ic}$, would permit higher vessel start-up and cool-down rates. Inclusion of WPS effects would benefit core operation because current guidelines[9] impose an additional 40°F "margin" on the core-operation upper P-T limit relative to the allowable start-up and cool-down rates determined based on Sect. III, App. G, of the *ASME Code*.

11.3.3 Probability of Vessel Failure

Inclusion of WPS effects would reduce the calculated probability of vessel failure under postulated accident conditions. The potential benefits would apply to both TS (large-break-loss-of-coolant) and PTS (small-break-loss-of-coolant) transients. The current probabilistic fracture safety-margin assessment method is based on a probabilistic treatment of $K_{IRef} = K_{Ic}$ for the prediction of crack initiation and a probabilistic treatment of $K_{IRef} = K_{Ia}$ for the prediction of crack arrest.[12–16] Current methodology for the evaluation of the calculated probability of vessel failure does not permit consideration of the potential benefits from WPS;[17] that is, crack initiation is assumed to take place when the applied K_I exceeds K_{Ic} during the transient, regardless of the history of K_I as a function of transient time up to $K_I = K_{Ic}$. Determination of crack reinitiation is similarly based on comparison of the applied K_I and K_{Ic} subsequent to crack arrest without regard for the loading history. While the reasons for not considering WPS effects are not explicitly stated in Ref. 17, it is believed they are related to consideration of WPS stability, as discussed in Ref. 15 and in the next paragraph.

There is a wide range of analysis conditions during a TS or PTS transient for which the magnitude of the applied K_I first exceeds K_{Ic} at a time in the transient at which K_I is decreasing with transient time (type-I WPS) as indicated in Fig. 11.5. While current methodology would consider crack initiation to have taken place when $K_I \geq K_{Ic}$,

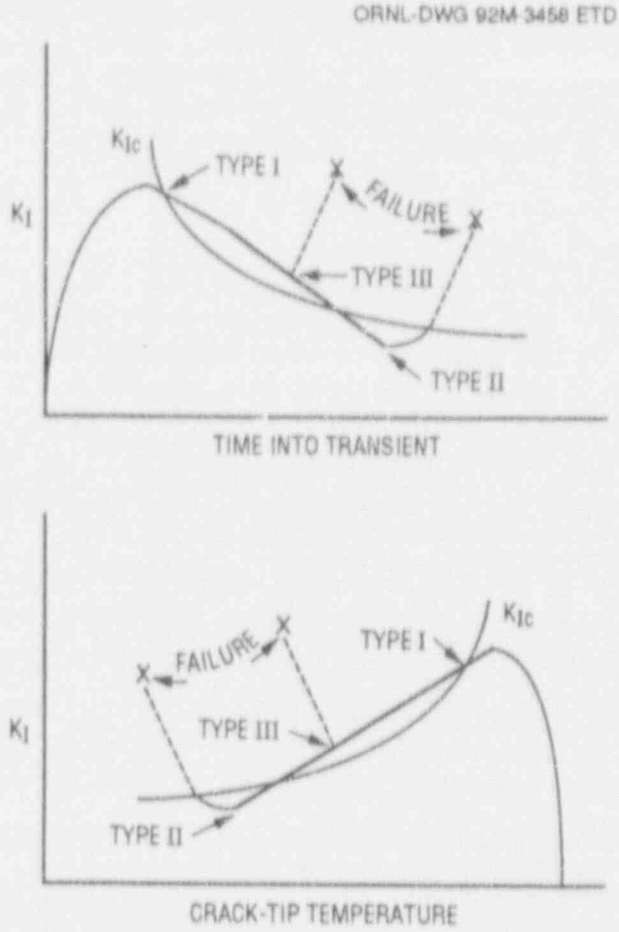

Figure 11.5 Schematic indicating times and range of crack-tip temperatures during a postulated TS or PTS transient for which inclusion of WPS effects would reduce the calculated probability of vessel failure

inclusion of type-I WPS effects would imply crack initiation would not take place under these analysis conditions. Furthermore, it is emphasized that type-II WPS would need to be addressed in cases where K_I could increase with time after passing previous maximum and local minimum values during a transient. A scenario for which K_I would increase with time after passing previous maximum value is a TS or PTS transient with repressurization at a later time in the transient. WPS stability in the present context refers to the magnitude of WPS toughness enhancement under types II and III conditions as indicated in Fig. 11.5. Similar considerations with respect to the potential benefits and stability of WPS apply to the determination of crack reinitiation. Evaluation of the stability of type-I WPS effects is part of the third-phase activities of this study.

References

1. F. J. Loss, R. A. Gray, Jr., and J. R. Hawthorne, Naval Research Laboratory, Washington, D.C., "Significance of Warm Prestress to Crack Initiation During Thermal Shock," USNRC Report NRL/NUREG &165, September 1977.*

2. F. J. Loss, R. A. Gray, Jr., and J. R. Hawthorne, "Investigation of Warm Prestress for the Case of Small DT During a Reactor Loss-of-Coolant Accident," *J. Press. Ves. Tech.* 101, 298–304 (1979).†

3. B. W. Pickles and A. Cowan, "A Review of Warm Prestressing Studies," *International Journal of Pressure Vessel and Piping* 14, 95–131, 1983.†

4. R. B. Stonesifer, E. F. Rybicki, and D. E. McCabe, Materials Engineering Associates, Lanham, Md., "Warm Prestress Modeling: Comparison of Models and Experimental Results," USNRC Report NUREG/CR-5208 (MEA-2305), 1989.*

5. U.S. Nuclear Regulatory Commission, *Regulatory Guide 1.99, Revision 2*, "Radiation Embrittlement of Reactor Vessel Materials," May 1988.‡

6. *The American Society of Mechanical Engineers Boiler and Pressure Vessel Code, Section III*, "Rules for Construction of Nuclear Power Plant Components," 1989.‡

7. *The American Society of Mechanical Engineers Boiler and Pressure Vessel Code, Section XI*, "Rules for Inservice Inspection of Nuclear Power Plant Components," 1989.‡

8. United States Nuclear Regulatory Commission, *Standard Review Plan Section 5.2.2 Rev. 3*, "Overpressure Protection," NUREG-0800, November 1988.*

9. United States Nuclear Regulatory Commission, *Standard Review Plan Section 5.3.2 Rev. 1*, "Pressure-Temperature Limits," NUREG-0800, July 1981.*

10. ASME Section XI Task Group on Reactor Vessel Integrity Requirements, "White Paper on Reactor

Vessel Integrity Requirements for Level A and B Conditions," prepared for ASME Sect. XI Working Group on Operating Plant Criteria, January 1991.†

11. R. N. Randall, "Overview of USNRC's Use of Radiation Damage Trend Curves," presented to Specialized Topic Workshop on Pressurized Thermal Shock, September 1990.

12. United States Nuclear Regulatory Commission, *Regulatory Guide 1154*, "Format and Content of Plant-Specific Pressurized Thermal Shock Safety Analysis Reports for Pressurized Water Reactors," January 1987.‡

13. T. J. Burns et al., Martin Marietta Energy Systems, Inc., Oak Ridge Natl. Lab., "Pressurized Thermal Shock Evaluation of the Oconee-1 Nuclear Power Plant," USNRC Report NUREG/CR-3770 (ORNL/TM-9176), May 1986.*

14. D. L. Selby et al., Martin Marietta Energy Systems, Inc., Oak Ridge Natl. Lab., "Pressurized Thermal Shock Evaluation of the Calvert Cliffs Unit I Nuclear Power Plant," USNRC Report NUREG/CR-4022 (ORNL/TM-9408), September 1985.*

15. D. L. Selby et al., Martin Marietta Energy Systems, Inc., Oak Ridge Natl. Lab., "Pressurized Thermal Shock Evaluation of the H. G. Robinson Unit 2 Nuclear Power Plant," USNRC Report NUREG/CR-4183 (ORNL/TM-9567, Vols. 1 and 2), September 1985.*

16. R. D. Cheverton and D. G. Ball, Martin Marietta Energy Systems, Inc., Oak Ridge Natl. Lab., "OCA-P, A Deterministic and Probabilistic Fracture-Mechanics Code for Application to Pressure Vessels," USNRC Report NUREG-3618 (ORNL-5991), May 1984.*

17. U.S. Nuclear Regulatory Commission, *Regulatory Guide 1.154*, "Format and Content of Plant-Specific Pressurized Thermal Shock Safety Analysis Reports for Pressurized Water Reactors," January 1987.‡

---

*Available for purchase from National Technical Information Service, Springfield, VA 22161.

†Available in public technical libraries.

‡Available in NRC Public Document Room for inspection and copying for a fee.

CONVERSION FACTORS[a]

SI unit	English unit	Factor
mm	in.	0.0393701
cm	in.	0.393701
m	ft	3.28084
m/s	ft/s	3.28084
kN	lb_f	224.809
kPa	psi	0.145038
MPa	ksi	0.145038
$MPa \cdot \sqrt{m}$	$ksi \cdot \sqrt{in.}$	0.910048
J	ft•lb	0.737562
K	°F or °R	1.8
kJ/m^2	$in.\text{-}lb/in.^2$	5.71015
$W \cdot n^{-3} \cdot K^{-1}$	$Btu/h\text{-}ft^2 \cdot °F$	0.176110
kg	lb	2.20462
kg/m^3	$lb/in.^3$	3.61273×10^{-5}
mm/N	$in./lb_f$	0.175127
T(°F) = 1.8(°C) + 32		

[a]Multiply SI quantity by given factor to obtain English quantity.

Prior Heavy-Section Steel Technology Reports

The work reported here was performed at Oak Ridge National Laboratory under the Heavy-Section Steel Technology (HSST) Program, W. E. Pennell, Program Manager. The program is sponsored by the Office of Nuclear Regulatory Research of the U.S. Nuclear Regulatory Commission (NRC). The technical monitor for NRC is S. N. M. Malik.

This report is designated HSST Report NUREG/CR-4219, Vol. 9, No. 1 (ORNL/TM-9593/V9&N1). Prior and future reports in this series are listed below.

1. S. Yukawa, General Electric Company, Schenectady, N.Y., *Evaluation of Periodic Proof Testing and Warm Prestressing Procedures for Nuclear Reactor Vessels*, HSSTP-TR-1, July 1, 1969.

2. L. W. Loechel, Martin Marietta Corporation, Denver, Colo., *The Effect of Testing Variables on the Transition Temperature in Steel*, MCR-69-189, November 20, 1969.

3. P. N. Randall, TRW Systems Group, Redondo Beach, Calif., *Gross Strain Measure of Fracture Toughness of Steels*, HSSTP-TR-3, November 1, 1969.

4. C. Visser, S. E. Gabrielse, and W. VanBuren, Westinghouse Electric Corporation, PWR Systems Division, Pittsburgh, Pa., *A Two-Dimensional Elastic-Plastic Analysis of Fracture Test Specimens*, WCAP-7368, October 1969.

5. T. R. Mager and F. O. Thomas, Westinghouse Electric Corporation, PWR Systems Division, Pittsburgh, Pa., *Evaluation by Linear Elastic Fracture Mechanics of Radiation Damage to Pressure Vessel Steels*, WCAP-7328 (Rev.), October 1969.

6. W. O. Shabbits, W. H. Pryle, and E. T. Wessel, Westinghouse Electric Corporation, PWR Systems Division, Pittsburgh, Pa., *Heavy-Section Fracture Toughness Properties of A533 Grade B Class 1 Steel Plate and Submerged Arc Weldment*, WCAP-7414, December 1969.

7. F. J. Loss, Naval Research Laboratory, Washington, D.C., *Dynamic Tear Test Investigations of the Fracture Toughness of Thick-Section Steel*, NRL-7056, May 14, 1970.

8. P. B. Crosley and E. J. Ripling, Materials Research Laboratory, Inc., Glenwood, Ill., *Crack Arrest Fracture Toughness of A533 Grade B Class 1 Pressure Vessel Steel*, HSSTP-TR-8, March 1970.

9. T. R. Mager, Westinghouse Electric Corporation, PWR Systems Division, Pittsburgh, Pa., *Post-Irradiation Testing of 2T Compact Tension Specimens*, WCAP-7561, August 1970.

10. T. R. Mager, Westinghouse Electric Corporation, PWR Systems Division, Pittsburgh, Pa., *Fracture Toughness Characterization Study of A533, Grade B, Class 1 Steel*, WCAP-7578, October 1970.

11. T. R. Mager, Westinghouse Electric Corporation, PWR Systems Division, Pittsburgh, Pa., *Notch Preparation in Compact Tension Specimens*, WCAP-7579, November 1970.

12. N. Levy and P. V. Marcal, Brown University, Providence, R.I., *Three-Dimensional Elastic-Plastic Stress and Strain Analysis for Fracture Mechanics, Phase I: Simple Flawed Specimens*, HSSTP-TR-12, December 1970.

13. W. O. Shabbits, Westinghouse Electric Corporation, PWR Systems Division, Pittsburgh, Pa., *Dynamic Fracture Toughness Properties of Heavy Section A533 Grade B Class 1 Steel Plate*, WCAP-7623, December 1970.

14. P. N. Randall, TRW Systems Group, Redondo Beach, Calif., *Gross Strain Crack Tolerance of A 533-B Steel*, HSSTP-TR-14, May 1, 1971.

15. H. T. Corten and R. H. Sailors, University of Illinois, Urbana, Ill., *Relationship Between Material Fracture Toughness Using Fracture Mechanics and Transition Temperature Tests*, T&AM Report 346, August 1, 1971.

16. T. R. Mager and V. J. McLaughlin, Westinghouse Electric Corporation, PWR Systems Division, Pittsburgh, Pa., *The Effect of an Environment of High Temperature Primary Grade Nuclear Reactor Water on the Fatigue Crack Growth Characteristics of A533 Grade B Class 1 Plate and Weldment Material*, WCAP-7776, October 1971.

17. N. Levy and P. V. Marcal, Brown University, Providence, R.I., *Three-Dimensional Elastic-Plastic Stress and Strain Analysis for Fracture Mechanics, Phase II: Improved Modelling*, HSSTP-TR-17, November 1971.

18. S. C. Grigory, Southwest Research Institute, San Antonio, Tex., *Tests of 6-in.-Thick Flawed Tensile Specimens, First Technical Summary Report, Longitudinal Specimens Numbers 1 through 7*, HSSTP-TR-18, June 1972.

19. P. N. Randall, TRW Systems Group, Redondo Beach, [illegible], *Effects of Strain Gradients on the Gross Strain [illegible]k Tolerance of A533-B Steel*, HSSTP-TR-19, [illegible]une 15, 1972.

20. S. C. Grigory, Southwest Research Institute, San Antonio, Tex., *Tests of 6-Inch-Thick Flawed Tensile Specimens, Second Technical Summary Report, Transverse Specimens Numbers 8 through 10, Welded Specimens Numbers 11 through 13*, HSSTP-TR-20, June 1972.

21. L. A. James and J. A. Williams, Hanford Engineering Development Laboratory, Richland, Wash., Heavy Section Steel Technology Program Technical Report No. 21, *The Effect of Temperature and Neutron Irradiation Upon the Fatigue-Crack Propagation Behavior of ASTM A533 Grade B, Class 1 Steel*, HEDL-TME 72-132, September 1972.

22. S. C. Grigory, Southwest Research Institute, San Antonio, Tex., *Tests of 6-Inch-Thick Flawed Tensile Specimens, Third Technical Summary Report, Longitudinal Specimens Numbers 14 through 16, Unflawed Specimen Number 17*, HSSTP-TR-22, October 1972.

23. S. C. Grigory, Southwest Research Institute, San Antonio, Tex., *Tests of 6-Inch-Thick Tensile Specimens, Fourth Technical Summary Report, Tests of 1-Inch-Thick Flawed Tensile Specimens for Size Effect Evaluation*, HSSTP-TR-23, June 1973.

24. S. P. Y[illegible]. Grigory, Southwest Research Institu[illegible]io, Tex., *Tests of 6-Inch-Thick Tens[illegible] Fifth Technical Summary Report, Acous[illegible] Monitorin[illegible]f One-Inch and Six-Inch-Th[illegible] Specimen[illegible]* HSSTP-TR-24, Novem[illegible]

25. R. W. Derby, J. G. Merkle, G. C. Robinson, G. D. Whitman, and F. J. Witt, Oak Ridge Natl. Lab., Oak Ridge, Tenn., *Test of 6-Inch-Thick Pressure Vessels. Series 1: Intermediate Test Vessels V-1 and V-2*, ORNL-4895, February 1974.

26. W. J. Stelzman and R. G. Berggren, Oak Ridge Natl. Lab., Oak Ridge, Tenn., *Radiation Strengthening and Embrittlement in Heavy Section Steel Plates and Welds*, ORNL-4871, June 1973.

27. P. B. Crosley and E. J. Ripling, Materials Research Laboratory, Inc., Glenwood, Ill., *Crack Arrest in an Increasing K-Field*, HSSTP-TR-27, January 1973.

28. P. V. Marcal, P. M. Stuart, and R. S. Bettes, Brown University, Providence, R.I., *Elastic Plastic Behavior of a Longitudinal Semi-Elliptic Crack in a Thick Pressure Vessel*, HSSTP-TR-28, June 1973.

29. W. J. Stelzman, R. G. Berggren, and T. N. Jones, Oak Ridge Natl. Lab., Oak Ridge, Tenn., *ORNL Characterization of Heavy-Section Steel Technology Program Plates 01, 02 and 03*, USNRC Report NUREG/CR-4092 (ORNL/TM-9491), April 1985.

30. Canceled.

31. J. A. Williams, Hanford Engineering Development Laboratory, Richland, Wash., *The Irradiation and Temperature Dependence of Tensile and Fracture Properties of ASTM A533, Grade B, Class 1 Steel Plate and Weldment*, HEDL-TME 73-75, August 1973.

32. J. M. Steichen and J. A. Williams, Hanford Engineering Development Laboratory, Richland, Wash., *High Strain Rate Tensile Properties of Irradiated ASTM A533 Grade B Class 1 Pressure Vessel Steel*, July 1973.

33. P. C. Riccardella and J. L. Swedlow, Westinghouse Electric Corporation, Pittsburgh, Pa., *A Combined Analytical-Experimental Fracture Study of the Two Leading Theories of Elastic-Plastic Fracture (J-Integral and Equivalent Energy)*, WCAP-8224, October 1973.

34. R. J. Podlasek and R. J. Eiber, Battelle Columbus Laboratories, Columbus, Ohio, *Final Report on Investigation of Mode III Crack Extension in Reactor Piping*, December 14, 1973.

35. T. R. Mager, J. D. Landes, D. M. Moon, and V. J. McLaughlin. Westinghouse Electric Corporation, Pittsburgh, Pa., *Interim Report on the Effect of Low Frequencies on the Fatigue Crack Growth Characteristics of A533 Grade B Class 1 Plate in an Environment of High-Temperature Primary Grade Nuclear Reactor Water*, WCAP-8256, December 1973.

36. J. A. Williams, Hanford Engineering Development Laboratory, Richland, Wash., *The Irradiated Fracture Toughness of ASTM A533, Grade B, Class 1 Steel Measured with a Four-Inch-Thick Compact Tension Specimen*, HEDL-TME 75-10, January 1975.

37. R. H. Bryan, J. G. Merkle, M. N. Raftenberg, G. C. Robinson, and J. E. Smith, Oak Ridge Natl. Lab., Oak Ridge, Tenn., *Test of 6-Inch-Thick Pressure Vessels. Series 2: Intermediate Test Vessels V-3, V-4, and V-6*, ORNL-5059, November 1975.

38. T. R. Mager, S. E. Yanichko, and L. R. Singer, Westinghouse Electric Corporation, Pittsburgh, Pa., *Fracture Toughness Characterization of HSST Intermediate Pressure Vessel Material*, WCAP-8456, December 1974.

39. J. G. Merkle, G. D. Whitman, and R. H. Bryan, Oak Ridge Natl. Lab., Oak Ridge, Tenn., *An Evaluation of the HSST Program Intermediate Pressure Vessel Tests in Terms of Light-Water-Reactor Pressure Vessel Safety*, ORNL/TM-5090, November 1975.

40. J. C. Merkle, G. C. Robinson, P. P. Holz, J. E. Smith, and R. H. Bryan, Oak Ridge Natl. Lab., Oak Ridge, Tenn., *Test of 6-In.-Thick Pressure Vessels. Series 3: Intermediate Test Vessel V-7*, USNRC Report ORNL/NUREG-1, August 1976.

41. J. A. Davidson, L. J. Ceschini, R. P. Shogan, and G. V. Rao, Westinghouse Electric Corporation, Pittsburgh, Pa., *The Irradiated Dynamic Fracture Toughness of ASTM A533, Grade B, Class 1 Steel Plate and Submerged Arc Weldment*, WCAP-8775, October 1976.

42. R. D. Cheverton, Oak Ridge Natl. Lab., Oak Ridge, Tenn., *Pressure Vessel Fracture Studies Pertaining to a PWR LOCA-ECC Thermal Shock: Experiments TSE-1 and TSE-2*, USNRC Report ORNL/NUREG/TM-31, September 1976.

43. J. G. Merkle, G. C. Robinson, P. P. Holz, and J. E. Smith, Oak Ridge Natl. Lab., Oak Ridge, Tenn., *Test of 6-In.-Thick Pressure Vessels. Series 4: Intermediate Test Vessels V-5 and V-9 with Inside Nozzle Corner Cracks*, USNRC Report ORNL/NUREG-7, August 1977.

44. J. A. Williams, Hanford Engineering Development Laboratory, Richland, Wash., *The Ductile Fracture Toughness of Heavy Section Steel Plate*, USNRC Report NUREG/CR-0859, September 1979.

45. R. H. Bryan, T. M. Cate, P. P. Holz, T. A. King, J. G. Merkle, G. C. Robinson, G. C. Smith, J. E. Smith, and G. D. Whitman, Oak Ridge Natl. Lab., Oak Ridge, Tenn., *Test of 6-in.-Thick Pressure Vessels. Series 3: Intermediate Test Vessel V-7A Under Sustained Loading*, USNRC Report ORNL/NUREG-9, February 1978.

46. R. D. Cheverton and S. E. Bolt, Oak Ridge Natl. Lab., Oak Ridge, Tenn., *Pressure Vessel Fracture Studies Pertaining to a PWR LOCA-ECC Thermal Shock: Experiments TSE-3 and TSE-4 and Update of TSE-1 and TSE-2 Analysis*, USNRC Report ORNL/NUREG-22, December 1977.

47. D. A. Canonico, Oak Ridge Natl. Lab., Oak Ridge, Tenn., *Significance of Reheat Cracks to the Integrity of Pressure Vessels for Light-Water Reactors*, USNRC Report ORNL/NUREG-15, July 1977.

48. G. C. Smith and P. P. Holz, Oak Ridge Natl. Lab., Oak Ridge, Tenn., *Repair Weld Induced Residual Stresses in Thick-Walled Steel Pressure Vessels*, USNRC Report NUREG/CR-0093 (ORNL/NUREG/TM-153), June 1978.

49. P. P. Holz and S. W. Wismer, Oak Ridge Natl. Lab., Oak Ridge, Tenn., *Half-Bead (Temper) Repair Welding for HSST Vessels*, USNRC Report NUREG/CR-0113 (ORNL/NUREG/TM-177), June 1978.

50. G. C. Smith, P. P. Holz, and W. J. Stelzman, Oak Ridge Natl. Lab., Oak Ridge, Tenn., *Crack Extension and Arrest Tests of Axially Flawed Steel Model Pressure Vessels*, USNRC Report NUREG/CR-0126 (ORNL/NUREG/TM-196), October 1978.

51. R. H. Bryan, P. P. Holz, J. G. Merkle, G. C. Smith, J. E. Smith, and W. J. Stelzman, Oak Ridge Natl. Lab., Oak Ridge, Tenn., *Test of 6-in.-Thick Pressure Vessels. Series 3: Intermediate Test Vessel V-7B*, USNRC Report NUREG/CR-0309 (ORNL/NUREG-38), October 1978.

52. R. D. Cheverton, S. K. Iskander, and S. E. Bolt, Oak Ridge Natl. Lab., Oak Ridge, Tenn., *Applicability of LEFM to the Analysis of PWR Vessels Under LOCA-ECC Thermal Shock Conditions*, USNRC Report NUREG/CR-0107 (ORNL/NUREG-40), October 1978.

53. R. H. Bryan, D. A. Canonico, P. P. Holz, S. K. Iskander, J. G. Merkle, J. E. Smith, and W. J. Stelzman, Oak Ridge Natl. Lab., Oak Ridge, Tenn., *Test of 6-in.-Thick Pressure Vessels, Series 3: Intermediate Test Vessel V-8*, USNRC Report NUREG/CR-0675 (ORNL/ NUREG-58), December 1979.

54 R. D. Cheverton and S. K. Iskander, Oak Ridge Natl. Lab., Oak Ridge, Tenn., *Application of Static and Dynamic Crack Arrest Theory to TSE-4*, USNRC Report NUREG/CR-0767 (ORNL/NUREG-57), June 1979.

55. J. A. Williams, Hanford Engineering Development Laboratory, Richland, Wash., *Tensile Properties of Irradiated and Unirradiated Welds of A533 Steel Plate and A508 Forgings*, USNRC Report NUREG/CR-1158 (ORNL/Sub/79-50917/2), July 1979.

56. K. W. Carlson and J. A. Williams, Hanford Engineering Development Laboratory, Richland, Wash., *The Effect of Crack Length and Side Grooves on the Ductile Fracture Toughness Properties of ASTM A533 Steel*, USNRC Report NUREG/CR-1171 (ORNL/Sub/79-50917/3), October 1979.

57. P. P. Holz, Oak Ridge Natl. Lab., Oak Ridge, Tenn., *Flaw Preparations for HSST Program Vessel Fracture Mechanics Testing; Mechanical-Cyclic Pumping and Electron-Beam Weld-Hydrogen Charge Cracking Schemes*, USNRC Report NUREG/CR-1274 (ORNL/ NUREG/TM-369), May 1980.

Prior

58. S. K. Iskander, Computer Sciences Div., Union Carbide Corp. Nuclear Div., Oak Ridge, Tenn., *Two Finite Element Techniques for Computing Mode I Stress Intensity Factors in Two- or Three-Dimensional Problems*, USNRC Report NUREG/CR-1499 (ORNL/NUREG/CSD/TM-14), February 1981.

59. P. B. Crosley and E. J. Ripling, Materials Research Laboratory, Glenwood, Ill., *Development of a Standard Test for Measuring K_{Ia} with a Modified Compact Specimen*, USNRC Report NUREG/CR-2294 (ORNL/Sub/81-7755/1), August 1981.

60. S. N. Atluri, B. R. Bass, J. W. Bryson, and K. Kathiresan, Computer Sciences Div., Oak Ridge Gaseous Diffusion Plant, Oak Ridge, Tenn., *NOZ-FLAW: A Finite Element Program for Direct Evaluation of Stress Intensity Factors for Pressure Vessel Nozzle-Corner Flaws*, USNRC Report NUREG/CR-1843 (ORNL/NUREG/CSD/TM-18), March 1981.

61. A. Shukla, W. L. Fourney, and G. R. Irwin, University of Maryland, College Park, Md., *Study of Energy Loss and Its Mechanisms in Homalite 100 During Crack Propagation and Arrest*, USNRC Report NUREG/CR-2150 (ORNL/Sub/79-7778/1), August 1981.

62. S. K. Iskander, R. D. Cheverton, and D. G. Ball, Oak Ridge Natl. Lab., Oak Ridge, Tenn., *OCA-I, A Code for Calculating the Behavior of Flaws on the Inner Surface of a Pressure Vessel Subjected to Temperature and Pressure Transients*, USNRC Report NUREG/CR-2113 (ORNL/NUREG-84), August 1981.

63. R. J. Sanford, R. Chona, W. L. Fourney, and G. R. Irwin, University of Maryland, College Park, Md., *A Photoelastic Study of the Influence of Non-Singular Stresses in Fracture Test Specimens*, USNRC Report NUREG/CR-2179 (ORNL/Sub/79-7778/2), August 1981.

64. B. R. Bass, S. N. Atluri, J. W. Bryson, and K. Kathiresan, Oak Ridge Natl. Lab., Oak Ridge, Tenn., *OR-FLAW: A Finite Element Program for Direct Evaluation of K-Factors for User-Defined Flaws in Plate, Cylinders, and Pressure-Vessel Nozzle Corners*, USNRC Report NUREG/CR-2494 (ORNL/CSD/TM-165), April 1982.

65. B. R. Bass and J. W. Bryson, Oak Ridge Natl. Lab., Oak Ridge Tenn., *ORMGEN-3D: A Finite Element Mesh Generator for 3-Dimensional Crack Geometries*, USNRC Report NUREG/CR-2997, Vol. 1 (ORNL/TM-8527/V1), December 1982.

66. B. R. Bass and J. W. Bryson, Oak Ridge Natl. Lab., Oak Ridge, Tenn., *ORVIRT: A Finite Element Program for Energy Release Rate Calculations for 2-Dimensional and 3-Dimensional Crack Models*, USNRC Report NUREG/CR-2997, Vol. 2 (ORNL/TM-8527/V2), February 1983.

67. R. D. Cheverton, S. K. Iskander, and D. G. Ball, Oak Ridge Natl. Lab., Oak Ridge, Tenn., *PWR Pressure Vessel Integrity During Overcooling Accidents: A Parametric Analysis*, USNRC Report NUREG/CR-2895 (ORNL/TM-7931), February 1983.

68. D. G. Ball, R. D. Cheverton, J. B. Drake, and S. K. Iskander, Oak Ridge Natl. Lab., Oak Ridge, Tenn., *OCA-II, A Code for Calculating Behavior of 2-D and 3-D Surface Flaws in a Pressure Vessel Subjected to Temperature and Pressure Transients*, USNRC Report NUREG/ CR-3491 (ORNL-5934), February 1984.

69. A. Sauter, R. D. Cheverton, and S. K. Iskander, Oak Ridge Natl. Lab., Oak Ridge, Tenn., *Modification of OCA-I for Application to a Reactor Pressure Vessel with Cladding on the Inner Surface*, USNRC Report NUREG/CR-3155 (ORNL/TM-8649), May 1983.

70. R. D. Cheverton and D. G. Ball, Martin Marietta Energy Systems, Inc., Oak Ridge Natl. Lab., Oak Ridge, Tenn., *OCA-P, A Deterministic and Probabilistic Fracture-Mechanics Code for Application to Pressure Vessels*, USNRC Report NUREG/CR-3618 (ORNL-5991), May 1984.

71. J. G. Merkle, Martin Marietta Energy Systems, Inc., Oak Ridge Natl. Lab., Oak Ridge, Tenn., *An Examination of the Size Effects and Data Scatter Observed in Small Specimen Cleavage Fracture Toughness Testing*, USNRC Report NUREG/CR-3672 (ORNL/ TM-9088), April 1984.

72. C. E. Pugh et al., Martin Marietta Energy Systems, Inc., Oak Ridge Natl. Lab., Oak Ridge, Tenn., *Heavy-Section Steel Technology Program—Five-Year Plan FY 1983–1987*, USNRC Report NUREG/CR-3595 (ORNL/TM-9008), April 1984.

73. D. G. Ball, B. R. Bass, J. W. Bryson, R. D. Cheverton, and J. B. Drake, Martin Marietta Energy Systems, Inc., Oak Ridge Natl. Lab., Oak Ridge, Tenn., *Stress Intensity Factor Influence Coefficients for Surface Flaws in Pressure Vessels*, USNRC Report NUREG/CR-3723 (ORNL/CSD/TM-216), February 1985.

74. W. R. Corwin, R. G. Berggren, and R. K. Nanstad, Martin Marietta Energy Systems, Inc., Oak Ridge Natl. Lab. Oak Ridge, Tenn., *Charpy Toughness and Tensile Properties of Neutron Irradiated Stainless*

Steel Submerged-Arc Weld Cladding Overlay, USNRC Report NUREG/CR-3927 (ORNL/TM-9309), September 1984.

75. C. W. Schwartz, R. Chona, W. L. Fourney, and G. R. Irwin, University of Maryland, College Park, Md., *SAMCR: A Two-Dimensional Dynamic Finite Element Code for the Stress Analysis of Moving CRacks*, USNRC Report NUREG/CR-3891 (ORNL/Sub/79-7778/3), November 1984.

76. W. R. Corwin, G. C. Robinson, R. K. Nanstad, J. G. Merkle, R. G. Berggren, G. M. Goodwin, R. L. Swain, and T. D. Owings, Martin Marietta Energy Systems, Inc., Oak Ridge Natl. Lab., Oak Ridge, Tenn., *Effects of Stainless Steel Weld Overlay Cladding on the Structural Integrity of Flawed Steel Plates in Bending, Series 1*, USNRC Report NUREG/CR-4015 (ORNL/TM-9390), April 1985.

77. R. H. Bryan, B. R. Bass, S. E. Bolt, J. W. Bryson, D. P. Edmonds, R. W. McCulloch, J. G. Merkle, R. K. Nanstad, G. C. Robinson, K. R. Thoms, and G. D. Whitman, Martin Marietta Energy Systems, Inc., Oak Ridge Natl. Lab., Oak Ridge, Tenn., *Pressurized-Thermal-Shock Test of 6-in.-Thick Pressure Vessels. PTSE-1: Investigation of Warm Prestressing and Upper-Shelf Arrest*, USNRC Report NUREG/CR-4106 (ORNL-6135), April 1985.

78. R. D. Cheverton, D. G. Ball, S. E. Bolt, S. K. Iskander, and R. K. Nanstad, Martin Marietta Energy Systems, Inc., Oak Ridge Natl. Lab., Oak Ridge, Tenn., *Pressure Vessel Fracture Studies Pertaining to the PWR Thermal-Shock Issue: Experiments TSE-5, TSE-5A, and TSE-6*, USNRC Report NUREG/CR-4249 (ORNL-6163), June 1985.

79. R. D. Cheverton, D. G. Ball, S. E. Bolt, S. K. Iskander, and R. K. Nanstad, Martin Marietta Energy Systems, Inc., Oak Ridge Natl. Lab., Oak Ridge, Tenn., *Pressure Vessel Fracture Studies Pertaining to the PWR Thermal-Shock Issue: Experiment TSE-7*, USNRC Report NUREG/CR-4304 (ORNL-6177), August 1985.

80. R. H. Bryan, B. R. Bass, S. E. Bolt, J. W. Bryson, J. G. Merkle, R. K. Nanstad, and G. C. Robinson, Martin Marietta Energy Systems, Inc., Oak Ridge Natl. Lab., Oak Ridge, Tenn., *Test of 6-in.-Thick Pressure Vessels. Series 3: Intermediate Test Vessel V-8A—Tearing Behavior of Low Upper-Shelf Material*, USNRC Report NUREG/CR-4760 (ORNL-6187), May 1987.

81. R. D. Cheverton and D. G. Ball, Martin Marietta Energy Systems, Inc., Oak Ridge Natl. Lab., Oak Ridge, Tenn., *A Parametric Study of PWR Pressure Vessel Integrity During Overcooling Accidents, Considering Both 2-D and 3-D Flaws*, USNRC Report NUREG/CR-4325 (ORNL/TM-9682), August 1985.

82. E. C. Rodabaugh, E. C. Rodabaugh Associates, Inc., Hilliard, Ohio, *Comments on the Leak-Before-Break Concept for Nuclear Power Plant Piping Systems*, USNRC Report NUREG/CR-4305 (ORNL/Sub/82-22252/3), August 1985.

83. J. W. Bryson, Martin Marietta Energy Systems, Inc., Oak Ridge Natl. Lab., Oak Ridge, Tenn., *ORVIRT.PC: A 2-D Finite Element Fracture Analysis Program for a Microcomputer*, USNRC Report NUREG/CR-4367 (ORNL-6208), October 1985.

84. D. G. Ball and R. D. Cheverton, Martin Marietta Energy Systems, Inc., Oak Ridge Natl. Lab., Oak Ridge, Tenn., *Adaptation of OCA-P, A Probabilistic Fracture-Mechanics Code, to a Personal Computer*, USNRC Report NUREG/CR-4468 (ORNL/CSD/TM-233), January 1986.

85. J. W. Bryson and B. R. Bass, Martin Marietta Energy Systems, Inc., Oak Ridge Natl. Lab., Oak Ridge, Tenn., *ORMGEN.PC: A Microcomputer Program for Automatic Mesh Generation of 2-D Crack Geometries*, USNRC Report NUREG/CR-4475 (ORNL-6250), March 1986.

86. G. D. Whitman, Martin Marietta Energy Systems, Inc., Oak Ridge Natl. Lab., Oak Ridge, Tenn., *Historical Summary of the Heavy-Section Steel Technology Program and Some Related Activities in Light-Water Reactor Pressure Vessel Safety Research*, USNRC Report NUREG/CR-4489 (ORNL-6259), March 1986.

87. C. Inversini and J. W. Bryson, Martin Marietta Energy Systems, Inc., Oak Ridge Natl. Lab., Oak Ridge, Tenn., *ORPLOT PC: A Graphic Utility for ORMGEN.PC and ORVIRT.PC*, USNRC Report NUREG/CR-4633 (ORNL-6291), June 1986.

88. J. J. McGowan, R. K. Nanstad, and K. R. Thoms, Martin Marietta Energy Systems, Inc., Oak Ridge Natl. Lab., Oak Ridge, Tenn., *Characterization of Irradiated Current-Practice Welds and A533 Grade B Class 1 Plate for Nuclear Pressure Vessel Service*, USNRC Report NUREG/CR-4880 (ORNL/TM-10387), July 1988.

89. K. V. Cook and R. W. McClung, Martin Marietta Energy Systems, Inc., Oak Ridge Natl. Lab., Oak Ridge, Tenn., *Flaw Density Examinations of a Clad Boiling Water Reactor Pressure Vessel Segment*, USNRC Report NUREG/CR-4860 (ORNL/TM-10364), April 1987.

Prior

90. D. J. Naus, B. R. Bass, C. E. Pugh, R. K. Nanstad, J. G. Merkle, W. R. Corwin, and G. C. Robinson, Martin Marietta Energy Systems, Inc., Oak Ridge Natl. Lab., Oak Ridge, Tenn., *Crack-Arrest Behavior in SEN Wide Plates of Quenched and Tempered A 533 Grade B Steel Tested Under Nonisothermal Conditions*, USNRC Report NUREG/CR-4930 (ORNL-6388), August 1987.

91. D. B. Barker, R. Chona, W. L. Fourney, and G. R. Irwin, University of Maryland, College Park, Md., *A Report on the Round Robin Program Conducted to Evaluate the Proposed ASTM Standard Test Method for Determining the Plane Strain Crack Arrest Fracture Toughness, K_{Ia}*, of Ferritic Materials, USNRC Report NUREG/CR-4966 (ORNL/Sub/79-7778/4), January 1988.

92. W. H. Bamford, Westinghouse Electric Corporation, Pittsburgh, Pa., *A Summary of Environmentally Assisted Crack-Growth Studies Performed at Westinghouse Electric Corporation Under Funding from the Heavy-Section Steel Technology Program*, USNRC Report NUREG/CR-5020 (ORNL/Sub/82-21598/1), May 1988.

93. R. H. Bryan, B. R. Bass, S. E. Bolt, J. W. Bryson, W. R. Corwin, J. G. Merkle, R. K. Nanstad, and G. C. Robinson, Martin Marietta Energy Systems, Inc., Oak Ridge Natl. Lab., Oak Ridge, Tenn., *Pressurized-Thermal-Shock Test of 6-in.-Thick Pressure Vessels. PTSE-2: Investigation of Low Tearing Resistance and Warm Prestressing*, USNRC Report NUREG/CR-4888 (ORNL-6377), December 1987.

94. J. H. Giovanola and R. W. Klopp, SRI International, Menlo Park, Calif., *Viscoplastic Stress-Strain Characterization of A533B Class 1 Steel*, USNRC Report NUREG/CR-5636 (ORNL/Sub/87-SA193/1), September 1989.

95. L. F. Miller et al., Martin Marietta Energy Systems, Inc., Oak Ridge Natl. Lab., Oak Ridge, Tenn., *Neutron Exposure Parameters for the Metallurgical Test Specimens in the Fifth Heavy-Section Steel Technology Irradiation Series Capsules*, USNRC Report NUREG/ CR-5019 (ORNL/TM-10582), March 1988.

96. Canceled.

97. D. J. Naus, J. Keeney-Walker, and B. R. Bass, Martin Marietta Energy Systems, Inc., Oak Ridge Natl. Lab., Oak Ridge, Tenn., *High-Temperature Crack-Arrest Behavior in 152-mm-Thick SEN Wide Plates of Quenched and Tempered A 533 Grade B Steel*, USNRC Report NUREG/CR-5330 (ORNL/TM-11083), April 1989.

98. K. V. Cook, R. A. Cunningham, Jr., and R. W. McClung, Martin Marietta Energy Systems, Inc., Oak Ridge Natl. Lab., Oak Ridge, Tenn., *Detection and Characterization of Indications in Segments of Reactor Pressure Vessels*, USNRC Report NUREG/CR-5322 (ORNL/TM-11072), August 1989.

99. R. D. Cheverton, W. E. Pennell, G. C. Robinson, and R. K. Nanstad, Martin Marietta Energy Systems, Inc., Oak Ridge Natl. Lab., Oak Ridge, Tenn., *Impact of Radiation Embrittlement on Integrity of Pressure Vessel Supports for Two PWR Plants*, NUREG/ CR-5320 (ORNL/TM-10966), February 1989.

100. D. J. Naus, J. Keeney-Walker, B. R. Bass, S. K. Iskander, R. J. Fields, R. deWitt, and S. R. Low III, Martin Marietta Energy Systems, Inc., Oak Ridge Natl. Lab., Oak Ridge, Tenn., *SEN Wide-Plate Crack-Arrest Tests* Utilizing *A 533 Grade B Class 1 Material: WP-CE Test Series*, USNRC Report NUREG/CR-5408 (ORNL/TM-11269), November 1989.

101. D. J. Naus, J. Keeney-Walker, B. R. Bass, S. K. Iskander, R. J. Fields, R. deWitt, and S. R. Low III, Martin Marietta Energy Systems, Inc., Oak Ridge Natl. Lab., Oak Ridge, Tenn., *High Temperature Crack-Arrest Tests Using 152-mm-Thick SEN Wide Plates of Low Upper-Shelf Base Material: Tests WP-2.2 and WP-2.6*, USNRC Report NUREG/CR-5450 (ORNL/TM-11352), February 1990.

102. Canceled.

103. D. J. Naus, J. Keeney-Walker, B. R. Bass, G. C. Robinson, S. K. Iskander, D. J. Alexander, R. J. Fields, R. deWitt, S. R. Low, C. W. Schwartz, and I.-B. Johansson, Martin Marietta Energy Systems, Inc., Oak Ridge Natl. Lab., Oak Ridge, Tenn., *Crack-Arrest Behavior in SEN Wide Plates of Low Upper-Shelf Base Metal Tested Under Nonisothermal Conditions: WP-2 Series*, USNRC Report NUREG/ CR-5451 (ORNL-6584), August 1990.

104. T. L. Dickson, R. D. Cheverton, and D. K. Shum, Martin Marietta Energy Systems, Inc., Oak Ridge Natl. Lab., Oak Ridge, Tenn., *Inclusion of Unstable Ductile Tearing and Extrapolated Crack-Arrest Toughness Data in PWR Vessel Integrity Assessment*, USNRC Report NUREG/CR-5473 (ORNL/ TM-11450), May 1990.

105. T. J. Theiss, Martin Marietta Energy Systems, Inc., Oak Ridge Natl. Lab., Oak Ridge, Tenn., *Recommendations for the Shallow-Crack Fracture Toughness Testing Task Within the HSST Program*,

USNRC Report NUREG/CR-5554 (ORNL/TM-11509), September 1990.

106. J. G. Merkle, Martin Marietta Energy Systems, Inc., Oak Ridge Natl. Lab., Oak Ridge, Tenn., *An Overview of the Low Upper Shelf Toughness Safety Margin Issue*, USNRC Report NUREG/CR-5552 (ORNL/TM-11314), August 6, 1990.

107. D. K. M. Shum, J. G. Merkle, J. Keeney-Walker, and B. R. Bass, Martin Marietta Energy Systems, Inc., Oak Ridge Natl. Lab., Oak Ridge, Tenn., *Analytical Studies of Transverse Strain Effects on Fracture Toughness for Circumferentially Oriented Cracks*, USNRC Report NUREG/CR-5592 (ORNL/TM-11581), April 1991.

108. J. D. Landes, The University of Tennessee for Martin Marietta Energy Systems, Inc., Oak Ridge natl. Lab., Oak Ridge, Tenn., *Extrapolation of the J-R Curve for Predicting Reactor Vessel Integrity*, USNRC Report NUREG/CR-5650 (ORNL/Sub/89-99732/1), January 1992.

109. J. Keeney-Walker, B. R. Bass, and J. D. Landes, (The University of Tennessee), Martin Marietta Energy Systems, Inc., Oak Ridge Natl. Lab., Oak Ridge, Tenn., *An Investigation of Crack-Tip Stress-Field Criteria for Predicting Cleavage-Crack Initiation*, USNRC Report NUREG/ CR-5651 (ORNL/TM-11692), September 1991.

110. G. R. Irwin, University of Maryland, for Martin Marietta Energy Systems, Inc., Oak Ridge Natl. Lab., Oak Ridge, Tenn., *Use of Thickness Reduction to Estimate Values of K*, USNRC Report NUREG/CR-5697 (ORNL/Sub/79-7778/5), November 1991.

111. P. Albrecht and X. Chen, University of Maryland for Martin Marietta Energy Systems, Inc., Oak Ridge Natl. Lab., Oak Ridge, Tenn., *Limit Pressure Analysis of PTSE-2 Vessel*, USNRC Report NUREG/CR-5698 (ORNL/Sub/79-7778/6) (to be published).

112. J. W. Dally, W. L. Fourney, and G. R. Irwin, University of Maryland for Martin Marietta Energy Systems, Inc., Oak Ridge Natl. Lab., Oak Ridge, Tenn., *Lower-Bound Initiation Toughness with a Modified-Charpy Specimen*, USNRC Report NUREG/CR-5703 (ORNL/ Sub/79-7778/7), November 1991.

113. S. K. Iskander, G. C. Robinson, W. R. Corwin, B. C. Oland, D. J. Alexander, and K. V. Cook, Martin Marietta Energy Systems, Inc., Oak Ridge Natl. Lab., Oak Ridge, Tenn., *Experimental Results of Tests to Investigate Flaw Behavior of Mechanically Loaded Stainless Steel Clad Plates*, USNRC Report NUREG/ CR-5785 (ORNL/TM-11950), April 1992.

114. S. T. Rolfe, University of Kansas for Martin Marietta Energy Systems, Inc., Oak Ridge Natl. Lab., Oak Ridge, Tenn., *Interpretive Report on the Application of Shallow-Flaw CTOD Test Data to the Structural Margin Assessment of Reactor Pressure Vessels with Flaws*, USNRC Report NUREG/CR-5767 (ORNL/Sub/90-SH640/1), November 1991.

115. D. E. McCabe, Martin Marietta Energy Systems, Inc., Oak Ridge Natl. Lab., Oak Ridge, Tenn., *Comparison of Weibull and β_{1c} Analysis of Transition Range Fracture Toughness Data*, USNRC Report NUREG/CR-5788 (ORNL/ TM-11959), January 1992.

116. R. D. Cheverton, T. L. Dickson, J. G. Merkle, and R. K. Nanstad, Martin Marietta Energy Systems, Inc., Oak Ridge Natl. Lab., Oak Ridge, Tenn., *Review of Reactor Pressure Vessel Evaluation Report for Yankee Rowe Nuclear Power Station (YAEC No. 1735)*, USNRC Report NUREG/CR-5799 (ORNL/ TM-11982), March 1992

117. T. L. Dickson, R. D. Cheverton, and J. W. Bryson, Martin Marietta Energy Systems, Inc., Oak Ridge Natl. Lab., Oak Ridge, Tenn., *Pressurized-Thermal-Shock Probobilistic Fracture Mechanics Sensitivity Analyses for Yankee Rowe Reactor Pressure Vessel*, USNRC Report NUREG/CR-5782 (ORNL/TM-11945) (to be published).

118. Cancelled

119. J. W. Dally, G. R. Irwin, X-J. Zhang, and R. J. Bonenberger, University of Maryland for Martin Marietta Energy Systems, Inc., Oak Ridge Natl. Lab., Oak Ridge, Tenn., *The Influence of Precompression on the Lower-Bound Initiation Toughness of A 533 B Reactor Grade Steel*, USNRC Report NUREG/ CR-5847 (ORNL/Sub/79-7778/8), May 1992.

120. Cancelled

121. C. W. Schwartz, University of Maryland for Martin Marietta Energy Systems, Inc., Oak Ridge Natl. Lab., Oak Ridge, Tenn., *Crack Speed Relations Inferred from Large SEN Specimens of A 533 B Steel*, USNRC Report NUREG/CR-5861 (ORNL/Sub/79-7778/9) (to be published).

122. A. R. Rosenfield and C. W. Marschall, Battelle Columbus Division for Martin Marietta Energy Systems, Inc., Oak Ridge Natl. Lab., Oak Ridge, Tenn., *Fracture-Mechanics-Based Failure Analysis*,

USNRC Report NUREG/CR-5860 (ORNL/Sub/82-17651/1), June 1992.

123. G. R. Irwin and X-J. Zhang, University of Maryland for Martin Marietta Energy Systems, Inc., Oak Ridge Natl. Lab., Oak Ridge, Tenn., *Gradient Study of a Large Weld Joining Two Forged A 508 Shells of the Midland Reactor Vessel*, USNRC Report NUREG/CR-5867 (ORNL/Sub/79-7778/10), June 1992.

124. J. Keeney-Walker and B. R. Bass, Martin Marietta Energy Systems, Inc., Oak Ridge Natl. Lab., Oak Ridge, Tenn., *ORNOZL: A Finite-Element Mesh Generator for Nozzle-Cylinder Intersections Containing Inner-Corner Cracks*, USNRC Report NUREG/CR-5872 (ORNL/TM-11049), September 1992.

125. J. Keeney-Walker and B. R. Bass, Martin Marietta Energy Systems, Inc., Oak Ridge Natl. Lab., Oak Ridge, Tenn., *A Comparison of Analysis Methodologies for Predicting Cleavage Arrest of a Deep Crack in a Reactor Pressure Vessel Subjected to Pressurized-Thermal-Shock Loading Conditions*, USNRC Report NUREG/CR-5793 (ORNL/TM-11969), September 1992.

126. T. J. Theiss, D. K. M. Shum, and S. T. Rolfe (University of Kansas), Martin Marietta Energy Systems, Inc., Oak Ridge Natl. Lab., Oak Ridge, Tenn., *Experimental and Analytical Investigation of the Shallow-Flaw Effect in Reactor Pressure Vessels*, USNRC Report NUREG/CR-5886 (ORNL/TM-12115), July 1992.

127. B. R. Bass, D. K. M. Shum, and J. Keeney-Walker, Martin Marietta Energy Systems, Inc., Oak Ridge Natl. Lab., Oak Ridge, Tenn., *Constraint Effects on Fracture Toughness for Circumferentially Oriented Cracks in Reactor Pressure Vessels*, USNRC Report NUREG/CR-6008, (ORNL/TM-12131), August 1992.

NUREG/CR-4219
Vol. 9, No. 1
ORNL/TM-9593/V9&N1
Dist. Category RF

Internal Distribution

1. D. J. Alexander
2. B. R. Bass
3. J. W. Bryson
4. E. W. Carver
5–6. R. D. Cheverton
7. J. M. Corum
8. W. R. Corwin
9. T. L. Dickson
10. F. M. Haggag
11. J. J. Henry
12. W. F. Jackson
13. J. E. Jones Jr.
14. S. K. Iskander
15. J. Keeney-Walker
16. W. J. McAfee
17. D. E. McCabe
18. J. G. Merkle
19. R. K. Nanstad
20. D. J. Naus
21–25. W. E. Pennell
26. C. B. Oland
27. C. E. Pugh
28. G. C. Robinson
29. D. K. M. Shum
30. C. C. Southmayd
31. R. L. Swain
32–35. T. J. Theiss
36. ORNL Patent Section
37. Central Research Library
38. Document Reference Section
30–40. Laboratory Records
41. Laboratory Records (RC)

External Distribution

42. L. C. Shao, Director, Division of Engineering, U.S. Nuclear Regulatory Commission, Washington, DC 20555
43. C. Z. Serpan, Jr., Division of Engineering, U.S. Nuclear Regulatory Commission, Washington, DC 20555
44. E. M. Hackett, Division of Engineering, U.S. Nuclear Regulatory Commission, Washington, D C 20555
45. A. L. Hiser, Division of Engineering, U.S. Nuclear Regulatory Commission, Washington, DC 20555
46–48. S. N. M. Malik, Division of Engineering, U.S. Nuclear Regulatory Commission, Washington, DC 20555
49. M. E. Mayfield, Division of Engineering, U.S. Nuclear Regulatory Commission, Washington, DC 20555
50. A. Taboada, Division of Engineering, U.S. Nuclear Regulatory Commission, Washington, DC 20555
51–56. J. W. Dally, Department of Mechanical Engineering, University of Maryland, College Park, MD 20742
57. W. L. Fourney, Department of Mechanical Engineering, University of Maryland, College Park, MD 20742
58. J. D. Landes, The University of Tennessee, Knoxville, TN, 37996-2030
59. S. T. Rolfe, The University of Kansas, Lawrence, KS 66045-2235
60. A. R. Rosenfield, Battelle Columbus Division, Columbus, OH 43201
61. C. W. Schwartz, Department of Civil Engineering, University of Maryland, College Park, MD 20742
62. E. T. Wessel, 312 Wolverine, Haines City, FL 33844
63. Office of Assistant Manager for Energy Research and Development, DOE–OR, Oak Ridge, TN 37831
64–65. Office of Scientific and Technical Information, P. O. Box 62, Oak Ridge, TN 37831

NRC FORM 335 (2-89) NRCM 1102, 3201, 3202

U.S. NUCLEAR REGULATORY COMMISSION

BIBLIOGRAPHIC DATA SHEET

(See instructions on the reverse)

1. REPORT NUMBER (Assigned by NRC, Add Vol., Supp., Rev., and Addendum Numbers, if any.)
NUREG/CR-4219
ORNL/TM-9593/V9&N1
Vol. 9, No. 1

2. TITLE AND SUBTITLE
Heavy-Section Steel Technology Program
Semiannual Progress Report for October 1991-March 1992

3. DATE REPORT PUBLISHED

MONTH	YEAR
November	1992

4. FIN OR GRANT NUMBER
B0119

5. AUTHOR(S)
W. E. Pennell

6. TYPE OF REPORT
Technical

7. PERIOD COVERED (Inclusive Dates)
October 1991-March 1992

8. PERFORMING ORGANIZATION - NAME AND ADDRESS (If NRC, provide Division, Office or Region, U.S. Nuclear Regulatory Commission, and mailing address; if contractor, provide name and mailing address.)

Oak Ridge National Laboratory
Oak Ridge, TN 37831-6285

9. SPONSORING ORGANIZATION - NAME AND ADDRESS (If NRC, type "Same as above"; if contractor, provide NRC Division, Office or Region, U.S. Nuclear Regulatory Commission, and mailing address.)

Division of Engineering
Office of Nuclear Regulatory Research
U.S. Nuclear Regulatory Commission
Washington, DC 20555

10. SUPPLEMENTARY NOTES

11. ABSTRACT (200 words or less)

The Heavy-Section Steel Technology (HSST) Program is conducted for the Nuclear Regulatory Commission (NRC) by Oak Ridge National Laboratory (ORNL). The program focus is on the development and validation of technology for the assessment of fracture-prevention margins in commercial nuclear reactor pressure vessels. The HSST Program is organized in 11 tasks: (1) program management, (2) fracture methodology and analysis, (3) material characterization and properties, (4) special technical assistance, (5) fracture analysis computer programs, (6) cleavage-crack initiation, (7) cladding evaluations, (8) pressurized-thermal-shock technology, (9) analysis methods validation, (10) fracture evaluation tests, and (11) warm prestressing. The program tasks have been structured to place emphasis on the resolution fracture issues with near-term licensing significance. Resources to execute the research tasks are drawn from ORNL with subcontract support from universities and other research laboratories. Close contact is maintained with the sister Heavy-Section Steel Irradiation (HSSI) Program at ORNL and with related research programs both in the United States and abroad. This report provides an overview of principal developments in each of the 11 program tasks from October 1, 1991 to March 31, 1992.

12. KEY WORDS/DESCRIPTORS (List words or phrases that will assist researchers in locating the report.)

Thermal Aging
Heavy-Section Steel Technology
Shallow-Crack Beam
Clad Cylinder
Cladding Evaluations
Full-Thickness Beams
Crack-Initiation
RPV-grade materials
PTS transients
Biaxial Loading
A 302 B
HSST Program
Thermal-Shock
Fracture Methodology
Cleavage-Crack
Warm Prestress
Crack-Tip Fields
WPS-Enhanced
Fracture Toughness
Out-Of-Plane Stress

13. AVAILABILITY STATEMENT
Unlimited

14. SECURITY CLASSIFICATION
(This Page)
Unclassified
(This Report)
Unclassified

15. NUMBER OF PAGES

16. PRICE

Federal Recycling Program

UNITED STATES
NUCLEAR REGULATORY COMMISSION
WASHINGTON, D.C. 20555-0001

OFFICIAL BUSINESS
PENALTY FOR PRIVATE USE, $300

SPECIAL FOURTH-CLASS RATE
POSTAGE AND FEES PAID
USNRC
PERMIT NO. G-67